Paleoenvironmental interpretation of the Beekmantown Group within the Ottawa Basin

A thesis presented to the
School of Graduate Studies, University of Ottawa

In partial fulfilment
of the requirements for the degree
Master of Science
in Geology

By

John I. Cass

June 1979

ABSTRACT

The Beekmantown Group consists of a siliciclastic and carbonate-transgressive sequence that was deposited in the Ottawa Basin between post-Hadryian and Middle Ordovician times. The Group is here divided into the Potsdam, Theresa, Buck Bridge and Beauharnois Formations.

No petrological or biostratigraphical evidence was found for the existence of major unconformities within the group. Both textural isolithic maps and conodont biostratigraphic studies of the Buck Bridge and Beauharnois Formations suggest a facies suite relationship between these formations. Intermittent penecontemporaneous instabilities along the Frontenac Axis, Adirondack Massif and Beauharnois Anticline are indicated by localized folding, faulting and angular unconformities near these structures.

The use of textural parameters to distinguish between various environments produced confusing and in some cases contradictory results when compared with the associated sedimentary structures. Only the log-probability method of curve dissection suggested by Visher produced results which were consistent with associated sedimentary structures.

Hydrodynamic conditions indicated by conglomerate clast sizes, ripple lengths and cross stratification heights, suggest that the Potsdam (Keeseville Member), Theresa, Bucks Bridge and Beauharnois Formations were deposited in a low wave energy, microtidal range paleoenvironment within the Ottawa Basin.

TABLE OF CONTENT

		Page
	ABSTRACT	i
	LIST OF FIGURES	v
	LIST OF TABLES	x
	NOTATIONS	xi
	EQUATIONS	xiv
CHAPTER 1	INTRODUCTION	1
	Problems and Objectives	1
	Study Area	2
	Previous Work	5
CHAPTER 2	STRUCTURE OF BASIN	
	General Description	13
	St Lawrence Graben	15
	Ottawa-Bonnechere Graben	17
	Frontenac Axis	17
	Beauharnois Anticline	18
	Folding	19
CHAPTER 3	STRATIGRAPHIC NOMENCLATURE OF THE BEEKMANTOWN GROUP	
	Beekmantown Group	20
	Potsdam Formation	21
	Basal member	22
	Ausable Member	23
	Keeseville Member	24
	Theresa Formation	26
	Bucks Bridge Formation	27
	Heuvelton member	28

Page

March Member 29

Beauharnois Formation 29

CHAPTER 4 PETROLOGY: TEXTURAL TRENDS

Method 31

Grain Size Distribution 35

Graphic Mean and First Moment Size .. 36

Statistical Tests 38

Grain Size Patterns 47

Grain Shape 53

Petrology and Paleoenvironment Evaluations 58

Log-Probability Grain Size Evaluation of Paleoenvironments 66

Conglomerate Textures 74

CHAPTER 5 SEDIMENTARY STRUCTURES AND PALEOENVIRONMENTAL INTERPRETATION

General 78

Sedimentary Structures in Siliciclastic Strata 79

Conglomerate Structures 79

Estimation of Wave Intensity 81

Ripples 84

Wave Paleohydrodynamics from ripples . 90

Asymmetric Ripples 100

Cross Strata 104

Paleohydrodynamics from Cross Strata . 107

Evaluation of Paleotides from Bedforms ... 115

Paleocurrents 117

Page

Channels 121

Flaser and Lenticular Bedding 122

Bioturbation 122

Carbonate Sedimentary Structures 125

Laminated to Bioturbated Micrite (SMF 19) .. 125

Stromatolitic Micrite (SMF 20) 126

Micrite with Large Onkoids (SMF 22) 131

Unlaminated Homogeneous Unfossiliferous Micrite (SMF 23) .. 131

Coarse Lithoclastic-Rudstone or Floatstone (SMF 24) .. 132

Lag Deposits (SMF 14) 132

Beach Profiles..... 135

Storm Beach Profile 135

High Tide Shingle Beach 135

Low Wave Energy Beach 137

Carbonate Tidal Flats 138

CHAPTER 6 WESTPORT-ATHENS DISTRICT

General 139

Isolithic Trends 139

Philipsville Sections 148

Location 61^{A} Section 150

Location 61 Section 151

Textural Interpretation 151

Tidalites and Intertidalites 155

Location 48 Section 158

Carbonate Strata within the District 161

Paleoenvironmental Interpretation 162

		Page
CHAPTER 7	SUMMARY	164
	Suggestions for Additional Studies	168
	ACKNOWLEDGEMENTS	170
	REFERENCES	171
	APPENDICES (see p. 32)	
Appendix	Title	
1	Consumer's Gas Well (Russell County)	1
	Table A1: Lithofacies terms used	2
	Table A2: Standard microfacies used	3
	Well log	5
2	Locations of samples	38
3	Inclusive graphic statistics	42
4	Moment statistics	61
5	Insoluble mud size distribution	74
6	Estimated paleowave and current conditions under which ripples formed	75
7	Estimated paleoflow conditions under which cross strata formed	84

LIST OF FIGURES

Figure	Title	
1-1	Distribution of the Beekmantown Group within the Ottawa Basin	3
1-2	Access to the Beekmantown Group within the Western Ottawa Basin	4
1-3	Biostratigraphy of the Beekmantown Group within the Ottawa Basin	8
2-1	Structures asscíated with the Ottawa Basin.	14
4-1a	Graphic mean vs first moment distribution	37

Figure	Title	Page
4-1b	Relationship of graphic mean & first moment to total mud content	37
4-2	Graphic mean vs inclusive graphic standard deviation	39
4-3	First vs second moments	40
4-4	Graphic mean vs inclusive graphic skewness.	41
4-5	First moment vs coefficient of skewness	42
4-6	Inclusive graphic skewness vs inclusive graphic standard deviation	43
4-7	Second moment vs coefficient of skewness	44
4-8	Transformed graphic kurtosis vs inclusive graphic skewness	45
4-9	Location map for grain size distribution study	51
4-10	Grain roundness vs sphericity	54
4-11a	Insoluble mud vs grain roundness in the Beekmantown Group	56
4-11b	Carbonate & mud vs grain roundness in the Beekmantown Group	56
4-12	Relation of sediment transport dynamics to populations and truncation points in a grain size distribution (modified after Visher, 1969)	67
4-13a	Visher's Environments with respect to Visher (1969) transport modes	69
4-13b	Distribution of samples with respect to Visher (1969) transport modes	69

Figure	Title	Page
4-14a	Distribution of fine truncation point grain size with respect to Visher (1969) transport modes	70
4-14b	Distribution of coarse truncation point grain size with respect to Visher (1969) transport modes	70
4-15	Clast projection sphericity (modified after Sneed & Folk, 1958)	76
5-1	Metaquartzite cobble and boulder clast conglomerate	80
5-2	Ripple length frequency distribution	85
5-3a	Ripple index frequency distribution	86
5-3b	Ripple symmetry index frequency distribution	89
5-4	Interference ripples	89
5-5	Relationship between ripple length & wave bottom orbital diameter (modified after Komar (1974) after Clifton (1976)	91
5-6	Estimation of wave period frequency spectrum from ripples	93
5-7	Estimation of deep water wave height spectrum from ripples	95
5-8	Estimation of depth at which ripples formed from waves	96
5-9	Fully developed sea forecast for limited fetch conditions from Bretschneider equations (in Seymour, 1977)	98
5-10a	Maximum Boundary linear current vs ripple asymmetry	102

Figure	Title	Page
5-11	Frequency distribution of estimated mean current velocity from ripples	103
5-12	Frequency distribution of planar cross strata height	105
5-13	Cross strata with reactivation surfaces	106
5-14	Symmetric herringbone cross strata	106
5-15	Froude number vs non-dimensional bed shear stress	111
5-16	Paleoflow power vs mean sediment size, showing bedform fields after Allen (1968)	112
5-17	Estimated mean depth range from cross stratal heights	113
5-18	Frequency distribution of estimated mean current velocity from cross strata	114
5-19a	Estimated paleocurrent mean velocities from bedforms	116
5-19b	Estimated bedforms depth of formation	116
5-20	Paleocurrent trends in the Beekmantown Group within the Ottawa Basin	119
5-21	Wavy flaser bedding	123
5-22	Lenticular bedding with connected flat lenses	124
5-23	Diplocraterion burrows	124
5-24	Extremely bioturbated sediments	124
5-25	Smooth mat type stromatolite (SMF 20)	127
5-26	Smooth mat and bulbous stromatolites(SMF 20)	128
5-27	Bulbous stromatolites (SMF 20)	128

Figure	Title	Page
5-28	Smooth mat type stromatolite (SMF 20) associated with sulphide mineralization..	129
5-29	Coarse lithoclastic rudstone (SMF 24)	124
5-30	Black coated sparite pebbles (SMF 14)	134
5-31	Interpreted beach profiles (a to d)	136
6-1	Westport-Athens district : sample location map	140
6-2	Westport-Athens district : graphic mean size isolithic map	142
6-3	Westport-Athens district : inclusive graphic standard deviation isolithic map	143
6-4	Westport-Athens district : inclusive graphic skewness isolithic map	144
6-5	Westport-Athens district : mud isolithic map.	145
6-6	Westport-Athens district : HCl soluble isolithic map	146
6-7	Philipsville cliff section 61	149
6-8	Primary sedimentary features at location 61.	152
6-9	Paleoenvironmental & paleocurrent trends at location 61	153
6-10	Location 61 section : roundness and other petrological trends	154
6-11	Location 48 section	160
6-12	Westport-Athens district : interpreted paleoenvironments	163

LIST OF TABLES

TABLE	Title	Page
4-1	Lithological terms adopted for study	33
4-2	Grain size trends of siliciclastic strata in the Ottawa Basin	48
4-3	Grain size comparison for areas within the western part of the Ottawa Basin	52
4-4	Petrological estimation of paleoenvironments	60
4-5	Distribution of sample classes in Visher's (1969) paleoenvironments	
4-5a	Based on sample population ratios	71
4-5b	Based on combination of population ratios and CT/FT size limits	72
4-5c	Based on combination of population ratios, CT/FT size limits and BW point	73
4-6	Conglomerate clast sizes	75
5-1	Estimation of wave activity during storms	82
5-2	Ripple statistics from the Beekmantown siliciclastic strata	87
6-1	Location 61: comparison of estimated paleotidal range from tidalites, textural parameters and estimated depth of cross strata formation	157

NOTATIONS

a = angle of wave approach to the beach nearest the breaking zone

d_o = wave particle orbital diameter near bottom (cm)

g = acceleration of gravity ($g = 987$ cm/sec)

h = mean water depth (cm)

k = wave number ($k = \frac{2\pi}{L}$)

r = sediment particle radius (cm)

t = time required to reduce wave height from H_i to H by viscous damping (sec)

$t_{(min)}$ = minimum duration for development of fully developed seas under specified wind, fetch and depth conditions (hr)

u_* = bed shear velocity (cm/sec)

^1u_m = Stoke's second order wave asymmetry velocity (cm/sec)

^2u_m = Longuet-Higgins water-mass transport velocity (cm/sec)

u_t = bed threshold velocity required to initiate ripple formation (cm/sec)

u_{t*} = bed threshold velocity required to initiate sediment movement (cm/sec)

z_o = hydrodynamic bed roughness element

$A_0, A_1, \ldots, A_4$ = Stein's rule coefficients

C = wave celerity (cm/sec)

C_g = wave group celerity (cm/sec).

D = sediment particle diameter.

E = total wave energy (ergs)

F = fetch (distance wind formed waves travel under deep water conditions)

Fr = Froude number

H = wave height (cm)

K_D = Hudson's clast stability coefficient (for quarry stone $K_D = 3.2$)

L = wave length (cm)

P_r = specific weight of clast ($P_r = 165$ lb/ft^3)

P_w = specific weight of water ($P_w = 64$ lb/ft^3)

T = wave period (sec)

U = wind mean velocity (m/sec)

$\bar{U}$ = mean current velocity (cm/sec)

U_z = surface current velocity (cm/sec)

W = weight of clast (lb)

Greek notation

α = beach face slope

β = lee side horizontal length of ripple (cm)

β_1, β_2 = Galvin's breaker type coefficients where

$\beta_1 > 8$	spilling breaker	$\beta_2 > 0.8$
$8 > \beta_1 > 0.1$	plunging breaker	$0.8 > \beta_2 > 0.05$
$0.1 > \beta_1$	surging or collapsing breaker	$0.05 > \beta_2$

δ = bottom (laminar flow) boundary layer thickness (cm)

θ = Shield-Bagnold non dimensional bed shear stress

κ = von Karman's constant ($\kappa = 0.4$)

λ = ripple length (cm)

ν = kinematic viscosity ($\nu = 1.21 \times 10^{-2}$ poise)

π = 3.141...

ρ = specific gravity of water ($\rho = 1.03$)

ρ_s = specific gravity of sediment particle ($\rho_s = 2.65$)

τ_o = bed shear stress (dynes)

ω = free falling settling velocity of sediments (cm/sec)

Φ = bedform amplitude (cm)

Subscripts and Special Notations

b = wave breaking conditions

o = bottom boundary conditions

s = solitary wave conditions

∞ = deep water conditions ($h > \frac{L_\infty}{2}$)

ϕ = phi size units ($D_\phi = -\log_2 D_{(mm)}$)

N = nautical miles

i = initial value

$(\frac{H}{L})_{max}$ = maximum wave steepness

$(\frac{H_\infty}{L_\infty})_{crit}$ = critical deep water wave steepness for summer or winter beach profile conditions

$F_{r\S}$ = estimated Froude number

EQUATIONS

The equations listed are those used in chapter 5 of this study. Information concerning the conditions under which the equations are applicable and their estimated accuracy may be found in the listed sources. Unlisted sources for equations are equations derived in this study and additional information concerning them may be found in chapter 5. The equations listed have been rearranged or modified to the form used in the study.

Equation	Source		
5-1	Dott (1974)	$u_{t*} = 9\ D^{1/2}$	(ft/sec)
5-2	Dott (1974)	$u_{t*} = 10D^{1/2.6}$	(ft/sec)
5-3	Dott (1974)	$C_{bs} \simeq 2\ u_{t*}$	(ft/sec)
5-4	Dott (1974)	$H_{bs} = \frac{C_{bs}^{\ 2}}{8}$	(ft)
5-5	Hudson (1958)	$H_b = \left[\frac{W \cdot K_D \{\frac{Pr}{P_w} - 1\}^3 \cot \alpha}{Pr}\right]^{1/3}$	(ft)
5-6	Silvester (1974; p.241)	$\frac{Hb}{H\infty} = 0.76\{a \cos\alpha\}^{1/7} \left(\frac{H\infty}{L\infty}\right)^{-1/4}$	
5-7	Komar (1974)	$d_o = 1.25\ \lambda$	(cm)
5-8	*	$d_o = \{16.43 - 2.92D_\phi - 1.57\ \ln\lambda\}$	(cm)
5-9	Clifton (1976; p. 133)	$\lambda = 60\ D^{1/2}$	(cm)
5-10	**	$\lambda = \{\frac{D\phi - 4.63}{0.82}\}$	(cm)

Equation	Source		
5-11a	Komar (1974)	$u_t = \frac{0.21(\rho_s - \rho)g \cdot D}{\rho} \{\frac{do}{D}\}^{1/2}$	(cm/sec)
5-11b	Komar (1974)	$u_t = \frac{0.46\pi(\rho_s - \rho)g \cdot D}{\rho} \{\frac{do}{D}\}^{1/4}$	$D \leq 0.5$ mm (cm/sec)
5-12	Komar (1976; p. 379)	$T \leq \frac{\pi \cdot do}{u_t}$	$D \geq 0.5$ mm (sec)
5-13	Komar (1976; p. 42)	$C\infty = \frac{g \cdot T}{2\pi}$	(cm/sec)
5-14	Komar (1976; p. 42)	$L\infty = T \cdot C\infty$	(cm)
5-15	Komar (1976; p. 61)	$(\frac{H}{L})_{max} = \frac{1}{16} \tanh kh$	
5-16	Komar (1976; p. 52)	$(\frac{H}{L})_{max} = \frac{1}{7} \tanh kh$	
5-17a	Dean (1973)	$(\frac{H\infty}{L\infty})_{crit} = \frac{1.7\pi \cdot \omega}{g \cdot T}$	
5-17b	Gibbs et al (1971)	$\omega = \frac{-3\nu + \sqrt{9\nu^2 + g \cdot r^2 \rho(\rho_s - \rho)(0.01576 + 0.19841r)}}{\rho(0.011607 + 0.14881r)}$	(cm/sec)
5-18	Komar (1976; p. 56)	$(\frac{H}{h})_{max} = 0.78$	
5-19	Komar (1976; p. 56)	$L = L\infty \tanh kh$	(cm)
5-20	Eagleson & Dean (1966; p. 65)	$\frac{L}{L\infty} = \frac{C}{C\infty} = \frac{k\infty}{k} \tanh kh$	(cm)
5-21	Eagleson & Dean (1966; p. 65)	$\frac{H}{L} = \frac{H\infty}{L\infty} = \{\frac{2 \cosh kh}{2kh + \sinh 2kh}\}^{1/2} \cdot \text{cotanh } kh$	

Equation	Source		
5-22	Inman (1957)	$do = \frac{H}{\sinh kh}$	(cm)
5-23	Eagleson & Dean (1966; p. 110)	$u_{t*} = \frac{\pi \cdot H}{T \cdot \sinh kh}$	(cm/sec)
5-24	Komar & Gaughan (1973)	$\frac{Hb}{H\infty} = \frac{0.563}{\{\frac{H\infty}{L\infty}\}^{1/5}}$	
5-25	Komar (1976; p. 45)	$E = \frac{1}{8} \rho \cdot g \cdot H^2$	(ergs)
5-26	King (1972)	$\alpha = 401.71 + 4.2D_{\phi} - 0.711\log E$	
5-27	Galvin (1968)	$\beta_1 = \frac{H\infty}{L\infty \cdot \alpha^2}$	
5-28	Galvin (1968)	$\beta_2 = \frac{H\infty}{g \cdot \alpha \cdot T^2}$	
5-29	**Miller et al. (1977; p.513)	$u_{t*} = 3.93D^{0.281}$ for $D \leq 0.6$ cm	(cm/sec)
5-30	**Miller et al. (1977; p.513)	$\hat{u}_{t*} = 8.23D^{0.545}$ for $D > 0.6$ cm	
5-31	Seymour (1977)	$H_{1/3} = \frac{0.283U^2}{g} \tanh(0.578\{\frac{g \cdot h}{U^2}\}^{0.75}) \cdot \tanh\left[\frac{0.0125\{\frac{g \cdot h}{U^2}\}^{0.42}}{\tanh(0.578\{\frac{g \cdot h}{U^2}\}^{0.75})}\right]$	(m)
5-32	Seymour (1977)	$T_{1/3} = \frac{7.54U}{g} \tanh(0.520\{\frac{g \cdot h}{U^2}\}^{0.375}) \cdot \tanh\left[\frac{0.077\{\frac{g \cdot h}{U^2}\}^{0.25}}{\tanh(0.520\{\frac{g \cdot h}{U^2}\}^{0.375})}\right]$	(sec)
5-33	Bretschneider (1966; p.141)	$t_{(min)} = \frac{FN}{1.14T_{1/3}}$	(hr)

Equation	Source		
5-34	Komar(1976; p.100)	$t = \frac{-g^2 \cdot T^4}{32\pi^4 \cdot \nu} \ln\{\frac{H}{H_i}\}$	(sec)
5-35	Komar(1976; p.95)	$C_g = \frac{1}{2} C\infty$	(cm/sec)
5-36	Clifton(1976; p.128)	$^1u_m = \frac{14.8H^2}{L \cdot T \cdot \sinh^4 kh}$	(cm/sec)
5-37	Clifton(1976; p.128)	$^2u_m = \frac{5}{4} \cdot \frac{^1u_m \cdot T}{L}$	(cm/sec)
5-38		$\Delta u = -21.28\ln(\beta/\lambda) - 13.77$	(cm/sec)
5-39	Silvester(1974; p.198)	$\delta = 2\,(T \cdot \pi \cdot \nu)^{1/2}$	(cm)
5-40	Harvey & Vincent (1977; p.724)	$z_o = \frac{\Phi}{30}$	(cm)
5-41	Harvey & Vincent (1977; p.722)	$u_* = \sqrt{\frac{\tau_0}{\rho}}$	(cm/sec)
5-42	Harvey & Vincent (1977; p. 722)	$U_z = \frac{u_*}{\kappa}\{\ln(h \pm z_o) - \ln(z_o)\}$	(cm/sec)
5-43	Massey (1970; p.317)	$\bar{U} = 0.85\, U_z$	(cm/sec)
5-44	Allen (1978; p.178)	$\theta = \frac{\tau_0}{(\rho_s - \rho)g \cdot D}$	
5-45	Allen (1978; p.178)	$\frac{\Phi}{h} = A_0 + A_1(\frac{\theta}{3})^1 + A_2(\frac{\theta}{3})^2 + A_3(\frac{\theta}{3})^3 + A_4(\frac{\theta}{3})^4$	

Equation	Source

where $A_0 = 0.079865$

$A_1 = 2.23897$

$A_2 = -18.1261$

$A_3 = 70.9001$

$A_4 = -88.3293$

5-46 Reineck & Singh (1975; p. 12) $Fr = \frac{\bar{U}}{\sqrt{g \cdot h}}$

5-47 ** $Fr_{\S} = 0.229 + 0.343 \ln \Phi$

---

* Equation derived by using multiple linear regression.

** Equations derived by using regressional curve fitting (HP programable card SD-03A).

For additional information concerning the source materials for these equations refer to text. In all cases unless otherwise stated both correlation coefficients and statistical significance limits for these equations were set at 0.95.

CHAPTER 1

INTRODUCTION.

Problems and Objectives

The Beekmantown Group in eastern Ontario consists of the lowest Paleozoic sedimentary succession in the area. It nonconformably overlies the Precambrian basement and underlies the Chazy Group of Middle Ordovician age. The group is gradational from sandstone below to carbonate beds above.

The objective of this study is to develop a model for the paleoenvironments of deposition in the Beekmantown Group. Constraints on the model were established on the basis of modern wave hydrodynamic theory.

To construct a depositional model for the group required integration and quantitative correlation of data from widely separated exposures. Major difficulties encountered in the study resulted from the limited exposures, scarcity of deep well data in the central basin and the complex, often conflicting stratigraphic nomenclature currently in existence. Recent biostratigraphical data based on conodont and gastropod studies of the Beekmantown Group were used for correlation where possible. A review of the stratigraphic nomenclature associated with the Beekmantown Group within the Ottawa Basin is necessary to assess the origin and validity of the many terms. The lithostratigraphy adopted in the study is considered to be not only realistic in terms of regional relationships of the units but also valid under the regulations of the Code of

Stratigraphic Nomenclature (Krumbein and Sloss, 1963; 621-636).

The study was divided into a general petrological investigation of the group in the basin, with respect to sediment composition, size, shape and general textural trends. A detailed investigation of the Westport-Athens district, where good biostratigraphical correlation and numerous accessible exposures of the group are available was also undertaken, to determine detailed lithofacies relationships.

Study Area

The study area includes most of the outcrops of the Beekmantown Group found within or adjacent to the Canadian portion of the Ottawa Basin.

This basin is a well defined rectangular embayment on the eastern margin of the Canadian Shield craton (figure 1-1). The basin lies within the Ottawa-St Lawrence Lowland and covers approximately 20,500 km^2, of which the Beekmantown Group outcrops constitute 12,900 km^2 (Wilson, 1946).

The Ottawa Basin is bordered on the north by the Laurentian Highlands, on the west by the Frontenac Axis and on the south by the Adirondack Massif. The eastern boundary is placed at the Beauharnois Anticline (Logan, 1843; p 90) which exposes inliers of Grenvillian rocks and lower Beekmantown Group siliciclastic strata between the Laurentian Highlands and Adirondack Massif (figure 1-1).

The Ottawa-St Lawrence Valley is covered by

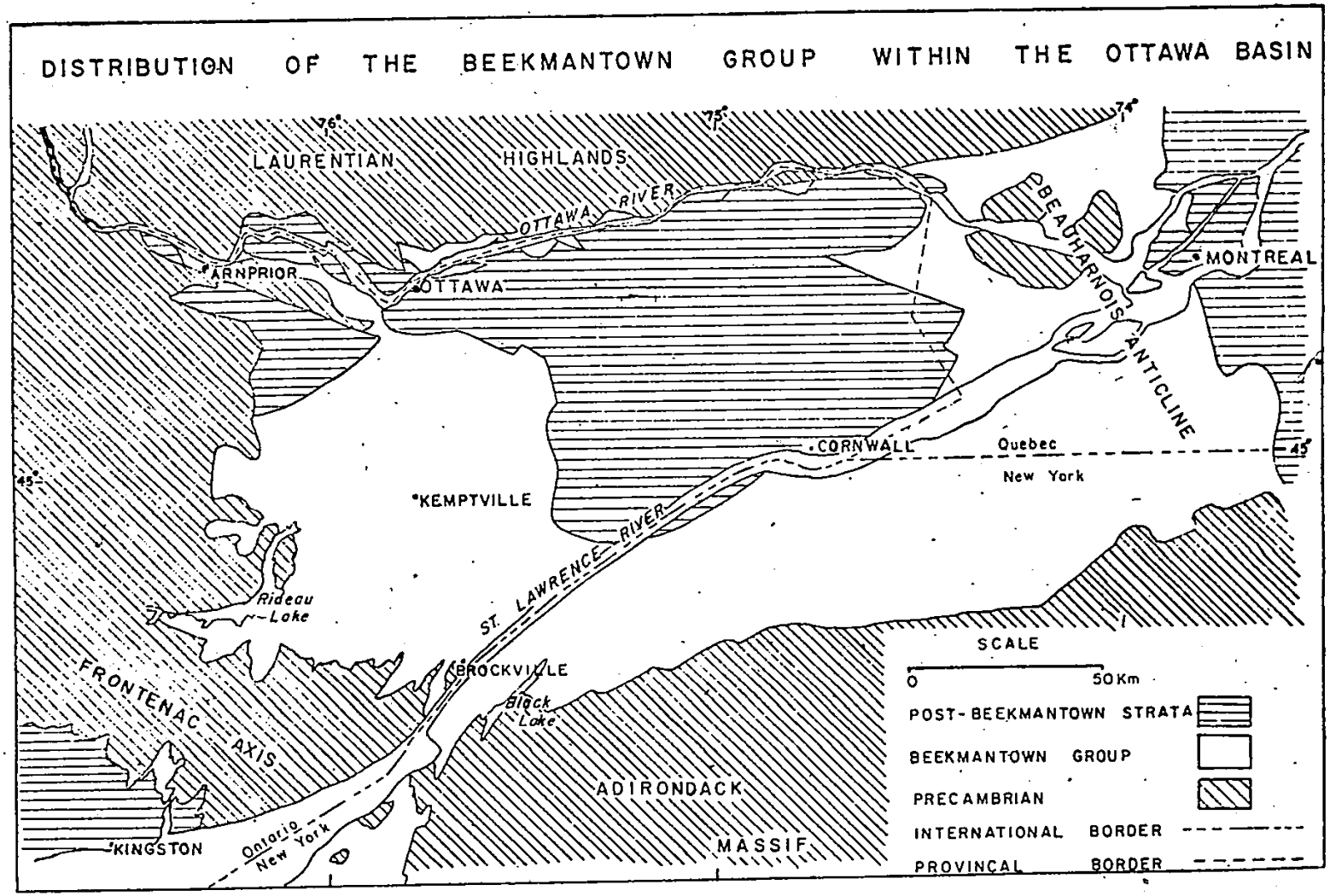

Figure 1-1 : Beekmantown Group location map for the Ottawa Basin

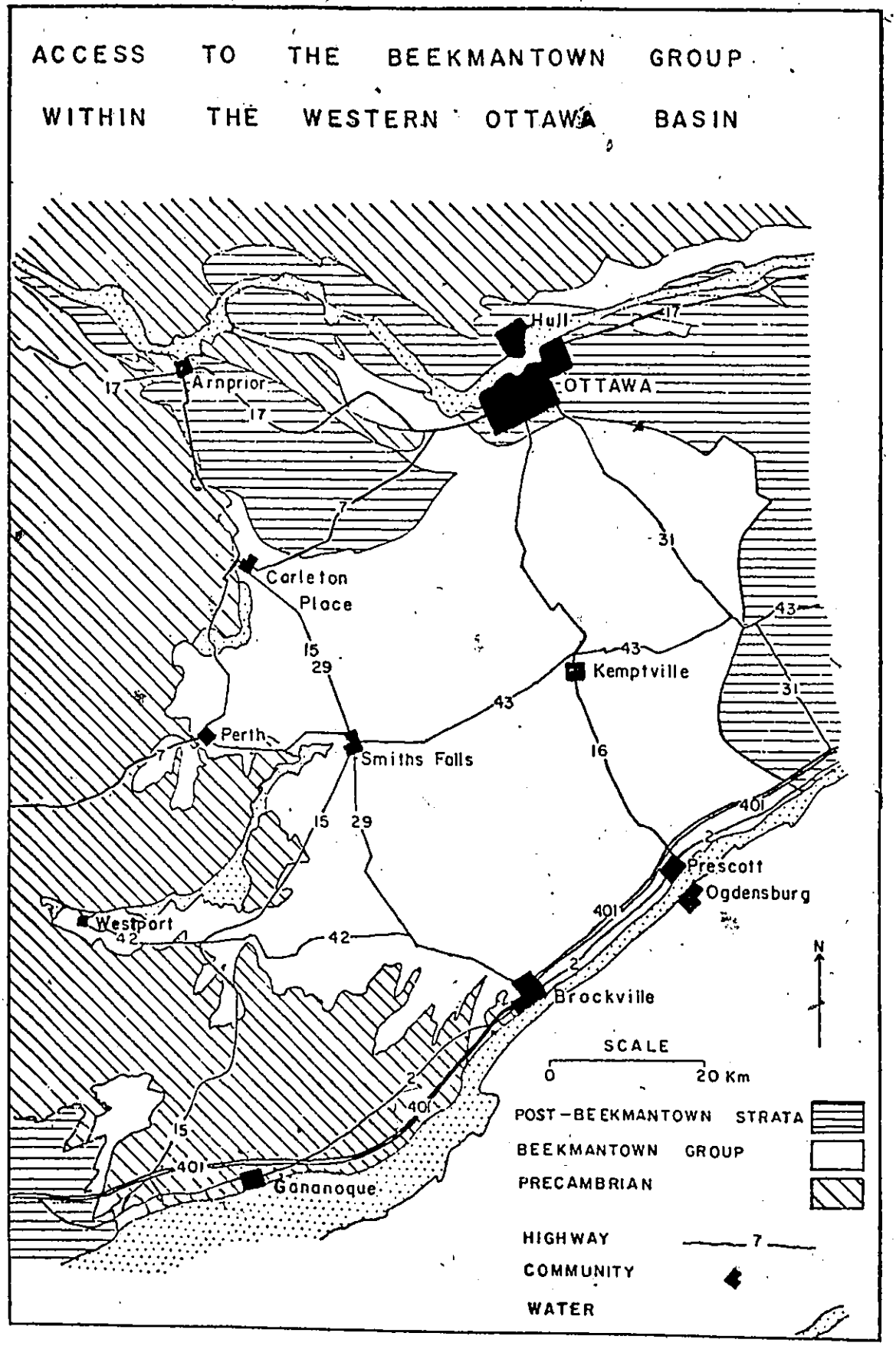

Figure 1-2: Access routes within the main study area.

extensive thin Quaternary glacial-marine deposits. The overburden varies from a thin veneer in the west (Chapman & Putman, 1973; p. 338-339) to thicknesses in excess of 60m in the east (ibid, p 360). Fluvial and marine reworking of glacial deposits has produced substantial deposits of silty sand and gravel along the Ottawa Valley and in eastern counties of Ontario.

In the western part of the Ottawa-St Lawrence Valley the topography reflects both the generally flat-lying nature of the bedrock and the thin marine deposits of the Champlain Sea, that extensively obscure the bedrock in places distal to the Frontenac Axis (ibid, p. 175, 336, 338).

Access to the study area is provided by an extensive network of primary and secondary roads (figure 1-2). East-west roads such as highways #401, #2, #42, #43, #7 and #17 cut the gently dipping strata and provide composite stratigraphic sections. North-south highways such as #15, #16, #29 and #31 generally follow the regional strike and provide laterally equivalent exposures of the strata.

Previous Work

The Beekmantown Group has been studied since early in the 19th century, resulting in a variety of stratigraphical interpretation and theories concerning its origin. Comprehensive summaries of previous work were given by Chadwick (1920), Lewis (1965) and Clark (1966) and this is further summarized here.

The earliest report on the Beekmantown Group was that of Amos Eaton (1824), who named the siliciclastic and carbonate rocks surrounding and overlapping the Adirondack Massif the Calciferous Sandrock. Emmons (1838, p. 214-215) separated the basal sandstone from the Calciferous Sandrock and renamed it the Potsdam Sandstone . These units were soon mapped into Ontario (Murray, 1849) and Quebec (Marcou, 1862; p. 241-242, 244, 249).

Chapman (1864, p. 186-190) divided the Potsdam Group in southwestern Quebec into the Kaministiquia Formation (consisting of sandstone and sandy carbonate strata) and the Beauharnois Formation (carbonate strata). Attempts to further divide the Calciferous Sandrock occurred when Brainerd and Seeley (1890;a,b) divided the Champlain Valley section into Divisions A to E. Clark and Schuchert (1899) recognized a major unconformity between Divisions B and C (Brainerd and Seeley, 1890; a,b) coinciding with the Cambro-Ordovician boundary. Divisions C to E were named the Beekmantown Dolomite. Cushing (1901) separated the alternating sandstone and dolomite beds from the Beekmantown Group in the western Adirondacks, naming them the Theresa Formation (Cushing; 1905, 1908) and correlating them with Division A of Brainerd and Seeley's (1890) section (Cushing, 1911). The Cambro-Ordovician boundary was considered by Ulrich and Cushing (1910) to lie between the middle of Division A and the base of Division C of Brainerd and Seeley (1890) section.

Raymond (1913, p. 137-162) applied the names Potsdam,

Theresa and Beauharnois Formations in Ontario and Quebec. The Theresa Formation was considered in part to be reworked Potsdam, and to be separated from the Potsdam Formation by an unconformity at the Cambro-Ordovician boundary. The Theresa and Beauharnois Formations, based on the occurrence of Ophileta complanata and Pleurotomaria canadensis were considered to be Ordovician and were correlated with the Beekmantown Dolomite in the Champlain Valley. The Beauharnois was considered by Raymond to be disconformably overlain by the Aylmer Formation of the Chazy Group, considered Middle Ordovician in age.

Chadwick (1915, p. 289) divided the transition beds in the northern Adirondacks into the Theresa Formation, a middle siliceous sandstone named the Heuvelton Sandstone and an upper mixed bed named the Bucks Bridge Formation, that was considered to be unconformably overlain by the Ogdensburg Formation dolomite beds. The Theresa Formation and Heuvelton Sandstone were considered to be separated by an unconformity that corresponded to the Cambro-Ordovician boundary. The Buck Bridge Formation was considered to disconformably overlie the Heuvelton Sandstone and on the occurrence of Palaeophycus beverleyensis was correlated with the lower Beekmantown strata. The Ogdensburg Formation was correlated with the upper Beekmantown strata. Chadwick (1920) renamed his upper Potsdam (Chadwick, 1915) as the Keeseville Sandstone suggesting that the Keeseville was separated from the typical Potsdam by an unconformity.

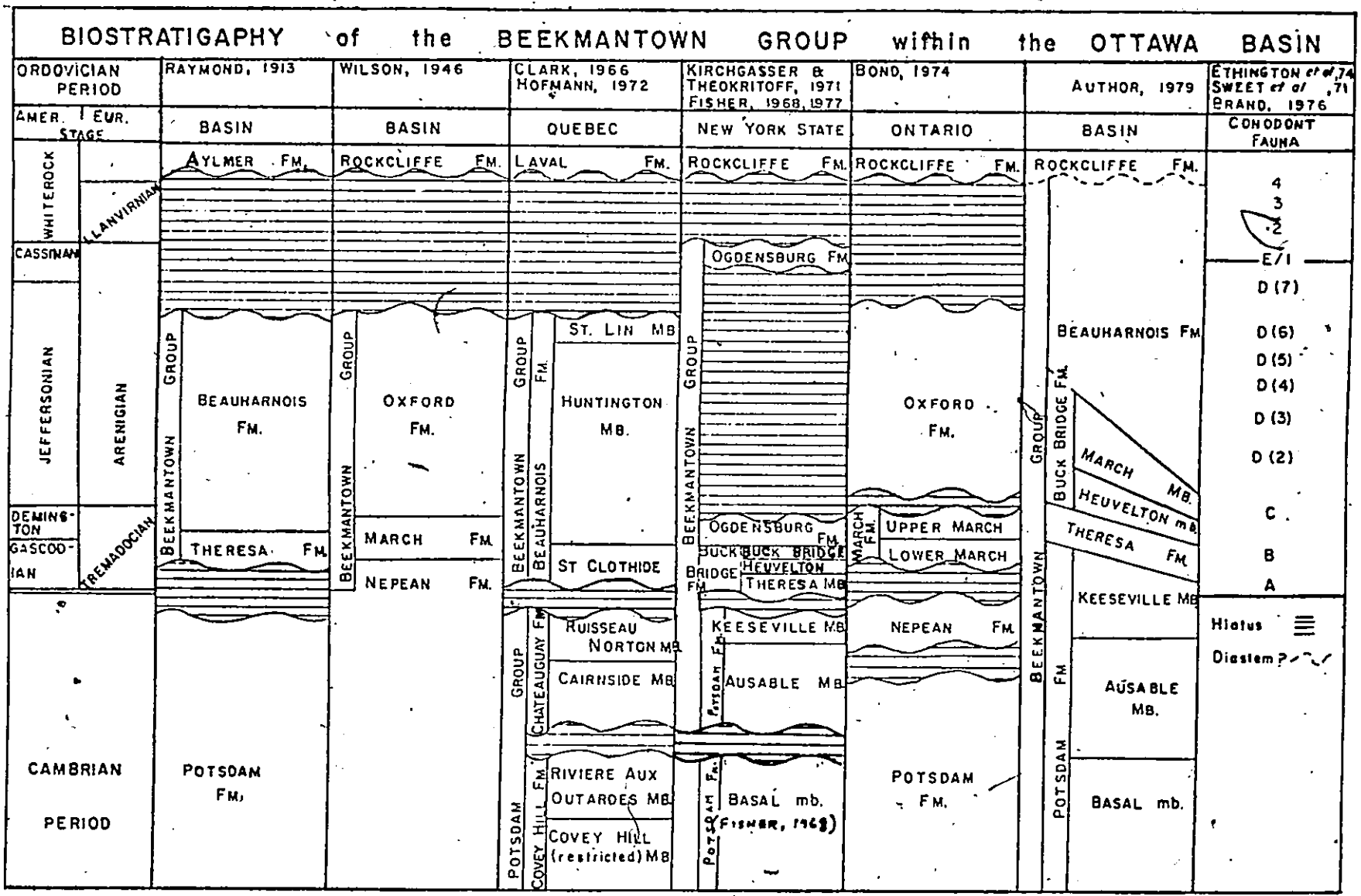

Figure 1-3: Changes in the biostratigraphical positions of the Beekmantown Group formations since 1900. Refer to text for detail discussion of figure.

Wilson(1946, p. 10) combined the sandstone formerly designated in the region as the Potsdam with the lower beds of Raymond's Theresa Formation and named them the Nepean Formation (figure 1-3). The upper strata of Raymond's (1915) Theresa were renamed the March Formation and the Beauharnois, renamed the Oxford Formation. The renaming of the strata was justified by Wilson primarily on biostratigraphical grounds. The Nepean was introduced to obviate the consideration of a variously placed contact between a possible Cambrian and an Ordovician formation (Wilson, 1946; p. 10). The March was introduced to replace the name Theresa on the grounds that the Theresa Formation in New York had been redefined and restricted to an Upper Cambrian age while the March strata were considered to be Ordovician in age (Wilson, 1946; p. 17). The March and Oxford Formations, containing Ophileta and Eccliomphalus faunas, were correlated with the lower Beekmantown strata. The Rockcliffe Formation of the Chazy Group was considered to disconformably overlie the Oxford Formation. The formation was correlated with the position of Camarotoechia plena in the upper Chazyian strata of the Champlain Valley (Cooper, 1956; chart 1).

Clark (1966) divided the Potsdam Group in southwestern Quebec into the basal Covey Hill Formation and the Chateauguay Formation (figure 1-3) placing an unconformity between them. The Beauharnois Formation, consisting of the St Clothide, Huntington and Sainte Lin Members, was assumed to unconformably overlie the Cambrian age Potsdam Group and was considered to be

Lower Ordovician in age.

Fisher (1954) advocated abandoning the name Beekmantown unless it was restricted to Middle Canadian age strata, the only known rocks of Canadian age outcropping in the vicinity of Beekmantown County, New York. The Potsdam and Theresa Formation were considered by Fisher (1955) to be both conformable and diachronous around the Adirondack Massif. Based on trilobite faunas the upper Potsdam and Theresa Formations were considered to be Middle Cambrian (Dresbachian Stage) in age near Saratoga Spring, but Early Ordovician (Gascondian Stage) in age in the vicinity of Alexandria Bay, New York. Fisher (1956) also found evidence for interfingering of the Keeseville and typical Potsdam; he rejected the idea of an unconformity separating them and consequently doubted the validity of using the term Keeseville Formation. The Potsdam Formation in the Plattsburgh district, New York, was divided into three members (Fisher, 1968), the Basal member, Ausable and Keeseville Members (figure 1-3).

Kirchgasser and Theokritoff (1971) redefined the transition beds in the northern Adirondacks. The transition beds were renamed the Bucks Bridge Formation, containing the Theresa, Heuvelton and Bucks Bridge Members. The Theresa Member was considered to be a tongue of the Theresa Formation from the western Adirondacks and the member was restricted to the extreme southwestern part of the Ottawa Basin. Kirchgasser and Theokritoff (1971) did not determine whether the Heuvelton Member conformably overlying the Theresa Member was a continuous

bed or lensoid. The Bucks Bridge Member conformably overlies the Heuvelton Member and was conformably overlain by the Ogdensburg Dolomite (figure 1-3).

Greggs and Bond (1971,1972; Bond, 1974; Bond and Greggs, 1975,1976) attempted to revise Wilson's stratigraphy in Ontario to take into account assumed unconformities in the sequence (figure 1-3). The Nepean Formation was correlated with the Upper Potsdam Formation of Kirchgasser and Theokritoff (1971) (Chadwick's (1920) Keeseville Formation) and was considered to be separated from the typical Potsdam Formation by an unconformity. The March Formation was considered to unconformably overlie the Nepean Formation. Based on conodont assemblages, the March was considered to be Tremadocian in age (Greggs and Bond, 1971, 1972, 1977; Bond, 1974).The Oxford Formation, with an Arenigian conodont assemblage was considered to disconformably overlie the March Formation (Bond, 1974; Bond and Greggs, 1976; figure 1-3).

Yochelson and Copeland (1974) found gastropods within the Oxford Formation in Ontario and considered them to be Late Canadian in age (Cassinian Stage). Fisher (1977) suggested the existence of a significant intraformational disconformity within the Ogdensburg Formation based on the apparent absence of a Jeffersonian Stage fauna.

Brand and Rust (1977 a,b) found the Nepean / March formational boundary to be conformable near Ottawa, where both the Nepean and March contain conodonts of Fauna D (lower Arenig; Barnes et al., 1976; p. 222). Recent studies of the March and

Oxford Formational boundary (March Member of Bucks Bridge Formation and Beauharnois Formation) show it to be diachronous, changing from Fauna C (Tremadocian) near Brockville, to Fauna D (Arenigian) near Ottawa (Brand, 1976; personal communications). Samples collected between Westport and Athens (locations 33, 43, 48 and 56) show no distinguishable age difference (Fauna D2/D3; Brand, 1977; personal communications) between the March and Oxford Formations.

Preliminary conodont studies of the Oxford-Rockcliffe formational boundary in the Arnprior, Cumberland and Montreal vicinities have shown that conodonts of Fauna 4 transgress the boundary (Whiterockian Stage, Barnes et al, 1976, p. 222; Brand, 1978; personal communications). The consistency of this trangression at all locations suggests that the boundary is marked by either a minor diastem or is predominantly conformable within the Ottawa Basin. Preliminary conodont studies of the Beauharnois and Chateauguay Formations in southwestern Quebec by Sandi (1978; personal communications), showed the Beauharnois Formation (Clark, 1966) to have a similar age range as the Oxford in Ontario (Fauna D to 4). The Buisseau Norton Member of the Chateauguay Formation showed a similar age as the March Formation at Brockville (Fauna C).

CHAPTER 2

STRUCTURE OF BASIN

General Description

The deposition of the Beekmantown Group was influenced by the structural configuration of the Ottawa Basin. Hence, the structural development of the basin must be appreciated for an understanding of the evolution of lithofacies.

The Ottawa Basin is a rectangular structural depression infilled by Paleozoic and Hadrynian strata (Hofmann, 1972: p. 4). The generally horizontal strata within the basin are disrupted by a well developed system of east-west trending normal faults that are associated with the northeast trending St Lawrence Valley fault system (figure 2-1).

The St Lawrence Valley has long been regarded as the site of a graben system termed the St Lawrence Graben (Laflamme, 1908; Gregory, 1929; Keith, 1930; Hodgson and Doxes, 1930). An associated, generally east-west fault system called the Ottawa-Bonnechere Graben (Kay, 1942) occupies the northern edge of the Ottawa Valley and joins the St. Lawrence Graben near Montreal. Kumarapeli & Saull (1966) and Hodder & Hollister (1974) presented additional geological, physiographical and geophysical evidence to substantiate the existence of major grabens in the area.

Although the time at which the graben systems were initiated is uncertain, radiometric dating of pseudotachylites from faults near St Alexis des Monts, Quebec (Philpotts and Miller,

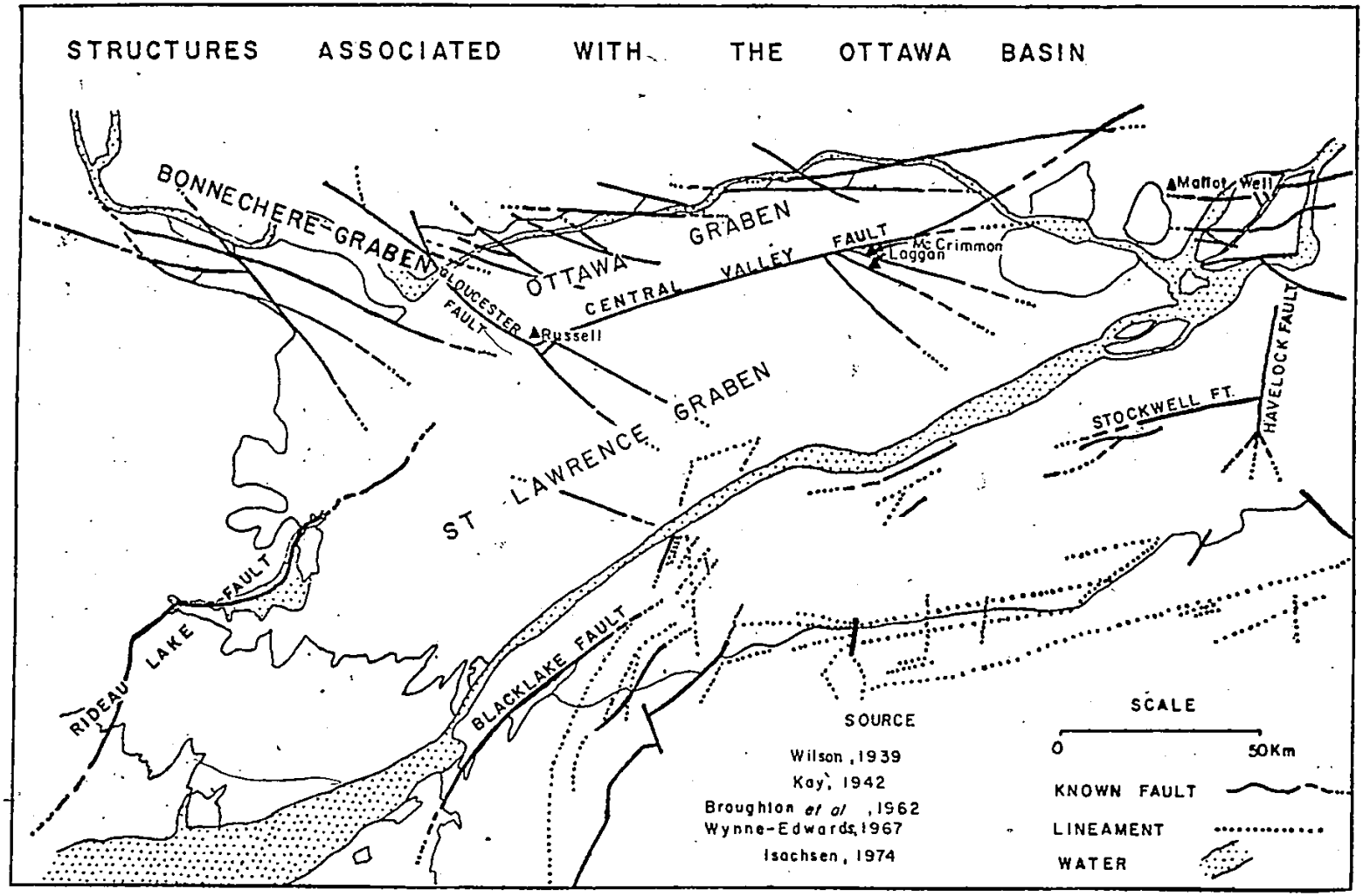

Figure 2-1: Primary structures associated with the Ottawa Basin. For detail discussion of figure refer to text.

1963) suggests a possible late Neohelikian age (975 ± 45 million years). Dates from carbonatites and igneous intrusions along the western part of the Ottawa-Bonnechere Graben system suggest continued instability occurred along the system from Middle Cambrian to Early Cretaceous time (Gittins et al, 1967; Hodder and Hollister, 1974; p. 454).

St Lawrence Graben

The St Lawrence Graben section of the Ottawa Basin is larger and less well defined than the Ottawa-Bonnechere Graben. The former is recognizable only through discontinuously exposed faults and lineaments shown on air or satellite photos.

The northern boundary of the graben is marked by a fault extending from the Beauharnois Anticline west to the Gloucester Fault. Intermittently exposed faults connect this fault to the Rideau Lake Fault that extends across the Frontenac Axis (figure 2-1). This fault system is traceable for at least 280 km. Wynne-Edwards (1967) postulated that movement along the Rideau Lake Fault initiated as a strike slip of unknown extent. The occurrence of Potsdam Formation overlying and in other places cut by the fault suggests several reactivations. Brecciated Oxford Formation at Narrow Lock was attributed to Lower Ordovician movement of the fault (Wynne-Edwards, 1967; p, 87).

The southern boundary of the graben is marked by a series of north dipping normal faults and linear features along

the Adirondack Massif (Isachsen, 1974). The northern series of faults extends from the Black Lake Fault (Kirchgasser and Theokritoff, 1971) in the west to the Stockwell Fault (Clark, 1966) in the east, by a series of linear features. Numerous parallel faults to the south possibly represent antithetic and synthetic faults associated with the graben (Hills, 1972; p.190). Based on the distance separating the Rideau Lake-Central Valley Faults and the Black Lake-Stockwell Faults the graben's minimum width ranged between 45 and 78 km, with a mean distance of 60 km.

The amount of subsidence in the St Lawrence Graben is uncertain due to the scarcity of deep well data within the central portion of the basin. Well data and field measurements suggest that the Potsdam Sandstone along and east of the Beauharnois Anticline ranges between 517 m and 760 m thickness (Clark, 1966; Lewis, 1971; p. 857) while the Beauharnois Formation is reported to range between 305 m and 432 m (Belyea, 1952; Clark, 1952). In Ontario well data from Laggan and Mc Crimmon Corners (figure 2-1) show the minimum post-Potsdam thickness of the Beekmantown Group to be between 270 m and 400 m. At Williamsburg the minimum post-Potsdam thickness of the Beauharnois Formation is 220 m (Bond and Greggs, 1976; p. 22). Uplift along the Frontenac Axis has resulted in the erosion of the Beekmantown Group east of Iroquois, making the estimation of the degree of subsidence during deposition of the group there impossible. In the vicinity of Rideau Lake occurrence of the lower members of the Potsdam Formation (Dugas, 1952; Wynne-Edwards, 1967) suggests that the complete Beekmantown Group extended at

least as far west as the Frontenac Axis.

Ottawa-Bonnechere Graben

The Ottawa Graben is bordered on the north by the Grenville and associated faults that separate it from the Laurentian Highlands and on the south by the Central Valley Fault that parallels the edge of the Laurentian Highlands. The Graben varies from 15 to 35 km in width and is traceable from Lachute, Quebec to Russell, Ontario where it terminates at the Gloucester Fault. West of the Gloucester Fault the Bonnechere Graben trends northwestward, leaving the Ottawa Basin near Renfrew and continues as a system of fault blocks (figure 2-1).

Well data indicate that the floor of the Ottawa Graben dips southward, reaching depths in excess of 900 m in the Russell area by Upper Ordovician time (Beard, 1969; p. 46). Kay (1942; p. 610) estimated the relief between the top of the Laurentian Highlands and the floor of the Bonnechere Graben to be of the order of 300 m.

Frontenac Axis

The date of initial uplifting of the Frontenac Axis has been for sometime a matter of conjecture. Occurrence of the Potsdam Formation on both sides of the axis and of isolated outliers across it has been considered by some workers to be evidence for the absence of a land barrier prior to the Lower

Ordovician (Bond, 1974; p. 4). Others have noted the distribution of outliers in bands along depressions across the axis (Wright, 1923) or of paleocurrent deflections in areas adjacent to the axis (Lewis, 1963), which suggest some form of barrier contemporaneous with deposition. Conodont studies (Brand, 1977; personal communications) suggest that the tonguing of the Theresa Formation into the basin over the southern edge of the Frontenac Axis occurred during the Gascodian Stage. Outliers in the Westport-Athens district (chapter 6) show isolithic continuity with the Jeffersonian Stage basin strata, suggesting that uplift along the Frontenac Axis was initiated in the south and continued throughout most of the Lower Ordovician.

Beauharnois Anticline

The Beauharnois Anticline (Logan, 1863) extends from the Laurentian Highlands to the Adirondack Massif as a broad structural ridge at the eastern limits of the Ottawa Basin. Only in the upper strata of the Potsdam Formation do shallow water sedimentary features such as desiccation cracks, paleocurrent deflection patterns and small scale ripples and cross stratification occur (Logan, 1863; Lewis, 1963; Clark, 1966) that may indicate early uplift of the anticline. Within the Keeseville Member (Cairnside Member) Clark (1966; p. 24) found local evidence of sub-aerial exposures, represented by an interformational disconformity.

During most of the Beekmantown Group deposition the

Beauharnois Anticline appears to have been a low intermittently exposed shoal separating the Ottawa Basin sea from the Apetus Sea (Keppie, 1977; figure 1, p. 31) to the east.

Folding

Intervals of instability along the Frontenac Axis and southern Beauharnois Anticline during the Lower Ordovician are evident from gently folded strata or local diastems within the Beekmantown strata.

Along the Frontenac Axis in the vicinity of Rideau Ferry (location DW-9) an intraformational angular unconformity occurs within the Keeseville Member. South of Kemptville, at the junction of Oxford Road and Highway #16 small open folds of Beauharnois strata are draped by adjacent beds. Conodont studies (Brand, 1977; unpublished data) show the section at this location to be conformable and of Arenigian age.

CHAPTER 3

STRATIGRAPHIC NOMENCLATURE OF THE BEEKMANTOWN GROUP

Beekmantown Group

The term Beekmantown Group as used in New York State prior to 1977 (Fisher, 1962a,b; Fisher and Hanson, 1951; Flagler, 1966; Richard, 1973), was restricted to the strata of Lower Ordovician age beneath the supposed disconformity at the base of the Chazy Group. As such the Beekmantown Group was a lithostratigraphic unit with a biostratigraphic lower boundary (Cambro-Ordovician boundary), contrary to article 4d of the Code of Stratigraphic Nomenclature (Krumbein and Sloss, 1963; p. 625). Fisher (1977) extended the lower boundary of the Beekmantown Group to include the Keeseville Member of the Potsdam Formation. Without conclusive evidence of a major disconformity at or near the assumed Cambro-Ordovician boundary or within the Potsdam Formation within the Ottawa Basin, the entire transitional sequence from sandstone resting nonconformably on the Precambrian basement to carbonate underlying the Chazy Group, has been termed the Beekmantown Group for the purpose of this report.

The sporadic distribution of exposures in different political regions has resulted in the establishment of three main schemes for stratigraphic subdivision of the Beekmantown Group (figure 1-3) within or flanking the Ottawa Basin. The most appropriate terminology appears to be a combination of these schemes. The sequence adapted in this report consists of four formations, the Potsdam, Theresa, Bucks Bridge and Beauharnois Formations.

Potsdam Formation

Wilson (1946) introduced the term Nepean Formation to replace the Potsdam and lower Theresa Formations of Raymond (1913), justifying the change on the grounds that it "... obviates the consideration of a variously placed, doubtful contact between a possible Cambrian and an Ordovician formation" (Wilson, 1946; p. 10). This however does not justify the replacement of a formational name that at the time of introduction was based on lithostratigraphical grounds (Murray, 1849). As a result the term Potsdam Formation as employed by Fisher (1968) is here used.

The Potsdam Formation within the Ottawa Basin non-conformably overlies the Precambrian basement and is conformably overlain by the Theresa, or in its absence, the Buck Bridge Formation. The Potsdam, consisting primarily of arkose, quartz arenites and quartzwacke (Pettijohn et al, 1973; p. 162-172) strata occasionally interlayered with oligomictic conglomerates, represents the lowest formation of the Beekmantown Group. The Potsdam is divided into the Basal member, Ausable and Keeseville Members.

Basal member

The informal Basal member (Fisher, 1968) nonconformably overlies the Precambrian basement and conformably underlies the Ausable Member. The upper boundary is taken to be below the highest continuous occurrence of hematitic arkose or lithic sub-

arkose.

The Basal member consists of red (5R8/2 to 5R3/4) hematite-rich arkose, lithic subarkose and lithic subarkosic wacke, with isolated orthoquartzitic or feldspathic paraconglomerate (Lewis, 1965; appendix 1). Exposures of the Basal member within the Ontario portion of the Ottawa Basin are scarce and occur primarily along the Frontenac Axis. Dugas (1952) described a 24 m section of feldspathic polymictic conglomerate cemented by carbonate along the eastern shore of Rideau Lake. The clasts consist of metaquartzite, granite, diabase, pegmatite and marble fragments with orthoclase, microcline and quartz crystals. Dugas (1952) considered the unit to be post-Grenvillian and pre-Nepean in age. A few kilometers south red hematitic arkose and feldspathic polymictic conglomerate occur sporadically, that more typically resemble the Basal member of Fisher (location 63; Wynne-Edwards, 1967; p. 120).

The Basal member is commonly exposed in southwestern Quebec, along the southern edge of the Beauharnois Anticline (Lewis, 1965; Clark, 1966; Hofmann, 1972) and the northern edge of the Adirondack Massif (Chadwick, 1920; Wiesnet, 1961). Similarly in the few deep wells that reach or almost reach basement (Mallet wells, in Lewis, 1965; Russell County well in appendix 1) the presence of the Basal member appears to indicate that the member at one time was extensive in the basin. Several studies of the Basal member (Lewis, 1971; p. 874; Hofmann, 1972; p. 4) have concluded that the member was deposited in an alluvial plain environment. Eastern oriented trough cross strata

(Hofmann, 1972; p. 4, 18) suggest the existence of a low-gradient eastward paleoslope for the deposition plain in the vicinity of Montreal (ibid; p. 18).

The member is correlated with the lower part of Chadwick's (1920) typical Potsdam in New York State and with Clark's (1966) Covey Hill (restricted) Member of the Covey Hill Formation in Quebec.

Ausable Member

The Ausable Member conformably overlies the Basal member of the Potsdam Formation, and conformably underlies the Keeseville Member of the same formation. The upper boundary is placed below the lowest continuous occurrence of quartzitic sandstone. The Ausable Member consists of arkose and subarkosic wacke in grey (N7 to N8), green (5G9/2) and pink (5R8/2) coloured laminae and lenses.

Lewis (1965) found the Ausable Member to be heterogeneous in its maturity and composition and to show wide variation in colour and grain sizes. The argillaceous content varies from a trace to 50 %, the amount increasing with depth. Lewis attributed the increase in argillaceous content to decomposition of feldspar grains, which increase in abundance with depth. In Ontario drill cores from Mc Crimmon and Russell show the member to consist of alternating laminae of pale green (5G9/2) and greyish pink (5R8/2) subarkose or subarkosic wacke. Clasts range from medium to fine sand size within the greenish

laminae and from fine sand to silt size within the pink laminae. The grain size and regularity of the laminae increase westward.

Lithologically similar sandstone was described by Logan (1863, p. 3), Wiesnet (1961, p. 7), Lewis (1965), Clark (1966) and Fisher (1968) from locations fringing the northern and eastern edge of the Adirondack Massif, along the Beauharnois Anticline and in a single outcrop north of Portland by the shore of Rideau Lake (Wynne-Edwards, 1967; p. 120). Based on distribution of exposures and occurrence in deep wells, the Ausable Member appears to represent a major sandstone body that extended across the Ottawa Basin and around the Adirondack Massif in the past.

Such features as thin alternating laminae of silt and fine sand, with regular colour changes associated with ripple bedding (appendix 1) are characteristic of modern prodelta environments (Reineck and Singh, 1975; p. 273). The occurrence of a delta front environment that retrograded during an Ordovician or Cambrian transgression, is consistent with the facies suite relationship suggested for the Beekmantown Group.

The Ausable Member is considered to be equivalent to the upper beds of Chadwick's (1920) typical Potsdam in New York State and to Clark's (1966) Rivière aux Outardes Member of the Covey Hill Formation in Quebec.

Keeseville Member

The Keeseville Member conformably overlies the Ausable

Member, or in its absence, nonconformably overlies the Precambrian basement. The member's upper boundary is placed at the first continuous unit of sandy dolomitized biomicrite of the Theresa Formation, or in its absence, quartzose sandstone of the Bucks Bridge Formation.

The Keeseville Member consists predominantly of quartzitic sandstone with isolated sporadic occurrence of feldspathic arenite, quartzose sandstone and hematitic quartz arenite. Grain size varies from silt to boulder size (-10ϕ to 4ϕ) with most grains being within the fine sand size (2ϕ to 3ϕ) range. Grain size, sorting, colour and quantity of accessory minerals varies dramatically over short vertical and lateral distances. Metaquartzitic clast oligomictic or polymictic conglomerate occur where the member rests on steep sloping resistent Precambrian basement. Minor conglomerate also occurs as bed load deposits within channels.

Within the study area the Keeseville Member is exposed on the west side of the Frontenac Axis between Kingston Mill and Loughborough Lake, Pitts Ferry(lot 32, concession II, Pittsburgh township, in county of Frontenac), Brown's Bay (location 10)and as isolated outliens across the Frontenac Axis. Similar quartz arenite has been reported along the northern Adirondacks (Cushing, 1905, 1908, 1916; Cushing et al, 1910; Chadwick, 1920; Wiesnet, 1961; Lewis, 1963; Sahakian, 1963), along the Beauharnois Anticline (Logan, 1861, 1863; Wilson, 1946; Clark, 1952, 1966; Hofmann, 1972) and west of the Frontenac Axis (Keith, 1949). The member is found in the subsurface throughout

the basin.

The Keeseville Member is considered to be equivalent to Clark's (1966) Cairnside Member of the Chateauguay Formation in Quebec and to most of the Nepean Formation of Wilson (1946) in Ontario.

Theresa Formation

The Theresa Formation conformably overlies the Keeseville Member of the Potsdam Formation, or in its absence, nonconformably overlies the Precambrian basement. The upper boundary is conformable with the overlying Bucks Bridge Formation. The upper boundary is placed at the lowest limit of noncontinuous greyish blue or bluish grey (5PB6/2 to 5B5/1), dolomitized, argillaceous, sandy biomicrite or quartzose sandstone.

Cushing (1908, p. 160-161) described the Theresa in its type area (Theresa, New York State) as a hard, tough, bluish grey sandy dolomite, which quickly weathers to iron-stained sandy crusts. The formation is characterized by the occurrence of large calcite grains which have a "... satiny luster, owing to the included sand grains " (ibid, p. 160). The formation was also reported to contain large Lingula, abundant gastropods, occasional cystoid plates and frequent fucoidal markings on the surfaces of some layers.

Kirchgasser and Theokritoff (1971) considered the Theresa Formation within the Ottawa Basin to be a tongue of the Theresa Formation west of the Frontenac Axis, and that the formation in New York State was restricted to the southwestern

corner of the basin. In Ontario, outcrops of the formation extend as a narrow band along the St. Lawrence River from Brown's Bay to Brockville and as far north as Athens. In the subsurface the Theresa is not found at Smith Falls, Russell, Mc Crimmon or Laggan, suggesting a restricted extension of the formation into the southwestern corner of the basin in Ontario.

Within the study area, the Theresa is characteristically a greyish blue (5B6/1), dolomitized, very fine to fine, quartzose sandstone that weathers to a greyish orange colour (10Y5/2 to 10YR6/2) to depths of 1 or 2 cm. Bioturbation ranges from moderate to extreme, commonly destroying the primary sedimentary structures. Fragments of brachiopods and gastropods are common. Both flaser and lenticular bedding are common.

The Theresa Formation is lithologically similar to Kirchgasser and Theokritoff's (1971) Theresa Member of the Buck Bridge Formation in New York, the upper part of the Nepean and lower part of the March Formations of Wilson (1946) in Ontario and the Lower March Dolomitic Sandstone of Greggs and Bond (1971) in Ontario (figure 1-3).

Bucks Bridge Formation

The Bucks Bridge Formation, consisting of the lower informal Heuvelton member and the March Member, conformably overlies the Theresa Formation, or Potsdam Formation, or, in their absence, nonconformably overlies the Precambrian basement. The upper conformable boundary with the Beauharnois Formation is placed above the highest visible continuous occurrence of

quartz sand grains disseminated within the carbonate lithofacies. The Bucks Bridge Formation includes most of the sandstone to carbonate transition strata of the Beekmantown Group within the basin.

The Bucks Bridge Formation is correlated with the Bucks Bridge Formation of Kirchgasser and Theokritoff (1971) in New York State.

Heuvelton member

The Heuvelton member consists of a wide variety of discontinuous beds of fine grained quartzose and quartzitic sandstones, or, where overlying the Theresa Formation, discontinuous or alternating beds of bluish grey, dolomitized, argillaceous, quartzose sandstone and grey quartzitic sandstone, becoming increasing quartzitic towards the central part of the member.

The lower boundary of the Heuvelton member is placed below the highest occurrence of continuous quartzitic sandstone of the Keeseville Member, or, below the highest continuous occurrence of bluish grey argillaceous sandy biomicrite or quartzose sandstone of the Theresa Formation. The upper boundary of the Heuvelton member is placed below the start of quartz sand grains suspended within the carbonate strata of the March Member.

Although stratigraphically correlated with the Heuvelton Member of the Bucks Bridge Formation of Kirchgasser

and Theokritoff (1971), the Heuvelton member is insufficiently exposed to be directly traced to the New York type area. In addition, uncertainty as to whether or not the Heuvelton member is lensoid makes direct extension of the member into Ontario at this time questionable. As a consequence the informal member status is used here. The member is correlated with the Ruisseau Norton Member of the Chateauguay Formation in Quebec (Clark, 1966).

March Member

The March Member conformably overlying the Heuvelton member consists of the strata in which quartz sand grains are visibly disseminated within a carbonate lithofacies. The upper boundary is placed above the highest visibly continuous strata of quartz sand grains in carbonate strata.

The member outcrops in many places within March township and consists of the upper strata of Wilson's (1946) March Formation. The March is equivalent to Kirchgasser and Theokritoff's (1971) Bucks Bridge Member and Clark's (1966) St. Clothide Member of the Beauharnois Formation in Quebec.

Beauharnois Formation

The Beauharnois Formation conformably overlies the Bucks Bridge Formation, or in its absence, nonconformably overlies the Precambrian basement. The upper boundary is placed below the sharp and in places irregular, but apparently

conformable boundary with the Rockcliffe Sandstone.

The Beauharnois Formation consists primarily of thin beds of grey (N3 to N6) dolomitized pelmicrite and biomicrite that weathers to a yellowish brown (10YR6/2) colour. Lower beds of the formation show smooth algal mat laminae and bulbous stromatolitic beds, alternating with laminated to bioturbated pelleted micrite or dolomicrite beds. Higher intervals are dominated by medium to thick beds of laminated micrite or dolomicrite and unlaminated, homogeneous, unfossiliferous dolomicrite beds. The carbonate beds contain a very high disseminated mud content and are often interlayered with dark coloured (N2 to N4) shale laminae that increase up the section (appendix 1). Vugs of sparite, dolomite or quartz are common throughout the formation, while the degree of dolomitization increases away from the northwestern corner of the basin.

The Beauharnois Formation is equivalent to Raymond's (1913) Beauharnois and Wilson's (1946) Oxford Formations in Canada and Chadwick's (1915) Ogdensburg Dolomite in New York State.

CHAPTER 4

PETROLOGY: TEXTURAL TRENDS

Methods

Textural analysis of the quartz arenite sand fraction (greater than 4ϕ size) was conducted primarily by direct sieving techniques. Two kg chip samples with hand samples used for detailed description were collected from 295 beds at 97 locations (appendix 2) within the study area. Only 3 % of the samples were found to be sufficiently consolidated that disaggregation of the samples for sieving was impractical. Under such conditions the grain size parameters were studied in thin section and corrected to sieve parameters (Friedman, 1962; appendix 4).

Prior to disaggregation samples were separated based on their reaction with dilute hydrochloric acid. Quartzitic sandstones were broken down to -3ϕ size aggregates. A split sample of 50 to 70 gm was then carefully disaggregated and sieved between -3ϕ to 4ϕ sieves at ½ϕ intervals by the procedure outlined by Folk (1968; p. 34,35). Grain breakage and aggregates were limited to 5 % or less (by grain count) for each sieve size. Aggregates below 3ϕ size were found to be too fragile to be disaggregated without grain breakage exceeding the 5 % limit. As a consequence, the very fine sand grains were not disaggregated and a slightly negative skewness may exist in some samples. Estimates of the pan fraction carbonate content were determined by weight loss of 2 to 5 gm of the sample after treatment in a heated hydrochloric acid bath. Samples reacting with dilute hydrochloric acid were broken into -3ϕ in size aggregates.

Between 200 and 300 gm were then placed in a hydrochloric acid bath and processed as outlined by Folk (1968; p. 17,18). Both inclusive (appendix 3) and moment (appendix 4) analyses were performed on each sample (Folk, 1968; p. 45-48).

Grain size analysis of 10 pan fractions was performed on samples representing the Potsdam (Keeseville Mb.), Theresa, Bucks Bridge (Heuvelton mb. and March Mb.) and Beauharnois Formations. Size analysis was obtained by means of a EEL photoextinction sedimentometer using the method outlined with its instruction manual (appendix 5).

Calculations used in this study were performed on Hewlett-Packard programmable HP 67/97 calculators. Where possible preprogrammable cards from HP Standard Pac or Stat Pac I were employed. Unless otherwise stated, correlation coefficients and statistical significance limits were set at 0.95.

Appendix 1 shows the drill log of the Russell County well core (Beard, 1970; p. 165; Consumer Gas Company well, Consumer 16321) stored at the Geological Survey of Canada, Ottawa. Lithological terms adopted for the log and text are defined under table 4-1. Colour codes used within the texts and log were those given in The Geological Society of America, Rock Colour Chart (Goddard et al, 1970). Carbonate textures are defined under Wilson's (1975; p. 64-69) standard microfacies (SMF) coding system. Major standard microfacies found in the study area are defined in appendix A2.

Due to the size of the appendices they have not been included within the text. Copies of the appendices are available

TABLE 4-1

LITHOLOGICAL TERMS ADOPTED FOR STUDY

Siliciclastic Litholofacies

The siliciclastic lithofacies in the Keeseville Member of the Potsdam, and in the Theresa, Bucks Bridge and Beauharnois Formations consist, with few exceptions of a fine quartz arenite. Classification of the quartz arenite was subsequently based on matrix content, or cement type. Composition of sandstone cement was based on the reaction of the rock to dilute (10%) hydrochloric acid solution.

Arkose: sandstone with over 25% feldspar, with feldspar exceeding rock particles.

Subarkose: sandstone with 5 to 25% feldspar, with feldspar exceeding rock particles.

Quartzitic sandstone: quartz arenite with a silica (or non-soluble) cement.

Quartzose sandstone: quartz arenite with a non-silica (soluble) cement.

Quartzwacke: quartz arenite with greater then 10% argillaceous material and under 10% unstable mineral constituents.

Mud: insoluble pan fraction.

Carbonate Lithofacies

No thin sections of the Russell County drill core are currently available and as a result estimation of carbonate

TABLE 4-1 (continued)

types and abundance was based on the reaction of the samples to a dilute (10 %) hydrochloric acid solution. The Beauharnois Formation consists primarily of various micrites, dolomitized micrites and dolomicrites (Folk, 1968; p. 152-170) in the form of mudstone or wackstone (Wilson, 1975; p. 13). The classification used does not take into consideration the influence of varying amounts of insolubles in the carbonate that would tend to bias the results in favour of dolomitic values.

	Type of HCL Reaction	Time Limit
Limestone	violent	immediate
Dolomitic limestone	slow	< 15 sec
Calcitic dolomite	very slow	< 30 sec
Dolomite	nil	> 30 sec.

in the Department of Geology, University of Ottawa, Ottawa, Canada.

Grain Size Distribution

Greggs and Bond (1972; p. 937), comparing samples of the typical Potsdam (Chadwick, 1920) type section and their proposed typical Nepean reference section considered that there are significant petrological differences between the formations: " Microscopically the Potsdam and Nepean differ in grain size, rounding, sorting and cement. The Potsdam sandstone is much coarser, its grains are more rounded and better sorted than those of the Nepean sandstone. The Potsdam sandstone is well known for its secondary quartz overgrowths; few grains in the Nepean sandstone samples show secondary overgrowths but calcareous cement is abundant, particularly in higher parts of the section" (Greggs and Bond, 1972; p. 937).

To test this hypothesis of two distinct petrological units within the siliciclastic strata of the Beekmantown Group, both inclusive graphic and moment statistics were employed (figure 4-1 to 4-8). Samples were separated into five general lithofacies: class A: pebbly sandstone or conglomerate matrix (9 samples); class B: quartzitic sandstone;(138 samples); class C: quartzwacke (65 samples); class D: calcareous quartz-wacke and sandy carbonate (73 samples) and class E: arkose or subarkose (2 samples).

Graphic Mean and First Moment Size

Between the inclusive graphic and moment statistics of grain size distribution there are several significant differences. One of the most noticeable discrepancies occurs between the graphic mean (Mz) and first moment (m_1).

Figure 4-1a illustrates the size frequency histogram of Mz and m_1. The mean value of m_1 for the samples shows a finer grain size than that given by Mz. In general, the m_1 values were found to give finer grain sizes than those for Mz for classes A, B and E. In classes C and D, where a significant pan fraction occurs, the Mz gives a finer grain size than m_1. The relationship between m_1, the insoluble pan fraction (P%) and Mz is approximated by the equation:

equation 4-1 $$Mz = 0.0178 + 0.8211(m_1) + 0.0148(P\%).$$

In figure 4-1b it may be seen that for m_1 and Mz values given in equation 4-1, the mean sizes would predict that the mean insoluble pan fraction for all samples should be approximately 14.5 %, which is close to the actual mean value of 13.7 ± 0.8 % (appendix 3).

The disparity between the value of Mz and m_1 for samples of classes A, B and D appears to reflect the greater sensitivity of the moment analysis over the graphic method (Folk, 1968; p. 49). The variation possibly reflects the inability of the inclusive graphic method's selected percentile points to detect abrupt variation in grain sizes between their

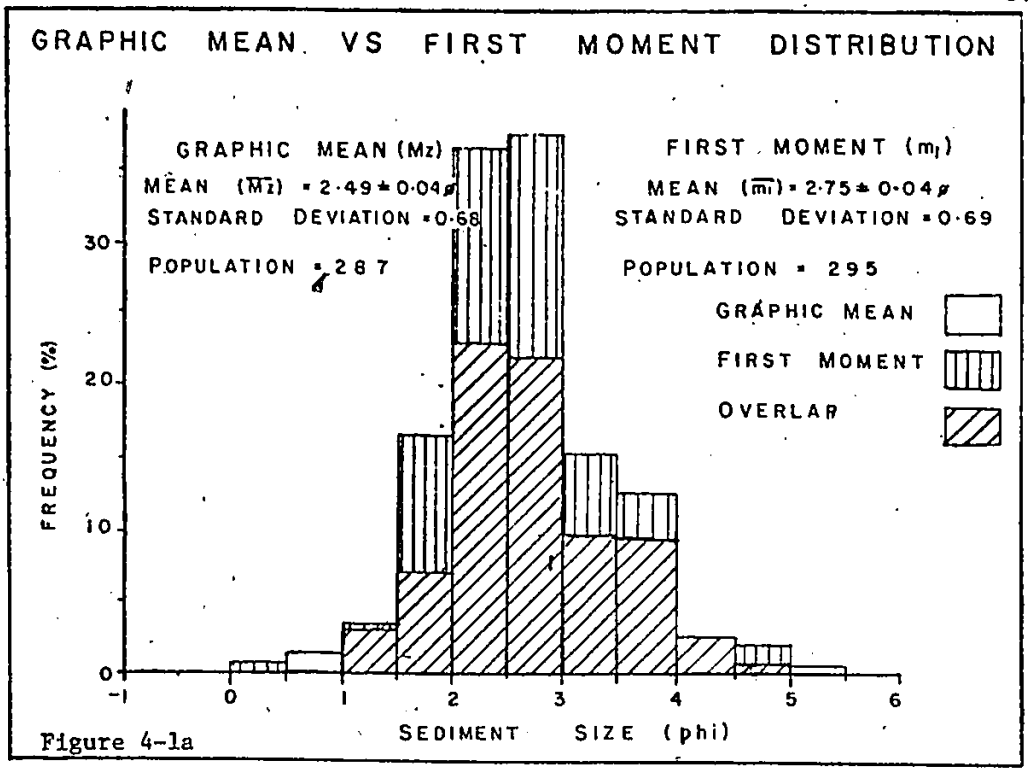

Figure 4-1a

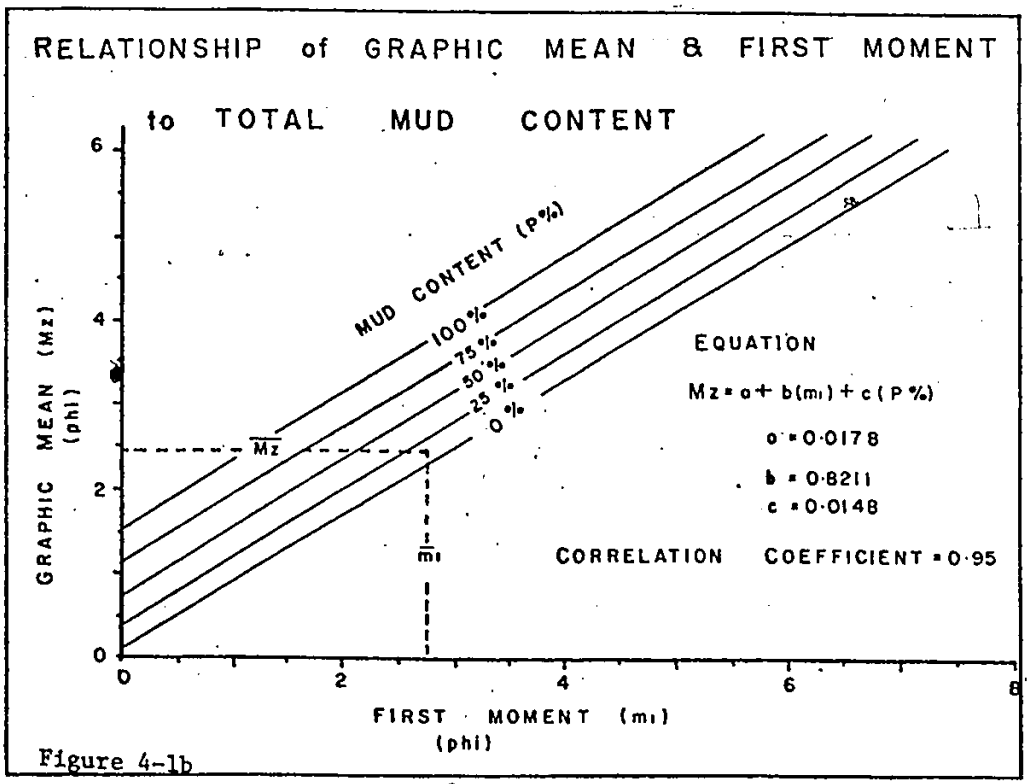

Figure 4-1b

Figures 4-1a and 4-1b: Refer to text for detailed discussion of figures.

positions. In argillaceous samples (classes C and D) the lower m_1 value may reflect the arbitrary lower limit used to estimate the fine sample fraction. Based on 10 pan fraction analyses of samples from the Beekmantown Group, over a wide area, the pan fraction mean Mz value was 5.25 ± 0.11ϕ. This value was used to represent the pan fraction midpoint. With high pan fractions, however, this approximation may not be realistic and may result in a general over-estimation of the actual grain size by m_1. This result is also reflected by other parameters, with sorting (m_2; figures 4-3 & 4-7) and skewness ($m_3/m_2^{3/2}$; figures 4-5 & 4-8) being lower than the corresponding inclusive graphic parameters.

Statistical Tests

In all comparisons of grain size distribution parameters no distinguishable cluster groups of samples could be found to support the existence of major petrological differences within Beekmantown Group clastics (figure 4-2 to 4-8). Gradual transition occurs from class B through to class D.

The distribution of plots in figure 4-2 shows a decrease in sorting (σ_I) with decrease in grain size (Mz) finer than 1.5ϕ. For grains coarser than 1.5ϕ, a weak continuous decrease in sorting is indicated by class A samples. Classes A to D show selective size ranges with class A occurring in Mz ≈ 2.5ϕ or coarser, class B between 1ϕ and 3ϕ, class C between 2ϕ and 3.5ϕ and class D with sizes finer than 2ϕ.

Plots of inclusive graphic skewness (S_{KI}) vs Mz

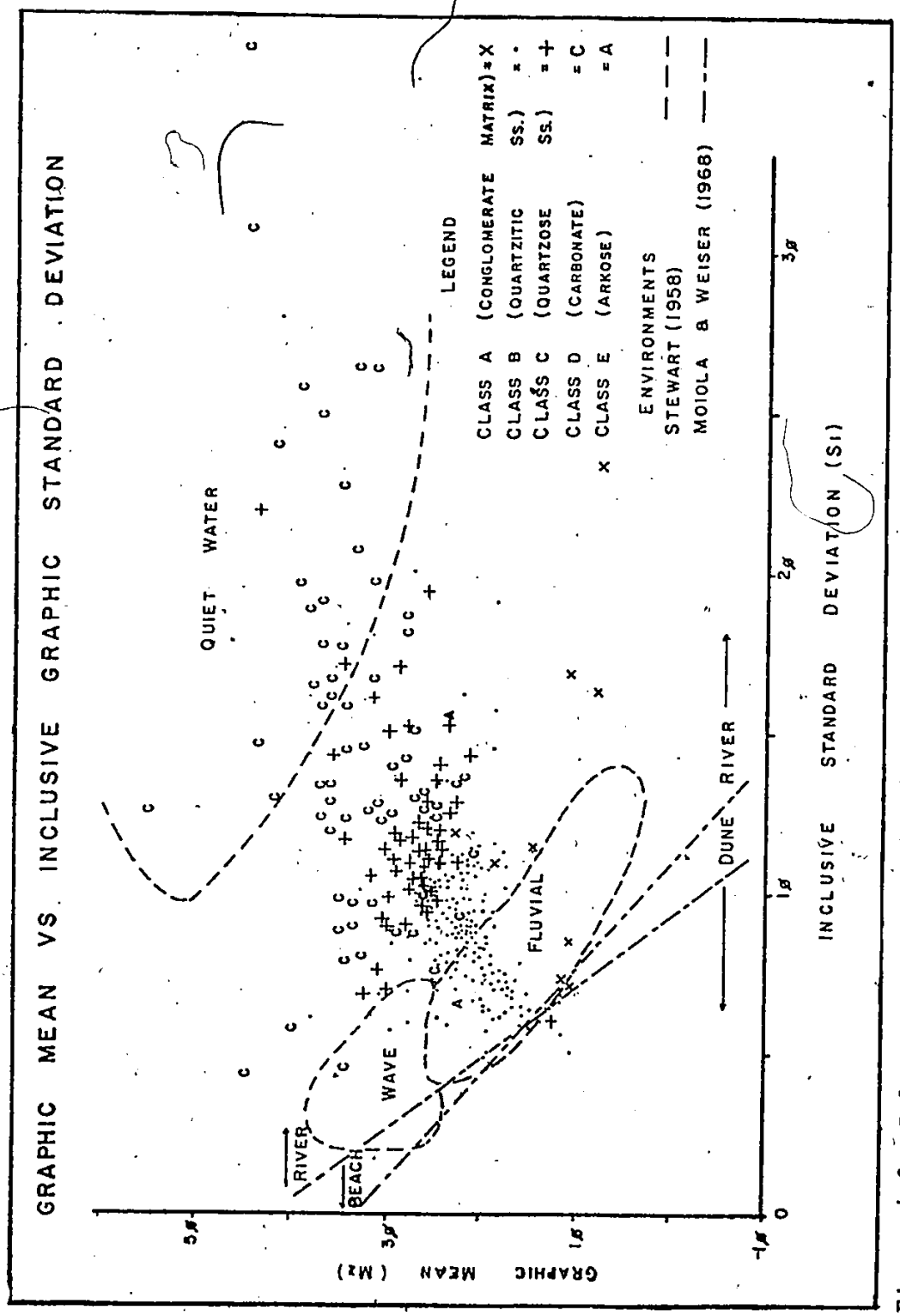

Figure 4-2: Refer to text for detailed discussion of figure.

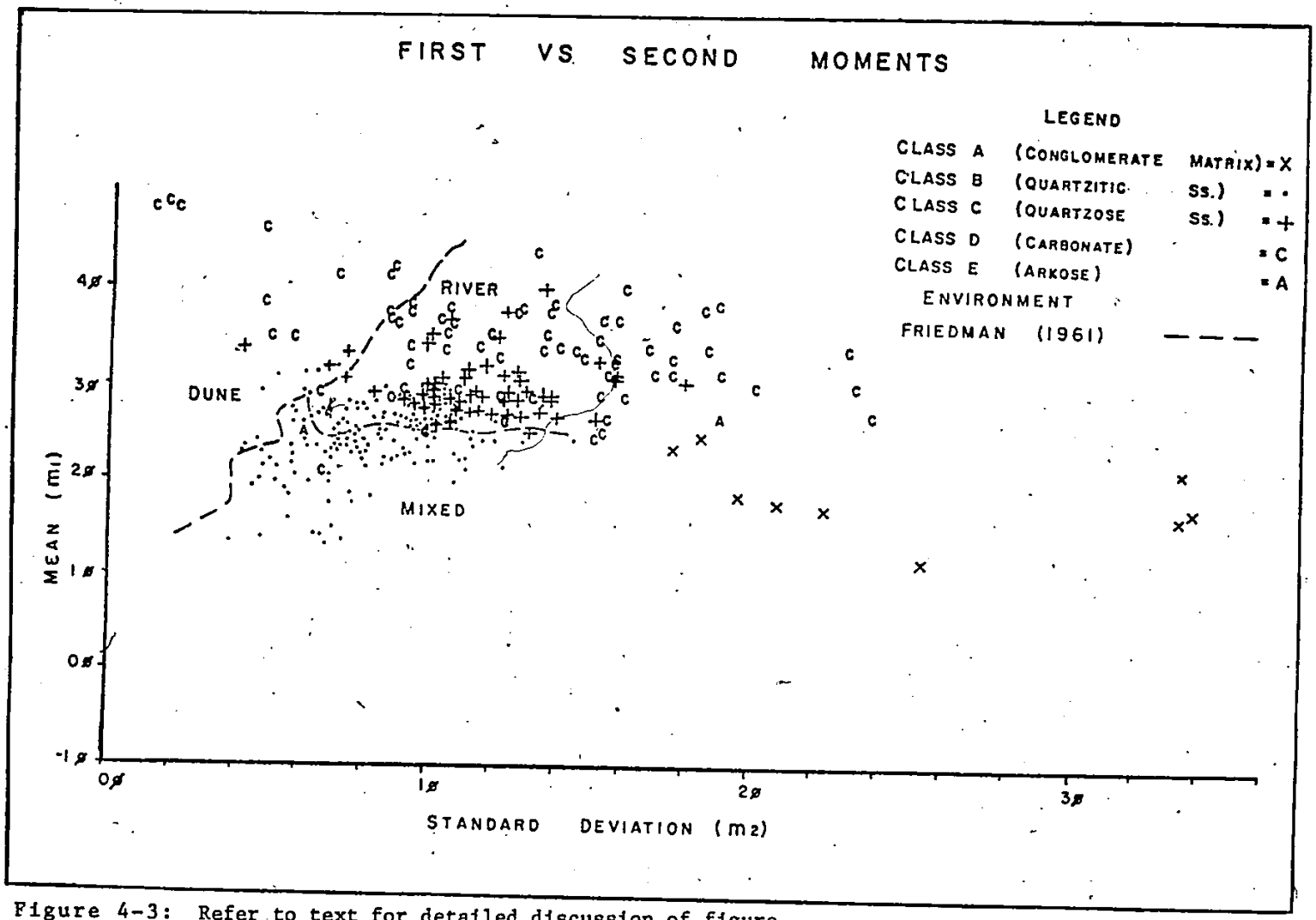

Figure 4-3: Refer to text for detailed discussion of figure.

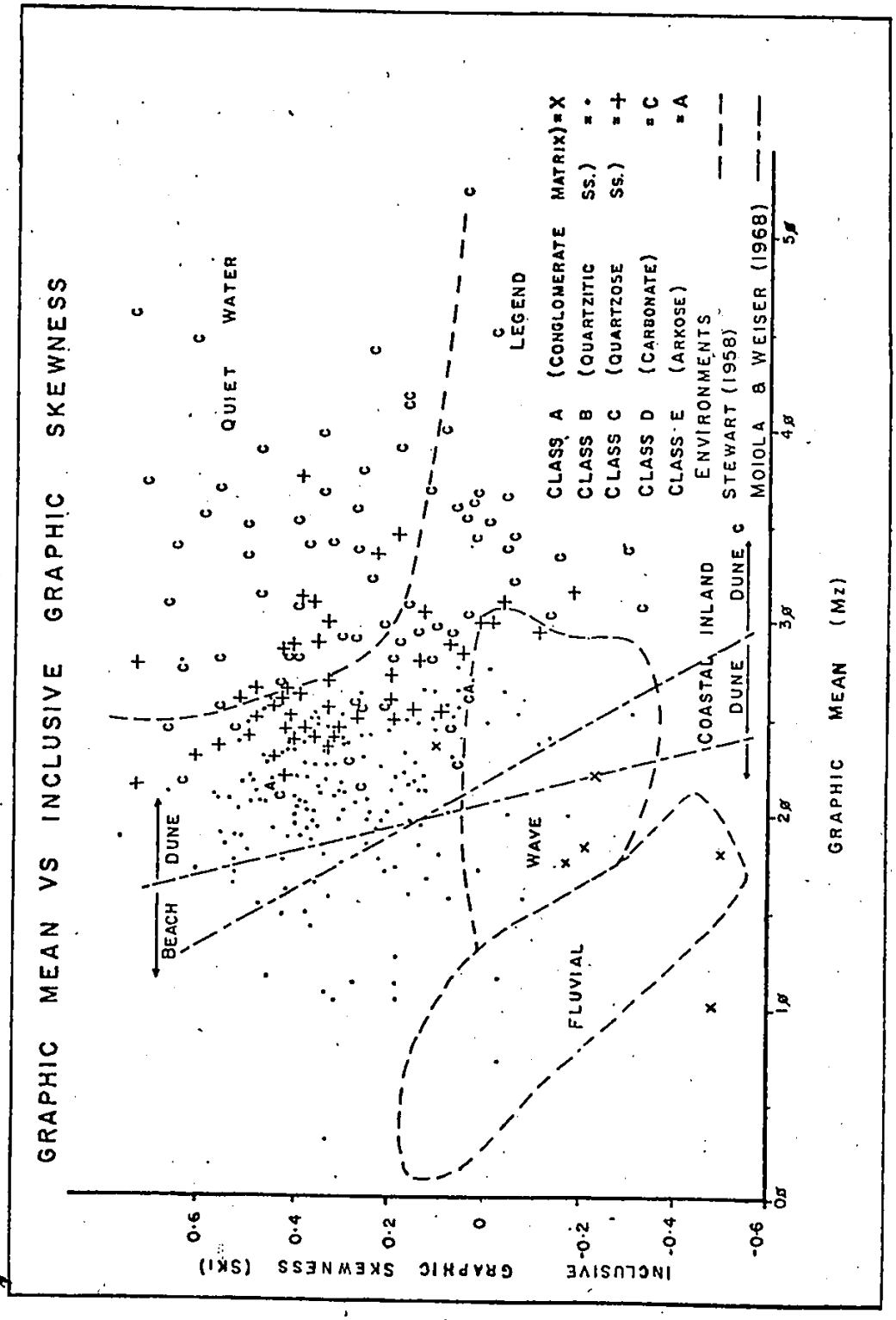

Figure 4-4: Refer to text for detailed discussion of figure.

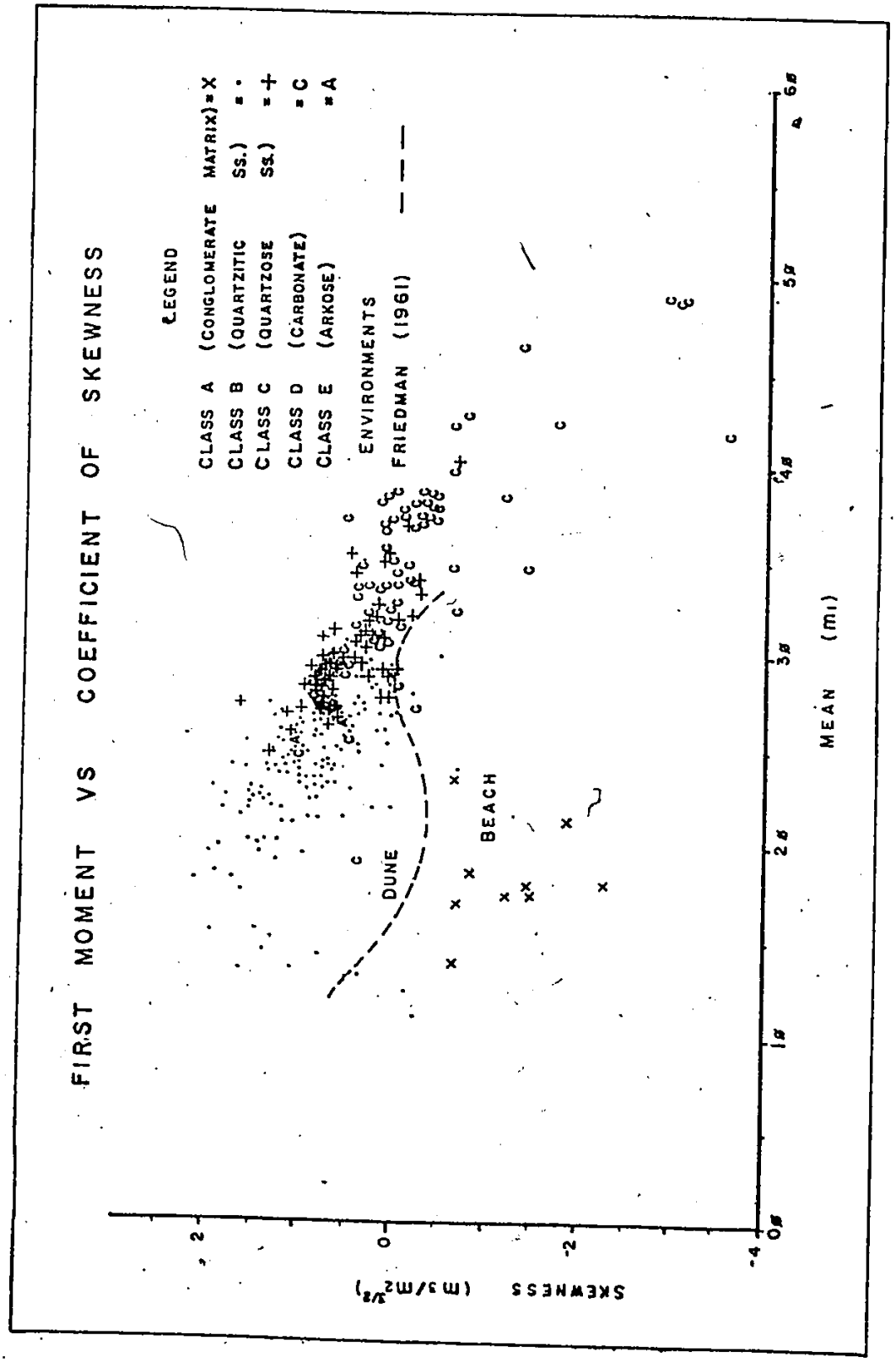

Figure 4-5: Refer to text for detailed discussion of figure.

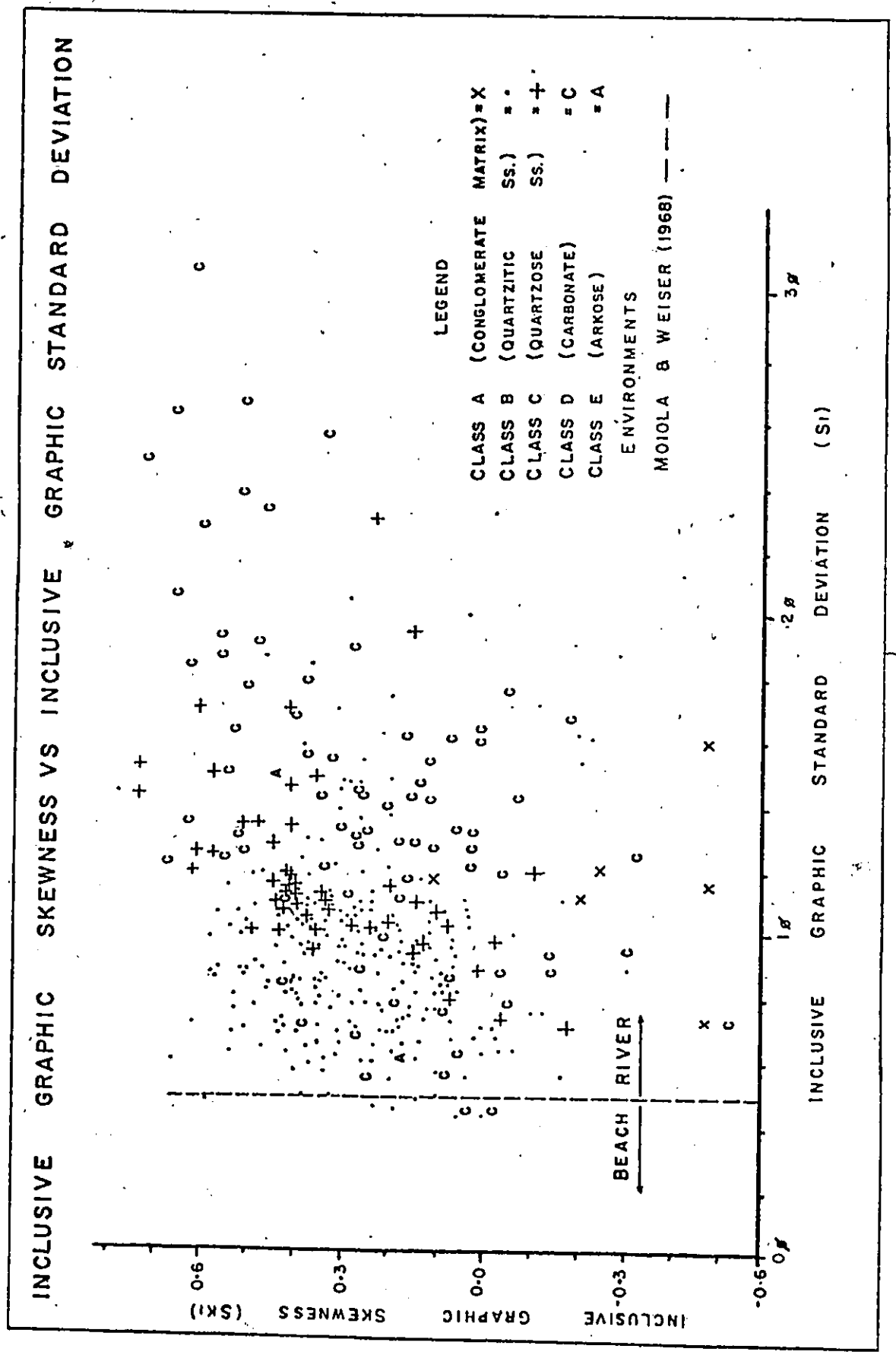

Figure 4-6: Refer to text for detailed discussion of figure.

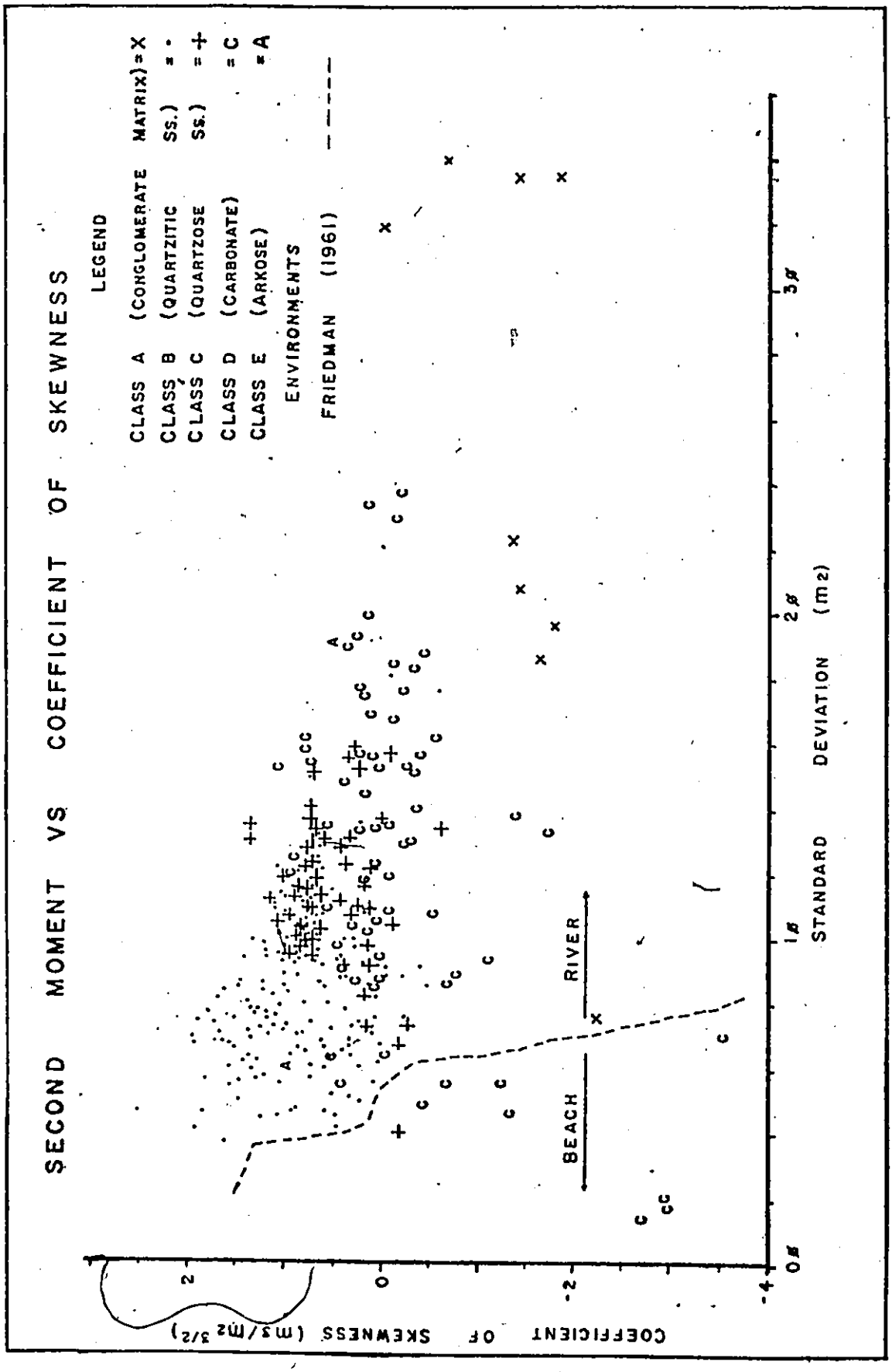

Figure 4-7: Refer to text for detailed discussion of figure.

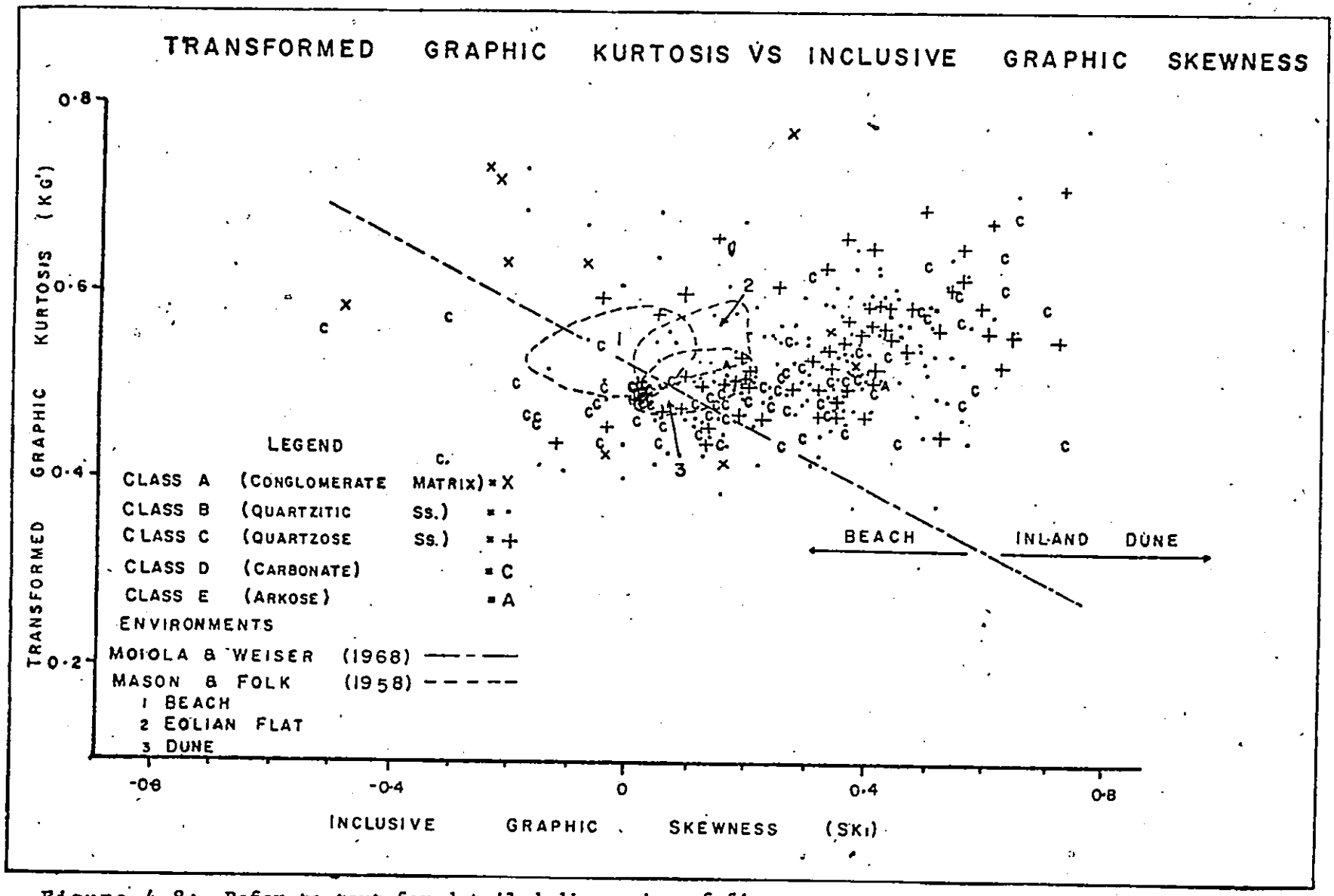

Figure 4-8: Refer to text for detailed discussion of figure.

(figure 4-4) show a continuous gradation characteristic of the classes. Again each class shows a preferred range, though less developed than in the figure 4-3 plot. Class A is negatively skewed, reflecting the strong bias toward the large clast modes with increase in Mz size. Class B, ranging in S_{KI} value between -0.3 and 0.7, shows no apparent correlation between grain size and skewness (mean S_{KI} = 0.30 ± 0.02). Class C ranges between S_{KI} -0.2 and 0.7 (mean S_{KI} = 0.31 ± 0.02) and overlaps the class B range. Class D ranges between -0.95 to 0.70 (mean S_{KI} = 0.24 ± 0.03) showing a slight bias toward the coarser grained fraction over that shown by class B or C. Increase in sample carbonate content appears not to directly influence the textural pattern of the samples, except for being associated with finer grain sediments. Such conditions are considered by Reineck and Singh (1975; p. 119) to be characteristic of tidal flat and shallow marine shelf environments.

The plot of S_{KI} vs σ_I (figure 4-6) clearly illustrates a trend to increased sorting and skewness from class D toward class B samples. Minimum σ_I values occur at S_{KI} values near 0 (classes B and D). Increasingly negative S_{KI} values correspond to decreasing degree of sorting within class A.

When the transformed graphic kurtosis (K'_G) is plotted against S_{KI} extensive class overlapping occurs (figure 4-8). The value of K'_G ranges from 0.38 to 0.88 with the mean K'_G value of 0.53 ± 0.004. The platykurtic nature of the size distribution peak (or peaks) would suggest a near normal kurtosis for the samples.

Evidence of sample clustering between or within the classes is not indicated by plots of textural parameters.

Grain Size Patterns

To test if distinct differences in grain size do exist within the siliciclastic strata of the Beekmantown Group, data from several sources were compared with Mz values obtained from all samples used in this study (Mz = 2.49 ± 0.04ϕ). Table 4-2 lists the mean values obtained from the data of various authors.

Data from Greggs and Bond (1972; p. 937) and Pettijohn et al. (1975; p. 223) were obtained from photographs of thinsections, measuring grains along five equally spaced ribbon transits. The size was then computed for the m_1 value, correcting to sieve size equivalent by the use of Friedman's (1962) equation. Insignificant numbers of grain counts and uncertainty of the Mz, m_1 and P% relationship made conversion to Mz by equation 4-1 impractical. It will be noted that Greggs and Bond's (1972) 'typical Potsdam' and Pettijohn et al (1975) 'Red Sandstone (Ordovician) Potsdam' are both from the type section at Hannawa Fall, New York. In all cases the Gaussian distribution was used to test the significance of the samples; values of 0.95 or greater were not considered significantly different.

Greggs and Bond's typical Nepean, Pettijohn's Red Sandstone (Ordovician) Potsdam, Wiesnet's (1961) Potsdam and samples collected in this study from Clark's (1966) Potsdam

TABLE 4-2

GRAIN SIZE TRENDS OF SILICICLASTIC STRATA IN THE OTTAWA BASIN

Samples collected in this study and from other independent studies are compared with respect to overall graphic mean (Mz) or first moment (m_1). Samples were tested, using normal probability statistics, to determine degree of similarily. See text for discussion of table.

$\overline{m_1}$ = first moment size

$\overline{Mz}$ = graphic mean size

t = estimated from thinsection

s = sieve data

Area from this study	Values
Western part of Ottawa Basin (A)	(s) $\overline{Mz} = 2.49 \pm 0.04\phi$
	$\overline{m_1} = 2.74 \pm 0.06\phi$
Chateauguay Area (B)	
Beauharnois Formation	
Huntington Member	(t) $m_1 = 2.72\phi$
St Clothide Member	(t) $m_1 = 1.37\phi$
Chateauguay Formation	
Ruisseau Norton Member	(t) $m_1 = 3.40\phi$
Cairnside Member	(t) $m_1 = 1.77\phi$
Covey Hill Formation	
Rivère aux Outardes Mb.	(t) $m_1 = 1.77\phi$.
Covey Hill (restricted) Mb.	(t) $m_1 = \underline{1.89\phi}$
	$2.15 \pm .31\phi$

TABLE 4-2 (continued)

Other Sources of data

Greggs and Bond (1972; p. 937)

(G) typical Potsdam (Hannawa Falls, N.Y.)
(t) $m_1 = 2.87 \pm 0.37\phi$

(D) typical Nepean (Ottawa, Ontario)
(t) $m_1 = 3.99 \pm 0.44\phi$

Pettijohn (1975; p. 223)

(E) Red Sandstone(Ord.) Potsdam (Hannawa Falls, N.Y.)
(t) $m_1 = 2.35 \pm 0.01\phi$

Wiesnet (1961; projected image of t)

(F) Potsdam Sandstone (Moore Quadrangle, N.Y.)
$m_1 = 1.32 \pm 0.34\phi$

	B	C	D	E	F
A	P_z (1.869) = 0.969	P_z (0.347) = 0.653**	P_z (2.815) = 0.998	P_z (6.412) = 1.000	P_z (3.534) = 1.000
B		P_z (1.492) = 0.932	P_z (3.419) = 1.000	P_z (0.645) = 0.741**	P_z (1.369) = 0.915*
C			P_z (1.948) = 0.974	P_z (1.405) = 0.920*	P_z (2.687) = 0.996
D				P_z (3.726) = 1.000	P_z (4.442) = 1.000
E					P_z (2.440) = 0.993

* significantly different at the 0.95 confidence limit.
** significantly different at the 0.90 confidence limit.

and Beekmantown Group (appendix 2) show no significant difference in grain size at the 0.95 confidence level from that of the western basin study area. Only Greggs and Bond's typical Potsdam shows significant difference from the western basin data ($P_{(z)} = 0.65$). However, their typical Potsdam and typical Nepean show no significant difference at the 0.95 confidence level ($P_{(z)} = 0.974$). In fact a larger difference exists between Pettijohn et al's Potsdam and Greggs and Bond's Potsdam ($P_{(z)} = 0.92$).

Because of the very limited number of samples, no prominent statistical difference appears to exist in the mean grain size of samples anywhere within the Ottawa Basin.

Differences in mean grain size in certain locations, particularly in the vicinity of the Frontenac Axis, appear to show consistent patterns. To test if regional patterns in grain sizes exist, four divisions of the study area were statistically tested for possible differences and the grain size parameters for the whole study area or between adjacent divisions were also tested. The divisions were: (1) west of the Frontenac Axis, (2) on the Frontenac Axis, (3) between Brown's Bay and Brockville, and (4) between Westport and Athens (figure 4-9). For each division the mean ($\bar{x}$) and the standard deviation of the mean ($^{\Delta}\bar{x}$) for each Mz in the division were computed (table 4-3).

The results show that although a general decrease in grain size occurs eastward across the Frontenac Axis no significant difference at the 0.95 confidence limits is apparent. Only the Westport Athens division has a significantly different

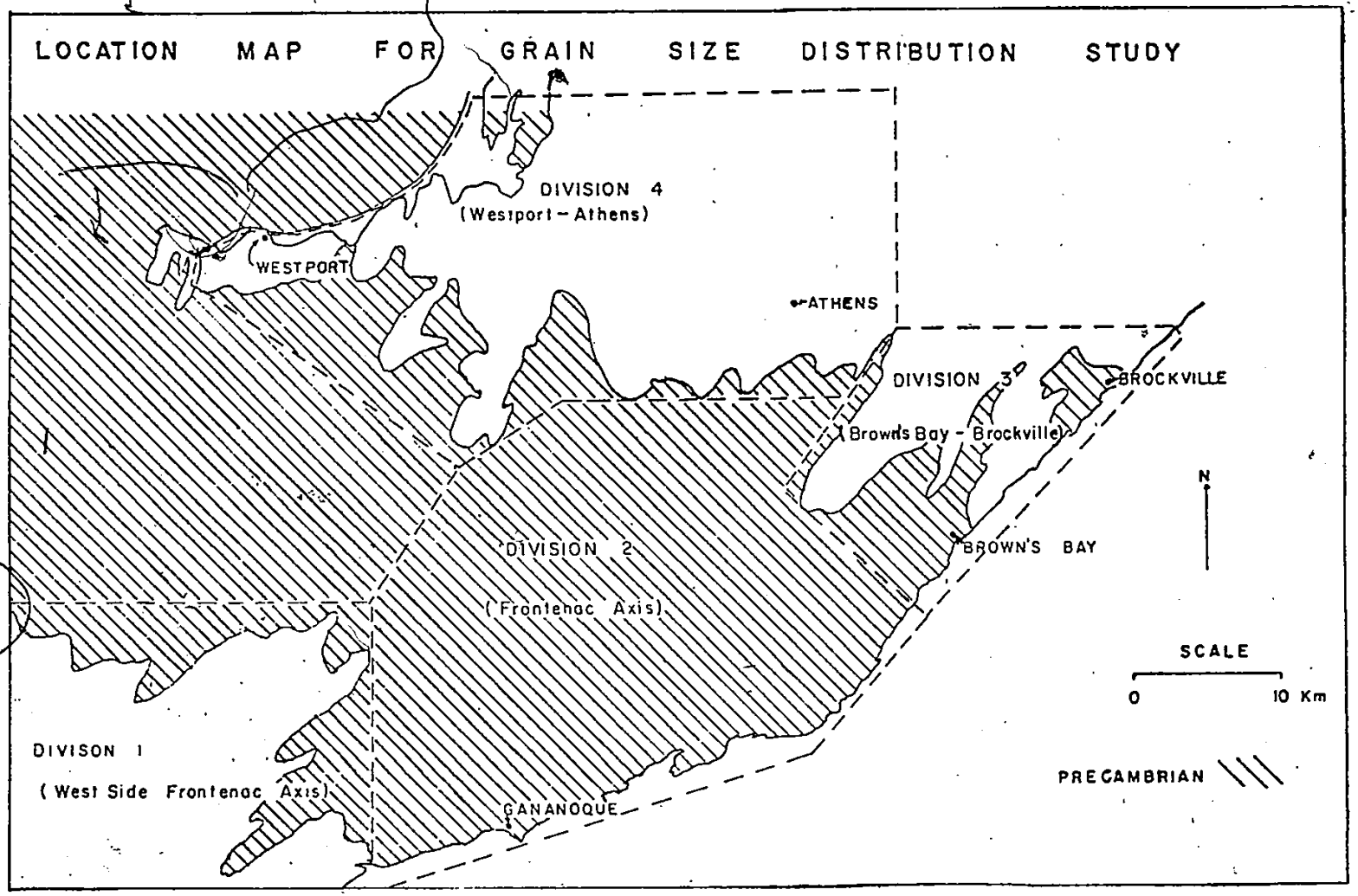

Figure 4-9: Divisions around the Frontenac Axis used in grain size distribution study. For detailed discussion refer to text.

TABLE 4-3

GRAIN SIZE COMPARISON FOR AREAS WITHIN THE WESTERN PART OF OTTAWA BASIN

The Four divisions used in this comparison correspond to the divisions shown on figure 4-9. Each division's overall graphic mean size ($\overline{Mz}$) was tested, using normal probability statistics, against the other divisions values of $\overline{Mz}$. Detailed discussion of this table may be found in text.

Location	Number of Samples	$\overline{Mz}$	Division
West of Frontenac Axis	9	1.55 ± 0.17ϕ	1
Frontenac Axis	27	2.16 ± 0.10ϕ	2
Brown's Bay to Brockville	64	2.82 ± 0.08ϕ	3
Westport-Athens District	146	2.41 ± 0.05ϕ	4
Overall Study Area	289	2.49 ± 0.04ϕ	A

	1	2	3	4
A	$P_z(5.382) = 1.000$	$P_z(3.064) = 0.999$	$P_z(3.690) = 1.000$	$P_z(1.249) = 0.894$**
1		$P_z(3.093) = 0.999$	$P_z(6.760) = 1.000$	$P_z(4.853) = 1.000$
2			$P_z(5.154) = 1.000$	$P_z(2.236) = 0.987$
3				$P_z(4.346) = 1.000$

* sigificantly different at 0.95 confidence limit.

** significantly different at 0.90 confidence limit.

Mz value from that of the entire study area. This difference is believed to be the result of the exceptionally high percentage of March and Beauharnois strata sampled in this area.

The change in mean grain size from west of the Frontenac Axis ($\overline{Mz}$ = 1.55 ± 0.17ϕ) across the Frontenac Axis ($\overline{Mz}$ = 2.16 ± 0.10ϕ) to division 3 ($\overline{Mz}$ = 2.82 ± 0.08ϕ) and division 4 ($\overline{Mz}$ = 2.41 ± 0.05ϕ) would appear to support a decreasing energy gradient of deposition from west to east across the Frontenac Axis.

Grain Shape

Attempts by several workers to determine the source area of the Beekmantown Group clastics by employing grain shape maturity have produced variable results (Wiesnet, 1961; Lewis, 1963). Greggs and Bond (1972, p. 937) attempted to employ grain shape as a criterion for distinguishing between the typical Potsdam and typical Nepean Formation.

To test the relationship between shape and stratigraphical position, 145 samples were selected for grain shape analysis. From each sample, between 200 and 300 whole grains from the 2.5ϕ sieve fraction were analysed for sphericity and roundness using Krumbein's (1941) roundness and Rittenhouse's (1943) sphericity outline charts. Rechecks on 50 samples over the interval of the study showed the variation in estimating the grain shape parameters were normally within the limits of the standard deviation of the means.

As a whole, samples from the western part of the basin

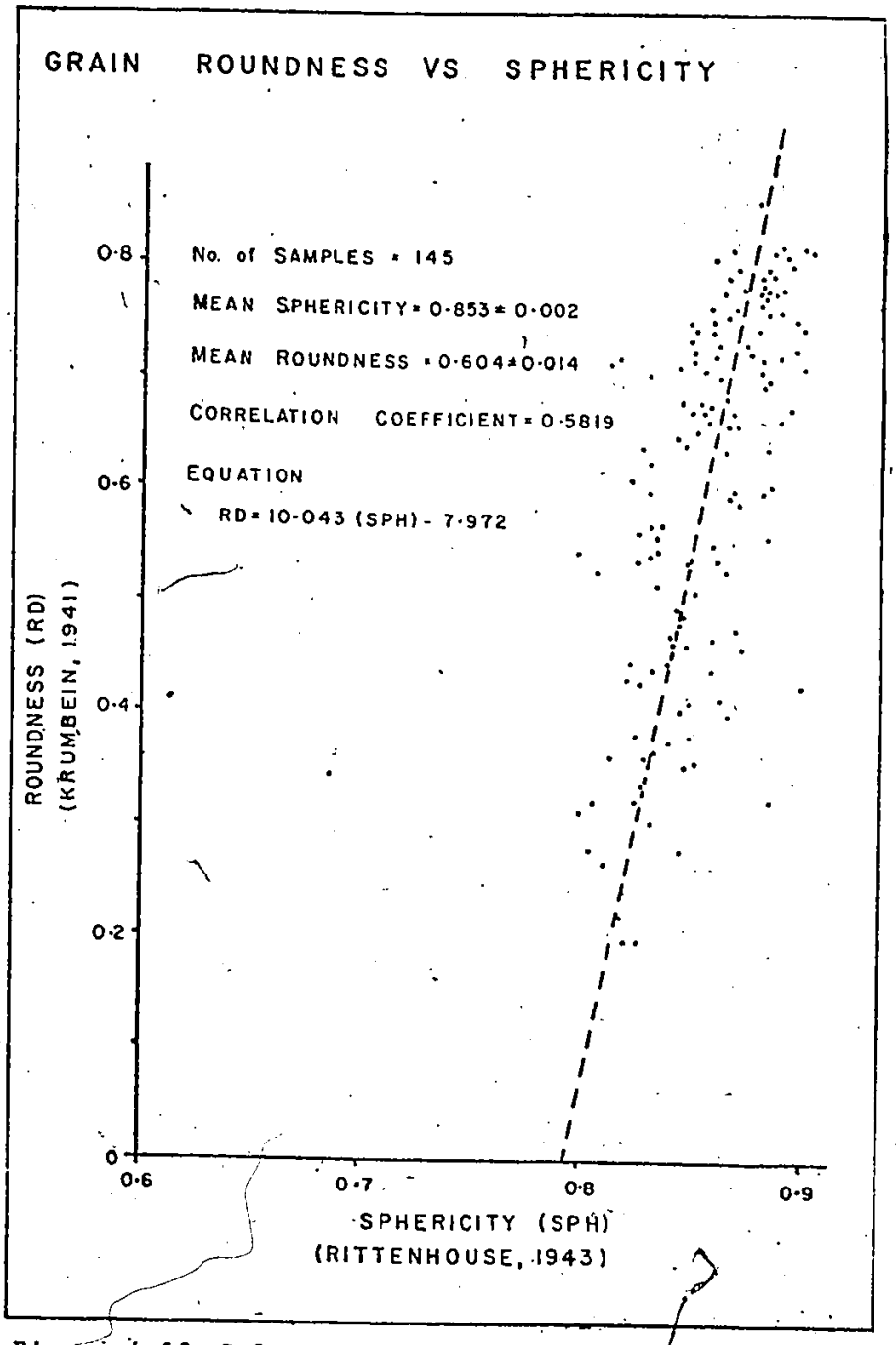

Figure 4-10: Refer to text for detailed discussion of figure.

show relatively high roundness (0.604 ± 0.014) and sphericity (0.853 ± 0.002) values with a significant linear relationship between them (figure 4-10). Grain shape parameters were found to change dramatically between adjacent beds. These changes were frequently greater than that found between samples of widely spaced locations (figure 6-9)? These variations were found in all units of the Beekmantown Group. With such wide variation in shape parameters between adjacent beds, the application of grain shape parameters to distinguish between different formations, or directions of source areas must be questioned.

The variation of grain shape in vertical sections was found to follow a repetitive pattern that corresponds to changes in certain grain size distribution parameters (figure 4-11). The strongest correlation appears to be between grain roundness and proportion of total mud fraction. When both carbonate and mud fraction (CP) are plotted against roundness (R_D) reasonable correlation occurs for CP content less than 30 % of the total sample (figure 4-11b). Beyond 30 % CP content, the correlation with roundness rapidly decreases. Similarly, if the insoluble mud fraction (P) is plotted against roundness an identical trend occurs (figure 4-11a). The correlation coefficient in figures 4-11a and 4-11b suggests that the insoluble mud fraction is the principal control on grain roundness with carbonate content only slightly improving the degree of correlation.

Studies by Heald and Baker (1977; p. 74-75) have shown a positive correlation between the amount of illite coating and degree of secondary quartz growth within the Rose Run Sandstone.

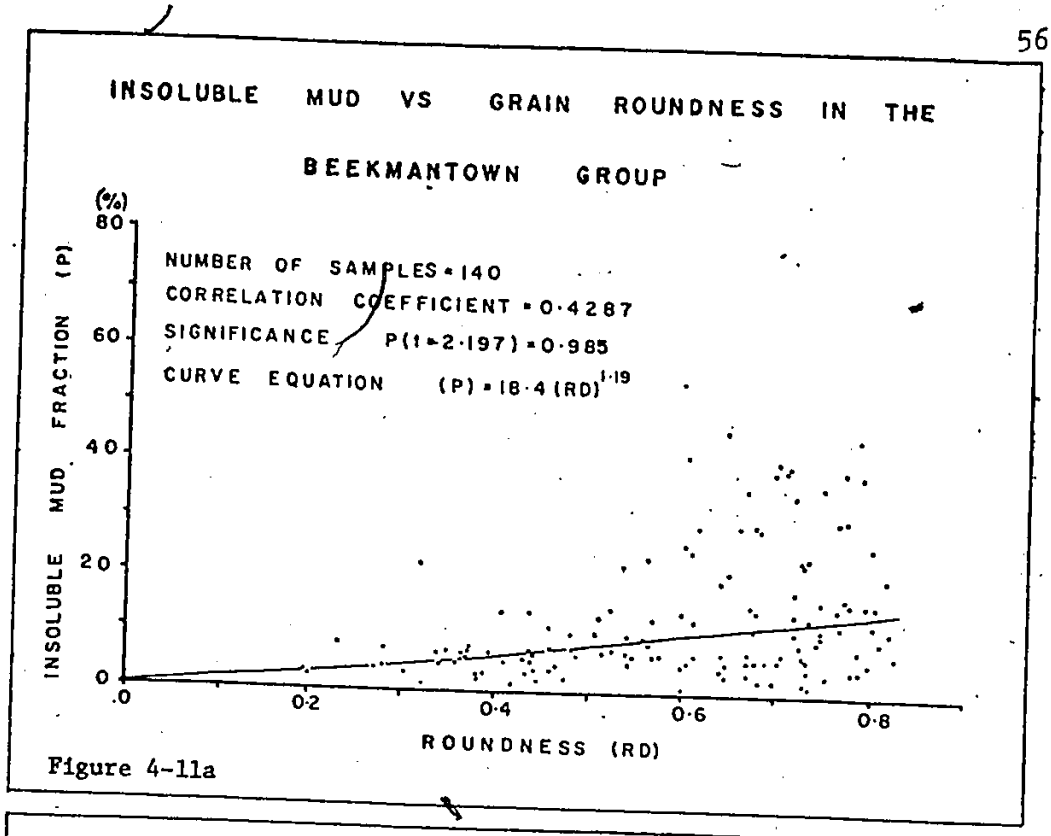

Figure 4-11a

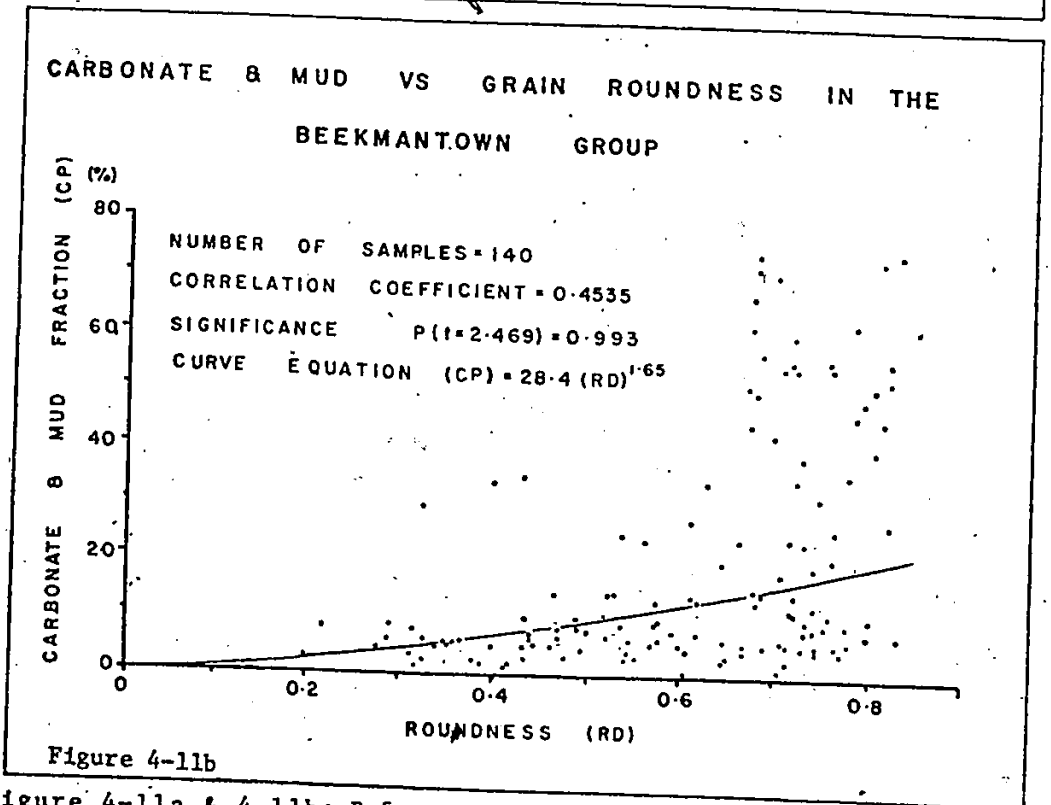

Figure 4-11b

Figure 4-11a & 4-11b: Refer to text for detailed discussion of figures.

Small quantities of clay coating the quartz grains were found to be sufficient to inhibit the development of secondary quartz. This trend may explain the increase in roundness with increase in mud content within the Beekmantown clastics, as well as the rapid decline in correlation with large mud content when a small fraction of the mud actually influences the grain shape.

Wiesnet (1961) found a correlation between the grain shape of the Potsdam Formation and the distance from the Precambrian rocks. The trend was attributed to mechanical abrasion of the grains with transport distance from the source area. However, when the mud fraction (P) obtained from his cumulative frequency curves (ibid, p. 8) are plotted against distance (D) from the nearest Precambrian rock (ibid, p. 9) a logarithmic correlation of the form:

equation 4-2 $$(P)\% = 5.30 + 4.19 \ln (D)$$

was obtained. The curve has a correlation coefficient of 0.82 and is significant at the 0.95 confidence limit (t- test statistic). As a result Wiesnet's correlation of grain shape with distance from the Precambrian rocks may alternatively be attributed to the increase of sample mud fraction away from the Precambrian exposures.

Use of quartz grain shapes to differentiate between formations or determine source areas of ancient sediments must be approached cautiously. Correlation of mud and carbonate content with grain shape suggests that overgrowths are not always apparent and this approach may result in misleading interpret-

ation of shape data (Folk, 1968; p. 78). No apparent distinction based on grain shape can be made between the Potsdam, Theresa and Bucks Bridge Formations of the Beekmantown Group.

Petrology and Paleoenvironmental Evaluations

For several decades attempts have been made to use grain size distribution to deduce depositional environments. The aim behind these attempts has been to develop methods by which sedimentary paleoenvironments may be recognized.

Few studies have been made of ancient sediments in which grain size may have been altered by disaggregation, authigenic growth or pressure solution (Amaral and Pryor, 1977; p. 38). In this study, the Beekmantown Group siliciclastics are relatively easily disaggregated with generally high roundness and sphericity values, suggesting minimum influence from authigenic growths. As a result the Beekmantown siliciclastics should be suitable for testing the ability of textural analysis to discriminate environments.

Stewart (1958), Moiola and Weiser (1968) and Friedman (1961) suggested that plots of inclusive graphic standard deviation (σ_I) vs graphic mean (Mz) or median (Md) or plots of the first (m_1) and second (m_2) moment could be employed to discriminate between various environments. Stewart (1958) found that quiet water, fluvial and wave-influenced environments could be distinguished by plotting σ_I vs Md. In figure 4-2, Stewart's environmental boundaries (corrected from Md to Mz values; table 4-4)are plotted with respect to the lithofacies classes.

Only a third of the samples lie within Stewart's boundaries (table 4-4), with most occurring between fluvial and quiet water environments. Class D samples occur primarily within the quiet water environment (32 % of class D) as would be expected. Classes A and B dominate the classes within the fluvial environment (11 % and 46 % respectively). With only 1 % of the total samples lying within the limits of a wave-active environment, Stewart's criteria would suggest that the Beekmantown Group was primarily deposited in fluvial environments.

Moiola and Weiser (1968) suggested that plots of Mz to σ_I could be used to distinguish between beach and fluvial or dune and fluvial environments (figure 4-2). According to these criteria most of the present samples (97 % to 98 %) fall within the fluvial environments, including all of class D samples. Occurrence of stromatolites, high micrite or dolomicrite content and marine fauna within class D samples show that this interpretation is incorrect.

Friedman (1961) applied the first (m_1) vs second (m_2) moments to distinguish between dune, mixed and fluvial environments (figure 4-3, table 4-4). Similarly to Moiola and Weiser's (1968) interpretation of σ_I vs Mz plots, the predicted environment is fluvial for 56 % of the samples. However, again, most of class D samples (86 %) are undoubtedly marine, making Friedman's criteria questionable.

Stewart (1958) suggested that the plot of median (Md) and inclusive graphic skewness (S_{KI}) may be used to distinguish his three environments of deposition. Figure 4-4 (table 4-4) shows

TABLE 4-4

PETROLOGICAL ESTIMATTION OF PALEOENVIRONMENTS

Table 4-4 is a summary of the data illustrated in figures 4-2 to 4-8. For detailed discussion of the table reference is give to the text.

Parameters	Authors	Class	Environments (%)			
			Wave	River	Quiet Water	Undefined
Md vs σ_I	Stewart (1958)	A	0	11	0	89
		B	3	46	0	52
		C	0	0	3	97
		D	1	0	31	68
		E	0	50	0	50
		Total	1	23	8	68

			Beach		Dune	
				River		River
Mz vs σ_I	Moiola & Weiser (1968)	A	0	100	11	89
		B	4	96	4	96
		C	2	98	2	98
		D	0	100	0	100
		E	0	100	0	100
		Total	2	98	3	97

			Dune	River	Mixed	Undefined
m_1 vs m_2	Friedman (1961)	A	0	22	0	78
		B	7	64	67	0
		C	5	5	2	0
		D	13	86	1	0
		E	0	50	50	0
		Total	8	56	34	2

TABLE 4-4 (continued)

Parameters Authors

Md vs S_{KI} Stewart (1958)

Class	Environment (%)			
	Wave	River	Quiet Water	Undefined
A	33	11	0	56
B	9	1	1	89
C	6	0	18	76
D	1	0	47	52
E	0	0	0	100
Total	7	1	18	74

Mz vs S_{KI} Moiola & Weiser (1968)

	Beach	Dune	Coastal Dunes	Inland
A	89	11	100	0
B	25	75	21	79
C	0	100	0	100
D	1	99	2	98
E	0	100	0	100
Total	15	85	Total 15	85

m_1 vs $m_3 / m_2^{3/2}$ Friedman (1961)

	Beach	Dune	Undefined
A	100	0	0
B	4	96	0
C	0	100	0
D	6	84	10
E	0	100	0
Total	6	92	2

S_{KI} vs σ_I Moiola & Weiser (1968)

	Beach	River
A	0	100
B	1	99
C	0	100
D	3	97
E	0	100
Total	1	99

TABLE 4-4 (continued)

Parameters	Authors	Class	Environment (%)	
			Beach	River
m_2 vs $m_3/m_2^{3/2}$	Friedman (1961)	A	0	100
		B	0	100
		C	2	98
		D	11	89
		E	0	100
		Total	3	97

Parameters	Authors	Class	Environment (%)	
			Beach	Inland Dune
K_G' vs S_{KI}	Moiola & Weiser (1968)	A	33	67
		B	18	82
		C	11	89
		D	38	63
		E	0	100
		Total	22	78

Parameters	Authors	Class	Environment (%)			
			Beach	Aeolian Flat	Dune	Undefined
K_G' vs S_{KI}	Mason & Folk (1958)	A	0	0	0	100
		B	7	9	7	77
		C	2	3	17	78
		D	8	4	13	75
		E	0	0	50	50
		Total	6	6	11	77

Overlapping fields = 48%

Md = Median size

M_z = Graphic mean size

σ_I = Inclusiye graphic standard deviation

S_{KI} = Inclusive graphic skewness

K_G' = Transformed Kurtosis

m_1 = first moment

m_2 = second moment

$m_3/m_2^{3/2}$ = moment coefficient of skewness

TABLE 4-4 (continued)

DISTRIBUTION OF LITHOFACIES CLASSES IN THE BEEKMANTOWN GROUP

Class	Symbol used in figures	Number	Lithofacies
A	X	9	Pebbly sandstone and conglomerate matrix
B	.	138	quartzitic sandstone
C	+	63	quartzwacke
D	C	73	quartzose sandstone & sandy carbonate
E	A	2	arkose or subarkose

Unit	Class	Fraction of Class (%)
Beauharnois Formation	D	8
Bucks Bridge Formation		
March Mb.	D	47
Heuvelton mb.	A	45
	B	84
	C	50
	D	13
Theresa Formation	A	11
	C	29
	D	32
Potsdam Formation		
Keeseville Mb.	A	44
	B	16
	C	21
Basal mb.	E	100

that 26 % of the samples fall within his environments. Classes C and D again represent the bulk of the samples within the quiet water environment. Unlike the Md vs σ_I plot, samples representing the quiet water environment predominate over those representing the fluvial environment. Most samples (74 %) lie between the wave and quiet water environments, possibly indicating a transition zone between these environments.

Moiola and Weiser (1968) plotted Mz vs S_{KI} to distinguish between beach and dune or coastal and inland dune environments (figure 4-4, table 4-4). Under both tests 85 % of the samples fall within the limits of dune or inland dune environments including most of classes C, D and E. The efficient aeolian sorting and mechanical abrasion would normally be expected to remove the finer and softer clasts from the sediment rapidly (Reineck and Singh, 1975; 183-185). In addition the inland dune environment is not supported by primary sedimentary structures such as oscillatory and current ripples, desiccation cracks, herringbone cross stratification and flaser bedding.

Friedman plotted the first moment (m_1) against the moment coefficient of skewness ($m_3/m_2^{3/2}$) to distinguish between beach and dune environments (figure 4-7, table 4-4). The plot suggests that the predominant environment was one of dunes (92 % of samples), including most of classes B' C' D and E. (96 %, 100 %, 84 % and 100 %, respectively). Again, the argument used against Moiola and Weiser's (1968) Mz vs S_{KI} plot is applicable.

Moiola and Weiser (1968) and Friedman (1961) also considered sorting vs skewness plots as useful in distinguishing

beach from fluvial environments. Moiola and Weiser (1968) plotted σ_I vs S_{KI} to distinguish these environments (figure 4-6). Most of the present samples fall within this fluvial environment criterion (99 %). Again, the previous argument against the existence of a carbonate-rich fluvial environment is applicable. Friedman (1961) suggested that a plot of m_2 vs $m_3/m_2^{3/2}$ could distinguish between beach and fluvial environments. Like the σ_I vs S_{KI} plot, the majority of the samples (97 %) lie within the limits of the fluvial environment (figure 4-7, table 4-4).

Both studies by Moiola & Weiser (1968) and those of Mason & Folk (1958) have employed the transform kurtosis (K'_G) vs (S_{KI}) to distinguish environments. Moiola and Weiser used the K'_G vs S_{KI} parameters to distinguish between beach and inland dunes (figure 4-8, table 4-4). The plots suggest that the majority of the samples are in the inland dune environments (78 %) including the majority of classes C, D and E samples. The argument used against their Mz vs S_{KI} boundaries may again be used.

Mason and Folk (1958) tried to differentiate between beach, aeolian flat and dune environments by the use of K'_G vs S_{KI}. Only 23 % of the samples fall within their environmental limits. The data suggest thet 85 % of the samples represent dune sediments (between dune vs beach environments) including all of classes C, D and E. The high occurrence of argillaceous sandstone (class C), carbonate (class D) and arkose (class E), would be an unusual condition and must be questioned. Of the samples that do fall within their limits, the dune environment dominates. Nearly half (48 %) of the samples overlap environmental boundaries.

Again, the dune environment is questionable with the large number of argillaceous (class C) and carbonate (class D)-rich samples present.

The results indicate little to no consistency in the indicated paleoenvironments from grain size distribution parameter plots. As a consequence, the application of these parameters to recognize paleoenvironments in the Beekmantown Group is questionable.

Log Probability Grain Size Evaluation of Paleoenvironments

An alternative procedure that has been employed to distinguish between various paleoenvironments is the analysis of log-probability grain size curves (Visher, 1969).

Visher (1969) interpreted breaks in the curves as the consequence of intermixing of truncated lognormal populations representing the various modes of transport of the grain populations. Both flume and modern environmental studies suggest that the transition from saltation to suspension transport populations normally occurs between grain sizes of 3.3ϕ and 3.9ϕ, while the saltation and traction transition occurs near 2ϕ size grains (ibid; p. 1076). Based on the similar positions of the log-probability breaks and size of transport mode change, Visher divided the log-probability curves into populations: saltation (A), suspension (B) and traction (C) (figure 4-12).

Based on the size of each population and the position of the breaks, Visher (1969, p. 1104) defined 10 environments of deposition. These environments and their limits with respect to

RELATION OF SEDIMENT TRANSPORT DYNAMICS TO POPULATIONS AND TRUNCATION POINTS IN A GRAIN SIZE DISTRIBUTION (modifed after Visher, 1969)

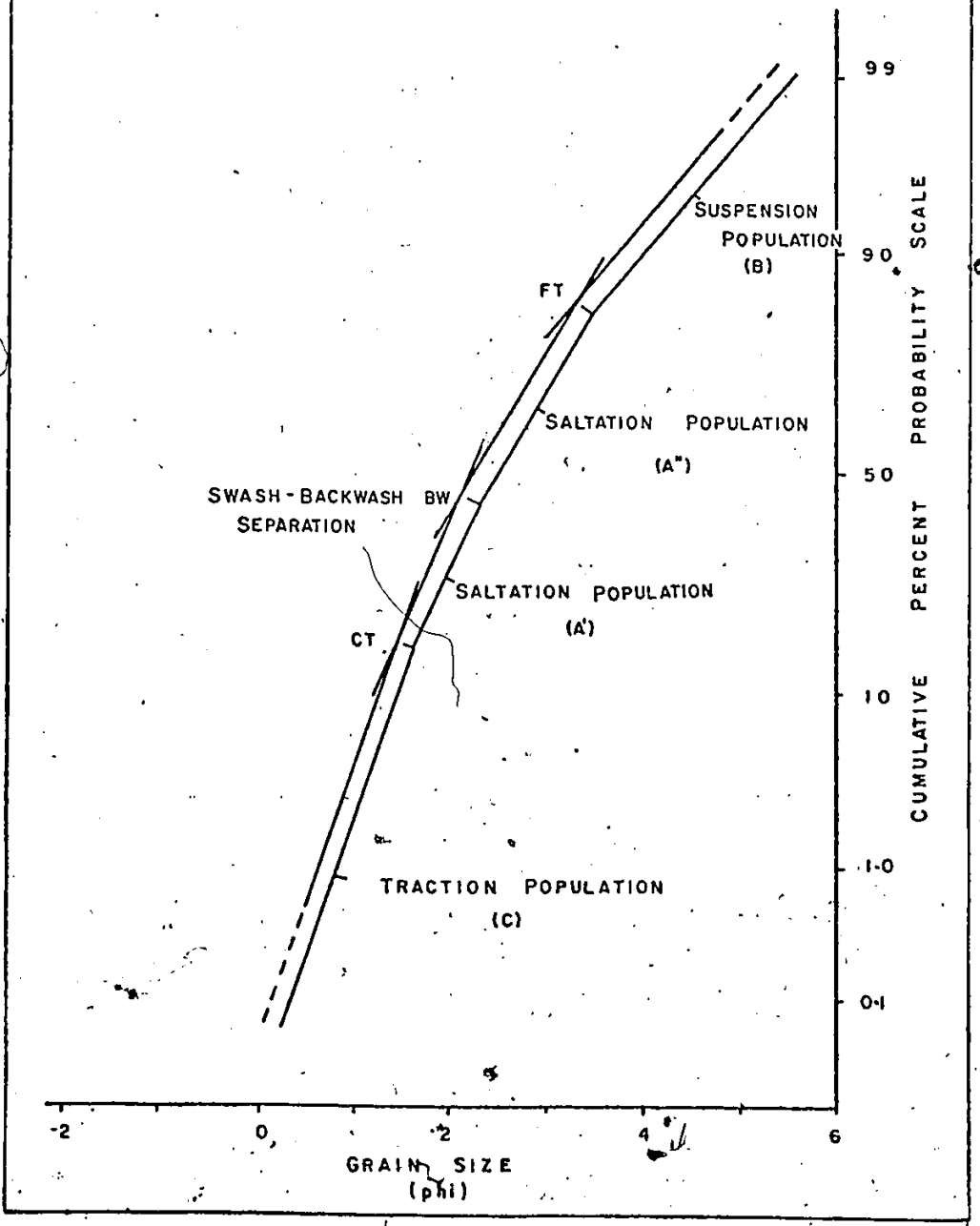

Figure 4-12: Refer to text for detailed discussion of figure.

each population are plotted in figure 4-13a. When the classes are plotted with respect to their populations (figure 4-13b), classes A to D are gradational from saltation to suspension dominant populations. From the distribution of populations, the suggested paleoenvironments are tidal channel (58 %), wave zone (54 %), fluvial (51 %), turbidity zone (32 %) and beach (29 %). The remaining environments are represented by less than 10% of the samples (table 4-5a). Only 10 % of class D samples occur marginally within the fluvial environment. This, however, represents only 3 % of the total samples, and as such none of the suggested environments may be eliminated.

Distribution patterns of the coarse truncation point (CT) size and fine truncation point (FT) size with respect to the populations (figures 4-14a and 4-14b, respectively), suggest a gradual decrease in CT size occurs from the saltation to the suspension populations, while the FT size decreases from the suspension to saltation dominant populations.

When the CT and FT size criterion is added to the environmental criteria of Visher (1969, p. 1104), the dominating environments become tidal channel (56 %), wave zone (51 %), turbidity zone (30 %) and beach (28 %). Both fluvial and dune environments are eliminated, restricting the possible environments to lacustrine or marine (table 4-5b).

In beach or nearshore environments a third truncation break within the saltation segment of the curve commonly occurs (figure 4-12). Visher (1969, p. 1083) attributed the truncation point (BW) to grain sorting by the swash and backwash wave motion.

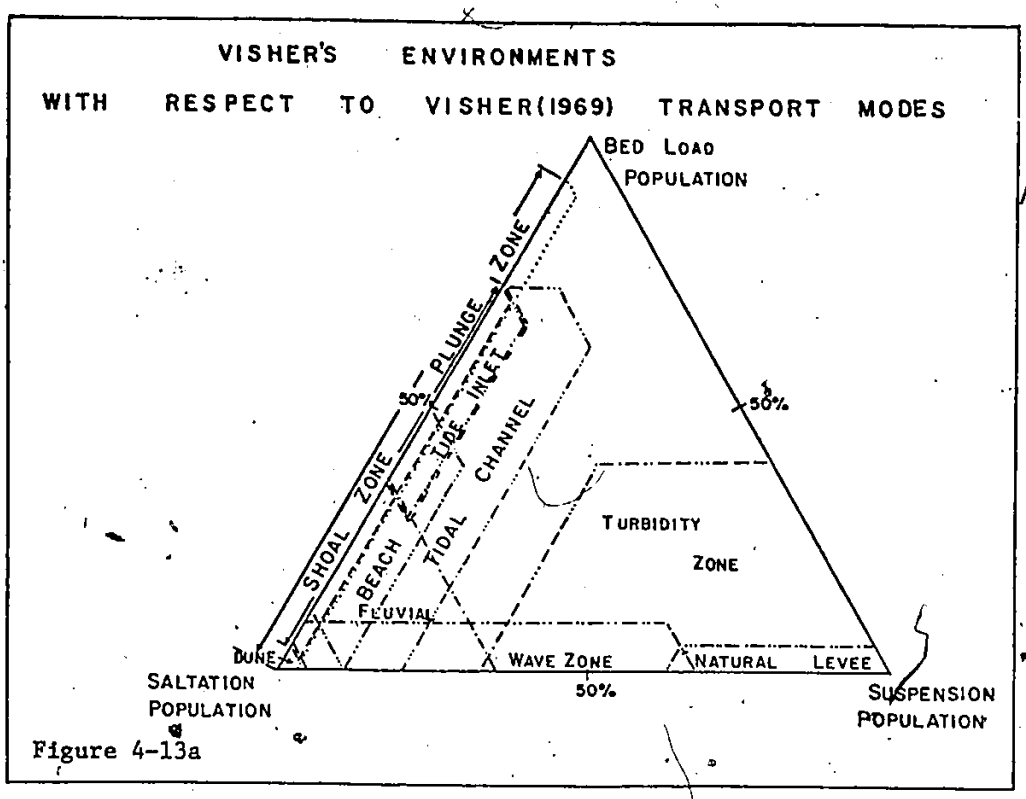

Figure 4-13a

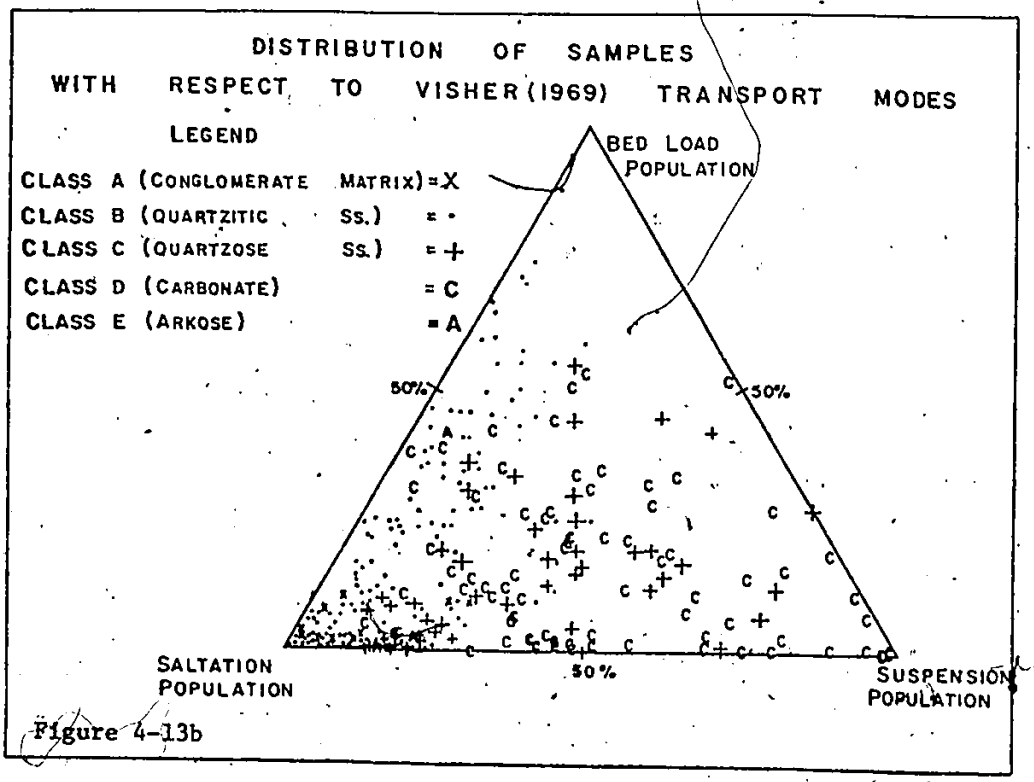

Figure 4-13b

Figure 4-13a and 4-13b: Refer to text for detailed discussion of figure.

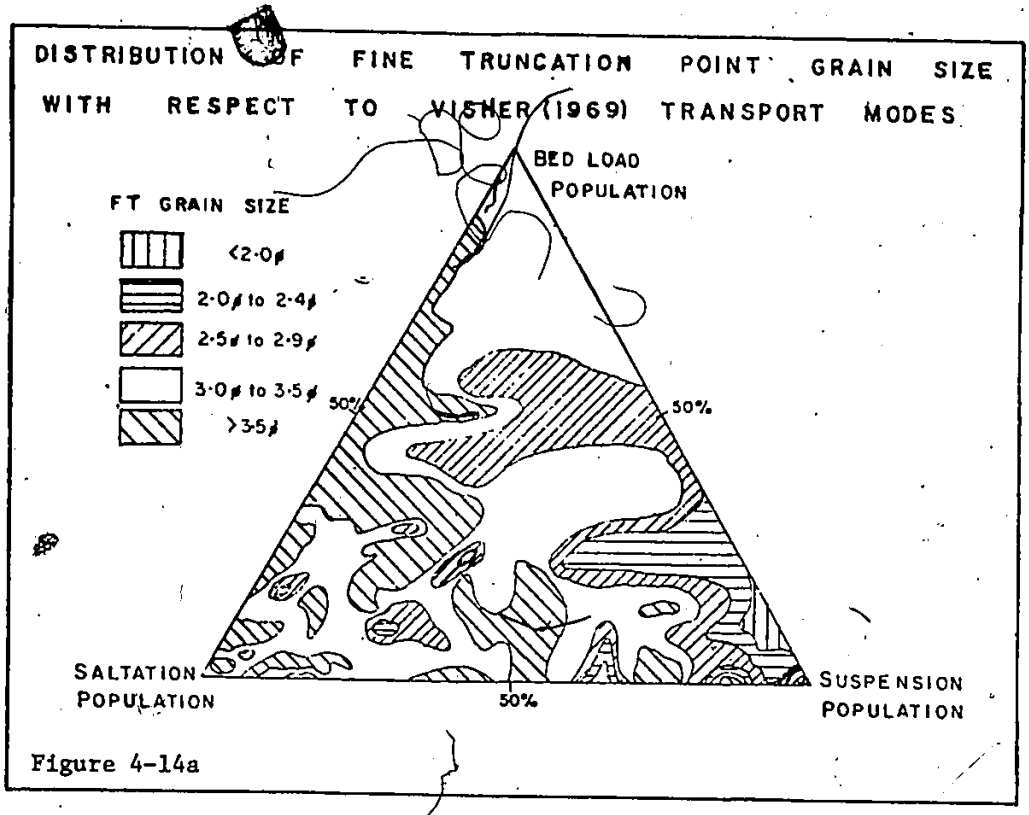

Figure 4-14a

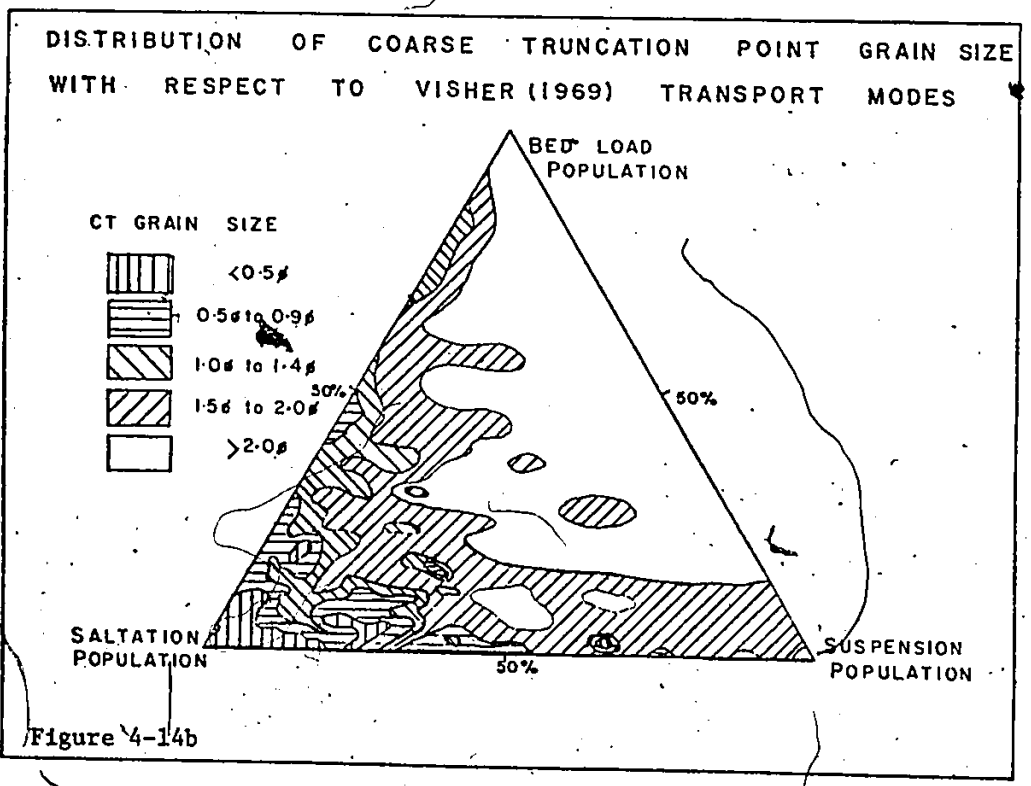

Figure 4-14b

Figures4-14a and 4-14b: Refer to text for detailed discussion of figure.

TABLE 4-5a

DISTRIBUTION OF SAMPLE CLASSES IN VISHER'S (1969)

PALEOENVIRONMENTS

Based on sample population ratios

For a detailed discussion of the table refer to text.

Classes	Tidal Channel	Wave Zone	Fluvial	Turbidity Zone	Beach	Undefined
A %	78	89	89	0	78	0
B %	88	56	71	2	46	3
C %	21	35	35	36	2	12
D %	11	36	10	78	4	13
E %	50	50	50	0	50	50
Total %	58	54	51	32	29	7

Classes	Plunge Zone	Natural Levee	Tidal Inlet	Shoal Zone	Dune
A %	22	0	0	0	22
B %	5	0	6	3	1
C %	0	3	0	0	0
D %	1	11	1	1	0
E %	0	0	0	0	0
Total %	5	2	2	1	1

Overlapping samples in more than one environment = 142 %

TABLE 4-5b

DISTRIBUTION OF SAMPLE CLASSES IN VISHER'S (1969)

PALEOENVIRONMENTS

Based on combination of population ratios and CT/FT size limits

For a detailed discussion of the table refer to text.

Classes		Tidal Channel	Wave Zone	Turbidity Zone	Beach	Undefined	Tidal Inlet
A	%	78	89	0	78	0	0
B	%	88	56	2	46	3	6
C	%	21	35	36	2	12	0
D	%	11	36	78	4	13	1
E	%	50	50	0	50	50	0
Total	%	56	51	30	28	8	6

Classes		Natural Levee	Plunge Zone	Shoal Zone	Dune	Fluvial
A	%	0	22	0	0	0
B	%	0	5	3	1	0
C	%	2	0	0	0	0
D	%	9	1	1	0	0
E	%	0	0	0	0	0
Total	%	4	4	1	0	0

Overlapping samples in more than one environments = 88 %

TABLE 4-5c

DISTRIBUTION OF SAMPLE CLASSES IN VISHER'S (1969)

PALEOENVIRONMENTS

Based on combination of population ratios, CT/FT size limit and presence of BW point

For a detailed discussion of the table refer to text.

Classes		Beach	Turbidity Zone	Tidal Channel	Undefined	Natural Levee	Plunge Zone
A	%	78	0	0	22	0	0
B	%	84	0	10	0	0	3
C	%	56	3	3	2	2	0
D	%	51	41	1	3	9	0
E	%	100	0	0	0	0	0
Total	%	70	18	7	6	3	1

Classes		Shoal Zone	Wave Zone	Tidal Inlet	Fluvial	Dune
A	%	0	0	0	0	0
B	%	3	0	1	0	0
C	%	0	0	0	0	0
D	%	0	3	0	0	0
E	%	0	0	0	0	0
Total	%	1	1	0	0	0

Overlapping samples in more than one environments = 7 %

When the samples with (BW) breaks are added to those required in the beach environment, the possible environments become beach (70 %), turbidity zone (18 %) and tidal channel (7 %; table 4-5c). The remaining samples are either undefined (6 %) or overlap into natural levee, plunge zone, shoal or wave zone environments (13 %). None of these environments can be eliminated on the grounds of textures or sedimentary structures present.

Although the BW point is characteristic of beach environments, only 28 % of the samples fulfil all the criteria required for beach environments. This discrepancy may indicate an overlapping of environmental conditions such as may occur over a tidal flat, or a similar sorting mechanism in other environments. Of the various methods of determining paleoenvironments from the siliciclastic size distribution, only the log-probability curve method appears to give results that have some degree of reliability, being consistent with both sedimentary structures and fossils.

Conglomerate Textures

Conglomerates within the Beekmantown Group occur primarily where the group is in abrupt contact with granitic or metaquartzitic Precambrian ridges. These conglomerates are oligomictic, consisting exclusively of metaquartzitic clasts that locally range in size from small pebbles to boulders with a mean diameter of $-7.4 \pm 0.2\phi$ (table 4-6). Roundness on the Powers scale (1953) varies from sub-angular to well rounded.

When clast axes are plotted on a simplified Sneed and

TABLE 4-6

CONGLOMERATE CLAST SIZES

Location	Mean Axis Diameter	Number of Clasts	Largest Clast's Diameter
401 - 4	19.81 ± 0.47 cm -7.63 ± 0.03ϕ	75	66.7 cm -9.4ϕ
14	15.43 ± 0.27 cm -7.27 ± 0.02ϕ	130	39.0 cm -8.6ϕ
61[A]	8.40 ± 0.43 cm -6.39 ± 0.07ϕ	50	24.3 cm -7.9ϕ
10	9.41 ± 0.22 cm -6.56 ± 0.03ϕ	100	21.2 cm -7.7ϕ
DW - 6	10.06 ± 0.16 cm -6.65 ± 0.03ϕ	65	17.8 cm -7.5ϕ
Total	13.11 ± 0.10 cm -7.03 ± 0.02ϕ	420	39.3 cm -8.6ϕ

Locations for the location code are given in appendix 2.

Refer to text for additional information concerning table.

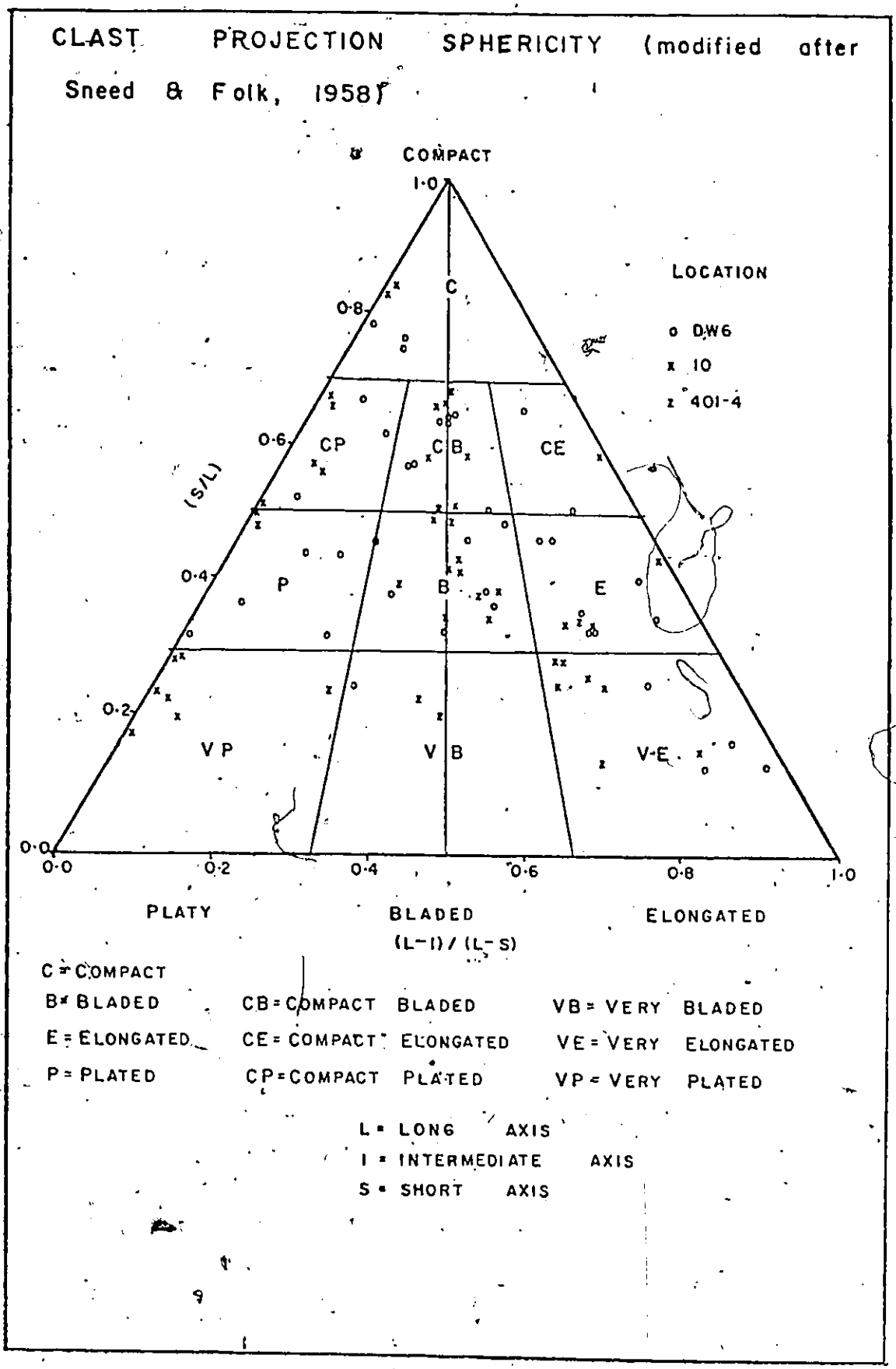

Figure 4-15: Refer to text for detailed discussion of figure.

Folk (1958) projection sphericity diagram (figure 4-15) a continuous distribution from very elongate larger clasts to compact platy smaller clasts is indicated. Dobkins and Folk (1970) suggested that clasts from fluvial environments have low roundness and high sphericity values with neither platy nor elongated shapes predominating. Clasts from high energy beaches were found to have highest roundness and lowest sphericity values with platy shapes prevailing. Low energy beaches have clasts with intermediate roundness and sphericity values with small clasts tending to be platy and larger ones being elongated.

From figure 4-15 the indicated conditions under which the conglomerate clasts were worn would appear to have been in a low energy beach environment.

CHAPTER 5

SEDIMENTARY STRUCTURES AND PALEOENVIRONMENTAL INTERPRETATION

General

Within the Beekmantown Group certain sedimentary structures are clearly associated with particular lithofacies. The siliciclastic strata, such as the Potsdam, Theresa or Bucks Bridge Formation are characterized by structures associated with wave and tidal environments. Carbonate-rich strata such as the March Member or Beauharnois Formation are dominated by biogenic or sedimentary structures associated with restricted tidal environments.

Preliminary conodont biostratigraphic studies within the study area (Brand, 1976; personal communications) suggest that lithofacies suites in the Beekmantown Group are diachronous in a north - south direction. As a result any paleoenvironmental model proposed must explain the presence of both lithological and structural variation within the group.

Sedimentary Structures in Siliciclastic Strata

The siliciclastic strata considered in this study are restricted to the Keeseville Member of the Potsdam, Theresa and Heuvelton member of the Bucks Bridge Formations, exposed along the fringes of the Precambrian Highlands. Within these strata there are six major sedimentary structures which in scale and form reflect the influence of sediment size, hydrodynamic flow conditions and degree of biogenic activity at the time of formation.

Conglomerate Structures

Features such as imbrication of clasts and low angle cross strata dipping away from basement contacts similar to those found at location 10 and 401-4 (figure 5-1), would appear to support a beach environment. At other locations (locations 61^{A}, WD-9) alternating beds of conglomerates and cross stratified sandstone dipping gently away from the basement contact, or the occurrence of Lingula shells trapped between cobble clasts (location DW-9) and interfingering of the conglomerate with sandy carbonate beds (location 401-4), would appear to suggest that the transport and deposition of clasts at these locations were infrequent and that a marine shingle beach with predominately low wave energy was the probable paleoenvironment.

Figure 5-1

Metaquartzite cobble and boulder clast conglomerate; clasts imbricated against monzonitic ridge (left) and interfinger with sandy dolomite beds of the Theresa Fm. on the right. Keeseville Member from location 401-4 (Mac Donald-Cartier Highway).

FIGURE 5-1

Estimation of Wave Intensity

Dott (1974) employed the solitary wave theory to estimate the minimum storm wave height required to round conglomerate clasts of the Baraboo District. Using equation 5-1* or 5-2 to estimate the threshold velocity necessary to initiate clast movement and assuming the velocity to be equal to the unidirectional bottom current beneath the solitary breaking wave, the wave celerity (equation 5-3) and breaker wave height (equation 5-4) may be obtained. The results suggest that under conditions in which the solitary wave is applicable, waves with breaker heights greater than 0.75 m were sufficient to initiate movement of the mean clast size (table 4-6), while the largest clasts would require waves on the order of 3.5 m high to initiate movement. Dott (1974, p. 245) considered his method to have about 25 % accuracy.

Dott's (1974) method depends on the assumption that the waves have shoaled sufficiently to become solitary. For short period waves breaking on a steeply sloping beach or against a steep cliff; this condition may not be fulfilled. Silvester (1974, p. 164) found that only waves with periods greater than 6 seconds should be considered under the cnoidal wave theory. Since the solitary wave is a special case of the cnoidal wave (ibid, p. 171) the solitary wave equations should not be employed for wave periods less than 6 seconds.

An alternative method of estimating the wave condition

---

* List of equations used in chapter 5 may be found on page xiv

TABLE 5-1

ESTIMATION OF WAVE ACTIVITY DURING STORMS

Dott's (1974) method

For detailed explanation of this table refer to text.

Clast sizes (mean axis diameter)

Mean size = 13.1 cm

Largest size = 66.7 cm

Threshold Velocity (converted to m/sec)	Equations 5-1	5-2	Mean
Mean clast size	1.80	2.20	2.00 ± 0.20
Largest clast size	4.05	4.11	4.08 ± 0.04
Wave Breaker Height (cm)			
Mean clast size	66	99	83 ± 16
Largest clast size	337	348	343 ± 6

Hudson's (1958) method

Estimated Breaker Heights (cm)

Mean clast size = 36

Largest clast size = 205

Means of both methods

Mean breaker height for mean clast size = 60 ± 24 cm

Mean breaker height for largest clast size = 274 ± 69 cm

Estimate of Offshore Wave Height from equation 5-6.

For mean clast size H_∞ = 48 ± 19 cm

For largest clast size H_∞ = 218 ± 55 cm

necessary for clast movement is provided by Hudson's (1958) equation. The equation was developed to estimate the breaker height that would initiate damage to a breakwater structure consisting of variously shaped armors. Using the experimental damage coefficient for freshly quarried stone and the mean conglomerate cross-stratification slope found in the study area ($\sim 15^{\circ}$), a minimum breaker height limit may be estimated from equation 5-5. For the mean clast size, a wave height of 0.4 m was sufficient, whereas for the largest clast size, a wave height of 2.0 m was sufficient to initiate movement of angular clasts. The result of waves breaking on steep beach slopes or cliffs suggests that the wave height to move a given clast size is roughly half the height required by the solitary waves. Part of the difference may be the consequence of wave reflection off the steep beach slope increasing the wave energy transmitted to the clast. The dominant breaker height that actually moved the mean and largest clasts probably was somewhere between Dott's and Hudson's predicted values (mean 60 ±24 cm and 274 ±69 cm, respectively; table 5-1).

If the storm waves did not break until reaching the sloping beach face (a possible condition for short period waves during high tide or storm surges) the slope itself influences the breaking process. The slope increases both the breaker height and the water depth of wave breaking (Silvester, 1974; p. 241). Le Méhauté and Koh (1967)used equation 5-6 to determine the ratio of wave breaker height to the deep water wave height. Under conditions of maximum deep water steepness ($\frac{H_{\infty}}{L_{\infty}} = \frac{1}{16}$) and

perpendicular wave incidence on the shoreline, equation 5-6 predicts that the offshore wave heights required to move the mean and largest clasts were 0.5 m and 2.2 m respectively (table 5-1).

Ripples

Small scale ripples predominate within the Ottawa Basin (figure 5-2; table 5-2), having a wide range in indices. (figure 5-3a and 5-3b; table 5-2) and widely diverse forms. Both mean ripple index (RI = 10.8 ± 0.2) and mean ripple symmetry index (RSI = 2.7 ± 0.5) lie within the limits of asymmetric ripples while their modal values occur within the limits of symmetric ripples (table 5-2; Reineck and Singh, 1975; p. 27-28)

Ripple indices show considerable variability within individual ripple sets (defined as 25 or more ripples on a bedding plane having same orientation and size). Some ripples having RSI values of one may show RI values from 4 to 43. With such wide ranges in indices classification of individual ripples into symmetry classes was not always possible. Suggestions by Reineck and Wunderlich (1968) that compaction of strata in ancient sediment may distort the ripple index and size does not appear to have been the cause within the study area. High porosity (Wilson, 1946; p. 13), generally high roundness and sphericity values (chapter 4) and absence of significant pressure solution features appear to eliminate major diagenetic compaction. In support of this, occurrences of interference ripple sets

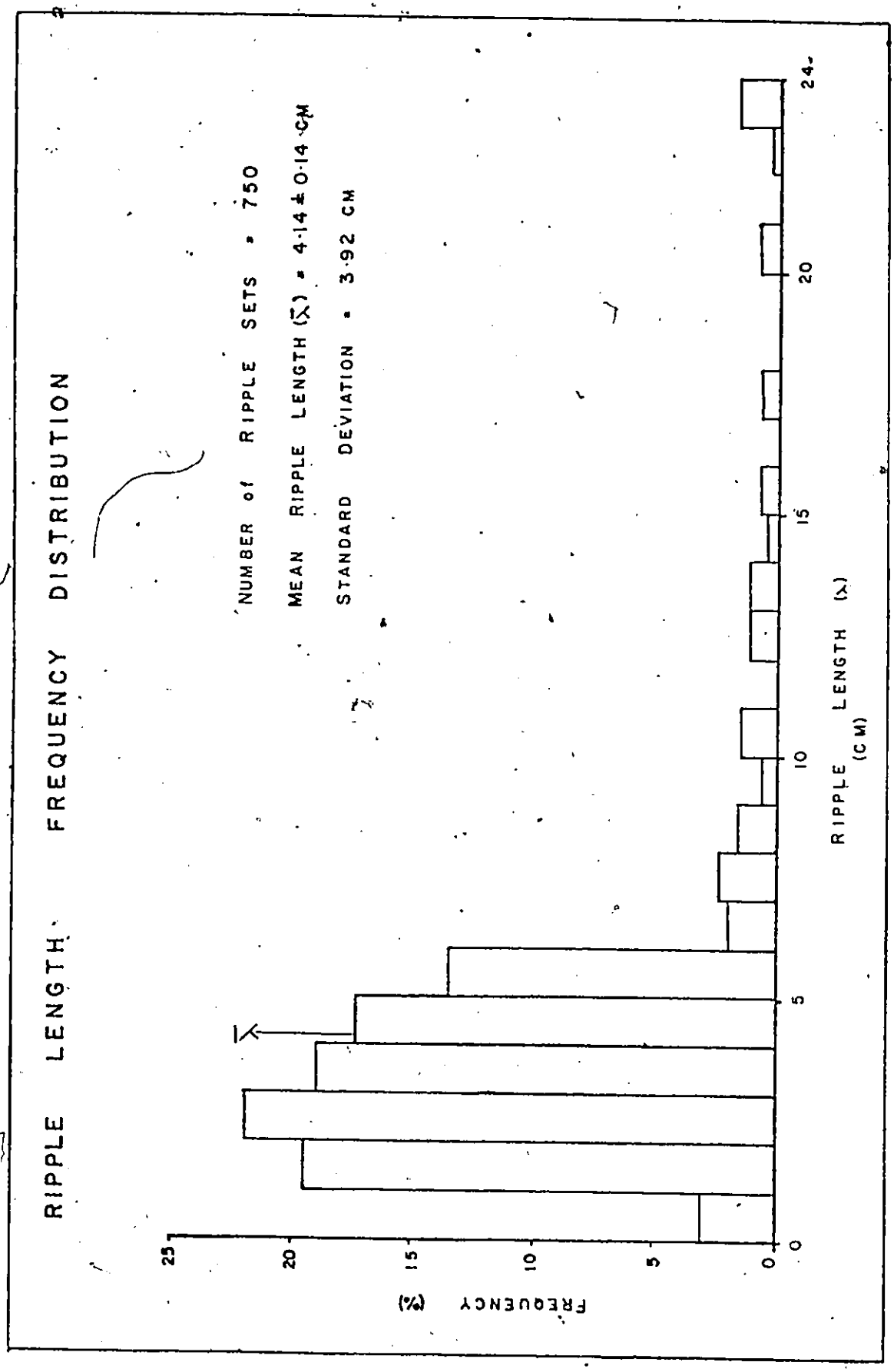

Figure 5-2: Refer to text for detailed discussion of figure.

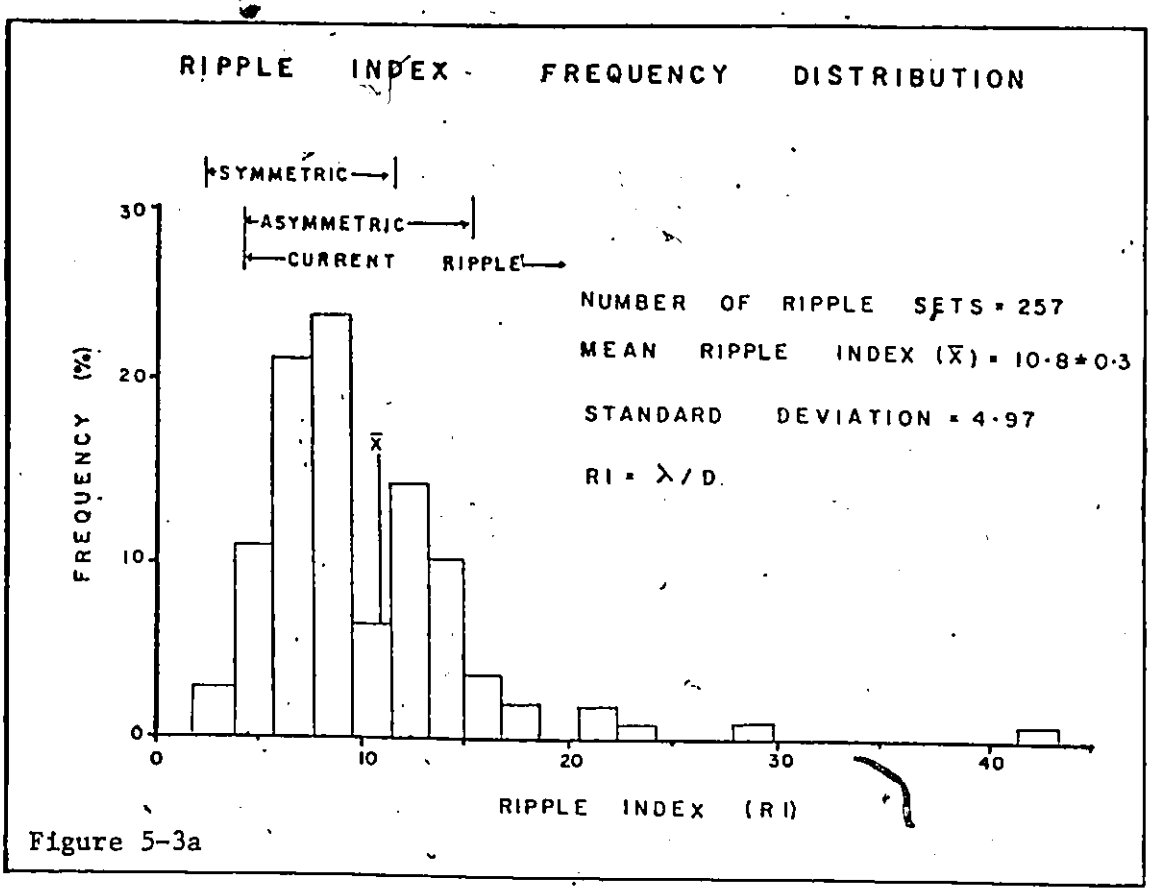

Figure 5-3a

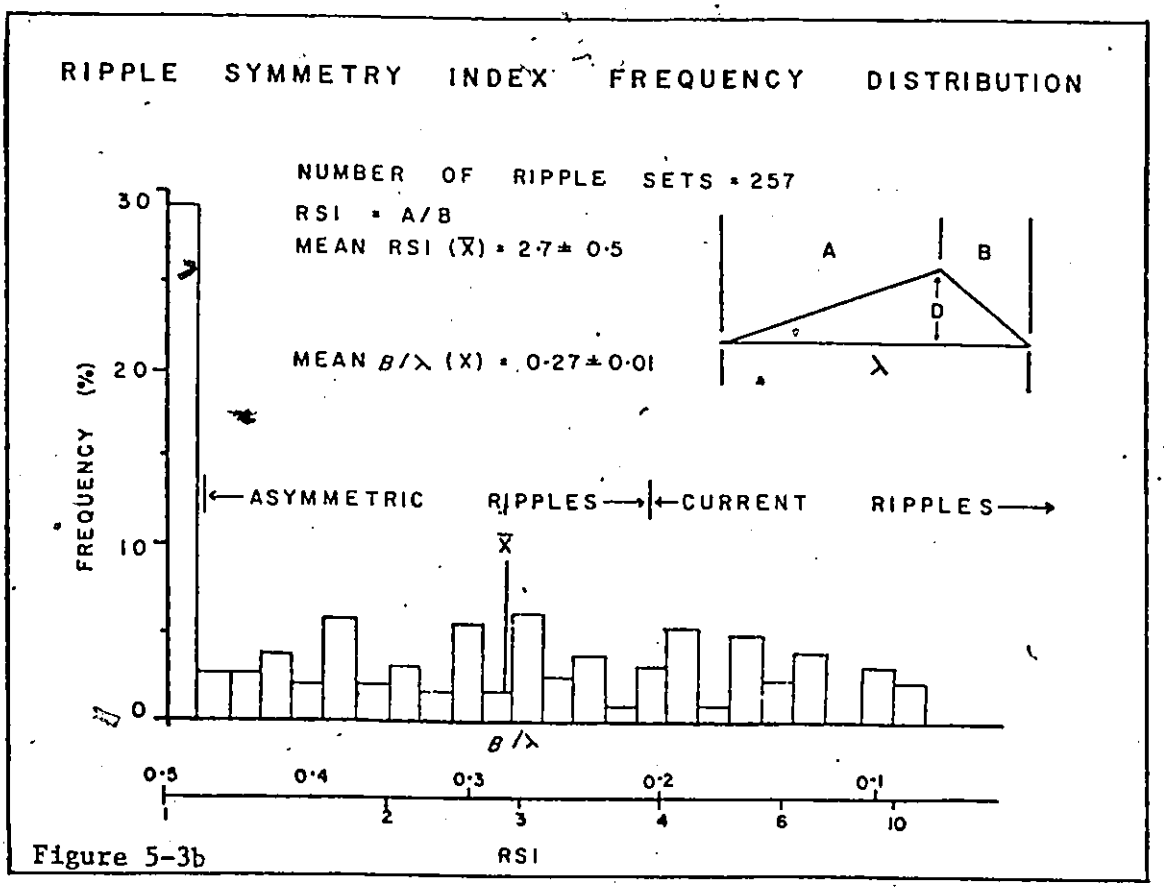

Figure 5-3b

Figures 5-3a and 5-3b: Refer to text for detailed discussion of figures.

TABLE 5-2

RIPPLE STATISTICS FROM THE BEEKMANTOWN SILICICLASTIC STRATA

Number of measured ripple sets = 750

Mean ripple length (λ) = 4.14 ± 0.14 cm

Range of ripple lengths = 0.8 to 24 cm

Mode ripple length = 2.5 cm

$$\text{Ripple Index (RI)} = \frac{\text{ripple length}}{\text{ripple height}}$$

Mean RI = 10.77 ± 0.18

RI range = 1 to 43

RI mode = 8.4

$$\text{Ripple Symmetry Index (RSI)} = \frac{\text{Length of horizontal projection of stoss side}}{\text{Length of horizontal projection of lee side}}$$

Mean RSI = 2.7 ± 0.5

SI range = 1 to 14

RSI mode = 1.04

(Reineck and Singh, 1975; p.27)

showing consistent variation in both indices with changes in ripple size or orientation suggest that index variability is a characteristic of the original bedform.

Interference ripples represent 48 percent of the ripple sets measured in the study. The most common form consists of symmetric straight or slightly undulatory crested ripples, crossed by smaller asymmetric or current ripples (Reineck and Singh, 1975; p. 27-28) that tend to be orientated perpendicular to the symmetric ripple crests (figure 5-4). Similar ripple patterns have been reported from tidal flats (Reineck and Singh, 1975; p. 366-369: Komar, 1976; p. 376: Klein, 1977; p. 14), where decreasing water depth during ebb tide changes the symmetric wave ripples to increasingly asymmetric forms as the wave symmetry is progressively altered on shoaling (Komar, 1976; p. 376) or superimposed tidal current increase. Late stage drainage between the larger ripple crests forms current ripples as the offshore ebb flow is directed toward larger channels (Komar, 1976; p. 376). Frequent occurrence of truncated ripple crests (location 8, 48, 57, 61, RR2, O-4), glauconitic lag deposits coating ripples (location 32, 47, 48) and desiccation cracks cutting the ripples (occur at 30 % of the locations) suggest periodic emergence.

The ripples occur in fine grained (mean Mz = 2.47 ± 0.05ϕ) quartz arenite or quartzwacke beds showing low to moderate bioturbation in the form of Skolithos and Diplocraterion burrows and generally low mud content (mean 14.2 ± 0.08 %). Although the abundance of interference ripples and desiccation

Figure 5-4

Figure 5-4a

Interference ripples; straight crested symmetric ripples (trough axes parallel to pen) crossed by later stage undulating, crested asymmetric ripples (paleoflow in direction of pen tip).

Figure 5-4b

Ripples showing the presence of Repichnia marking. Both figures 5-4a & 5-4b show thin glauconitic lag deposits over ripples.

Heuvelton member

Location 48

Scale: pen = 16 cm

FIGURE 5-4a

FIGURE 5-4b

cracks suggests an upper intertidal setting for the ripples, the generally low mud content within these sediments indicates sufficient wave activity to transport the mud offshore. The conditions would appear to support an intermediate situation between a wave- and tide- dominant setting.

Wave Paleohydrodynamics from Ripples

Dingler (in Clifton, 1976; p. 133) introduced three forms of symmetric ripples. Orbital ripples are ripples in which a linear relationship exists between the wave bottom orbital diameter (do) and ripple length (λ). Komar (1974) found the relationship to be given by equation 5-7 (figure 5-5). Suborbital ripples (Clifton, 1976; p. 133) are ripples with length dependent upon both the wave bottom orbital diameter and sediment size. From Inman's (1957) approximation curves (figure 5-5) equation 5-8 was obtained. This equation for fine grained sediments is in reasonable agreement with Inman's curve but, for coarser sediments the agreement rapidly decreases. With the majority of the ripples occurring in the fine grained sand (Mz = 2.47 ± 0.05ϕ), equation 5-8 is considered adequate for the estimation of the wave bottom orbital diameter in this study. Anorbital ripples (Clifton, 1976; p. 133) are ripples with lengths independent of the wave bottom orbital diameter, depending only on the sediment size by the relationship given in equation 5-9.

By employing equation 5-10 to separate the orbital and suborbital ripple conditions, it is possible to evaluate

RELATIONSHIP BETWEEN RIPPLE LENGTH & WAVE BOTTOM ORBITAL DIAMETER (modified after Komar (1974) and Clifton (1976).)

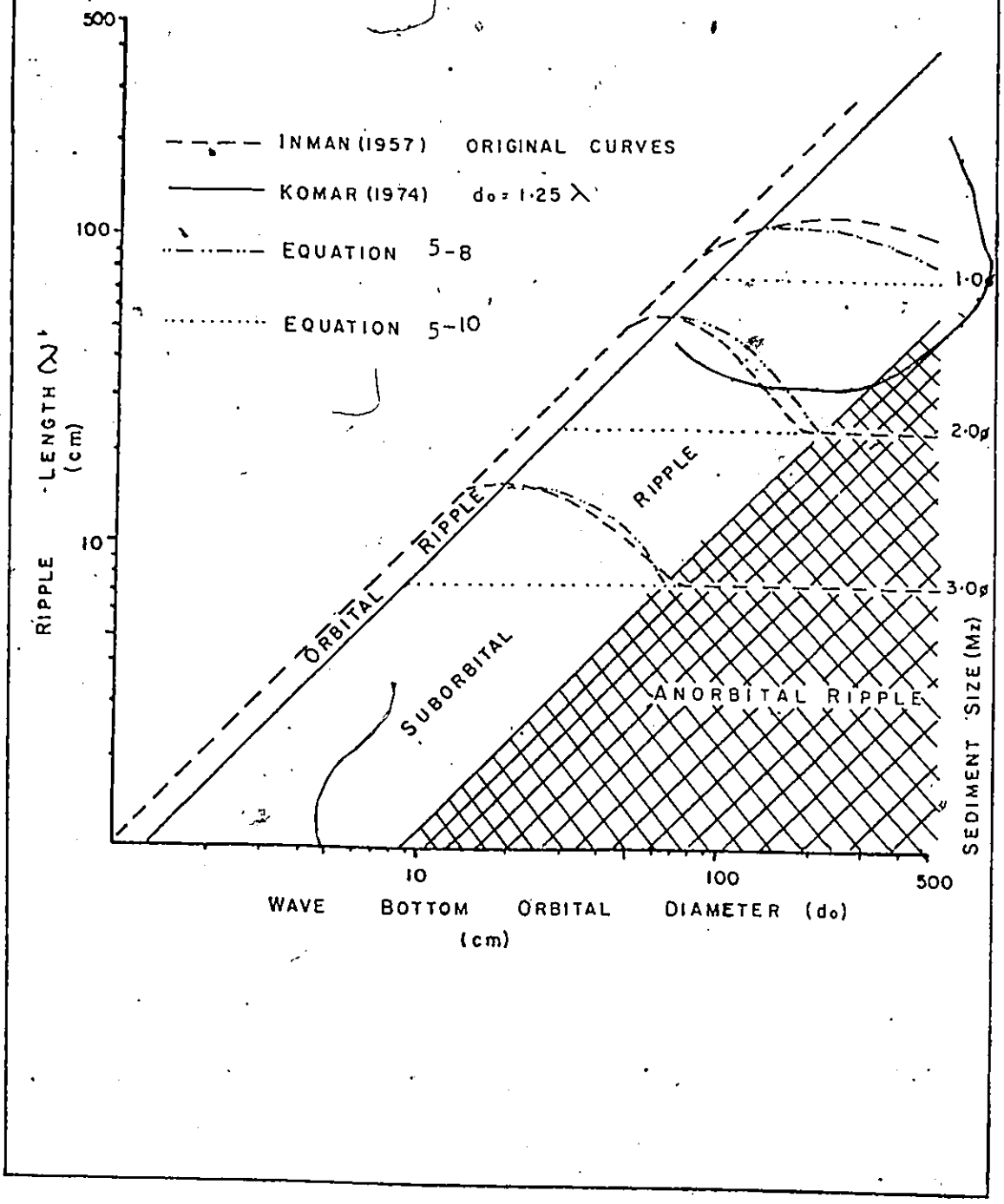

Figure 5-5 : Refer to text for detailed discussion of figure.

the ripple form and approximate the wave or bital diameter. From 200 ripple sets measured, only 7 show values transitional between orbital and suborbital types. When calculations were made from these ripple sets to evaluate the deep water wave conditions, only 1 ripple set indicated marginal suborbital conditions.

Komar (1974) found that the bottom threshold velocity required to initiate the formation of ripples by waves may be approximated by equation 5-11. From the wave bottom orbital diameter and wave orbital velocity, an estimate of the maximum wave period for the waves that formed the ripples may be determined from equation 5-12 (ibid). This procedure suggests that the mean wave period was 1.36 ± 0.07 seconds with a maximum wave period of 3.7 seconds (figure 5-6; appendix 6). Under open oceanic conditions waves normally have periods between 5 and 15 seconds (Silvester, 1974; p. 40) indicating the marine body within the basin at the time of ripple formation had a limited fetch.

From the wave period the deep water (depth greater than half the deep water wavelength; Komar, 1976; p. 42) celerity and wavelength may be directly estimated from equations 5-13 & 5-14 respectively. Evaluation of the deep water wave height is complicated by its independence of other wave parameters (ibid; p. 37). From the Airy wave theory the maximum wave steepness for any depth is given by equation 5-15, while the physical limit of wave steepness is given by equation 5-16. Such extreme wave conditions are unlikely to have prevailed for long within a limited fetch condition. An alternative approach is to estimate wave height by Dean's (1973)

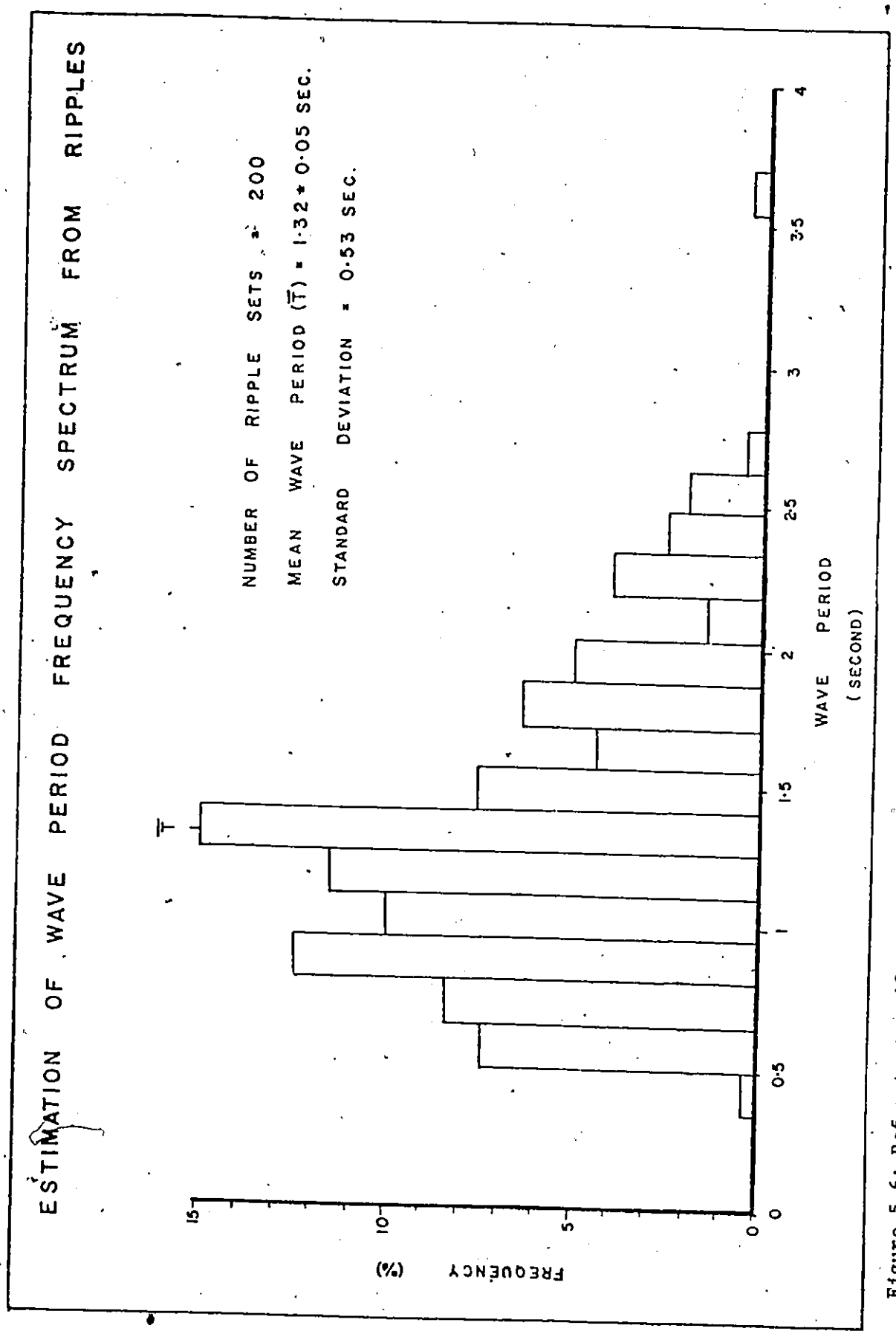

Figure 5-6: Refer to text for detailed discussion of figure.

equation 5-17a that estimates the critical wave steepness at which the shore profile changes from summer to winter profile (Komar, 1976; p. 289). The scarcity of recognizable offshore bars within the study area suggests a prevailing summer beach profile with wave steepness less than or equal to the value in equation 5-17a The predicted mean wave deep water height is 5.28 ± 0.18 cm, with the maximum wave height of 14 cm (figure 5-7).

In water shallower than half the deep water wavelength, shoaling of the wave initiates. Under this condition both the wave celerity and length progressively decrease as the height initially decreases then increases prior to breaking. Wave breaking occurs when the maximum wave steepness is obtained (equation 5-16) or maximum wave height to depth ratio (equation 5-18) is reached. From equations 5-19, 5-20, and 5-21 the wave celerity, length and height may be estimated for any depth. The water depth at which the ripples formed may be obtained using equation 5-22 and 5-23 to estimate the wave bottom orbital diameter and velocity at various depths. The mean predicted depth at which the ripples formed is 48.9 ± 2.0 cm (figure 5-8; appendix 6).

Additional hydrodynamic sedimentary characters may be predicted from the wave parameters obtained from the ripples. Komar et al (1973) found that the wave breaker height may be estimated from equation 5-24. From the wave breaker energy (equation 5-25) and sediment size, King (1972; p. 330-331) found that the beach face slope for sand size sediment may be

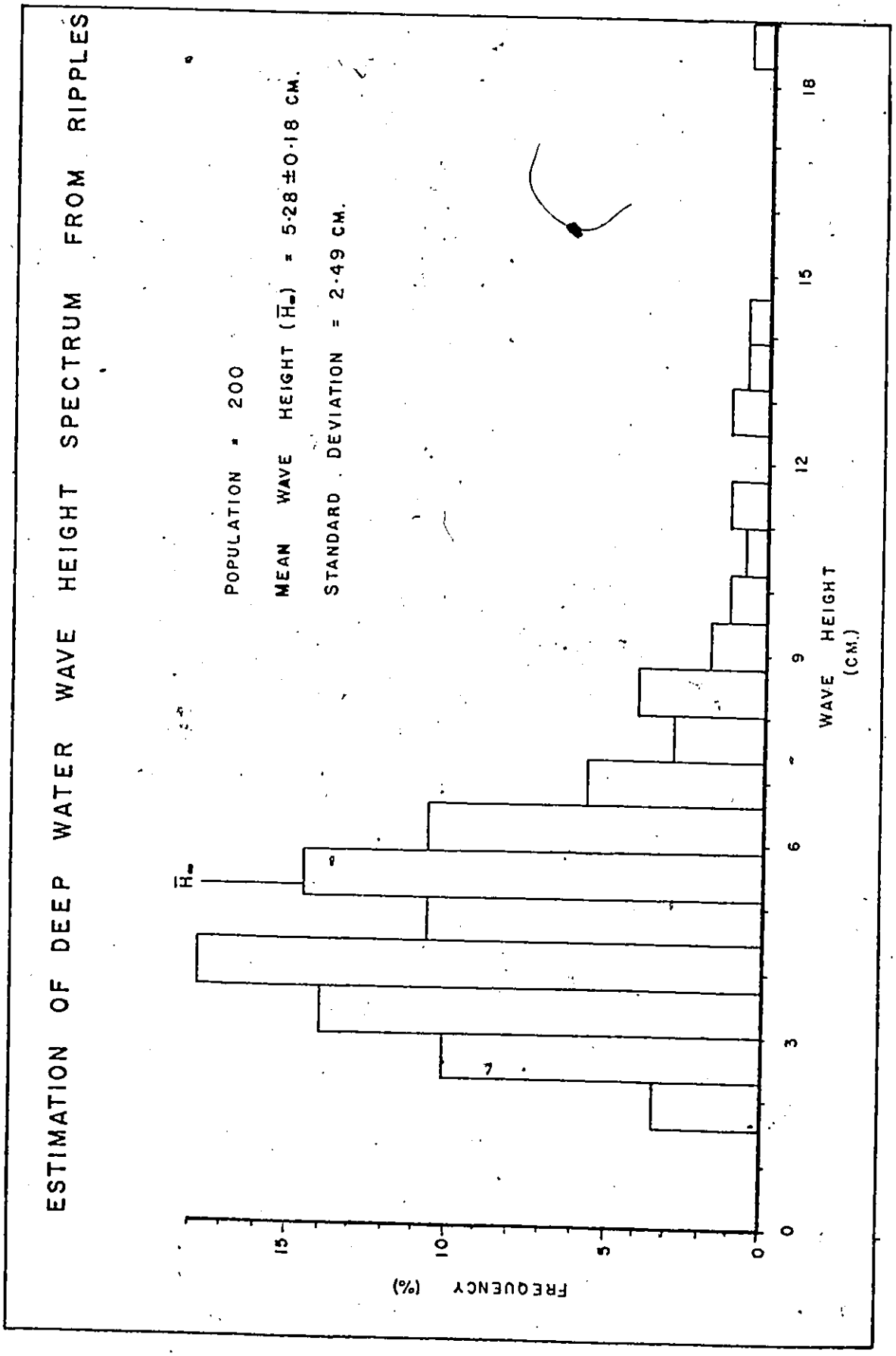

Figure 5-7: Refer to text for detailed discussion of figure.

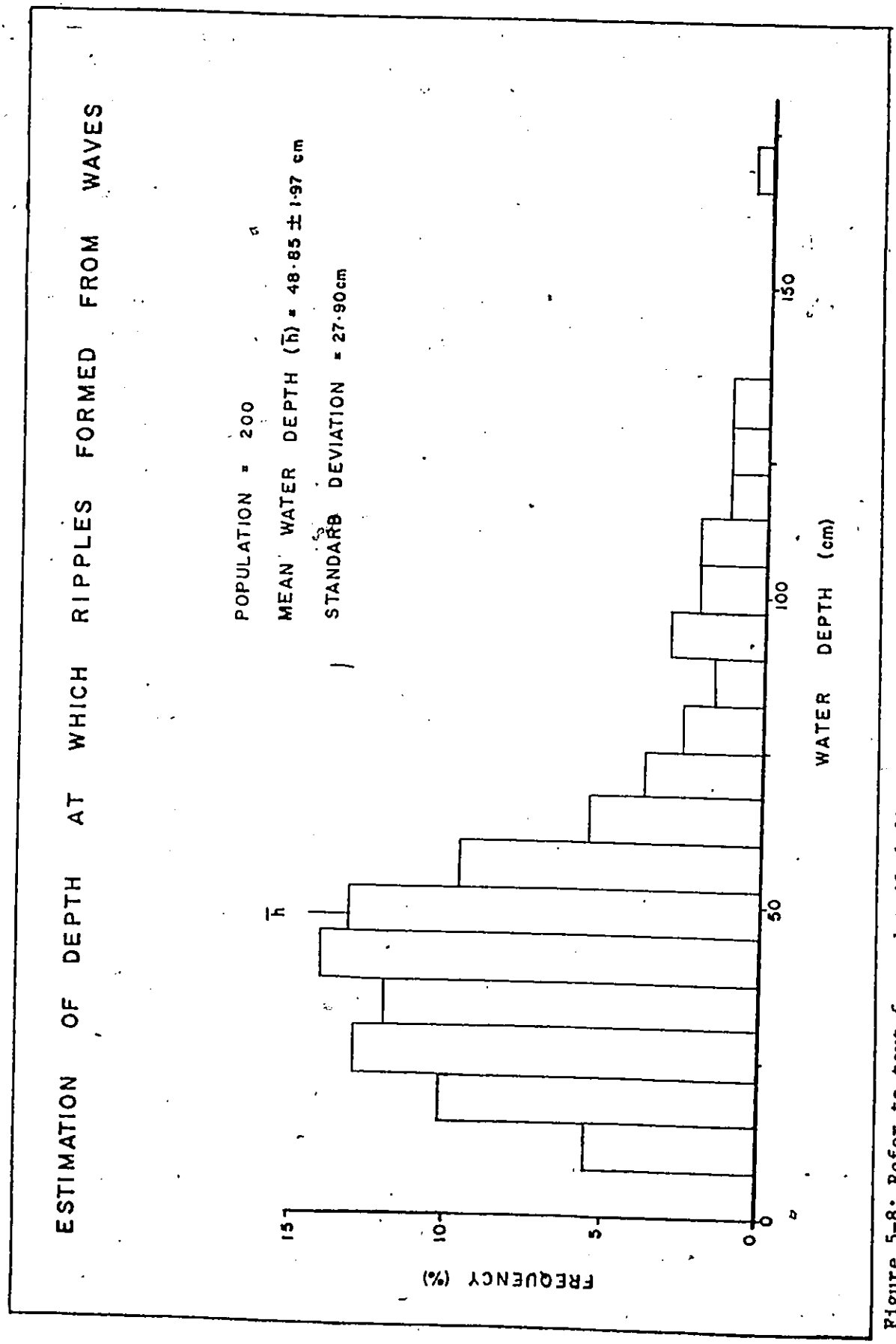

Figure 5-8: Refer to text for a detailed discussion of figure.

approximated by equation 5-26. The predicted beach face slope for the mean sediment size in the study area is 1:415. This gradient is too low to be noticed in the field with the limited available exposures and may explain the scarcity of such recognized features. Galvin (1968) found that the breaker type occurring along a shoreline could be predicted by equations 5-27 or 5-28. Both equations suggest that a spilling breaker type prevailed within the study area. Miller (1976, p. 106) in his study of the surf zone showed that offshore bars were formed by plunging type breakers, whereas spilling breakers tended to erase them. The apparent scarcity of major bar features within the study area would tend to support the spilling breaker type.

Equations 5-29 and 5-30 were obtained from the Miller et al (1977,p.563) curve for the threshold velocity for incipient movement of quartz grains under unidirectional currents. A rough estimate of the depth at which incipient movement of 4ϕ size sand occurs may be estimated from equations 5-23 and 5-29. The predicted depth is $\frac{L_\infty}{2.3}$ or $\simeq$ 1.3 m, which for a beach face slope of 1:415 would give for the prevailing wave conditions, a zone of sand movement roughly 0.5 km wide.

Wave parameters predicted by Airy's wave theory appear to be consistent with the bedforms observed within the study area. Based on the ripple data, the prevailing wave condition appears to have been one of low energy, short period waves that shoaled over a broad, gently sloping, sandy bottom. Spilling type breakers prevailed along most shorelines.

Bretschneider (in Seymour, 1977; p. 252-253) found

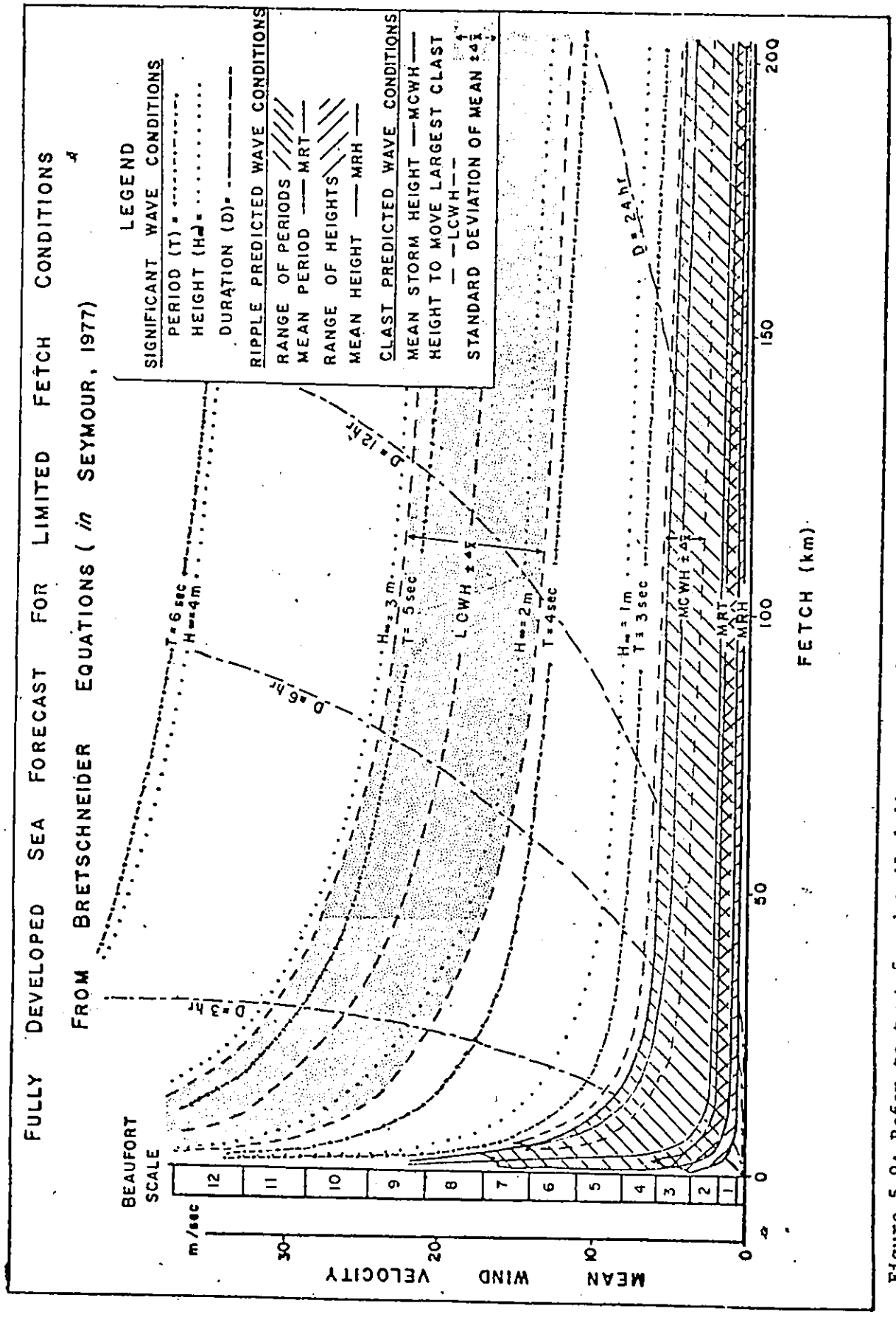

Figure 5-9: Refer to text for detailed discussion of figure.

that the significant wave height and period (greatest 1/3 of their respective magnitude spectrum) under limited fetch conditions could be estimated from the mean wind velocity over a given fetch and given mean water depth (arbitarily taken as = 15 m) by equations 5-31 and 5-32 respectively (figure 5-9). These equations are dependent upon the duration of the prevailing mean wind speed that is given by Bretschneider's (1966, p. 141) equations (equation 5-33) and is incorporated in figure 5-9.

For a basin with a limited fetch of 200 km and mean depth of 15 m wind velocities of breeze force (Fairbridge, 1967; p. 991) would be sufficient to generate the wave parameters predicted from the ripple data. The mean wave height and period could have been obtained from winds of light breeze force (1.1 to 3.3 m/sec; Fairbridge, 1967) while the predicted deep water wave height required to move the mean conglomerate clast required winds of only gentle breeze force (3.4 to 5.4 m/sec; ibid) over 3 hours and a fetch greater than 20 km. The largest clast size required winds of fresh gale force (17.2 to 20.7 m/sec; ibid) over a minimum duration of 5 hours and a fetch over 50 km.

Based on wave parameters obtained from both ripple and conglomerate clast sizes, the model of a restricted fetch across the basin appears reasonable. A barrier isolating the basin from the Apetus Sea (Keppie, 1977; figure 1) to the east must have existed during deposition of the Beekmantown Group, in order to restrict the fetch.

Distances of the order of 200 km, similar to the distance between the Frontenac Axis and Beauharnois Anticline, appear to have been sufficient to generate the required wave intensity without the need for extraordinary wind intensities. From figure 5-9 a discrepancy between the expected mean wave height ($H_\infty \sim 17$cm) and the predicted mean height ($H_\infty = 5.28$ cm) is apparent. Assuming that the discrepancy is the result of internal viscous damping of the wave, an estimate of the time required to decay the wave height is given by equation 5-34. The distance over which the waves have travelled may be approximated from the wave group velocity (equations 5-13, 5-35). The results suggest that a distance of 92 km would be sufficient to dampen the wave height to the indicated value. Adding this distance to the minimum required distance for the wave height (1 km at 15 m/sec to 100 km for 1.5 m/sec wind velocity) the estimated distance across the basin was between 100 and 200 km.

Asymmetric Ripples

The degree of ripple asymmetry may be attributed to superimposition on to oscillatory wave motion of a current, such as a linear current generated by the wave asymmetry (equation 5-36, Clifton, 1976; p. 128), a mass transport current beneath the wave (equation 5-37; ibid, p. 128), a current independent of the shoaling waves, or a combination of these currents.

Clifton (1976; p. 138) plotted the maximum bottom current vs ripple asymmetry from data obtained in studies by Inman (1957) and Tannar (1971) and showed a direct relationship

existed (figure 5-10a). From this data the best fitting curve was obtained (equation 5-38). By subtracting the mean value of the predicted wave induced current from the predicted current required to produced the ripple's asymmetry, it should be possible to estimate the magnitude of any superimposed current (figure 5-10b; appendix 6). Wave induced linear currents appear sufficient to have caused the ripple asymmetry only for β/λ values greater than 0.45.

Silvester (1974; p. 198) found that the wave induced current within the boundary layer for a progressive wave was maximum at a distance of one-third the thickness of the boundary layer (equation 5-39). Knowing the maximum superimposed bottom current (figure 5-10b), the height above the bed where the bottom current is maximum and the bed roughness element (equation 5-40), an estimate of the near-bed velocity may be obtained from the Karman- Prandtl equation (equation 5-42). The estimated mean near-bed velocity ($U_* = 1.31 \pm 0.10$ cm/sec) is sufficient to maintain incipient movement of grains finer than 2.3ϕ size (equation 5-29). This roughly corresponds to the mean backwash truncation point obtained from the grain size distribution data (BW = 2.13 ± 0.03ϕ appendix 3).

Using the near-bed velocity and water depth, estimates of the mean superimposed current velocity may be obtained from from equation 5-42. The predicted current ranges from -2.2 (opposing direction of wave propagation) to 135 cm/sec, having a mean velocity of 27 ± 2 cm/sec (figure 5-11). These values are consistent with tidal current

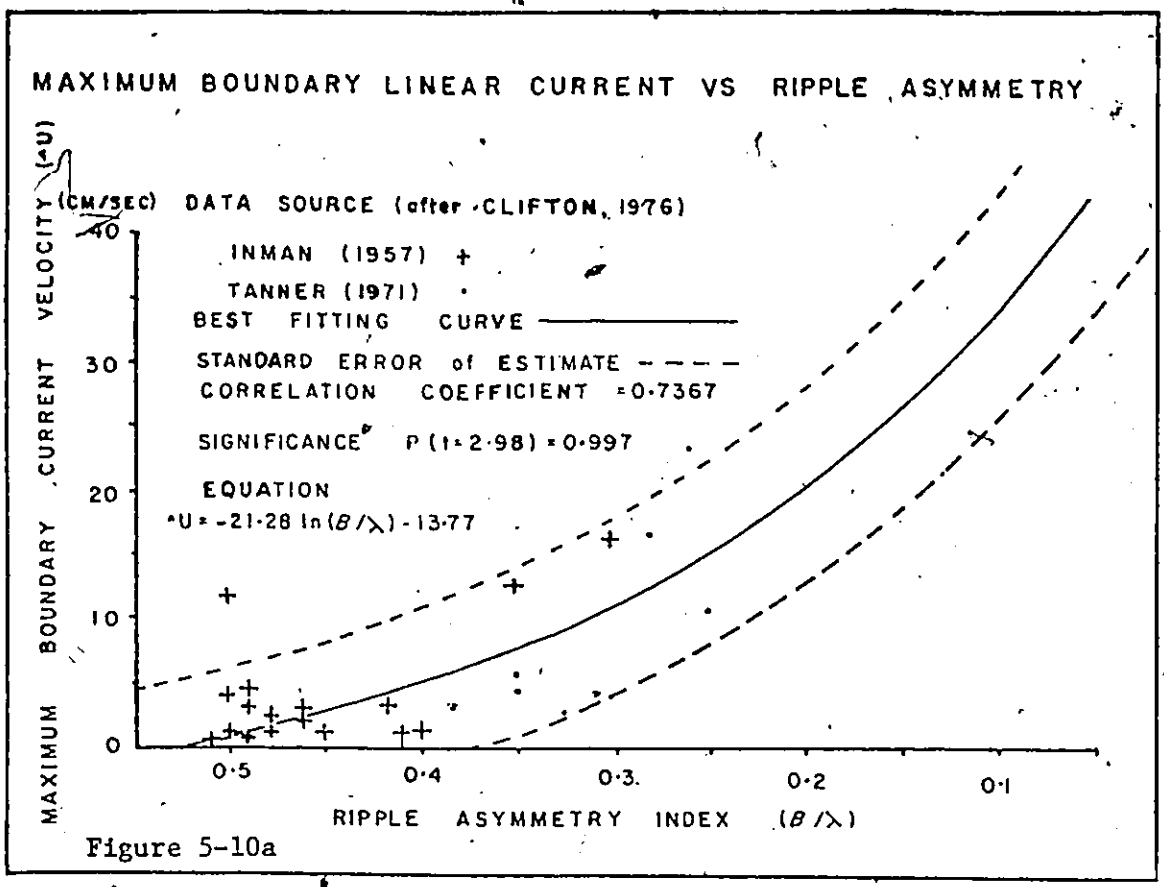

Figure 5-10a

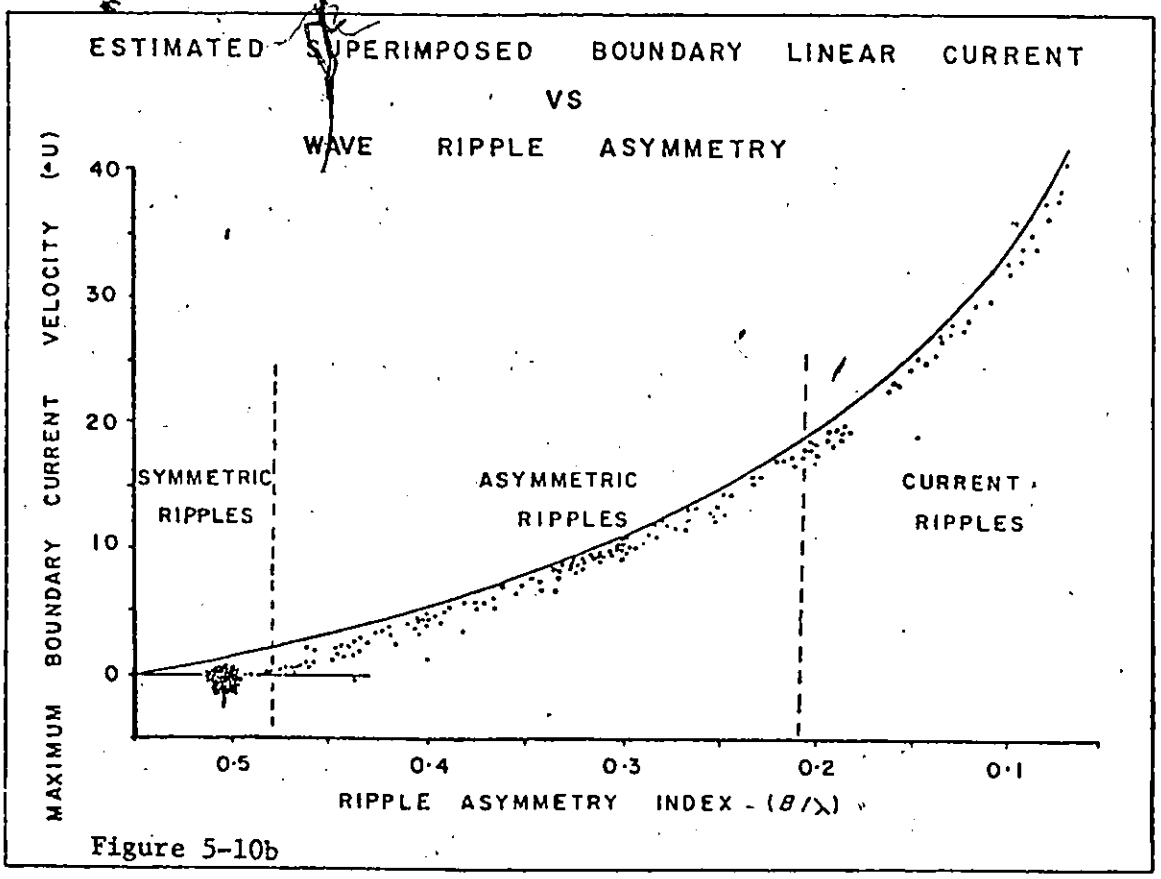

Figure 5-10b

Figures 5-10a and 5-10b: Refer to text for detailed discussion of figures.

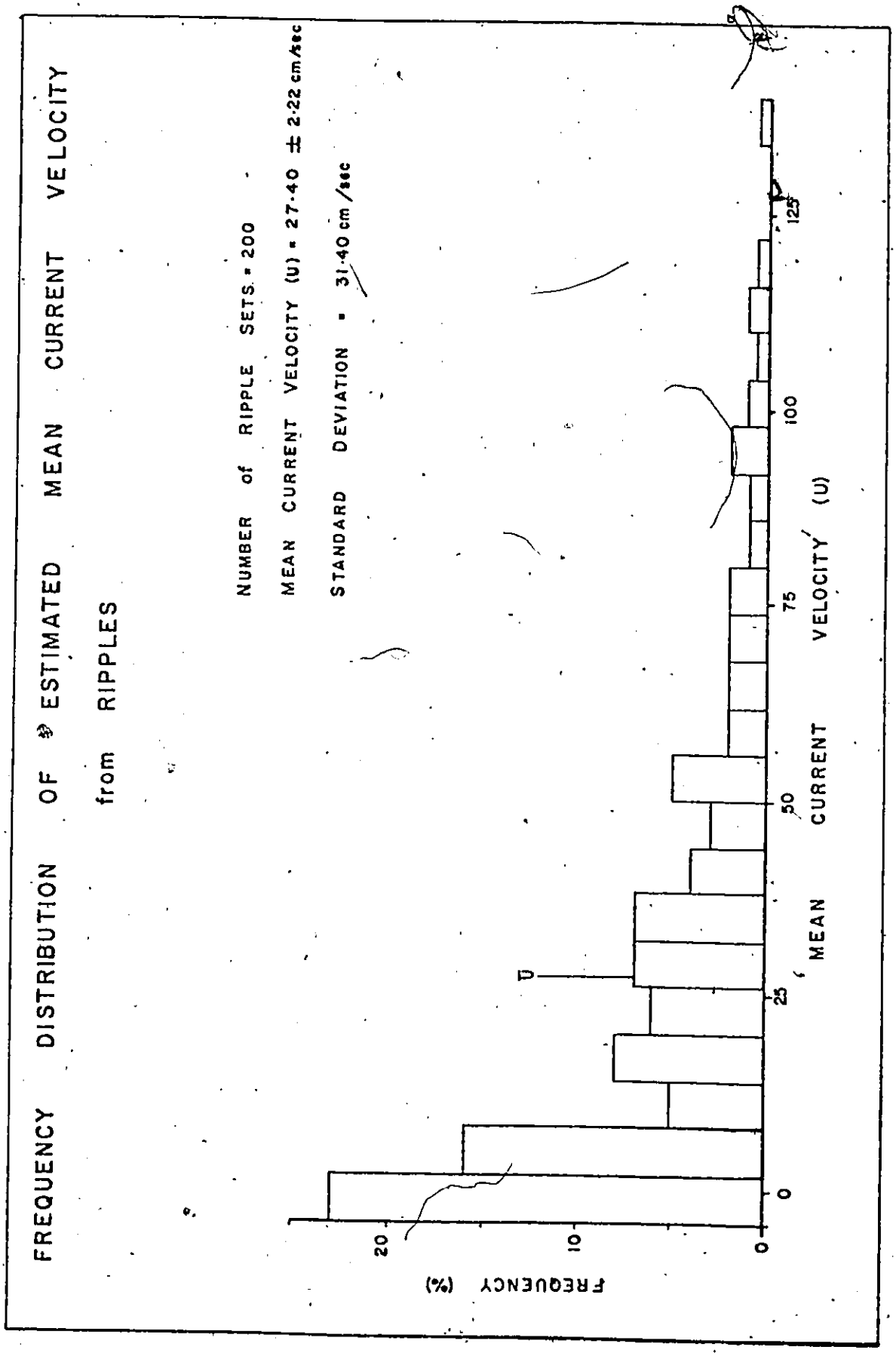

Figure 5-11: Refer to text for detailed discussion of figure.

velocities reported from tidal flats that range from 30 to 50 cm/sec and may reach 150 cm/sec in tidal channels (Reineck and Singh, 1975: p. 359).

Cross Strata

Cross strata within the study area are characterized by their generally small scale, which ranges from 1 to 70 cm in height (mean height = 9.7 ± 0.7 cm; figure 5-12). This range overlaps both the suggested 4 cm (Allen, 1970; p. 70) and 6 cm (Reineck and Singh, 1975; p. 29) height boundaries used to separate ripples from megaripples. Within the basin most cross strata are straight crested to weakly undulatory ripples and megaripples with angular to tangential foresets.

Large planar cross strata (greater than 30 cm in amplitude) occur locally in outliers on the southwestern edge of the Frontenac Axis (location 38, 40), near the southwestern corner (location 10) and northwestern corners of the basin (location 0-4), usually showing a unidirectional orientation. Smaller cross stratal sets commonly form symmetric or asymmetric herringbone cross stratification that frequently shows reactivation surfaces (figure 5-13 and 5-14). In several places (locations 47, 47, & 61) there are patterns of asymmetric herringbone cross strata in which the alternating sets have preferred orientations (figure 6-7). Such features have been interpreted by Klein (1977) as representing time-velocity asymmetry in tidal sequence. On average the mean cross strata are formed in coarser grained sediments ($\overline{Mz}$ =

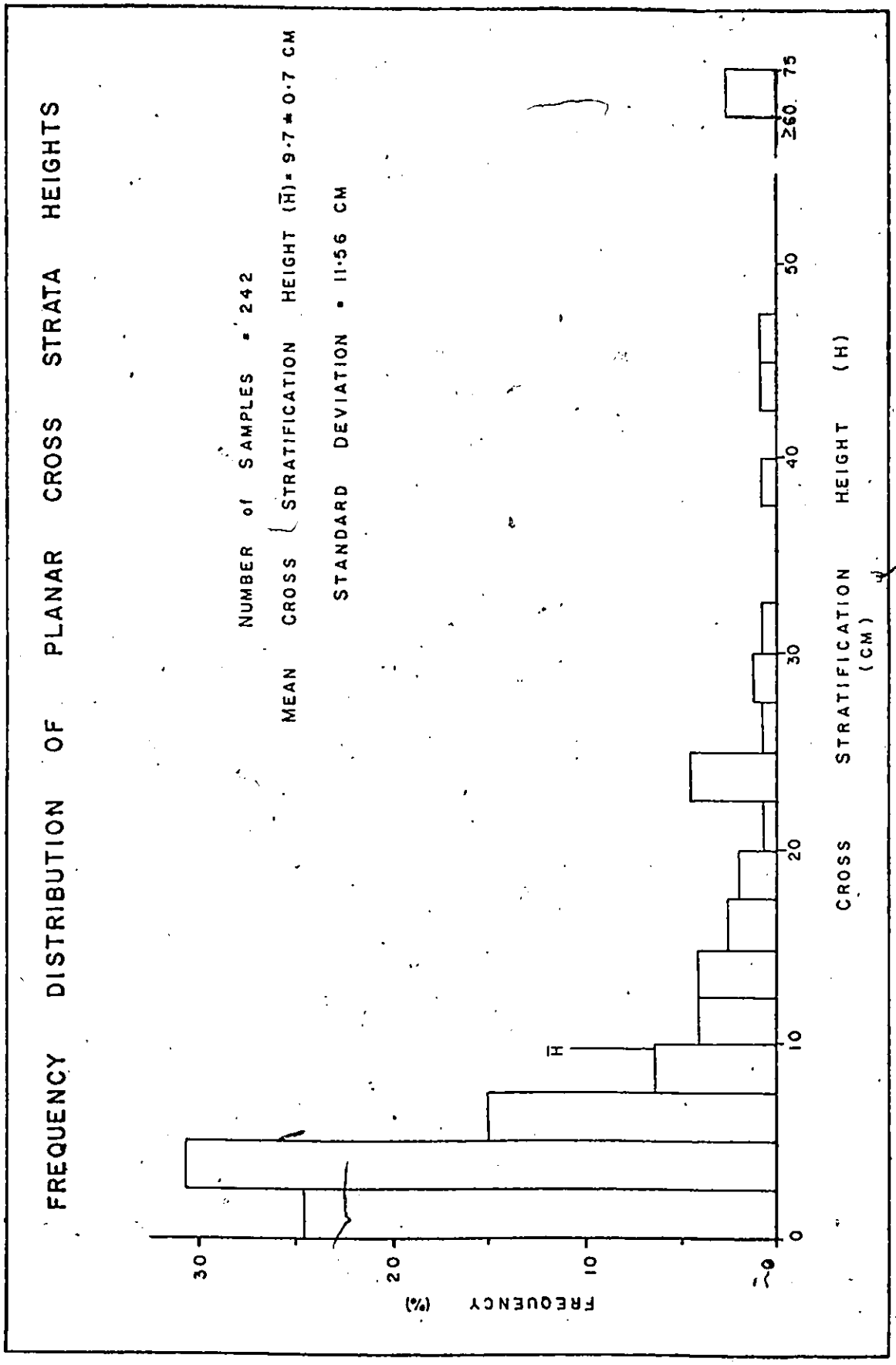

Figure 5-12: Refer to text for detailed discussion of figure.

Figure 5-13

Cross strata with reactivation surfaces (a). The section shows a regular pattern consisting of (1) asymmetric cross strata, (2) small scale ripple sets ?, (3) argillaceous parallel planar sets. Sample from the Heuvelton member, location RR 2.

Figure 5-14

Symmetric herringbone cross strata grading into argillaceous (darker areas at top) parallel planar sets. Dark spots in sections are Endichnia burrows rich in mud. Thin slab section of Heuvelton member, location O-4 (Queensway roadcut west of Ottawa).

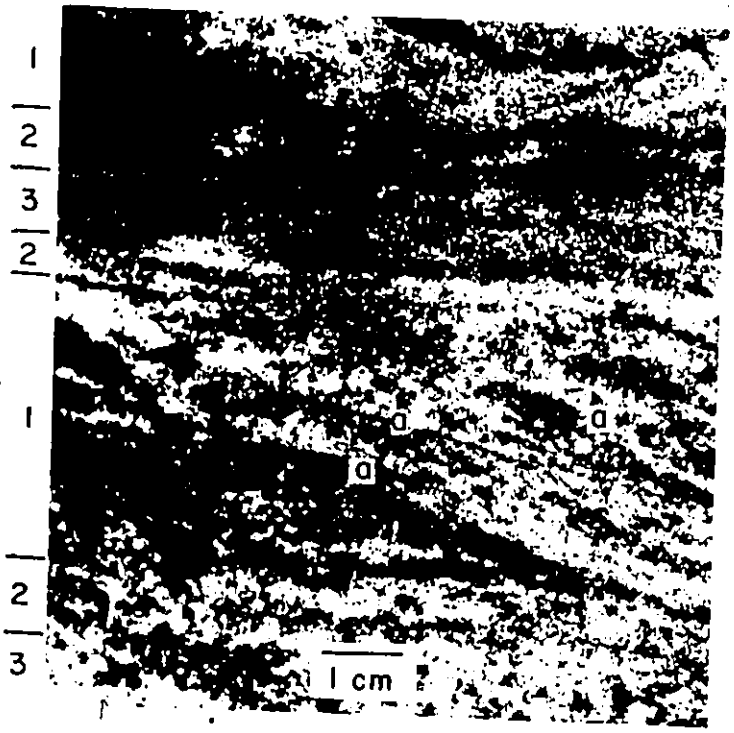

FIGURE 5–13

FIGURE 5–14

2.28 ± 0.08ϕ) than that in which ripple bedforms occur ($\overline{Mz}$ = 2.47 ± 0.05ϕ) suggesting that both the hydrodynamic flow and sediment size change contributed to the change in bedforms (Reineck and Singh, 1975; p.11-12).

Festoon shaped cross strata along the western flank of the Frontenac Axis (location 35, 37) range in thickness from 5 to 50 cm and are up to 1 m in width (location 39). These cross strata occur in medium grained sediments and are associated with large scale channels. Lunate megaripples of similar scale have been reported by Clifton et al (1971) in the inner rough zone of a non-barred high energy coast.

Low angle planar cross strata dipping between 5° and 15° toward the basin (location DW-10, 61^A) occur in some places. Alternation of these beds with conglomerate beds (location 61^A) or the alternating lamination of heavy minerals with quartz grains (location DW-10) suggests that they are beach foreshore deposits, such as sand runs (Bluck, 1967) or swash zone deposits (Clifton et al , 1971).

Paleohydrodynamics from Cross Strata

Analysis of paleoflow parameters is complicated by the unsteady reversible flow and changing depth associated with tidal environments as well as the dependence of the bedforms on sediment size and paleoflow parameters. A partial simplification of the various unknown paleoflow parameters is to assume that the Karman-Plandtl equation (equation 5-42) is valid and that paleoflow velocity is dependent on flow depth.

Allen (1978, p. 177-178) found that a plot of the relative height (defined as the ratio of bedform height to flow depth) versus the Shields-Bagnold non-dimensional bed shear stress, θ, (equation 5-43) relating bed shear stress and sediment mass, gave a continuous smooth curve (ibid ; p. 178). From this curve, Allen (1978; p. 177) obtained the polynomial equation (equation 5-44) that he named the " Stein rule" (ibid; p. 180). The Stein's rule curve initially shows an increase in relative height with increased bed shear stress, up to a critical shear stress ($\theta \sim 1.25$). It then rapidly decreases with additional shear stress until the relative height approaches zero ($\theta \sim 1.50$).

Allen (1978; p. 182-183) recognized three types of response in relative height, depending on the range and magnitude of the unsteady bed shear stress. In regime 1, in which the bed shear stress range is less than the critical shear stress($\theta \sim 1.25$), the relative height increased with increased shear stress. In regime 2, in which the bed shear stress is greater than the critical shear stress the relative height decreases with increasing shear stress. In regime 3, the bed shear stress ranges over the entire Stein's rule curve, the maximum values for the relative height occurring at minimum, intermediate and near maximum shear stress.

Under unsteady flow conditions bedforms may not be able to respond quickly enough to obtain the relative height values predicted by the Stein's rule. However, when the relative heights are averaged over a long time interval, Allen

(1978; p. 168) found the value to be within 10 % of the value predicted by Stein's rule. Since the migration of bedforms generates cross stratal sets, regularity of sets over considerable distances should provide long term averages of the paleoflow parameters using Stein's rule.

In equation 5-44 and 5-45 only the dimensional bed shear stress and the paleoflow depth are unknown and must be estimated independently of the Stein's rule equation. Simons and Richardson (1962) found, in steady unidirectional flow, that the bedform height increased with increase in Froude number (equation 5-46) within the lower flow regime (Reineck and Singh, 1975; p. 8). This is similar to the Stein's rule, regime 1 condition. Since the Froude number relates the mean flow velocity and flow depth, an independent estimate of these parameters by means of the Froude number and Stein's rule can be obtained from bedform height, under limited conditions. The bed shear stress, τ_0, is related to the mean velocity by equations 5-41, 5-42 and 5-44. Using the arbitary boundaries for the initiation of ripples at 0.1 cm height (minimum measurable height) at Fr = 0.15, initiation of megaripples at 4 cm height (Allen, 1970; p. 70) for Fr = 0.30 and the maximum megaripple height of 150 cm (Reineck and Singh, 1975; p. 34) at Fr = 0.40, equation 5-47 was obtained. Under conditions of regime 1 (subcritical flow) a given bedform height should give a similar value of the Froude number through the Stein's rule and by equation 4-47. If the flow conditions were in regime 2 or 3, the calculated Froude number should be less than the

value given by equation 5-47.

With straight or undulatory crested ripples and megaripples with planar sets dominant within the basin, low to moderate tranquil flow conditions (regime 1) appear to have prevailed. By increasing the value of θ by increments in equation 5-45 and testing the resulting Froude number against equation 5-47, an estimate of the paleoflow conditions is obtained (appendix 7). For regime 2 or 3 conditions in which the Stein's rule estimate and equation 5-47 values of the Froude number are not the same, the closest approaching values of Froude number was taken ($\theta = 1.25$).

Figure 5-15 illustrates the relationship of equation 5-44 and the Stein's rule for various sediment sizes for the mean cross strata height ($\overline{H} = 9.7$ cm). For sediment finer than 2.3ϕ size, regime 2 or 3 conditions should prevail, while coarser sediments would prevail in regime 1 conditions. It will be noted that the critical sediment size is close to the mean sediment size for the cross strata found in the study ($D\phi = 2.28 \pm 0.08\phi$. As a test of the validity of the above assumptions the estimated paleoflow strength to sediment graphic mean size was plotted against Allen's (1968, p. 144) bedform fields in figure 5-16. Despite the crudity of some of the approximations used (such as the relationship of bedform height to Froude number) there is good agreement between the Allen's bedform fields and the data over the range in which Allen had experimental data for sediments defining these fields. For regime 2 and 3 data finer than 2.5ϕ size the data no longer fall within Allen's transition field. Absence of direct experimental data in this range prevents

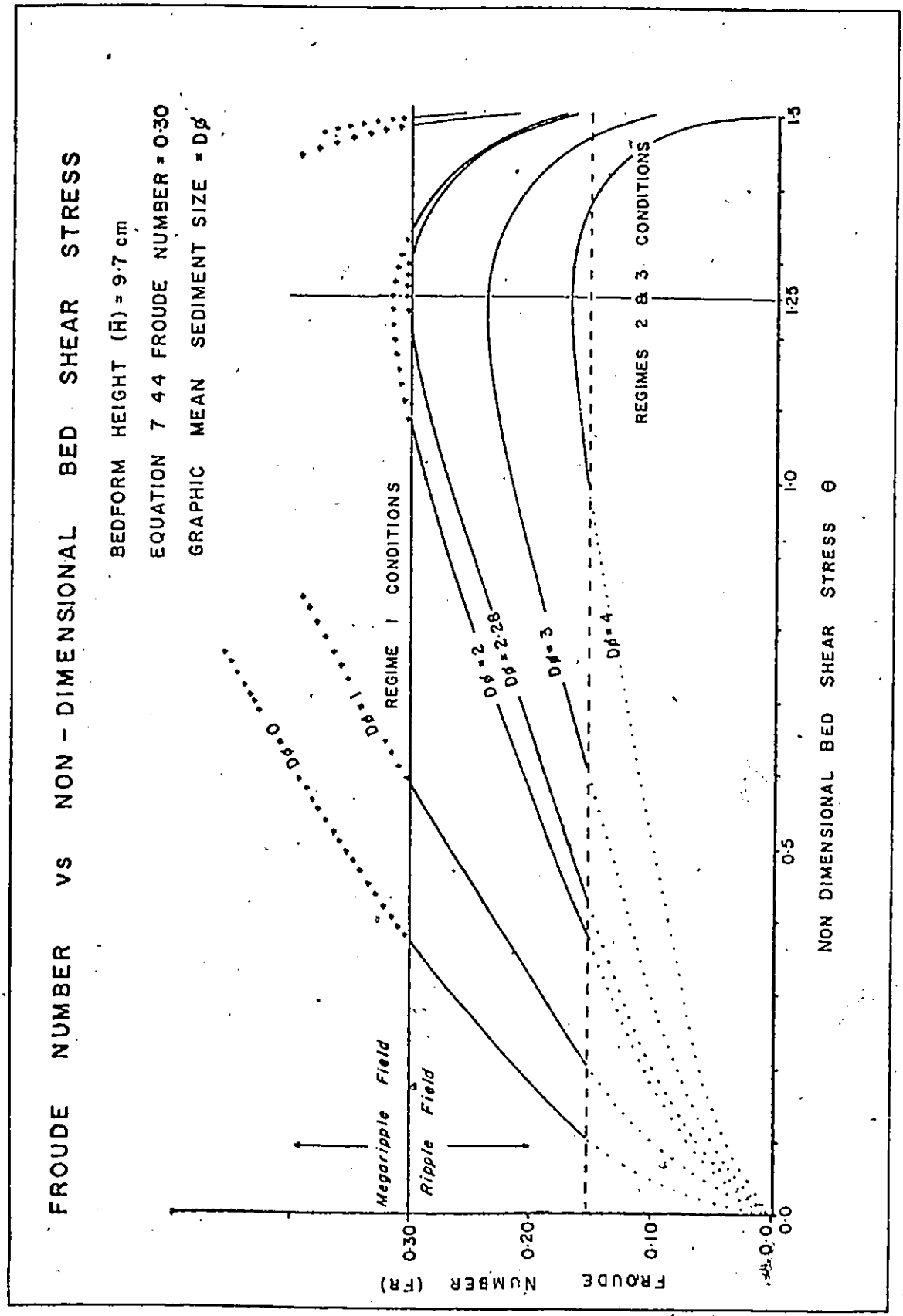

Figure 5-15: Refer to text for detailed discussion of figure.

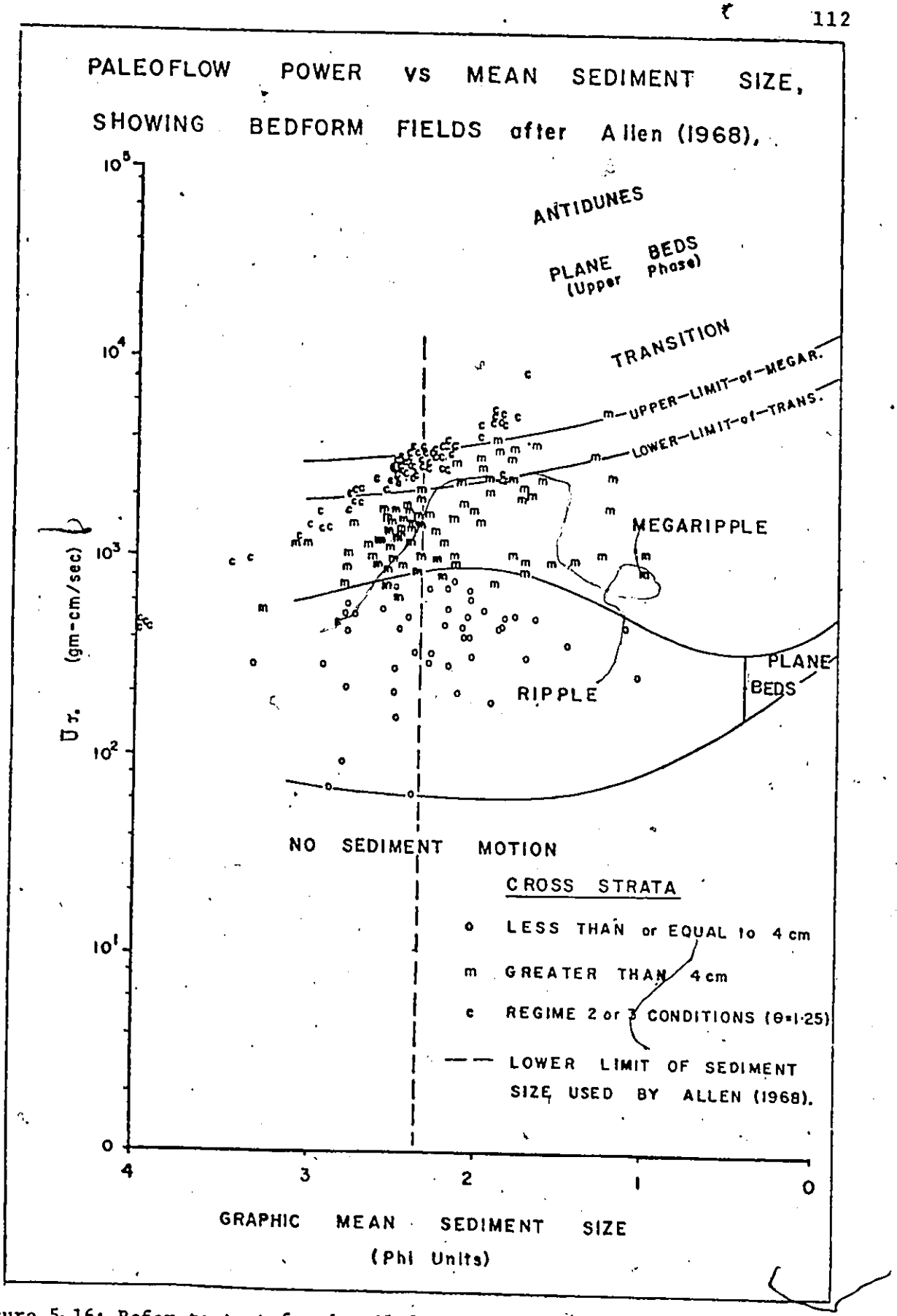

Figure 5-16: Refer to text for detailed discussion of figure.

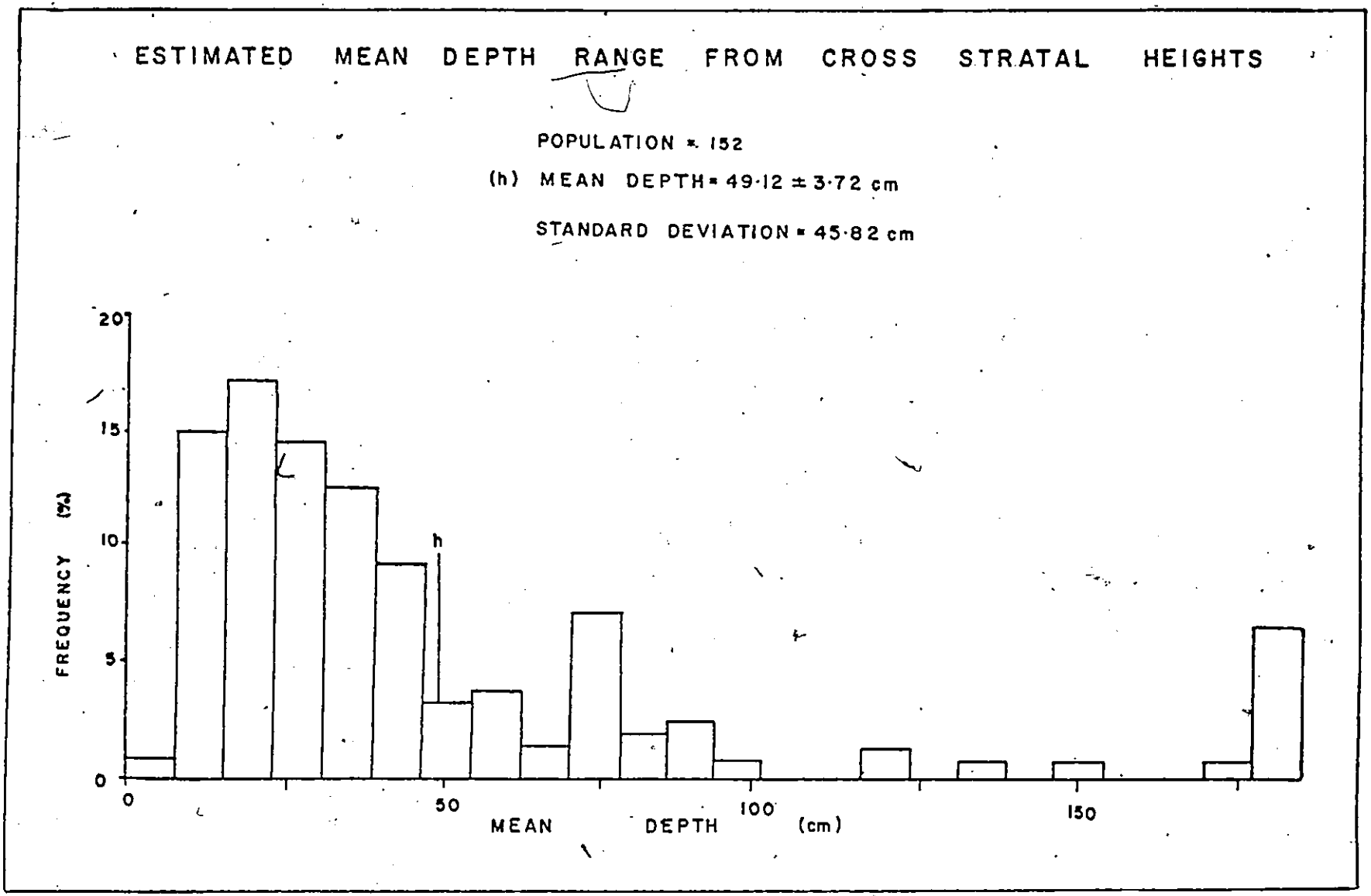

Figure 5-17: Refer to text for detailed discussion of figure.

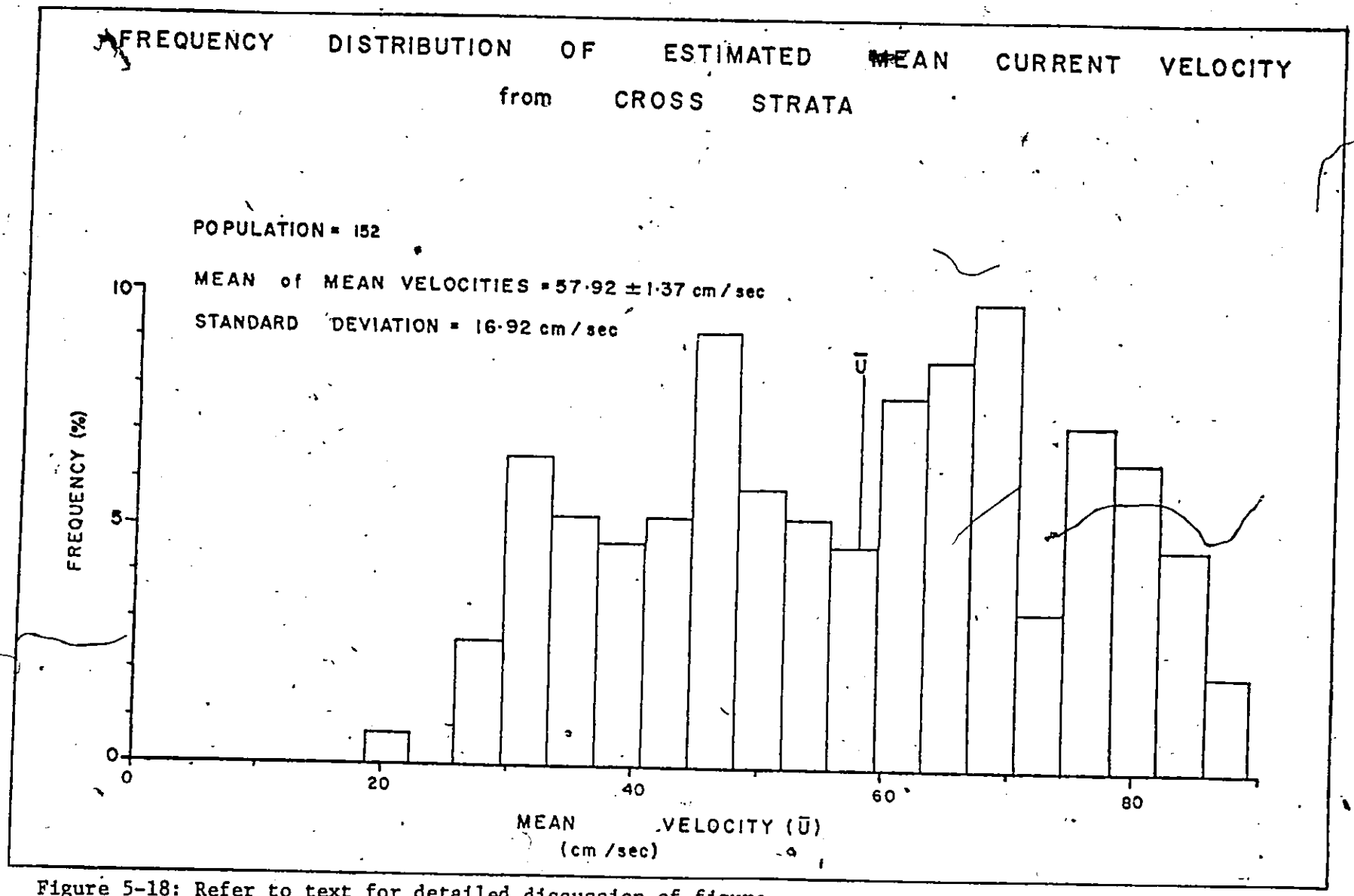

Figure 5-18: Refer to text for detailed discussion of figure.

the testing of these data as to validity.

The predicted cross stratal mean depth (h = 49.1 ± 3.7 cm; figure 5-17) is comparable to the value obtained from ripples using wave theory (48.9 ± 2.0 cm), while the predicted flow velocity, ranging between 8 and 90 cm/sec (mean velocity = 62.8 ± 5.2 cm/sec; figure 5-18) is consistent with velocities reported for modern tidal flats (Reineck and Singh, 1975; p.359).

Evaluation of Paleotides from Bedforms

A regular transition in bedforms appears to occur with increasing current velocity : symmetric ripples ($\overline{U}$ = 1.0 ± 0.1 cm/sec), asymmetric ripples ($\overline{U}$ = 22 ± 1 cm/sec) ripple-sized cross strata ($\overline{U}$ = 36 ± 1 cm/sec), megaripple-sized cross strata ($\overline{U}$ = 70 ± 5 cm/sec) and current ripples ($\overline{U}$ = 71 ± 3 cm/sec figure 5-19a). In contrast, studies by Fleming (1977; figure 6) of the Langebaan Lagoon show the bedform sequence with increasing current velocity in medium sand ($D\phi \simeq 1.7\phi$) sediments was from current ripples to megaripples. Allen (1968, p.144) plotted stream power versus median grain size (figure 5-16) and showed that under the same stream power, a decrease in sediment size may result in a change from megaripple to ripple bedforms. Such a change in sediment size with the bedforms was noted in the study area, with ripples occurring in sediment of Mz = 2.47ϕ size compared to Mz =2.28ϕ size for cross strata.

The response of the bedform to increasing water depth shows a similar transition of bedforms as that occurring

FIGURE 5-19a

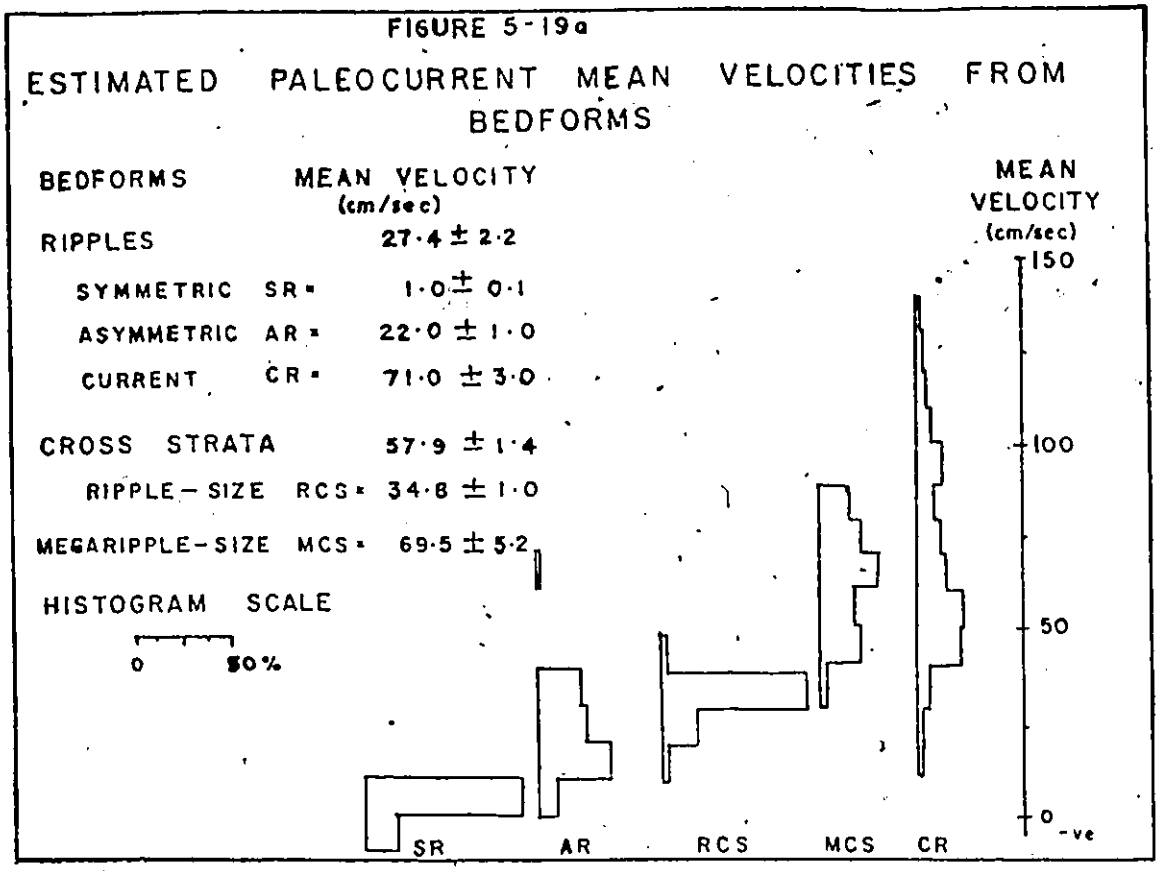

FIGURE 5-19b

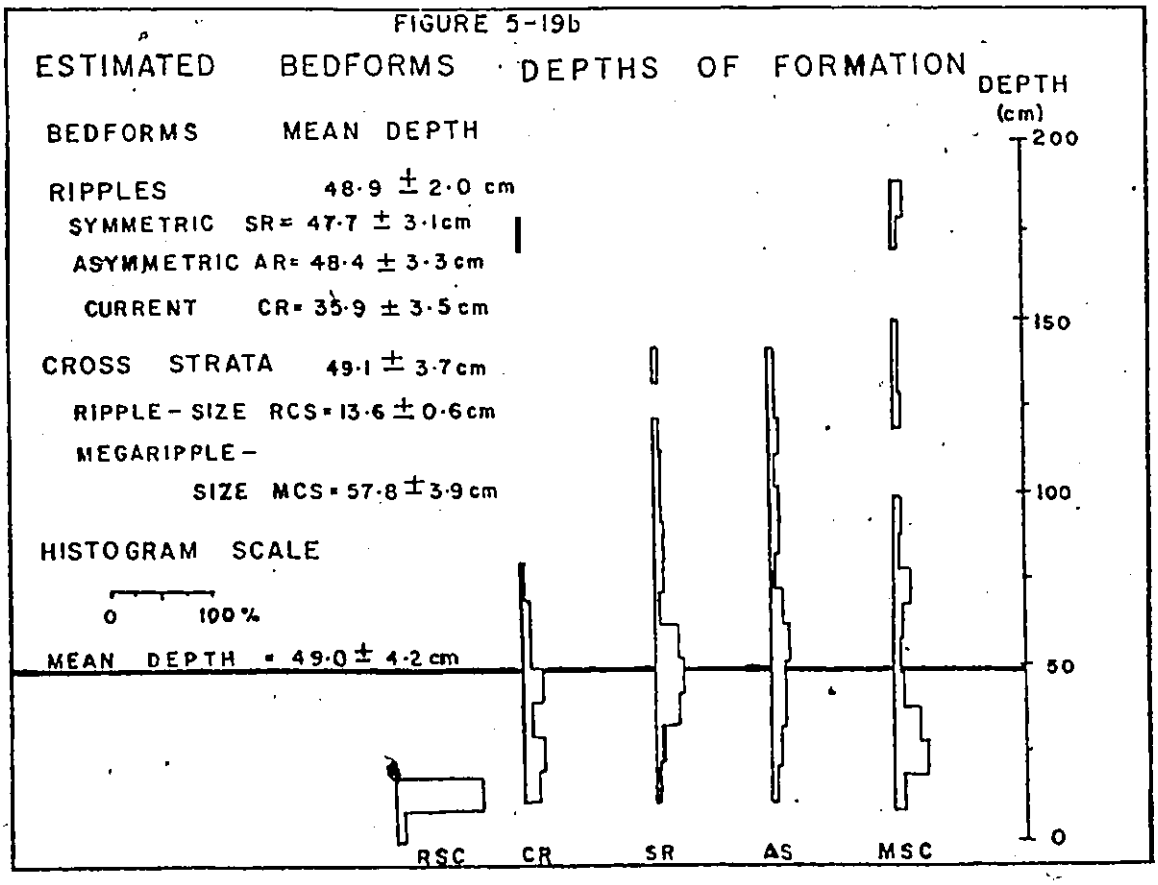

Figures 5-19a and 5-19b: Refer to text for detailed discussion of figures.

with increasing current velocity: ripple-sized cross strata (h = 13.6 ± 0.6 cm), current ripples (h = 36 ± 4 cm), symmetric & asymmetric ripples (h = 48 ± 3 cm) and megaripple-sized cross strata (h = 58 ± 4 cm; figure 5-19b). Figure 5-19b shows that symmetric and asymmetric ripples occurred at depths under 1.4 m, suggesting this was the maximum depth at which waves normally could disturb the sediment. Megaripple-sized cross strata, however appear not to have been so strongly controlled by water depth as were waved-formed ripples. The cross strata occur in water as deep as 1.9 m, suggesting the current velocity has the greatest influence on these bedforms.

Based on either the maximum depth at which the bedforms occur (h = 185 cm) or the doubled value of the mean depth (h = 98 cm) the tide would appear to have a microtidal range (Komar, 1975; p. 137).

Paleocurrents

Examination of ripples and cross strata suggests that the paleocurrent pattern within the Ottawa Basin was more complex than had been indicated by previous studies.

Lewis (1963) did a regional paleocurrent analysis of all exposures of the Potsdam Sandstone (siliciclastics of the Beekmantown Group) in Ontario, Quebec and New York State. The analysis was based on a two-dimensional moving average of the vector means of cross strata occurring within a quadrangle grid system. The results of this study suggested:

1. The prominent paleocurrent directions appeared to

trend south and southeast within the basin.

2. Current deviations adjacent to the Adirondack Massif, Beauharnois Anticline and Frontenac Axis suggested the occurrence of structural highs at these locations at the time of deposition.

3. Consistency of the vector direction in various lithofacies was interpreted as indicating a stable paleocurrent pattern over a long interval of time.

Clark (1966, figure 7) plotted both ripple marks and cross stratification from the Covey Hill and Chateauguay Formations in the Chateauguay region. In his study ripple axes were plotted to the nearest degree while cross strata were plotted to the inter-cardinal points (45 degrees interval; figure 5-20). The rose diagram shows a prominent southeast to east paleocurrent direction in the area southeast of the Beauharnois Anticline, supporting the trend noted by Lewis (1963). Despite displacement of the order of 450 m along the Stockwell-Havelock Faults (Clark, 1966; p.43), no distinguishable change in the paleocurrent pattern across the fault is evident. This would appear to indicate a stable eastward paleoslope throughout the deposition of the Potsdam Formation, east of the Beauharnois Anticline.

Physical differences in the bedforms have been reported between the Potsdam members in this area. The Basal member (Covey Hill (restricted) Member) is characterized by trough cross strata that range from 0.1 to 0.5 m in height (Clark, 1966; p. 16; Hofmann, 1972; p. 17-18). The Ausable Member (Rivière aux Outardes Member) contains large swales (8 m wide by 1.5 m deep;

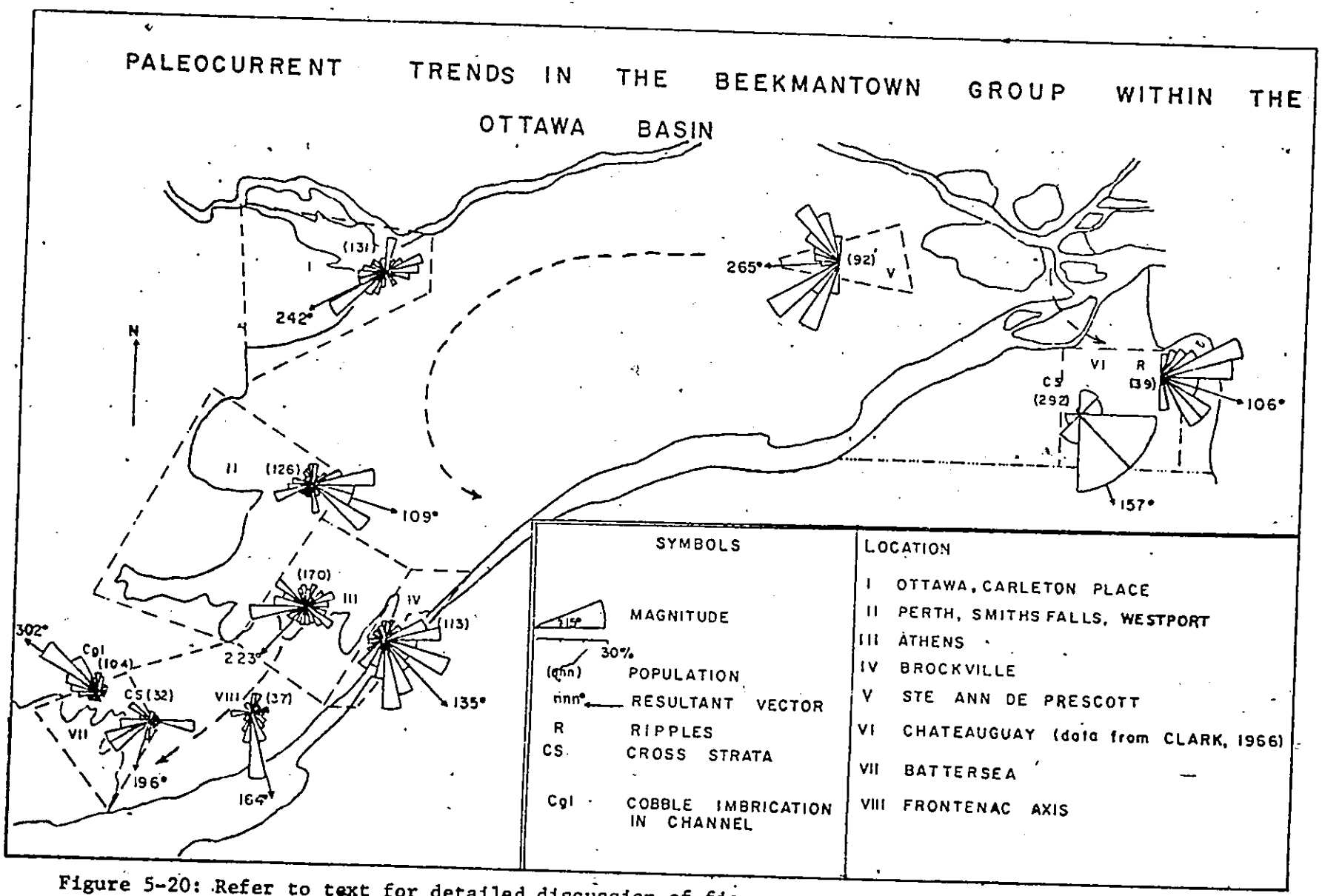

Figure 5-20: Refer to text for detailed discussion of figure.

Clark, 1966; p. 16) and ripples. The Keeseville Member (Cairnside Member) is dominated by small scale cross strata less than 10 cm high (Lewis, 1963; p. 37) and abundant ripples (Clark, 1966; p. 24). These changes in bedform scale are interpreted as representing a decrease in wave energy from the deposition of the Ausable to the deposition of the Keeseville Member.

Preliminary paleocurrent measurements of ripples and cross strata within the study area established that ripple orientation normally gave just as consistent paleocurrent orientations as did the cross strata and that both bedforms gave multimodal orientations. Both bedforms were subsequently grouped in regional rose diagrams and plotted at 15 degree intervals (figure 5-20).

The resultant vectors of the 7 regional rose diagrams show a prominant counter clockwise circulation within the basin. Directional modes are either bipolar (area 2 and 3), bimodal (area 4 and 6) or multimodal (area 5 and 7). Mode peaks are often separated by as little as 45 degrees, suggesting that larger size intervals than 15 to 20 degrees would not be able to resolve the individual modes (Clark, 1966; figure 7).

In some sections (location 48 and 61) the bedforms show preferred orientations with ripples forming one mode and cross strata another (figure 6-9). These orientations are interpreted as resulting from velocity asymmetry during different intervals of the tidal cycle. On a regional scale this time phase asymmetry in orientation averages out and no apparent orientation is dominated by the ripples or cross strata.

Deflection patterns in the paleocurrent orientation

near the edges of the Frontenac Axis are similar to those observed by Lewis (1963, figure 17), suggesting the existence of a structural barrier along the axis during siliciclastic deposition. Outliers occurring across the Frontenac Axis show a weak bimodal orientation with the major orientation towards the south. The pattern may indicate the occurrence of restricted flow across the Frontenac Axis.

Channels

Within the basin, channels are marked by extreme bioturbation, Skolithos burrowing to depths of 20 to 60 cm and petrological differences from beds they cut (such as increased mud, carbonate or feldspar). These channels range between a few centimeters and a meter in depth (location 61) and vary in width to depth ratio from 15 to over 50. The channels are commonly surrounded by herringbone cross stratified beds and are considered to be tidal in origin. The infrequency of these channels at most locations suggests that the tidal flat gradient and tidal range were low.

West of the Frontenac Axis there are large scale channels (location 36) up to 7 m deep with width to depth ratio less than 3. The channels are filled with medium grained, poorly sorted quartzitic sandstone marked by channel-fill cross strata (Reineck and Singh, 1975; p.91). Bed load deposits of small cobble size clasts occur in some channels with the clasts dipping in a northwestern direction paralleling the channel axis (figure 5-20). The nature of these channels suggests both high-

er energy and volume of drainage of the tidal flats in the west side of the Frontenac Axis than those within the basin.

Flaser and Lenticular Bedding

Flaser and lenticular bedding (Reineck and Singh, 1975; p. 97-113) occur within the Theresa and Buck Bridge Formations. Within the Heuvelton member, flaser bedding ranging from simple to bifurcated wavy types (ibid; p. 98), with both shale and micrite lenses occurs within the quartzose sandstone (figures 5-21). Wavy and lenticular bedding occur within the Theresa Formation and March Member, where fine quartzose sandstone lenses occur in argillaceous dolomitized micrite (figure 5-22). Gradation from flaser to lenticular bedding occurs both vertically and laterally in the section, reflecting variation in paleoflow velocities and duration.

Bioturbation

Bioturbation within the siliciclastics ranges from traces in the Keeseville, to extreme within the Theresa Formation (figure 5-24). The bioturbation tends to increase with increased mud and carbonate content.

Skolithos and Diplocraterion burrows occur widely within the Heuvelton member. Diplocraterion burrows commonly show high density along regularly spaced bed intervals (figure 5-23). Burrows range from 5 to 15 cm in depth, frequently show reactivation features (Reineck and Singh, 1975;

Figure 5-21

Wavy flaser bedding; having long laminae of mud (dark) lenses in very fine to fine quartzitic sandstone laminae, with small scale ripples. Heuvelton member, location 0-4 (Queensway section west of Ottawa).

Figure 5-22

Lenticular bedding with connected flat lenses; argillaceous dolomitized micrite (dark) with lenses of medium quartzose sandstone partly disturbed by burrowing. March Member, location 56 (Highway 42, 6 km east of Soperton).

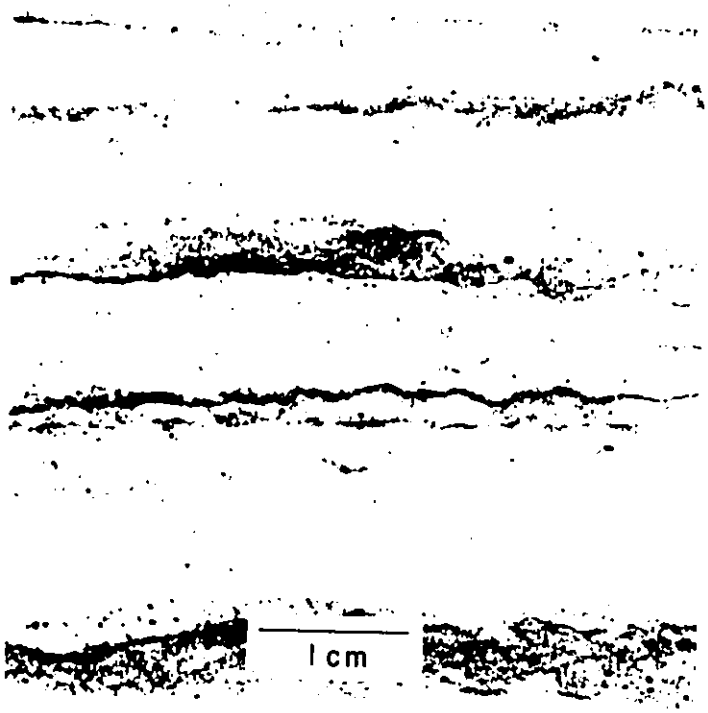

FIGURE 5-21

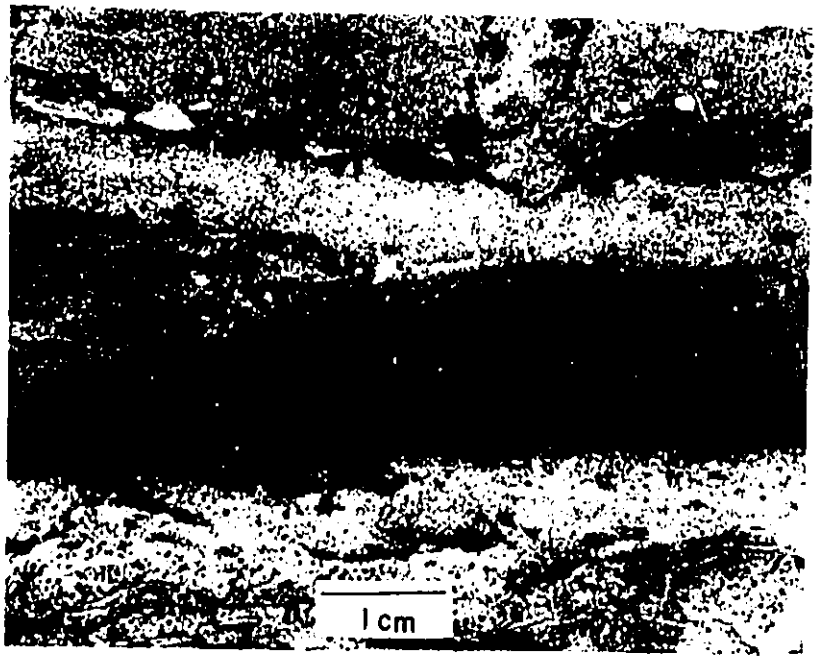

FIGURE 5-22

Figure 5-23

Diplocraterion burrows at regularly spaced intervals in the Heuvelton member. Location 17 (hammer = 35 cm long).

Figure 5-24

Extremely bioturbated sediments; bioturbation has destroyed all evidences of primary sedimentary structures in this Theresa Formation sample. Sample from near top of formation shows lenses of fine quartzitic sandstone (a). Brachiopod shell fragments (black clasts) common. Location 401-6 (junction of MacDonald-Cartier and Thousand Island Highways).

FIGURE 5-23

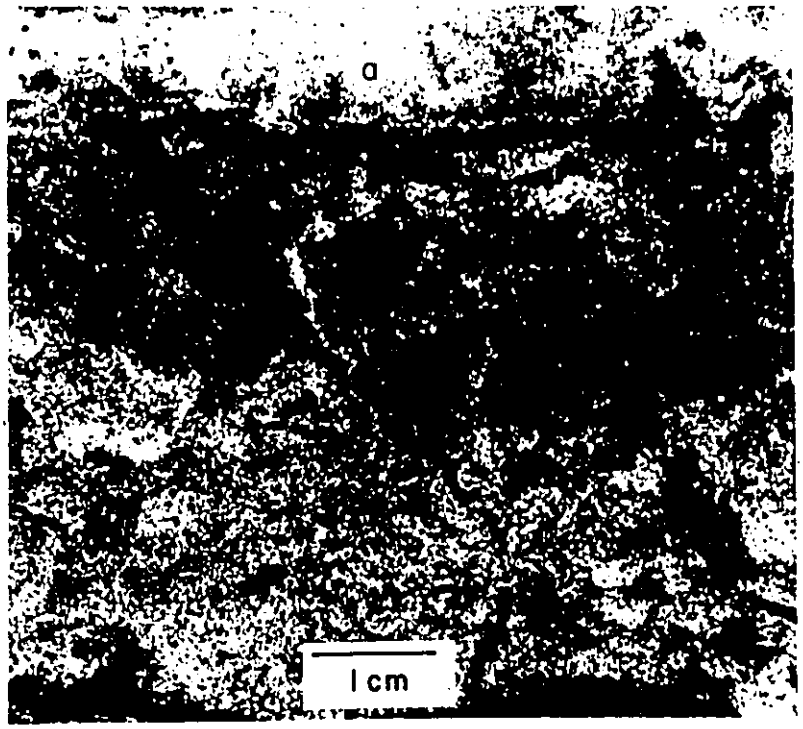

FIGURE 5-24

p. 152). Skolithos burrows range from 5 to 20 cm in depth along most beds, but in large tidal channels may extend to depths of 60 cm.

Conodonts were found in all siliciclastic beds in which sufficient carbonate exists to permit extraction, suggesting a wide distribution of the fauna within the basin. Gastropod fragments particularly Ophileta and Eccliomphalus shells occur sparsely throughout the Buck Bridge Formation.

Carbonate Sedimentary Structures

The carbonate strata (March Member and Beauharnois Formation) within the study area may be grouped into six standard microfacies (Wilson, 1975; p. 63-69) that are predominantly associated with restricted lagoons or protected supratidal or intertidal environments. Occurrence of rhythmite bedding transitional between the siliciclastic and carbonate strata supports the occurrence of a gradual change in paleoenvironments between these within the March Member.

Laminated to Bioturbated Micrite (SMF 19)

Laminites occur extensively within the middle and upper strata of the Beauharnois Formation (appendix 1). The microfacies occurs as a finely interlaminated dark argillaceous dolomitized micrite (N2 to N3) and lighter dolomicrite (N3 to N5). Fine sand or silt size grains are frequently scattered along the dolomitized micrite laminae. In some places

the normally millimeter thick laminae thicken to centimeter scale beds consisting of dolomitized pelmicrite. The microfacies grades from stromatolitic calcisiltite and rhythmite beds to homogeneous unlaminated dolomitized micrite.

Gastropods are the only recognizable fauna within the microfacies. Vugs of sparite and small desiccation cracks occur sporadically. The microfacies is considered to represent deposition in very restricted tidal bays and ponds (Wilson, 1975; p. 68). Its position between the stromatolitic and homogeneous micrite microfacies as well as the high degree of bioturbation favours a low subtidal or nearshore environment where aerobic conditions prevailed, with occasional storm-generated waves to disturb the bottom sediments.

Stromatolitic Micrite (SMF 20)

Stromatolite microfacies prevail within the March and lower Beauharnois strata. The microfacies consist of alternating laminae of trapped detrital mud, sand or micrite up to 1 cm thick with thinner darker micrite laminae (N3-N4). Thinning and thickening of laminae is common, particularily over irregularities. Both smooth mat (Kinsman and Park, 1976) and columnar stromatolites (Hoffman, 1976) occur.

The smooth mat stromatolites (figures 5-25) consist of generally regular laminae of fine sand or mud rich micrites that alternate with thinner dark micrite. The detrital laminae range from a few mm to nearly a cm in thickness with most laminae less than 5 mm thick. Gebelein (1976, p. 385) considered

Figure 5-25

Smooth mat type stromatolite (SMF 20); Dolomitized micrite or dolomicrite alternating with shale and calcisiltite laminae. Lamination irregular, cut by small scale desiccation cracks to depths of one or more laminations. Beauharnois Formation, location 0-6.

FIGURE 5-25

Figure 5-26

Smooth mat and bulbous stromatolites (SMF 20); small scale bulbous stromatolites (right of hammer head) interfingering with arenaceous smooth mat type stromatolites. March Member, location WRR 3 (hammer handle = 35 cm long).

Figure 5-27

Bulbous type stromatolites(SMF 20); overturned large scale bulbous stromatolite showing internal basal smooth mat type laminations. The stromatolitic top has been truncated with further growth occurring horizontally in the direction of primary paleocurrent flow (?). SMF 24 microfacies on crest of stromatolite probably caused by wave action. Beauharnois Fm., location 0-8 (hammer handle =35 cm long).

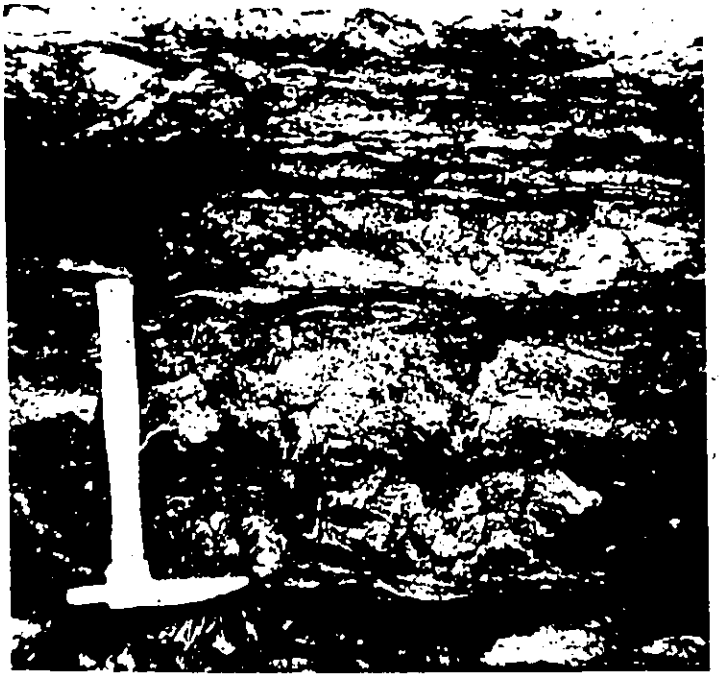

FIGURE 5-26

FIGURE 5-27

Figure 5-28

Smooth mat type stromatolite (SMF 20) associated with sulphide mineralization; stromatolitic lamination interfingering and overlapping sulphide mineralization. Pyrite and galena (1) infill vugs that are blackened by sulphide mineralization. Onkoids and rip-up clasts of the underlying beds occur in center. Quartz and sparite replace gypsum (?) in vugs (2) and partly fill burrow. Beauharnois Formation from location HW 16.

FIGURE 5-28

the smooth mats to prevail in low to moderate wave energy upper tidal zones where reworking and injection of surface sediments by grazing and burrowing invertebrates is retarded. In modern environments the lower boundary of the smooth mats, where invertebrate reworking eliminates laminated sediments, occurs between the 25% and 50% submergent frequency (Gebelein, 1976). Frequent occurrence of desiccation cracks and glauconitic lag deposits associated with the smooth mats substantiates the intermittent exposures of the mats, while onkoids and ripped up intraclasts with concentrations of sand grains suggest intervals of high energy currents over the mats (locations 44, 46, 48, 56 and 0-6).

Columnar stromatolites (figure 5-26 and 5-27) occur less frequently and are generally closely associated with smooth mat form. Sizes range from small domed mounds (locations RR3, 0-6 and 0-7) to massive columns up to 0.5 m high and 0.8 m wide (location 0-8; figure 7-25). The presence of onkoids between the larger columns and truncation of their tops suggest that these stromatolites occur within a high energy wave zone, such as a surf zone.

At a few locations (location HW16) vugs of sparite, dolosparite, galena or pyrite distort the laminations of the stromatolite, suggesting syngenetic deposition (figure 5-28). One possible origin for the metal sulphide deposits within a dominantly oxidizing shallow water environment may be the co-precipitation of metals in the host rock dolomite under conditions of hypersalinity. During subsequent dolomitiz-

ation the metals formed complexes with products of algal decomposition and were released into pore solutions that migrated to the site of deposition (Trudinger and Mendelson, 1976; p. 670).

Micrite with large Onkoids (SMF 22)

Dolomicrite or dolosiltite onkoids ranging in diameter from a few mm to several cm occur between columnar stromatolites (location 0-8) as channel lag deposits (location 0-7) or intermixed with ripped up intraclasts in beds alternating with SMF 19 and SMF 21 microfacies (location RR3; appendix 1). The microfacies occurs in places of high energy aggregation such as on the edges of shoals lagoons or channels (Wilson, 1975; p. 69).

Unlaminated Homogeneous Unfossiliferous Micrite (SMF 23)

Unfossiliferous deposits of unlaminated homogeneous dolomitized micrite increase in abundance up the Beauharnois succession. The microfacies consists of homogeneous micrite in thin to thick beds with no evidence of macrofauna. Mud content varies widely, sometimes approaching the composition of calcisiltites (location 15 and 48). Selenite crystals, vugs and sheet cracking on or within dolomicrite beds suggest formation in evaporitic tidal ponds (location 43 and 401-3; appendix 1) while the occurrence of allochthonous gastropod deposits at the boundary of SMF 19 and SMF 23 beds favours an environment marginal to euxinic conditions within the subtidal zone (locat-

ions 43, 55 and 73). At other locations, rapid changes from SMF 19 and SMF 23 to SMF 24 microfacies indicate the deposition was influenced by major storm waves.

Coarse Lithoclastic-Rudstone or Floatstone (SMF 24)

Clasts of SMF 19 or SMF 23 microfacies in a matrix of quartzose sandstone or sandy calcisiltite occur widely throughout the carbonate strata. The deposits were found as thin to medium thick beds over the beds of SMF 19, SMF 20 and SMF 23 microfacies or as channel fills and are considered to have formed by high energy storm or tidal activity (Wilson, 1975; p. 62; figure 5-29).

Lag Deposits (SMF 14)

Sand or mud rich glauconitic deposits occur within the Heuvelton (locations 27, 28, 47 and 48) and lower March (locations 46, 49, 57 and 0-4). They range from thin mud laminae coating ripples (locations 47 and 48) figure 5-4) to medium sand rich beds several centimeters thick (location 46). The presence of desiccation cracks cutting the microfacies suggest periodic exposures.

Round black coated sparite pebbles occur within the cross strata at location 48. They are thought to have been formed as algal coats in subaerially exposed saline ponds in supratidal environments (Wilson, 1975; p. 81; figure $5\text{-}3_0$).

Figure 5-29

Coarse lithoclastic rudstone (SMF 24); Channel deposit consisting of dolomicrite and dolomitized micrite clasts in an argillaceous dolomicrite cement. Beauharnois Formation from location 0-6.

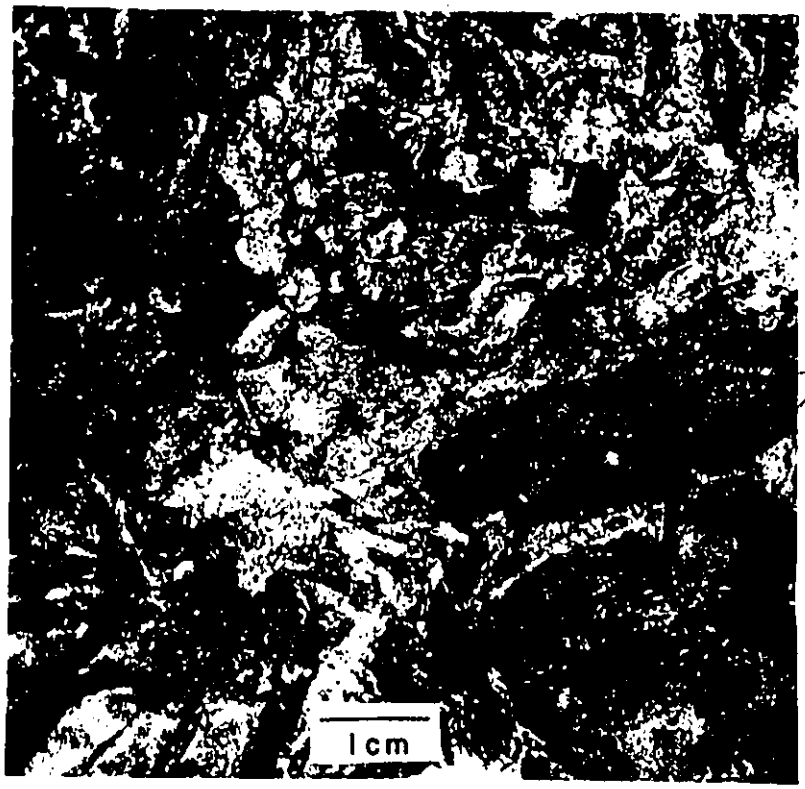

FIGURE 5-29

Figure 5-30

Black coated sparite pebbles (SMF 14); the coating on the clasts vary from a few mm thick to the entire clast. The clasts occur in quartzitic sandstone cross strata with sets dipping in direction of pen tip. Heuvelton member, location 48.

Scale: pen = 16 cm.

FIGURE 5-30

Beach Profiles

The sedimentary structures and textures suggest four types of beach profile within the study area. The form of the profile was dependent upon the relief of the basement which the beach overlaps or terminates against, the sediment size and type available, the type and activity of organisms and or wave intensity in relation to the strength and range of the local tides (figure 5-31).

Storm Beach Profile

Cobble and boulder size clasts were deposited at the base of steeply sloping basement ridges where the waves were abruptly broken before significant shoaling had occurred. Only under severe storm conditions could the largest clasts be moved significantly (figure 5-1). Their rapid gradation into lenticular carbonate strata (location 401-4) or normal wave and tidal controlled sandstone (location 10) support the infrequent movement of these clasts (figure 5-31a).

High Tide Shingle Beach

Pebbles were deposited where the basement slope was gentle enough to disperse some of the wave energy by shoaling prior to breaking (locations 19, DW-3, DW-6, DW-11). Deposition occurred primarily along the high tide terrace.

The transition from the shingle beach to the swash

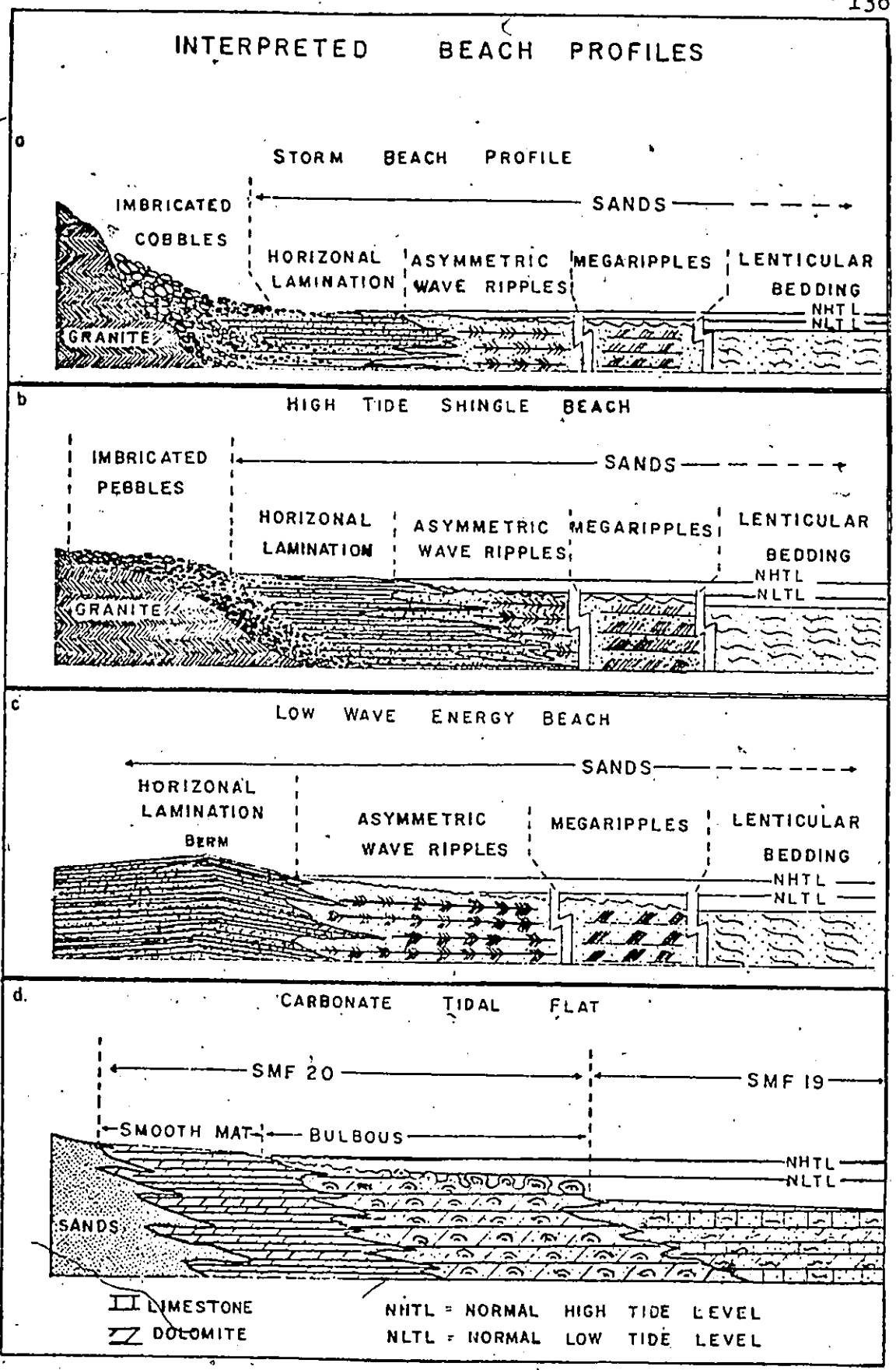

Figures 5-31 a to d: Refer to text for detailed discussion of figures.

zone sand beds was more gradational than that occurring on storm beaches. Pebbles occur sporadically within the nearly horizontal laminae of the swash zone. Seaward of the zone the normal wave and tidal profile developed (figure 5-31b).

Low Wave Energy Beach

Under ideal conditions the low wave energy beach would be expected to initiate from a high tide beach berm. However under the predicted prevailing wave breaker heights, the berm height given by Bagnold (in Komar,1976; p. 308) for fine sand beaches would be roughly 10 cm. Such small scale structures would be difficult to distinguish, particularly with limited exposures, and none were found in this study.

Seaward of the berm the normal wave and tidal profile occurred with four major zones. Seaward of the berm nearly horizontal sand laminae are deposited within the swash zone. The zone rapidly changes seaward of the high tide breaker zone to rippled beds, where interference ripples dominate. In the lower reaches of the ripple zone Diplocraterion and Skolithos burrows and flaser bedding become prominent. Rapid deposition of sediment at turning tide resulted in laminae of rhythmite or lenticular mud or micrite that is locally extremely bioturbated. The zone probably marks the normal subtidal boundary. The lower offshore zone in which strong tidal currents dominate is marked by sparsely bioturbated sandstone with megaripples. Further offshore the siliciclastic strata grade into planar bedded

lenticular sandstone-micrite beds that grade eventually into SMF 19 carbonate microfacies (figure 5-31c).

Carbonate Tidal Flats

Rocks representing carbonate tidal flats are best exposed within the boundaries of March Township in the vicinity of Malwood. The sequence starts on the gentle northern slope of the basement inlier where a low energy beach of fine sand developed. Smooth mat stromatolites developed on the sand base, occasionally being buried during high energy storm conditions by SMF 24 microfacies deposits. Over a distance of 2 to 3 km the smooth mat stromatolites changed from thin mm thick laminated calcisiltite and sandstone laminae cut by desiccation cracks to cm thick lenticular micrite and calcisiltite laminae in thick beds (locations 0-6, and 0-7). Northward in the offshore direction the smooth mat stromatolites are succeeded by columnar forms that over a distance of 1 to 2 km increase in height from a few cm to more than 0.5 m (locations 0-7 and 0-8; figure 5-31d).

CHAPTER 6

WESTPORT-ATHENS DISTRICT

General

The Westport-Athens district is the largest and most westerly extending embayment along the Frontenac Axis. The district contains roughly 35 % of the exposures of the Beekmantown Group in the western Ottawa Basin with numerous easily accessible, small exposures of the group's various formations (figure 6-1).

The embayment is bordered on the north by the Westport Plutons (Wynne-Edwards, 1967) that abruptly rise along the Rideau Lake Fault, and in the south by the north-dipping Grenville metasediments that extend beneath the Beekmantown strata.

Recent conodont biostratigraphic studies within the district show a similar faunal age at several widely spaced locations (locations 16, 56, 32, 43, and 48) despite lithological changes (Arenigian; Fauna D2-D3; Brand, 1977, personal communications). As a result, detailed sedimentological studies of this area should be useful in modeling the local paleoenvironments.

Isolithic Trends

Petrological studies of 43 exposures of the Beekmantown Group in the Westport-Athens district were performed (figure 6-1; appendix 3). Parameters from beds at each location were averaged to obtain isolithic maps of the district (figures

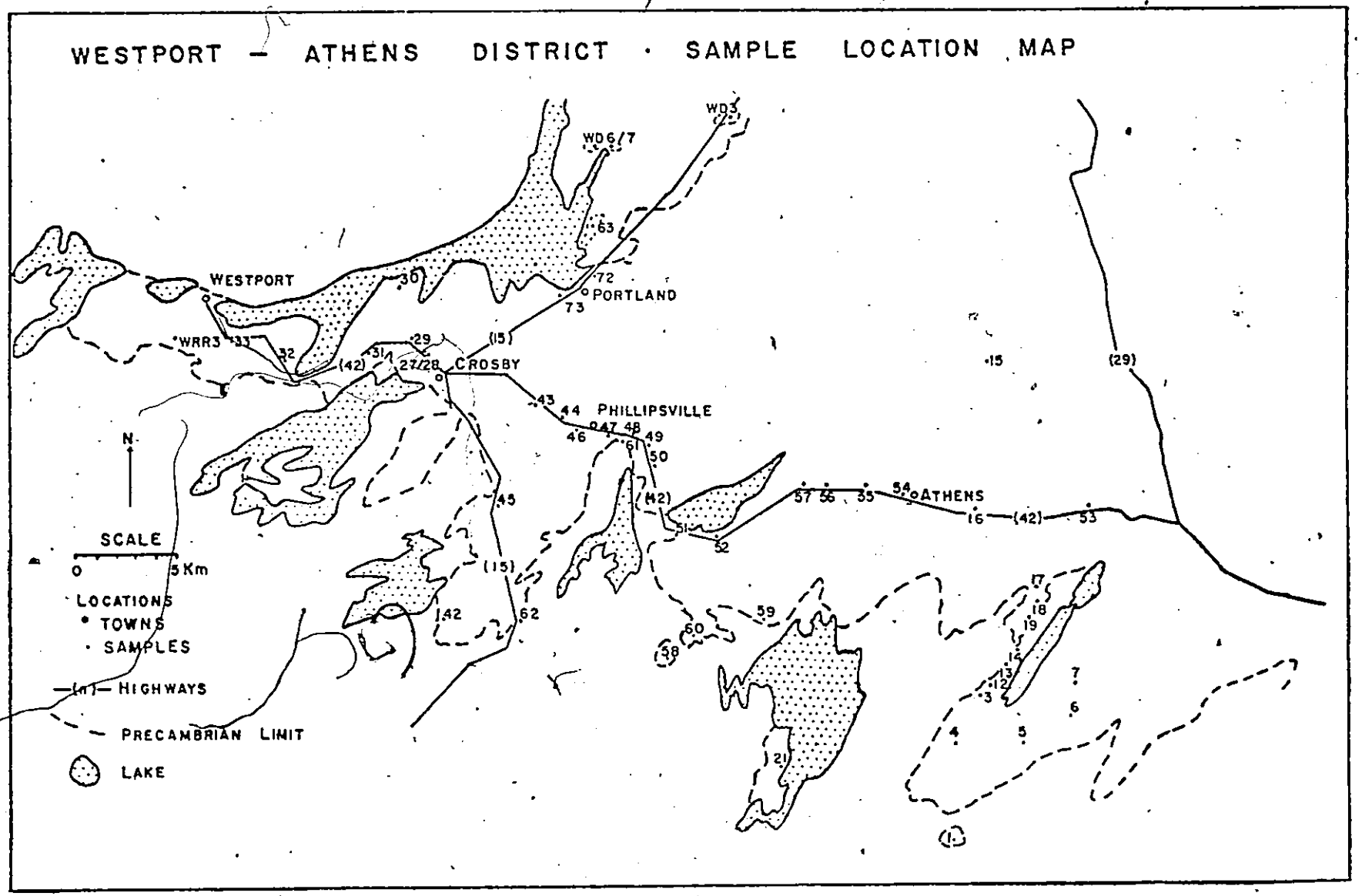

Figure 6-1: Primary sample locations used in the Westport-Athens District.

6-2 to 6-6).

Isolithic maps of the graphic mean size (figure 6-2), inclusive graphic standard deviation (figure 6-3), inclusive graphic skewness (figure 6-4), insoluble mud fraction (figure 6-5) and soluble (carbonate) fraction (figure 6-6) show similar distribution patterns. Symmetry of the isolithic lines show little evidence of prior extensive overlap of the facies on to the Shield, suggesting that the present limits of the embayment are close to the maximum extent of the Group at the time of deposition.

The graphic mean size isolithic map shows a general decrease in grain size away from the embayment edges (figure 6-2) while the standard deviation increases in value (figure 6-3). These patterns may be attributed to coastal wave action in which finer sediment is removed from the nearshore areas and transported offshore to lower energy zones. The consequence would be an increase in grain size and sorting in the higher energy nearshore area. Support for the transport of fines offshore is also provided by the mud (figure 6-5) and skewness isolithic patterns (figure 6-4), the latter showing increased positive skewness offshore.

Studies by Ingle (1966) and Fox et al (1966) of wave dominant beaches have shown that the sorting of the sediment is minimal at the breaker zone. The low degree of sorting was attributed to intermixing of coarse and fine sediment modes, where the backwash and wave front converge. Fox et al (1966) found that the skewness is generally negative in nearshore areas, except in the vicinity of the breaker zone. The

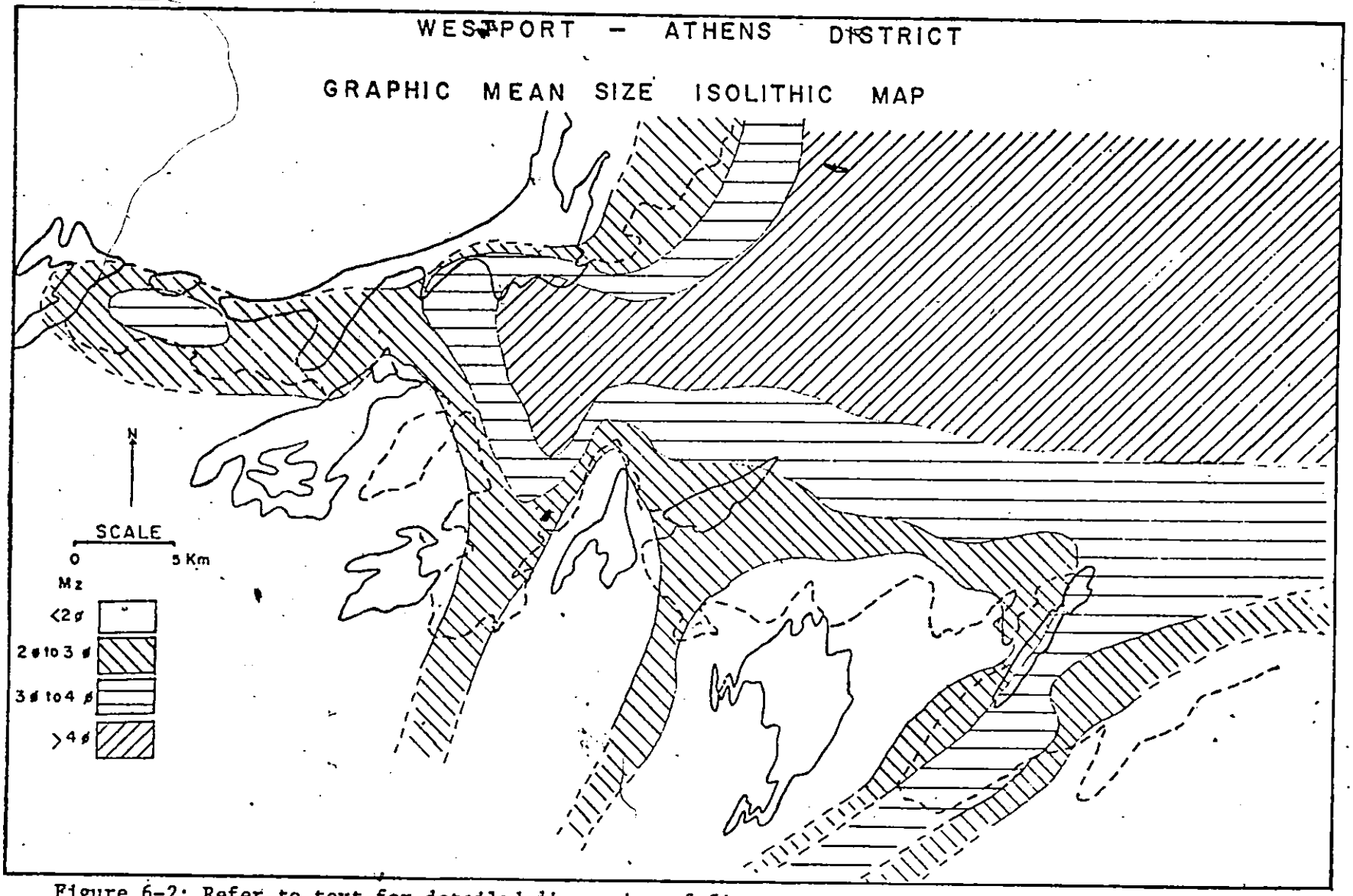

Figure 6-2: Refer to text for detailed discussion of figure.

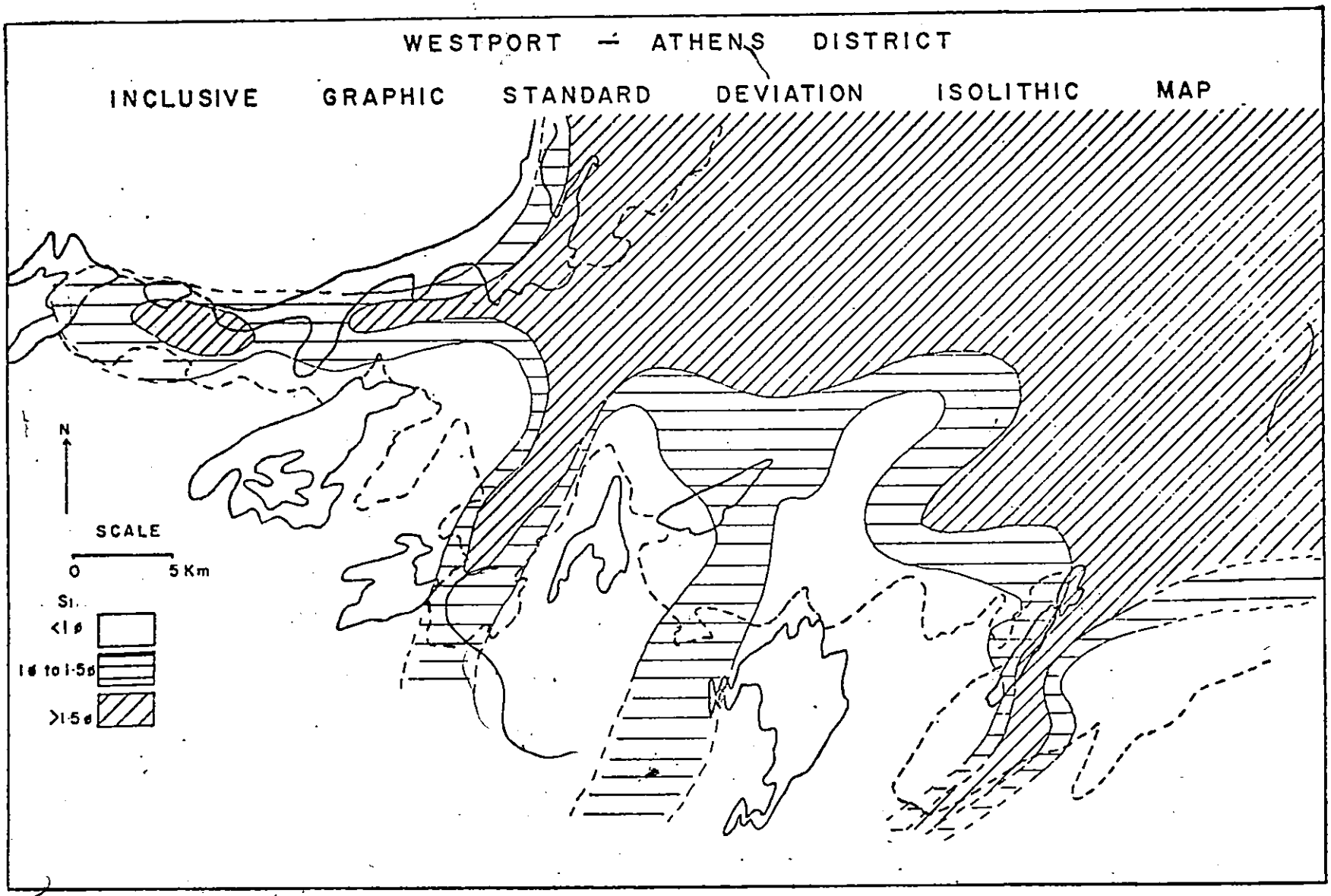

Figure 6-3: Refer to text for detailed discussion of figure.

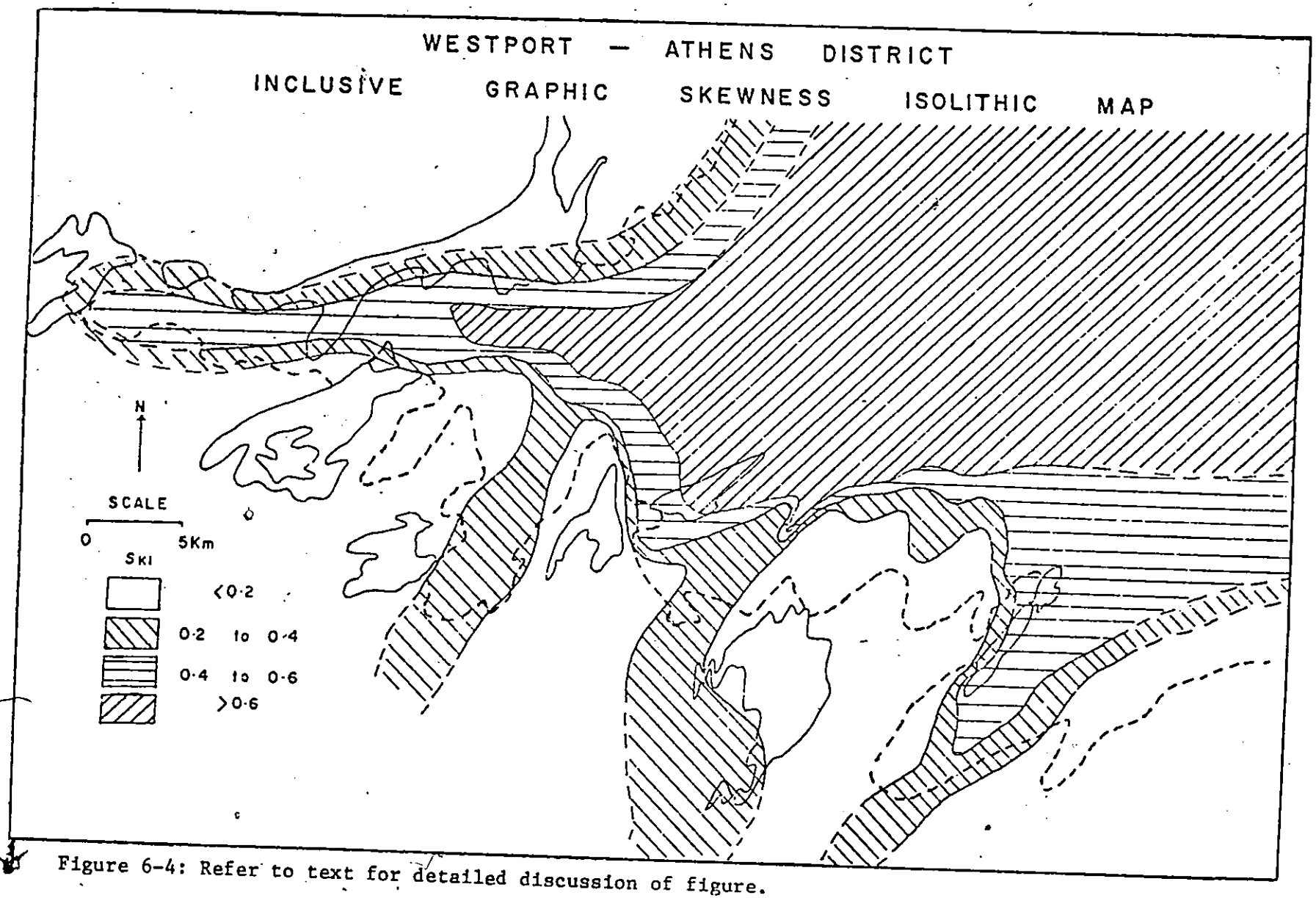

Figure 6-4: Refer to text for detailed discussion of figure.

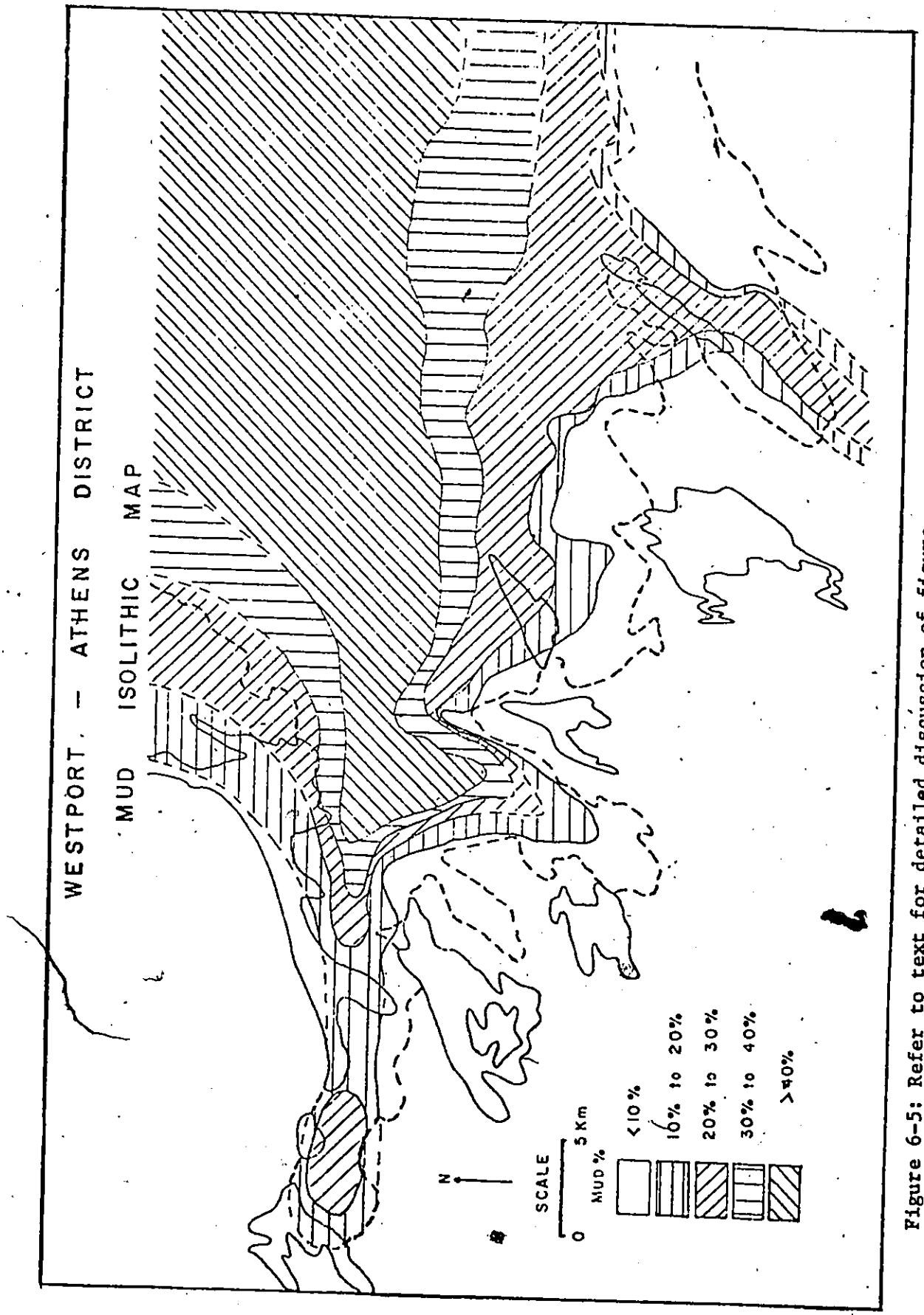

Figure 6-5: Refer to text for detailed discussion of figure.

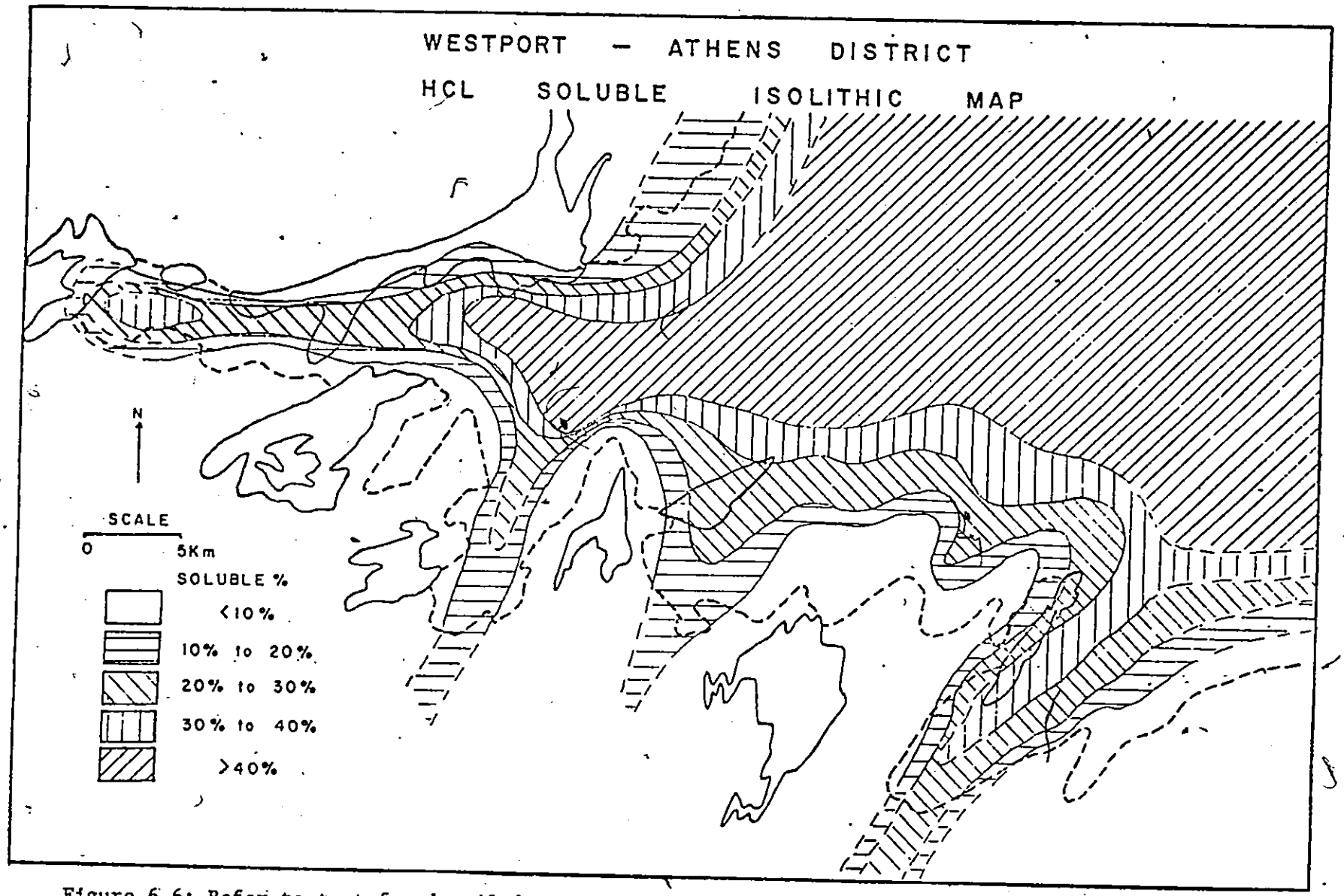

Figure 6-6: Refer to text for detailed discussion of figure.

negative skewness was attributed to the presence of a small granular fraction within the sand size sediment. The positive skewness in the breaker zone was considered to be the result of the mixing of the granule and medium sand modes where the sand dominates the granule mode. The presence of a nearshore zone of low sorting or high skewness is not apparent within the district (figures 6-2 to 6-4).

The textural differences between the present examples and Ingle's (1966) may in part be the result of differences in the wave breaker types. Whereas in studies by both Ingle and Fox et al plunging breakers occur, the breaker predicted from ripple data in the study area suggest a spilling type breaker. Miller (1976, p.108) found that the plunging breaker disturbed the bottom sediment while spilling breakers generated a steady back and forth bottom shear stress which tends to sort the sediments and erase bottom topographical irregularities.

Extending southward from the embayment and across the Frontenac Axis are three zones in which isoliths of grain size (figure 6-2), sorting (figure 6-3) and skewness (figure 6-4) are symmetrical about the zonal axes. Grain size and sorting decrease toward the zone axes while skewness increases. The zones are interpreted as deep water (below normal low tide wave base) channels across the Frontenac Axis. Grain size (chapter 5) generally increases westward across the Frontenac Axis. If the rocks in these zones are penecontemporaneous, then the channels may represent restricted inlets from a higher

energy sea west of the Ottawa Basin. General decrease in sorting and increase in skewness eastward along these zones is consistent with this hypothesis.

Distribution of total sample solubles (figure 6-6) shows a direct correlation with increased insoluble mud content (figure 6-5). This contrasts with the suggestion of Blatt et al (1972, p. 412) that the average ancient limestone contains less than 5% detrital silicate particles. They attributed low insoluble content to mechanical and chemical removal of the carbonate grains in silicate rich sediments or to the inhibition of carbonate precipitating organisms by large concentrations of silicate sediments.

In order to explain the presence of both high soluble fraction and high insoluble mud rich sediments, a detrital origin for one or both must be considered. Decrease in both mud and soluble southward into the channels crossing the Frontenac Axis suggests that the source of the mud and carbonate was primarily within the basin.

Phillipsville Sections

In the vicinity of Phillipsville (figure 6-1) several major exposures of the Beekmantown Group occur. From these sections a composite section representing the Keeseville, Heuvelton, March Members and lower strata of the Beauharnois Formation can be obtained (figures 6-7 and 6-11).

The exposures in the vicinity of Phillipsville are

Figure 6-7

Phillipsville cliff section 61; central section showing units c to oo (see figure 6-8 for unit scales). Weathering of the section reflects range in textural and lithological variation between units. Massive central units (eg. cc) are composed of subarkose and quartzwacke with deep Skolithos burrows (Heuvelton member).

FIGURE 6-7

primarily the result of erosion of strata exposed on the northern limb of a Precambrian anticlinal uplift, known locally as The Mountain (Wynne-Edwards, 1967). The Mountain consists of metaquartzite and marble strata. Additional exposures of the Beekmantown Group have resulted from road improvements along highway 42.

Location 61^{A} Section

Isolated from the main cliff exposure at location 61 there are several outliers of the Keeseville Member showing features interpreted as representing high tidal shingle beach and low tidal terraces. The exposures consist of metaquartzite pebble oligomictic conglomerate alternating with thick beds of medium to fine grained quartzitic sandstone, with low angle cross stratification. Clasts range from small pebbles to large cobbles (-2ϕ to -7.9ϕ) with a mean size of -6.4 ± 0.1ϕ. The cobbles range in shape from subangular to rounded.

Cobble imbrication within the conglomerate shows a polymodal distribution with a weakly developed principal mode of C axes dipping towards the south (figure 6-9). The modal imbrication is interpreted as resulting from wave action during high flood tide while the westward imbrication may be the result of ebb tidal flow around the point formed by The Mountain . Weak northward imbrication is interpreted as wave induced from limited southward advancing wave fronts on the beach.

Location 61 Section

The largest Heuvelton member exposure is a 16.5 m cliff at location 61, 0.3 km east of Phillipsville off highway 42 (figures 6-7, 6-8, 6-9 and 6-10). Here fine grained quartzitic and quartzose sandstone are intermittently interbedded with fine grained, poorly sorted, feldspathic litharenite (Keith, 1949). Based on texture and primary sedimentary structures 47 units were recognized (figures 6-8 and 6-9).

Textural Interpretation

Visher's (1969) environmental criteria (chapter 4) were used to interpret the most probable paleoenvironment of each of the units (figure 6-8). The criteria corresponded to only six of Visher's environments: beach, plunge zone, wave zone, tidal channel, tidal inlet and turbidity zone. Overlapping of characteristics of more than one environment is common (60%).

The most frequent overlaps occur between beach, plunge zone and wave zone environments (figure 6-8). A sequence of herringbone cross strata grading into flaser bedding and terminating in shaly or lenticular bedding occasionally marked by desiccation cracks supports this transition and may indicate a tide-dominant nearshore paleoenvironment. Another possible paleoenvironment is the tidal channel or inlet, whose textural criteria are fulfilled by half the units. Features such as small scale channels, convolute bedding, extreme bioturbation in

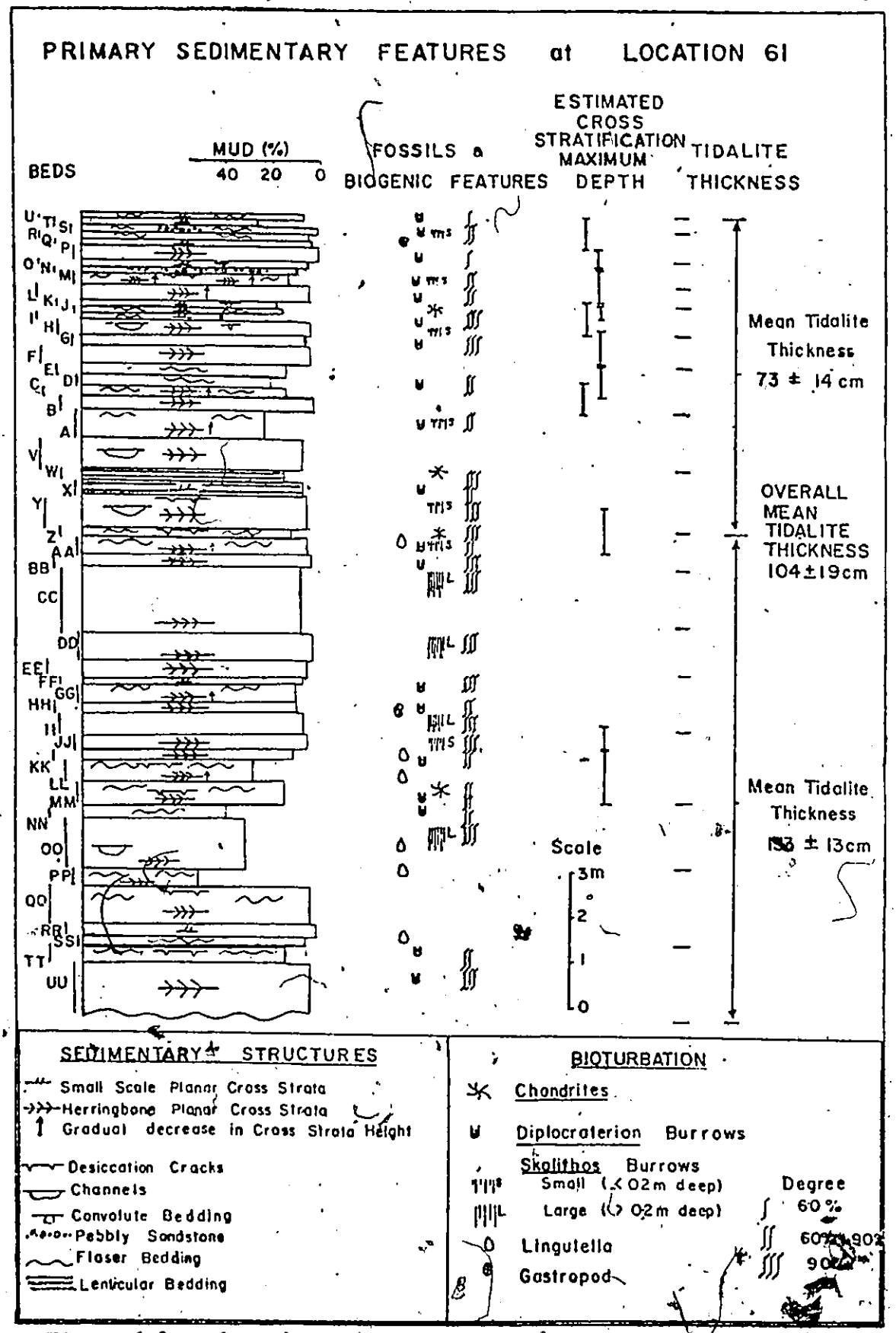

Figure 6-8: Refer to text for detailed discussion of figure.

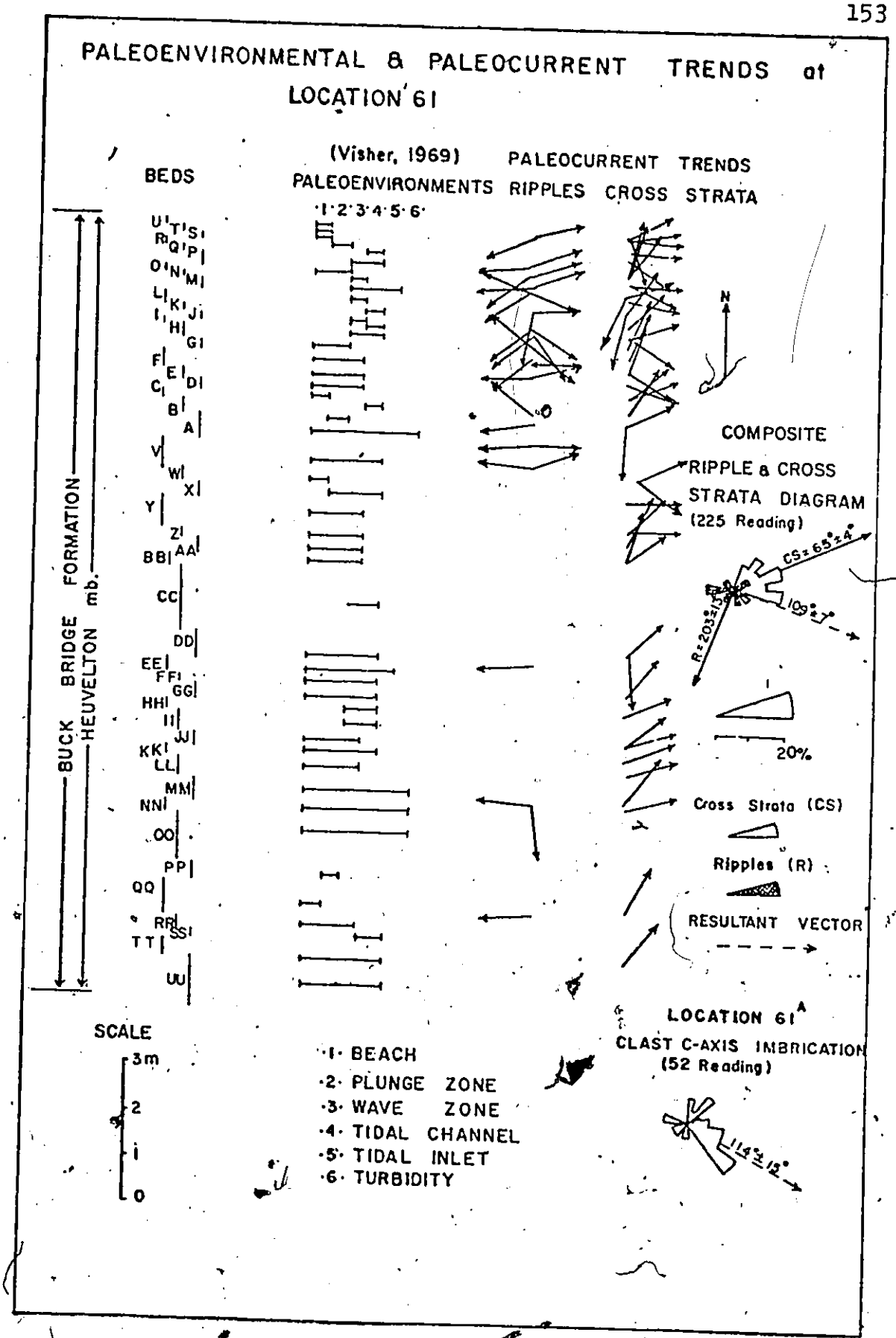

Figure 6-9: Refer to text for detailed discussion of figure.

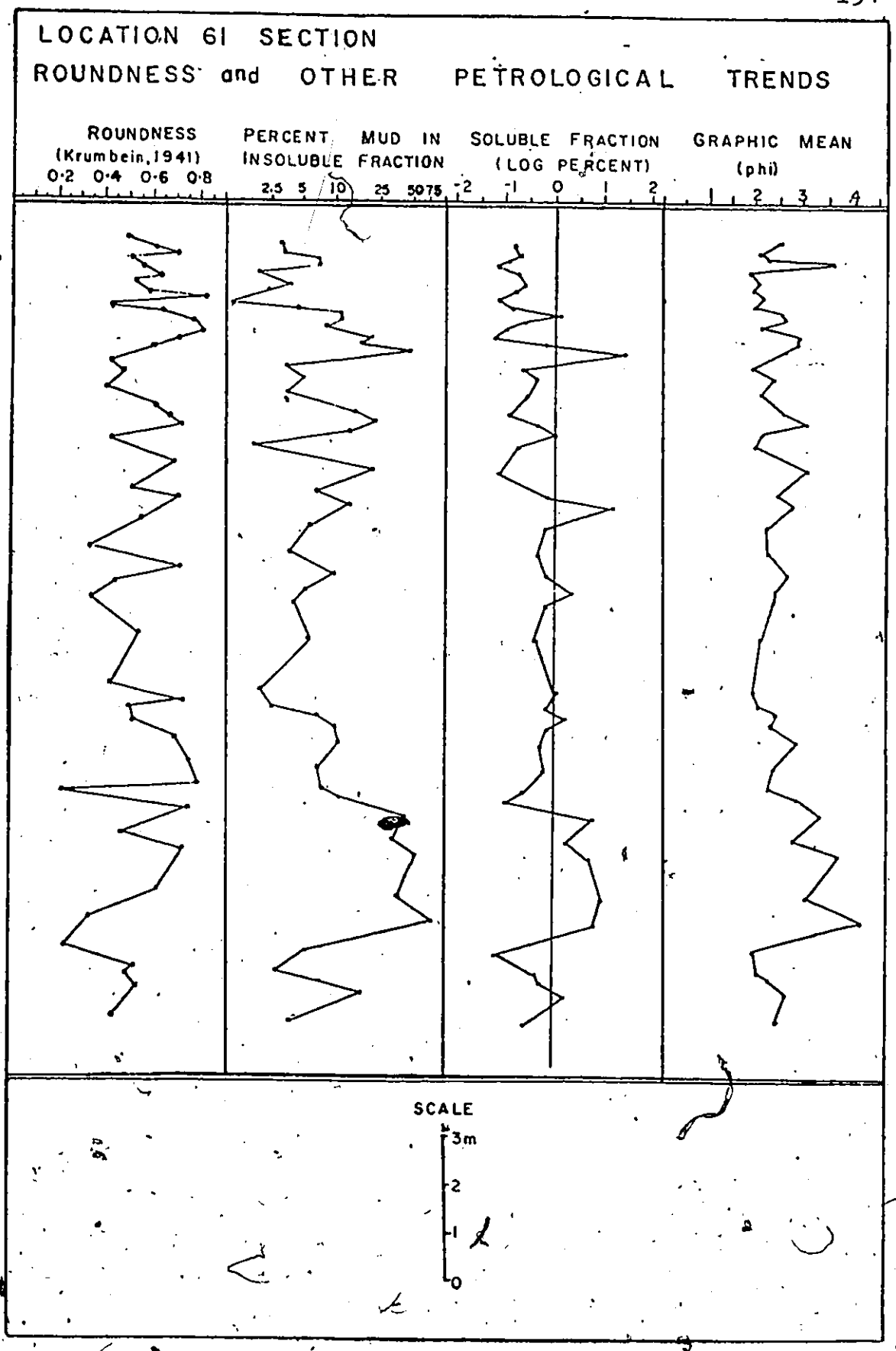

Figure 6-10: Refer to text for detailed discussion of figure.

feldspathic litharenite, thick and massive beds that feather out into the adjacent quartzose sandstone and large scale Skolithos burrows (range from 20 to 60 cm in length) are consistent with tidal channel origin. However they are present in only 26 % of the units in which texture suggests tidal channel origin. A partial explanation for the high incidence of apparent tidal channel environments may be found in the grain size criteria used by Visher (1969) to define his environments.(figure 4-13a). The criteria for tidal channel environments are transitional between beach, plunge zone and wave zone. Intermixing of closely spaced beds during sampling or partial reworking of beds at the time of deposition may duplicate the petrological criteria for the tidal environment.

Turbidity zone criteria are indicated by 13 % of the units. In each case either moderate to extreme bioturbation or rhythmite bedding (Reineck and Singh, 1975; p.108) are present. The turbidity zone of Visher (1969) is characterized by a low saltation population relative to traction and suspension populations. Either alternating laminae of the rhythmites, or selective removal of the fine sand fraction by bioturbation (Rick et al, 1977; p. 1425) may duplicate this criterion.

Tidalites and Intertidalites

Klein (1971, p. 2585) introduced the term tidalite to describe the distinct combination of sedimentary structures, vertical sequences, textures and lithologies that reflect phases of tidal sediment transport and deposition. A special

type of the tidalite was the intertidalite which was defined as the complete tidalite showing evidence of exposures during late stage emergence (Klein, 1971). Using criteria for recognizing the different transport phases within an intertidalite, Klein (1971; p. 2586-2587) suggested that the tidalite thickness can be measured and the paleotidal range estimated therefrom.

Using Klein's (1971) criteria, 27 tidalites or intertidalites were distinguished at locations 61 and 48 (figures 6-7 to 6-11). At location 61 the tidalites show a general decrease in thickness from 1.3 ± 0.1 m for the lowest 8 tidalites to 0.7 ± 0.1 m for the mean size of the upper 8 tidalites, giving a mean tidalite thickness of 1.0 ± 0.1 m for the section (figure 6-9). Textural parameter mode points, which may indicate changes in sediment size, transport mode and the transporting current energy, appear at similar intervals within the succession (mean spacing 0.9 ± 0.2 m; figure 6-9; table 6-1).

Within the section several massive units (units CC, DD, II and OO; figures 6-8 and 6-9) show features that differ from others in the section. These units consist of calcareous sub-arkose that feather out laterally over distances of the order of hundreds of meters (Keith, 1949). The units are also unique in having Skolithos burrows up to 60 cm deep in the upper parts. Texturally all four units fulfil Visher's criteria for tidal channels (figure 6-8). Taking these units to represent large scale tidal channels and the depth of the burrows as evidence of intervals of exposure, a rough estimate of the paleotidal

TABLE 6-1

LOCATION #61 COMPARISON OF ESTIMATED PALEOTIDAL RANGE FROM TIDALITES, TEXTURAL PARAMETERS, AND ESTIMATED DEPTH OF CROSS STRATA FORMATION.

For detailed discussion of this table refer to text. Textural parameter patterns refer to repeating patterns of peak parameter values found in the section (figure 6-10).

Parameter	Peak value intervals
Graphic mean size	Mz = 85 ± 10 cm
First percentile size	1% = 86 ± 10 cm
Inclusive graphic standard deviation	σ_I = 86 ± 12 cm
Inclusive graphic skewness	S_{KI} = 114 ± 17 cm
Grain Roundness	R_D = 95 ± 9 cm
Coarse Truncation Point	CT = 94 ± 14 cm
Fine Truncation Point	FT = 80 ± 14 cm
Traction Population	C = 99 ± 11 cm
Saltation Population	A = 89 ± 9 cm
Parameter mean spacing	= 92 ± 17 cm
Mean tidalite thickness	= 104 ± 19 cm
Tidal Channel mean thickness	= 73 ± 19 cm

Mean of estimated max. depth for Cross Strata formation = 87 ± 10cm

range is possible. The mean thickness of the four largest channels is 0.73 ± 0.2 m, which is of similar magnitude to the mean tidalite thickness and textural mode spacing (table 6-1).

Estimates of the maximum depth under which each cross strata was formed from 11 units show a positive correlation with the gradual increase in tidalite thickness up the section (figure 6-9). The mean maximum depth estimate of the cross strata is 0.76 ± 0.11 m, again of similar magnitude to the range suggested by other sources (table 6-1). The results appear to indicate a prevailing microtidal range existed at this location at its time of deposition and the gradational changes in the tidal range occur over its history.

Cross strata show a dominant eastward paleoflow possible resulting from rapid ebb flow toward the basin. Ripples, however, show a bipolar orientation dominated by a westward modal orientation (figure 6-8), reflecting wave action during slack tide intervals.

Location 48 Section

Directly north of the cliff face of location 61, a road cut on highway 42 has exposed a 6 m fresh section showing the upper Heuvelton member, March Member and lower strata of the Beauharnois Formation. Here ten intertidalite sequences are recognized (figure 6-11).

The intertidalites consist of four parts: an asymmetric herringbone cross strata zone, a strongly bioturbated

sideritic zone, a Diplocraterion burrow zone and glauconitic sandstone lag deposit marked by desiccation cracks and interference ripple marks (figures 5-4 to 6-11). The tidalites continue the trend from location 61 of decreasing in thickness up section for the lower 3.5 m, before starting to increase in thickness again (figure 6-11). Both the maximum estimated depth of formation of cross strata and ripples show similar trends.

The cross stratification zone is marked by simple tangential planar sets or asymmetric herringbone cross strata with dominant sets oriented westward. This appears to indicate a dominant flood tidal current at this location.

Teodorovich (in Larsen and Chilingar, 1967; p. 13-16) suggested that the siderite facies without significant amounts of other carbonate was most prominent in a weakly reducing marine environment of neutral acidity (pH = 7.2 to 6.6). The condition was considered to occur at the sediment-water interface. Glauconitic facies were considered to indicate weakly oxidizing zones of weakly alkaline to neutral acidity (pH = 8.0 to 6.6). Such conditions were considered to occur below the sediment-water interface. The presence of wave formed ripples cut by desiccation cracks in the glauconite-rich beds would, however, suggest formation at the sediment-water interface, rather than below, while the siderite facies appear to have formed just below the interface, where bioturbation was maximum. Glauconite was found in both carbonate and sandstone throughout the Westport-Athens district as a lag deposit that appears to occur at regular intervals.

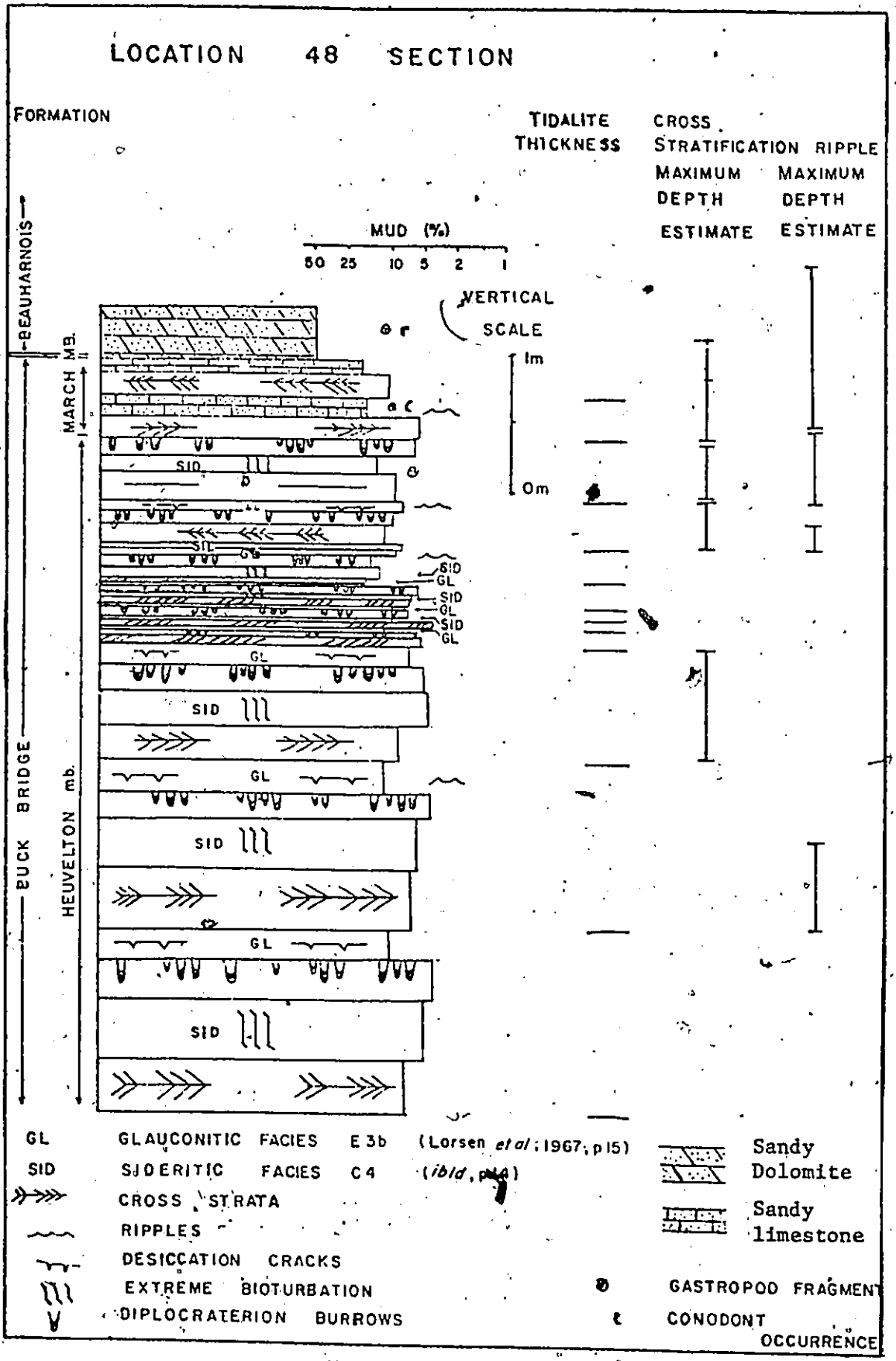

Figure 6-11: Primary sedimentary and biogenic structures at section 48. Refer to text for detailed discussion of figure.

Within the cross stratal zone, black coated sparite pebbles occur, with their greatest concentration in eastward orientated sets. These pebbles are interpreted as formed in subaerially exposed hypersaline tidal ponds west of location 48.

Detrital carbonate constituents, intermixed with fine quartz grains, grade rapidly into carbonate-dominated beds in the upper meter of the section. Bond and Greggs (1976, p. 21) considered the apparently sharp contact between the carbonate-rich beds and underlying quartzose and quartzitic sandstone to represent a possible disconformity between the March and Oxford Formations. Present at several locations along the contact, however, are cross strata that cross this boundary, indicating a penecontemporaneous relationship. The highest occurring strata in the section consist of dolomicrite with gastropod shell fragments. The dolomicrite contains a high insoluble mud fraction (± 40 %) and few sand size grains (± 15 %), and as a consequence is considered to represent the Beauharnois Formation at this location.

Carbonate Strata Within The Philipsville District

Laminated to bioturbated sandy or dolomitized calcisiltite and pelmicrite (SMF 19) occur frequently within the district (locations 33, 44, 46, 55, 56 and 73) often showing rhythmite-like bedding. The microfacies occurs in close association with the unfossiliferous homogeneous dolomicrite of SMF 23, which contains allochthonous gastropods near boundaries. The beds are frequently

separated by beds of intraformational dolomitized intermicrite (SMF 24). The boundary between the aerobic conditions represented by SMF 19 microfacies and the occasionally anaerobic conditions of the SMF 23 microfacies may be placed at or near storm wave base. For wave intensities sufficient to move the largest clast size (figure 5-9), waves between 4 and 5 second periods would be needed, corresponding to a probable depth (for $\frac{L_\infty}{4}$) of between 6 and 10 m.

Smooth mat type stromatolites are characterized by being cut by desiccation cracks, separated by glauconitic lag deposits and being separated and incorporated into SMF 24 microfacies, suggesting high intertidal conditions. The microfacies is gradational into SMF 19 microfacies (locations 33, 44, 46, 53, 55, 56 and WRR3; figure 5-26).

Paleoenvironmental Interpretation

The Westport-Athens district appears to have occupied a generally low wave energy, microtidal paleoenvironment in which saline conditions prevailed. Glauconitic lag deposits and black coated sparite clasts suggest periodic supratidal conditions on flats in the area west of Phillipsville that were flooded and drained through large channels connecting the embayment to the basin (figure 6-12). Conglomerate deposits found primarily along the southeast corner of the embayment suggest that the prevailing storm direction was from the northeast.

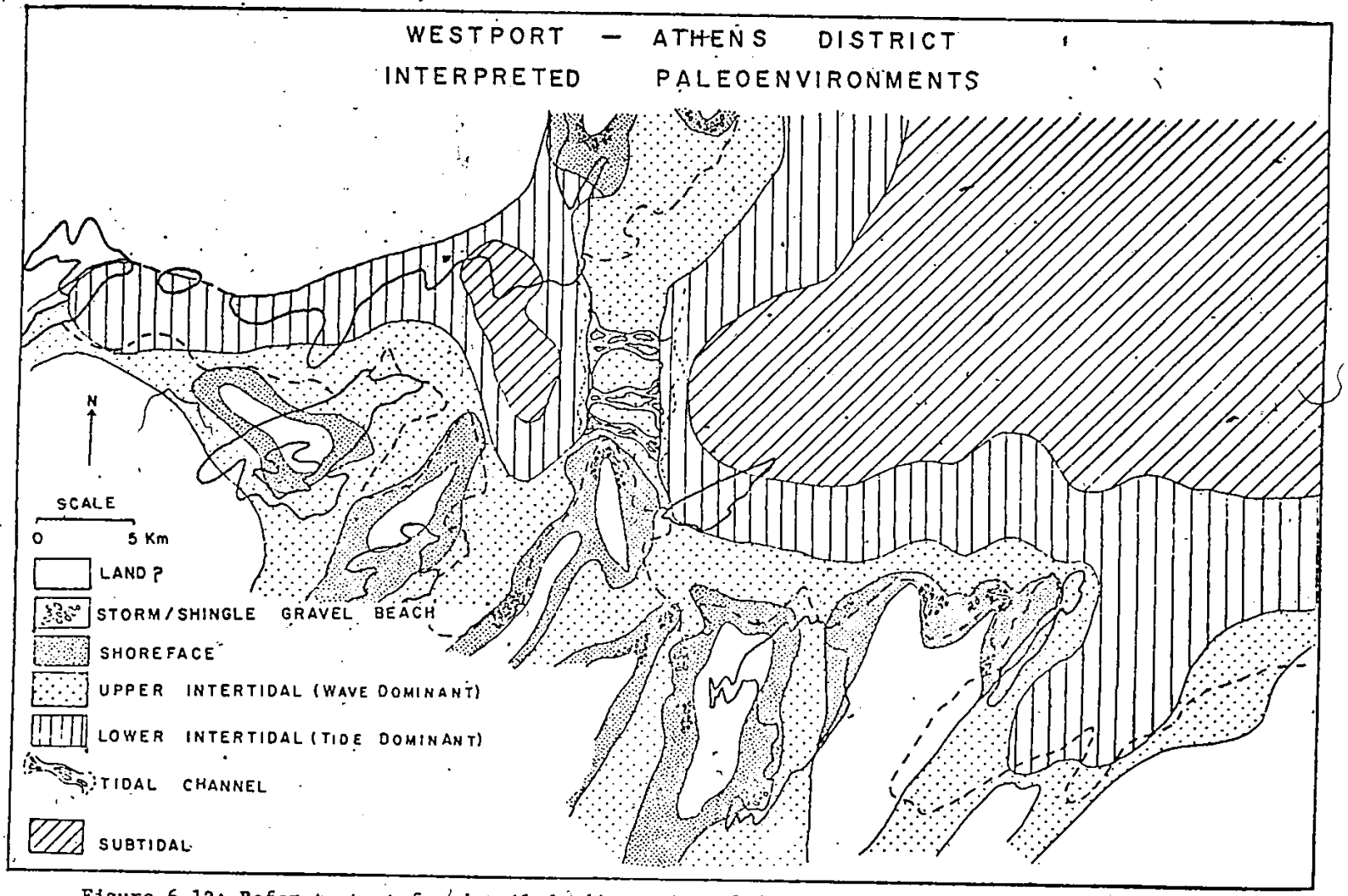

Figure 6-12: Refer to text for detailed discussion of figure.

CHAPTER 7

SUMMARY

The Ottawa Basin formed as a graben complex near the southeastern flank of the Canadian Shield between Hadrynian and Middle Ordovican times. Within this subsiding structure the siliciclastic and carbonate strata of the Beekmantown Group were deposited in a nearly continuous sequence. Localized diastems, faults and penecontemporaneous folding of the strata within the group near the Frontenac Axis, Beauharnois Anticline and Adirondack Massif are evidence of intermittent instability along the basin's southern margin.

Comparison of the lithologies of the Beekmantown Group in the Ontario, Quebec and New York State parts of the basin, within a framework of recent conodont biostratigraphy and drill-core data, suggests that a single lithostratigraphical scheme can be applied throughout. A nomenclature consistent with the Code of Stratigraphic Nomenclature (Krumbein & Sloss, 1963; p. 621-636) is proposed. Under this system the Beekmantown Group consists of the Potsdam, Theresa, Bucks Bridge and Beauharnois Formations. Conodont biostratigraphy indicates that the Theresa and Bucks Bridge Formations near the southwestern edge of the basin were deposited during the Tremadocian Stage while the Potsdam, Buck Bridge and Beauharnois Formations are diachronous within the basin, decreasing in age toward the north (Brand, 1976; personal communications). Consistency in age of the boundary between the Chazy & Beekmantown Groups (Whiterock Stage; Brand, 1977; personal communications) at Arnprior, Cumberland and in the vicinity of

Montreal suggest that the sharp contact is conformable, or represents at most a diastem.

The group may be divided into facies representing three major paleoenvironments. The Basal member of the Potsdam, consisting of hematitic arkose and subarkose with eastward orientated trough cross strata, was deposited in an alluvial plain paleoenvironment (Lewis, 1971; p. 871; Hofmann, 1972; p. 4). The Ausable Member of the Potsdam, consisting of green and pink laminae of silt and subarkose that become more pronounced toward the western part of the basin (appendix 1; Lewis, 1965), may represent a delta front paleoenvironment (Lewis, 1971; p. 879; Reineck and Singh, 1975; p. 270). The Keeseville Member of the Potsdam and the Theresa, Bucks Bridge and Beauharnois Formations were deposited in a microtidal, low wave energy sea.

Suggestions by some workers (Chadwick, 1920; Greggs and Bond, 1972; p. 937) that major regional unconformities are present within the Beekmantown Group in the basin could not be supported. Greggs and Bond (1972; p. 937) proposed that grain textural parameters, cement, degree of bioturbation or colour in the siliciclastic strata were sufficiently distinct to indicate distinct formations, that possibly are disconformable (Bond, 1974; p. 19-20, figure 3). Statistical tests of sediment size from widely separated areas and various stratigraphical positions within the group showed no significant differences at the 0.95 significance level. Rapid variation in grain shape, particularly roundness over short horizontal and vertical distances were found to be too random to be used as a criterion to discrim-

inate the formations. The fluctuation in roundness was found to have a significant correlation with mud and carbonate content, suggesting that present grain shape is primarily the result of diagenesis rather then abrasion during mechanical transport. Isolithic maps of grain size, sorting, skewness, mud and carbonate content for the western part of the region show a regular, continuous gradation from Keeseville Member fringing the Frontenac Axis, to the Beauharnois Formation within the basin. Evidence of lateral facies changes within the upper Beekmantown Group is shown by the presence of similar conodont zones at different lithostratigraphic positions in the Westport-Athens district.

Paleoenvironmental determinations based on grain textural parameters were found to be inconsistent, inconclusive and frequently unrealistic with respect to associated sedimentary structures. However the plots of various textural parameters do show a uniform transition from one lithofacies to another with no evidence of abrupt changes that may be attributed to major disconformities. Only Visher's (1969) method using a log-probability grain size curve provides an estimate of the paleoenvironment which is mostly consistent with the sedimentary structures. Discrepancies with respect to sedimentary structures in these suggested paleoenvironments are primarily associated with complex rhythmite sequences or highly bioturbated sediments and suggest that the method is ineffective under these circumstances.

Hydrodynamic controls interpreted from wave formed ripples and cross strata suggest that the basin was shallow, had a limited fetch (between 100 to 200 km) and was microtidal.

Absence of offshore bars, coarse sediment size and the apparent presence of wide low angle beach faces supports the low wave energy suggested by ripple hydrodynamics. Removal of mud from the beach by wave action and transport to offshore areas within this microtidal range sea can explain the lithofacies suite found in the upper Beekmantown Group.

Climatic conditions suggested by the wave energy estimated from sedimentary structures indicate prevailing calm to light wind conditions with occasional storms of gale force. Such conditions are currently associated with equatorial doldrum climates. The counter-clockwise circulation within the basin suggested by the paleocurrent orientation of cross strata and ripples may indicate a southern hemisphere position of the basin during Ordovician times. Consistency of the paleocurrent directions in the Potsdam, Bucks Bridge and Beauharnois Formations support a prolonged stability in the general basin configuration, with only partial tidal connection of the basin with the eastern Theic Ocean. Paleotectonic maps by Keppie (1977) suggest that the Ottawa Basin was situated in the southern equatorial latitudes and are consistent with these predictions.

Tidal ranges estimated from tidalite thickness, textural trends, and ripple & cross stratal depth of formation are consistent, suggesting microtidal ranges within the basin throughout the deposition of the Buck Bridge Formation. The consistency of the various methods also provides support for Klein's (1971) tidalite model for estimating paleotidal range, as well as suggesting an alternative method using cross strata or ripples to estimate depth.

Suggestions for Additional Studies

(1) Detailed conodont biostratigraphy of the type section of the Beekmantown and Chazy Groups in the Champlain Valley are necessary to adequately correlate these units within the region and elsewhere in North America. Previous macrofaunal correlations that have been adopted appear to be severely limited.

(2) Relationships between wave bottom orbital diameter and ripple length are known primarily for short period waves and small ripples in fine sand. Additional flume and field study of ripple formation in medium to coarse sand by intermediate (3 to 15 second) period waves are necessary to fully understand and apply the relationship of wave theories to ripple formation.

(3) Insufficient data are available to estimate with certainty the relationship between ripple asymmetry and bottom unidirectional currents. In addition, the influence of different sediment sizes on the relationship is unknown; more experimentation is necessary to refine this model.

(4) Attempts to estimate paleoflow conditions from planar cross strata by relating Stein's rule to the Froude number give reasonable agreement when plotted on a Paleoflow power vs sediment size diagram for particles coarser than 2ϕ. However, finer sediment departs significantly from Allen's extrapolated bedform boundaries. Experimental studies of the behaviour

of ripples and megaripples in silt and very fine sand under unidirectional currents are needed to fully evaluate the Stein's rule-Froude number relationship. Regime 1 and 3 bedforms cannot be distinguished on the basis of cross stratification: further experiments should be performed to increase the potential resolution of this tool.

ACKNOWLEDGEMENTS

I would like to thank Dr. Brian Rust for suggesting this study. Critical reading of the manuscript by Drs. Rust and Owen A. Dixon considerably improved the text. Information and sometimes stimulating discussions concerning the study area were provided by Drs. Donald Fisher, Robert Greggs, Don Hogarth and Bruce Liberty.

Bruce Sanford provided access to the drill cores stored at the Geological Survey of Canada repository, Ottawa. Thanks are also extended to Ter Haar Romeny for logistical assistance while examining the cores. Important biostratigraphic information contributing to this study were provided by Uwe Brand and Elizabeth Sandi.

The study was financed by a National Research of Canada grant (to Brian Rust) and by a Ontario Petroleum Institute grant, whose generosity is graciously acknowledged.

REFERENCES

Allen, J.R.L.

1968: Current ripples, their relations to patterns of water and sediment motion; Amsterdam: North-Holland Publ. Co., 433p.

1970: Physical process of sedimentation. An introduction; London: G. Allen & Unwin, 248p.

1978: Computational models for dune time-lag: calculations using Stein's Rule for dune height; Sediment. Geol. v.20, 165 - 216.

Amaral, E.J. and Pryor, W.A.

1977: Depositional environment of the St. Peter Sandstone deduced by textural analysis; J. Sediment. Petrology, v.47, no. 1, 32 - 52.

Bagnold, R.A.

1963: Mechanism of marine sedimentation; in The Sea, ed. Hill, M.N., v.3; 507 -528; Interscience, New York:

Barnes, C.R., Jackson, D.E. and Norford, B.S.

1976: Correlation between Canadian Ordovician zonations based on Graptolites, Conodonts and Benthic macrofossils from key successions; in The Ordovician System, ed. Bassett, M.G.; Univ. of Wales Press, 209 - 226.

Beard, R.J.

1969: Guide to subsurface Paleozoic stratigraphy of Southern Ontario; Ont. Dep. Mines, Energy Resources Management; Paper 69 -2.

Beard, R.J.

1970: Guide to subsurface Paleozoic stratigraphy of Southern Ontario; Ont. Dep. Mines, Energy Resources Management; Paper 70 - 2.

Belyea, H.L.

1952: Deep wells and subsurface stratigraphy of part of the St. Lawrence Lowland, Quebec; Geol. Surv. Can., Bull 22, 7 - 11.

Blatt, H., Middleton, G.V. and Murray, R.C.

1972: Origin of sedimentary rocks; Prentice-Hall Inc., New Jersey, 634p.

Bluck, B.J.

1967: Sedimentation of beach gravels: examples from South Wales; J Sediment. Petrology, v.37, 128 - 156.

Bond, I.J.

1974: Lithostratigraphy and conodont biostratigraphy of the Lower Ordovician of the Ottawa - St. Lawrence Lowlands, Ontario and New York; Unpubl. Ph.D Dissertation, Queens University, Kingston; 467p.

Bond, I.J. and Greggs, R.G.

1973: Revision of March Formation (Tremadocian) in Southeastern Ontario; Can. J. Earth Sci., v.10, 1140 - 1155.

1976: Revision of the Oxford Formation (Arenig) of Southeastern Ontario and Northwestern New York State; Can. J. Earth Sci., v.13, 19 - 27.

Brainard, E. and Seekley, H.M.

1890a: The Calciferous Formation in the Champlain Valley;

Geol. Soc. Amer. Bull, v. 1, 501-516.

Brainard, E. and Seekly, H.M.

1890b: The Calciferous Formation in the Champlain Valley; Amer. Mus. Nat. Hist. Bull, v. 3, 1-23.

Brand, U.

1976: Lower Ordovician conodonts from the Kindblade Formation, Arbuckle Mountains, Oklahoma; Unpubl. MSc Dissertation, University of Missouri, Columbia, 110p.

Brand, U. and Rust, B.R.

1977a: The age and upper boundary of the Nepean Formation in its type section near Ottawa, Ontario; Can. J. Earth Sci., v. 14, no. 9, 2002-2006.

1977b: The age and upper boundary of the Nepean Formation in its type section near Ottawa, Ontario: Reply; Can. J. Earth Sci., v. 14, no. 11, 2671-2673.

Bretschneider, C.L.

1966: Wave generation by wind, deep and shallow water; in Estuary and Coastline Hydrodynamic, ed. Ippen, A.T.; McGraw-Hill Book Co., New York, 133-196.

Chadwick, G.H.

1915: Post Ordovician deformation in the Saint Lawrence Valley, New York; Geol. Soc. Amer. Bull, v. 26, 289-291.

1920: Paleozoic rocks of the Canton Quadrangle; New York State Mus. Bull, 1-60, 217-218.

Chapman, E.J.

1864: A popular exposition of the minerals and geology of Canada; part 5, Paleozoic Rocks of Canada, Can. Jour.

new ser. v.8, 185 - 210.

Chapman, L.J. and Putman, D.F.

1951: Physiographic map of Southern Ontario - eastern section; in The Physiography of Southern Ontario, ed. Chapman, L.J. and Putman, D.F.; Univ. of Toronto Press, Toronto.

1973: Physiography of Southern Ontario, 2nd ed.; Univ. of Toronto Press, Toronto; 386p.

Clarke, J.M. and Schuchert, C.

1899: The nomenclature of the New York series of geological formations; Science, new ser., v.10, 878 - 898.

Clark, T.H.

1952: Montreal Area - Laval and Lachine Areas; Que. Dep. Mines, Geol. Rept. 46, 159p.

1966: Châteauguay Area; Geol. Explor. Ser., Dep. Nat. Resour. Que., Geol. Rept. no. 122.

Clifton, H.E.

1976: Wave formed sedimentary structures - a conceptual model; in Beach and nearshore sedimentation, ed. Davis, R.A. Jr. and Ethington, R. Soc. Econ. Paleont. Mineral. Special Publ. no. 24, 126 - 148.

Clifton, H.E., Hunter, R.E. and Phillips, R.L.

1971: Depositional structures and processes in the non-barred high energy nearshore; J. Sediment. Petrology, v.41, 651 - 670.

Cooper, G.A.

1956: Chazyan and related brachiopods; Smithson. Misc. Collect., v.127, pt. 1.

Cushing, H.P.

1901: New York State Museum 53rd Annual Report; pt. 1, r39 - r69.

1905: Geology of the northern Adirondacks region; New York State Mus. Bull, v.95, 185.

1908: Lower Paleozoic section in northwestern New York; Geol. Soc. Amer. Bull, v.19, 155 - 176.

1911: Nomenclature of the Lower Paleozoic rocks of New York; Amer. J. Sci., (4), v.31, 35 - 145.

1916: Geology in the vicinity of Ogdensburg (Brier Hill, Ogdensburg, and Red Mills Quadrangles); New York State Mus. Bull, v.191, 64p.

Cushing, H.P., Fairchild, H.L., Ruedemann, R., and Smyth, C.H. Jr.

1910: Geology of the Thousand Islands Region (Alexandria Bay, Cape Vincent, Clayton, Grindstone and Theresa Quadrangles); New York State Mus. Bull, v.145, 1 - 194.

Dean, R.G.

1973: Heuristic models of sand transport in surf zone; in Conf. on Eng. Dyn. in the Surf Zone, Sydney, Austral., 7p.

Dobkins, J.E. and Folk, R.L.

1970: Shape development on Tahiti - Nui; J. Sediment. Petrology, v. 40, 1167 - 1203.

Dott, R.H. Jr.

1974: Cambrian tropical storms in Wisconsin; Geology, v. 2, no.5, 243 - 246.

Dugas, J.

1952: Geology of the Perth map - area, Lanark and Leeds

Counties, Ontario; Unpubl. Ph.D Dissertation, Mc Gill Univ., Montreal.

Eaton, A.

1824: A geological and agricultural survey of the district adjoining the Erie Canal in the state of New York; Albany, Packard and Van Benthuysen, 163p.

Eagleson, P.S. and Dean, R.G.

1966: Small amplitude wave theory; in Estuary and Coastline Hydrodynamics, ed. Ippen, A.T.; Mc Graw-Hill Book Co., New York, 1 - 92.

Emmons, E.

1838: Report of the second geological district of the state of New York; New York State Geol. Surv., 2nd Ann. Rept., 185 - 252.

Ethington, R.L.C. and Clark, D.L.

1971: Lower Ordovician conodonts in North America; in Symposium on conodont biostratigraphy, ed. Sweet, W.C. and Bergstrom, S.M.; Geol. Soc. Amer. Mem. 127, 63 - 82.

Fairbridge, R.W.

1967: The encyclopedia of atmospheric sciences and astrogeology; Encyclopedia of Earth Sciences ser., v.2, Reinhold Publ. Corp., New York, 1200p.

Fisher, D.W.

1954: Lower Ordovician stratigraphy of the Mohawk Valley; Geol. Soc. Amer. Bull, v.65, no. 1, 70 - 96.

1955: Time span of the Theresa and Potsdam Formations in the region peripheral to the Adirondack Mountains,

New York (abs.); Geol. Soc. Amer. Bull, v.66, 1558 - 1559.

Fisher, D.W.

1956: The Cambrian System of New York; in El Sistema Cambrico, su paleogeografia y el problema de su base, ed. Rogers, J.; Internatl. Geol. Cong. 20th, Mexico City Symposium, pt. 2, 321 - 351.

1962: Correlation of the Cambrian rocks in New York State; New York Mus. and Sci. ser., Geol. Surv. maps and chart ser., no. 2.

1962b: Correlation of the Ordovician rocks in New York State; New York Mus. and Sci. ser., Geol. Surv. maps and charts ser., no. 3.

1968: Geology of the Plattsburgh and Rouses Point, New York - Vermont, Quadrangles; New York State Mus. and Sci. ser., Geol. Surv. maps and charts ser., no. 18.

1977: Correlation of the Hadrynian, Cambrian and Ordovician rocks in New York State; New York State Mus. and Sci. ser., Geol. Surv. maps and charts ser., no. 25, 75p.

Fisher, D.W. and Hanson, G.F.

1951: Revision in the geology of Saratoga Springs, New York and vicinity; Amer. J. Sci., v.249, no. 11, 795 - 814.

Flager, C.W.

1966: Subsurface Cambrian and Ordovician of Trenton Group - Precambrian interval in New York State; New York State Mus. and Sci. ser., Geol. Surv. maps and charts ser., no. 8.

Flemming, B.W.

1977: Langebaan Lagoon: a mixed carbonate - siliciclastic tidal environment in a semi arid climate; Sediment., v.18, 61 - 95.

Folk, R.L.

1959: Practical petrographic classification of limestone; Amer. Ass. Petol. Geol., Bull, v.43, 1 - 38.

1968: Petrology of sedimentary rocks; Hemphills Book Store, Austin, Texas, 170p.

Folk, R.L. and Ward, W.C.

1957: Brazos River bar: a study in the significance of grain size parameters; J. Sediment. Petrology, v.27, 3 - 26.

Fox, W.T., Ladd, J.W. and Martin, M.K.

1966: A profile of the four moments measure perpendicular to a shoreline, South Haven, Michigan; J. Sediment. Petrology, v.36, no. 4, 1126 - 1130.

Friedman, G.M.

1961: Distinction between dune, beach and river sands from the textural characteristics; J. Sediment. Petrology, v.31, 514 - 529.

1962: Comparison of movement measures for sieving and thin section data in sedimentary petrological studies; J. Sediment. Petrology, v.32, no. 1, 15 - 25.

1967: Dynamic processes and statistical parameters composed for size frequency distributions of beach and river sands; J. Sediment. Petrology, v.37, 327 - 354.

Galvin, C.J.

1968: Breaker type classification on three laboratory beaches;

J. Geophys. Res., v.73, no. 12, 3651 - 3659.

Gebelein, C.D.

1976: Open marine subtidal and intertidal stromatolites (Florida, the Bahamas and Bermuda); in Stromatolites, ed. Walter, M.R.; Develop. Sedimentol., v.20, Elsevier Scientific Publ. Co., 381 - 388.

Gibbs, R.J., Matthew, M.D. and Link, D.A.

1971: Relationship between sphere size and settling velocity; J. Sediment. Petrology, v.41, no. 1, 7 - 18.

Gittins, J., Macintyre, R.M. and York, D.

1967: The age of carbonatite complexes in eastern Canada; Can. J. Earth Sci., v.4, 651 - 655.

Greggs, R.G. and Bond, I.J.

1971: Conodonts from the March and Oxford Formations in the Brockville Area, Ontario; Can. J. Earth Sci., v.8, 1455 - 1471.

1972: A principal reference section proposed for the Nepean Formation of probable Tremadocian Age near Ottawa, Ontario; Can. J. Earth Sci., v.9, 933 - 941.

1977: Discussion: The age and upper boundary of the Nepean Formation in its type section near Ottawa, Ontario; Can. J. Earth Sci., v.14, no. 11, 2669 - 2671.

Gregory, J.W.

1929: The earthquake south of Newfoundland and submarine canyons; Nature, v.124, p.945.

Goddard, E.N., Trask, P.D., De Ford, R.K., Rove, O.N., Singewald, J.T. Jr., and Overbeck, R.M.

1970: Rock - Color Chart; Geol. Soc. Amer., Boulder, Colorado.

Harvey, J.G. and Vincent, C.E.

1977: Observations of shear in near bed currents in the southern North Sea; Estuaries and Coastal Marine Sci. v.5, 715 - 731.

Heald, M.T. and Baker, G.F.

1977: Diagenesis of the Mt. Simon and Rose Run Sandstone in western West Virginia and southern Ohio; J. Sediment. Petrology, v.47, 66 - 77.

Hills, E.S.

1972: Elements of structural geology, 2nd ed.; John Wiley & Son Inc., New York, 502p.

Hodder, R.W. and Hollister, V.F.

1974: Some geologic distinctions among lineaments for the mineral explorationist; in Proceeding of the 1st International Conference on the New Basement Tectonics, ed. Hodgson, R.A., ParkerGay, S. Jr. and Benjamins, J.Y.; Utah Geol. Assoc. Publ., no. 5, 453 - 461.

Hodgson, E.A. and Doxes, W.W.

1930: The Grand Bank earthquake, November 18, 1929; Proc. Seismol. Soc. Amer., Eastern Section, 72p.

Hoffman, P.

1976: Stromatolite morphogenesis in Shark Bay, Western Australia; in Stromatolites, ed. Walter, M.R.; Develop. Sediment., v.20, Elsevier Scientific Publ. Co., 261 - 271.

Hofmann, H.J.

1972: Stratigraphy of the Montreal Area; Internat. Geol. Cong. 24th Section Guidebook, Excursion B-03.

Hudson, R.

1959: Laboratory investigation of rubble mound breakwaters; J. Waterways and Harbours Div. ASCE, v.85, 93 - 121.

Ingle, J.C. Jr.

1966: The movement of beach sand; Develop. Sediment., v 5, Elsevier Scientific Publ. Co., 221p.

Inman, D.L.

1957: Water generated ripples in nearshore sands; U.S. Army Corp. of Engineers Board Tech. Memo., no. 100; 67p.

Isachsen, Y.W.

1974: Fracture analysis of New York State using multi-stage remote sensor data and ground study; possible application to plate tectonic modeling; in Proceeding of 1st International Conference on the New Basement Tectonics, ed. Hodgson, R.A., ParkerGay, S. Jr. and Benjamins,J.Y.; Utah Geol. Assoc. Publ., no. 5, 200 - 217.

Kay, G.M.

1942: Ottawa - Bonnechère Graben and Lake Ontario Homocline; Geol. Soc. Amer., Bull, v.53, 585 - 646.

Keith, A.

1930: The Grand Bank earthquake; Proc. Seismol. Soc. Amer., Eastern Section (suppl.).

Keith, M.L.

1949: Sandstones as a source of silica sands in southwestern Ontario; Ont. Dep. Mines Ann. Rept., v.55, pt. 5, 36p.

Keppie, J.D.

1977: Plate tectonic interpretation of Paleozoic world maps (with emphasis on circum - Atlantic orogens & southern

Nova Scotia); Nova Scotia Dep. Mines, paper 77 - 3, 45p.

King, C.A.M.

1972: Beach and coasts, 2nd ed.; St. Martin's Press, New York, 570p.

Kinsman, D.J.J. and Park, R.K.

1976: Algal belt and coastal sabkha evolution, Trucial Coast, Persion Gulf; in Stromatolites, ed. Walter, M.R., Develop. Sediment., v.20; Elsevier Scientific Publ. Co., 421 - 433.

Kirchgasser, W. and Theokritoff, G.

1971: Precambrian and ~~Lower~~ Paleozoic stratigraphy, northwest St. Lawrence and Jefferson Counties, New York; in Geological Studies of the Northwest Adirondacks Region, Fieldtrip Guidebook, May 7 - 9, 1971, ed. Van Diver, B.B. ; 43rd Ann. Meeting, New York State Geol. Assoc., B0 - B24.

Klein, G. deV.

1971: A sedimentary model for determining paleotidal range; Geol. Soc. Amer. Bull, v.82, 2585 - 2592.

1977: Clastic tidal facies; CEPCO, Champaign, Ill., 149p.

Komar, P.D.

1974: Oscillatory ripple marks and the evaluation of ancient wave conditions and environments; J. Sediment. Petrology, v.44, 169 - 180.

1975: Beach processes and sedimentation; Prentice-Hill Inc., New Jersey, 429p.

Komar, P.D. and Gaughan, M.K.

1973: Airy wave theory and breaker height prediction; Proc. 13th Conf. Coast. Eng., 405 - 418.

Krumbein, W.C.

1941: Measurement and geological significance of shape and roundness of sedimentary particles; J. Sediment. Petrology, v.11, p. 68.

Krumbein, W.C. and Sloss, L.L.

1963: Stratigraphy and sedimentation, 2nd ed.; W.H. Freeman and Co., 660p.

Kumarapeli, P.S. and Saull, V.A.

1966: The St. Lawrence Valley System: a North American equivalent of the East African Valley System; Can. J. Earth Sci., v.3, no. 5, 639 - 658.

Laflamme, J.C.K.

1908: Les tremblements de terre de la région de Quebec; Proc. Roy. Soc., sect. 4, ser. 3, no. 1, p 157.

Larsen, G. and Chilingar, G.V.

1967: Diagenesis of sediments; Develop. Sedimentol., v.8, 551p.

Le Méhauté, B. and Koh, R.C.Y.

1967: On the breaking of waves arriving at an angle to the shore; J. Hydraul. Res., v.5, 67 - 80.

Lewis, D.W.

1965: Cambrian (Pre-Beekmantown) sedimentation in southwestern Quebec with especial reference to three wells near Montreal; Unpubl. Ph.D. Dissertation, McGill Univer., Montreal.

Lewis, D.W.

1971: Qualitative Petrographic interpretation of Potsdam Sandstone (Cambrian) southwestern Quebec; Can. J. Earth Sci., v.8, 853 - 882.

Lewis, T.L.

1963: A paleocurrent study of the Potsdam Sandstone of New York, Quebec and Ontario; Unpubl. Ph.D. Dissertation, Ohio Univer., Ohio.

Logan, Sir W.E.

1843: Preliminary report of progress 1842; Preliminary Rept., Geol. Surv. Can.

1861: On the track of an animal lately found in the Potsdam Formation; Can. Nat., v.5, 279-285.

1863: Geology of Canada; Geol. Surv. Can., Rept. of Prog. from commencement to 1863; 87-110.

Longuet-Higgins, M.S.

1953: Mass transport in water waves; Roy. Soc. London, Phil. Trans., Ser. A, v.245, 535-581.

Marcou, J.

1862: The Taconic and Lower Silurian rocks of Vermont and Canada; Boston, Proc. Nat. Hist. Soc., v. 8, 239-253.

Mason, C.C. and Folk, R.L.

1958: Differentation of beach, dune and aeolian flat environments by size analysis, Mustang Island, Texas; J. Sediment. Petrology, v.28, 211-226.

Massey, B.S.

1970: Mechanics of fluids; 2nd ed., Van Nostrand Reinhold Co., London; 508p.

Miller, M.C., Mc Cave, I.N. and Komar, P.D.

1977: Threshold of sediment motion under unidirectional currents; Sedimentol., V.24, 504 - 527.

Miller, R.L.

1976: Role of vortices in surf zone prediction: sedimentation and wave force; in Beach and nearshore sedimentation, ed. Davis, R.A. Jr. and Ethington, R.L., SEPM Special Publ. no. 24, 92 - 114.

Moiola, R.J. and Weiser, D.

1968: Textural parameters: an evaluation; J. Sediment. Petrology, v.38, 45 - 53.

Murray, A.

1849: On the geology of the country on the south side of the St. Lawrence from Montreal and Lake Champlain to the Chaudière River, Quebec; in Rept. Progress 1847 - 1848, ed. Logan, Sir W.E.; Geol. Surv. Can., 5 - 92.

Pettijohn, F.J., Potter, P.E. and Siever, R.

1973: Sand and sandstone; Springer-Verlag Publ., New York; 618p.

Philpotts, A.R. and Miller, J.A.

1963: A Precambrian glass from Alexis des Monts, Quebec; Geol. Mag., v.100, no.4, p 337.

Power, M.C.

1953: A new roundness scale for sedimentary particles; J. Sediment. Petrology, v.23, 177 - 219.

Raymond, P.E.

1913: Ordovician of Montreal and Ottawa; Geol. Surv. Can., Guide Book, no. 3, 137 - 162.

Reineck, H.E. and Singh, I.B.

1975: Depositional sedimentary environments with reference to terrigenous clastics; Springer-Verlag Publ., New York: 439p.

Reineck, H.E. and Wunderlick, F.

1968: Zur Unterscheidung von asymmetrischen Oszillationsrippeln und Stromungsrippeln; Senckenbergiana Lethaea, v.49, 321-345.

Richard, I.V.

1973: Stratigraphy and structure of the subsurface Cambrian and Ordovician carbonates in New York State; New York State Mus. and Sci. ser., Geol. Surv. maps and charts ser., no. 18.

Rick, M.J. and Moffat, J.S.

1977: Sedimentological significance of fecal pellets of Macoma balthica in Minas Basin, Bay of Fundy; J. Sediment. Petrology, v. 47, no. 4, 1425-1436.

Rittenhouse, G.

1943: A visual method of estimating two-dimensional sphericity; J. Sediment. Petrology, v. 13, 80-81.

Sahakian, A.S.

1963: Paleocurrent study of the Potsdam Sandstone of New York and Quebec; Unpubl. Ph.D. Dissertation, Harvard Univer., Cambridge, Mass., 118p.

Seymour, R.J.

1977: Estimating wave generation on restricted fetches; J. Waterway Port Coastal & Ocean Div., Amer. Soc. Civ.

Engrs., v. 103, no. WW2, 251-264.

Silvester, R.

1974: Coastal Engineering, 1, generation, propagation and influence of waves; Elsevier Scientific Publ. Co., 457p.

Simons, D.B. and Richardson, E.V.

1962: Resistance to flow in alluvial channels; Amer. Soc. Civ. Engrs., Trans., v. 127, 927-953.

Sneed, E.D. and Folk, R.L.

1958: Pebbles in the lower Colorado River, Texas, a study in particle morphogenesis; J. Geol., v. 66, 114-150.

Stein, R.A.

1965: Laboratory study of Total load and apparent bed load; J. Geophys. Res., v. 70, 1831-1842.

Stewart, H.B. Jr.

1958: Sedimentary reflections of depositional environments in San Miguel Lagoon, Baja California, Mexico; Amer. Ass. Petrol. Geol. Bull, v. 42, 2567-2618.

Sweet, W.C., Ethington, R.L. and Barnes, C.R.

1971: North American Middle and Upper Ordovician conodont fauna; in Symposium on conodont biostratigraphy, ed. Sweet, W.C. and Bergstrom, S.M.; Geol. Soc. Amer. Mem., v. 127, 163-206.

Tannar, W.F.

1971: Numerical estimates of ancient waves, water depth and fetch; Sedimentol., v. 16, 71-88.

Trudinger, P.A. and Mendelson, F.

1976: Biological processes and mineral deposition; in Strom-

atolites, ed. Walter, M.R.; Develop. Sedimentol. v. 20, 663-672.

Ulrich, E.O. and Cushing, H.P.

1910: Age and relations of the Little Falls Dolomite (Calciferous) of the Mohawk Valley; New York State Mus. Bull, v. 140, 97-140.

Visher, G.S.

1969: Grain size distribution and depositional processes; J. Sediment. Petrology, v. 39, 1074-1106.

Wiesnet, D.R.

1963: Composition grain size, roundness and sphericity of the Potsdam Sandstone (Cambrian) in northeastern New York; J. Sediment. Petrology, v. 1, 5-14.

Wilson, A.E.

1946: Geology of the Ottawa-St Lawrence Lowland, Ontario and Quebec; Geol. Surv. Can. Mem. 241, 66p.

Wilson, J.L.

1975: Carbonate facies in geologic history; Springer-Verlag Publ., New York; 471p.

Wilson, M.E.

1921: The relationships of the Paleozoic to the Precambrian along the southern border of the Laurentian Highlands in southeastern Ontario and adjacent portions of Quebec; Roy. Soc., Canada, Proc. and Trans, 3rd ser. 14, sec. 4, 15-24

Wright, J.F.

1923: Brockville-Mallorytown map area, Ontario; Geol. Surv.

Can. Mem. 134, 63p.

Wynne Edwards, H.R.

1967: Westport map-area, Ontario; with special emphasis on the Precambrian rock; Geol. Surv. Can. Mem. 346, 142p.

Yochelson, E.L. and Copeland, M.J.

1974: Taphonomy and taxonomy of the Early Ordovician Gastropod Ceratopea canadensis (Billing) 1865; Can. J. Earth Sci., v. 11, no. 1, 189-207.

Paleoenvironmental interpretation of the Beekmantown Group within the Ottawa Basin

Appendices 1 to 7

A thesis presented to the
School of Graduate Studies, University of Ottawa

In partial fulfilment of the
requirements for the degree
Master of Science
in Geology

By

John I. Cass

June 1979

LIST OF APPENDICES

Appendix	Title	Page
1	Consumer's Gas Well (Russell County)	1
	Table A1: Lithofacies terms used	2
	Table A2: Standard microfacies used	3
	Well log	5
2	Locations of samples	38
3	Inclusive graphic statistics	42
4	Moment statistics	61
5	Insoluble mud size distribution	74
6	Estimated paleowave and current conditions under which ripples formed	75
7	Estimated paleoflow conditions under which cross strata formed	84

Appendix 1

Consumer's Gas Company Well (Russell County)

The following well log of the Beekmantown Group is based on an examination of Consumer's Gas Company well, Consumers 16321. The well core is currently stored at the Geological Survey of Canada repository in Ottawa, Ontario, in tray no. 7336-37, index no. 404-23 (Beard, 1970; p. 165).

The core was examined under hand lens and a Heerbrugg variable power binocular microscope. No thin sections of the core are currently available and as a result estimation of carbonate types and abundance was based on the reaction of the samples to dilute (10%) solution of hydrochloric acid. Table A1 lists and defines the lithofacies used in this study. Under Folk's (1959) classification, most of the carbonate strata are micrite or dolomitized micrite. The classification used does not take into consideration the influence of varying amounts of insolubles in the carbonate that would tend to bias the results in favour of dolomitic values. Colour of the core was determined by comparing it with the Geological Society of America rock color chart (Goddard et al; 1970). Texture of the carbonate lithofacies were based on Wilson's (1975; 64-68) standard microfacies classification (Table A2).

Table A1

Carbonate Lithofacies

Classification	Type of reaction to dilute HCl	Time duration
Limestone	violent	immediate
Dolomitic limestone	slow	under 15 sec.
Calcitic dolomite	very slow	under 30 sec.
Dolomite	nil	over 30 sec.

Siliciclastic Lithofacies

Arkose: Sandstone with over 25% feldspar, with feldspar exceeding rock particles.

Mud: insoluble (in HCl) sediment fraction finer than 4 ϕ size.

Quartzitic sandstone: Quartz arenite with a non-carbonate cement.

Quartzose sandstone: Quartz arenite with a carbonate cement.

Quartzwacke: Quartz arenite with greater than 10% argillaceous material and under 10% unstable mineral constituents.

Subarkose: Sandstone with 5 to 25% feldspar, with feldspar exceeding rock particles.

Table A2

Wilson's(1975, 64-69) Standard Microfacies Classification

SMF 14: Lag

Coated and worn particles, in places mixed with ooids and peloids which are blackened and iron-stained, with phosphate. Allochthonous lithoclasts may be present. These lags are characteristically thin deposits, representing slow accumulation of coarse material in zone of winnowing.

SMF 19: Laminated to bioturbated pelleted lime mudstone-wackstone grading occasionally into pelsparite with fenestral fabric, Loferite.

An ostracod-peloid assemblage is common within these mudstones. Micrite with scattered foraminifera, gastropods and algae also occur. This biota represents deposition in very restricted bays and ponds.

SMF 20: Algal stromatolite mudstone

Dense and closely-spaced growth laminations swelling over protuberances characterize this sediment. Fine lime mud is preferentially trapped on the highest areas resulting in lamination contrary to gravity. Such stromatolitic structure is commonest in intertidal zone.

Table A2 (continued)

SMF 21: Spongiostrome mudstone fabric

Tuffeted algal fabric is preserved in fine lime mud sediment in tidal ponds.

SMF 22: Micrite and onkoids

Wackstone or floatstone texture. This is a quiet-water sediment with algal balls composed of light organic matter which is later calcifed or which traps fine detrital lime mud. They are typical of shallow water backreef environment, found typically on edges of ponds or channels.

SMF 23: Unlaminated homogeneous unfossiliferous pure micrite

This lime mudstone is mainly deposited in somewhat saline or evaporative tidal ponds. Selenite crystals may form at random or in rosettes in this sediment.

SMF 24: Coarse lithoclastic-bioclastic rudstone or floatstone

The clasts are generally of unfossiliferous micrite or calcisiltite, the matrix variable but sparse. Crossbedding and edgewise arrangement of pebbles may occur. The sediment is normally termed intraformational limestone pebble conglomerate. It is formed as a lag deposit in tidal channels.

Appendix 1

Consumer's Gas Company Well: Consumers 16321.

Lithofacies	Nomenclature	Depth (m)
	CHAZY GROUP	
	Rockcliffe Formation	
Fine quartzitic sandstone (N7) with calcitic dolomite clasts (N3); SMF 23		573.25
Sharp lithological break		
	BEEKMANTOWN GROUP	
	Beauharnois Formation	
Calcitic dolomite (N3/N4); SMF 23, cut by shale (N2) laminae		573.48
Calcitic dolomite (N3/N4); SMF 19		573.91
Shale (N2) grading into calcitic dolomite (N3); SMF 23.		574.71
Calcitic dolomite (N3); SMF 23		574.79
Shale (N2)		574.85
Calcitic dolomite (N3); SMF 23		575.32
Shale (N2)		575.36
Calcitic dolomite (N3); SMF 23		575.72
Calcitic dolomite (N3); SMF 19, interlayered with fine quartzose sandstone (N8), homogeneous		576.46
Calcitic dolomite (N3); SMF 19		576.43
Fine quartzitic sandstone (N8), homogeneous		576.46
Calcitic dolomite (N3/N4); SMF 23		579.09
Shale (N2)		579.11

Lithofacies Nomenclature	Depth (m)
Dolomitic limestone (N4); SMF 23	579.45
Shale (N2)	579.47
Dolomitic limestone (N4); SMF 19, alternating with shale (N2)	579.73
Calcitic dolomite (N3); SMF 23, grading into dolomitic limestone (N5); SMF 23	580.26
Dolomitic limestone (N5/N7); SMF 19	580.76
Dolomitic limestone (N5); SMF 24, intermixed with fine quartzose sandstone (N7)	580.80
Calcitic dolomite (N7); SMF 23	580.94
Shale (N2)	580.96
Calcitic dolomite (N3/N4); SMF 23	581.17
Shale (N2)	581.20
Dolomitic limestone (5Y6/1); SMF 19, alternating with calcitic dolomite (N6); SMF 19	581.49
Shale (N2)	581.64
Dolomitic limestone (N2/N6); SMF 19, argillaceous, traces of bioturbation, sparite vugs	582.04
Dolomitic limestone (N6); SMF 24	582.09
Shale (N2)	582.13
Calcitic dolomite (N5, 5Y6/1); SMF 23, scattered pyrite grains up to -2ϕ size	582.23
Shale (N2)	582.27
Calcitic dolomite (N5); SMF 19, interlayered with shale (N2)	582.32
Dolomitic limestone (N4); SMF 24, interlayered with	

Lithofacies Nomenclature	Depth (m)
shale (N2)	582.39
Calcitic dolomite (N4); SMF 19, interlayered with shale (N2)	582.63
Calcitic dolomite (N4); SMF 19, alternating with dolomitic limestone (N5); SMF 19	583.35
Calcitic dolomite (N5); SMF 19/22/23, alternating with dolomite (N5); SMF 23/24, clasts up to -3ϕ size, onkoids at base	583.45
Calcitic dolomite (N3); SMF 23, argillaceous	583.57
Calcitic dolomite (N3); SMF 19/23, shale (N2) flasers	583.62
Dolomitic limestone (N6); SMF 19, strongly bioturbated	583.85
Shale (N2)	584.06
Dolomitic limestone (N6); SMF 19	584.09
Calcitic dolomite (N3); SMF 19/23, alternating with shale laminae	584.69
Calcitic dolomite (N4); SMF 19, alternating with dolomitic limestone (N6); SMF 19	584.74
Dolomitic limestone (N6); SMF 19/24, with shale (N2)	585.14
Dolomitic limestone (N6); SMF 23	585.26
Dolomitic limestone (N6); SMF 19/24, alternating with calcitic dolomite (N4); SMF 19/24, sparite vugs	585.31
Calcitic dolomite (N4); SMF 19, alternating with dolomite (N3); SMF 23	585.52
Calcitic dolomite (N4); SMF 19/24, alternating with dolomite (N3/N4); SMF 23/24	586.13
Calcitic dolomite (N2); SMF 23, with shale (N2) laminae	586.18

Lithofacies Nomenclature	Depth (m)
Dolomitic limestone (N6); SMF 19/22, alternating with calcitic dolomite (N3); SMF 19/22, sparite veinlets, strongly bioturbated	586.73
Dolomitic limestone (N6/N7); SMF 23	586.90
Dolomitic limestone (N6); SMF 24, interclasts up to -3ϕ size	586.95
Shale (N2), grading into dolomitic limestone (N5); SMF 19	587.00
Calcitic dolomite (N3/N4); SMF 23	588.31
Dolomite (N5, 5Y6/1); SMF 23	588.43
Shale (N2)	588.51
Dolomite (5Y6/1); SMF 23	588.53
Dolomite (5Y6/1); SMF 19/24, alternating with calcitic dolomite (N5/N6); SMF 19/24, sparite vugs	588.60
Calcitic dolomite (N5); SMF 19, with shale (N2)	588.84
Calcitic dolomite (N5); SMF 23	589.34
Calcitic dolomite (N2); SMF 23 grading into dolomitic limestone (N2); SMF 23	589.52
Calcitic dolomite (N2); SMF 19/22/24, alternating with dolomitic limestone (5Y6/1); SMF 19/22	589.72
Calcitic dolomite (N3/N5); SMF 22/24	589.79
Calcitic dolomite (N3/N5); SMF 19, alternating with dolomitic limestone (5Y6/1); SMF 19, soft sediment deformation at 3 to 4 cm intervals, moderate bioturbation	590.64

Lithofacies Nomenclature	Depth (m)
Calcitic dolomite (N3); SMF 19, alternating with dolomitic limestone (5Y5/1); SMF 19	590.90
Dolomitic limestone (5Y5/1); SMF 19, alternating with calcitic dolomite (N5); SMF 19 and shale (N2)	591.22
Calcitic dolomite (N3); SMF 23	591.37
Dolomitic limestone (N3, 5Y3/1); SMF 19, alternating with calcitic dolomite (N3); SMF 19	591.75
Dolomitic limestone (5Y6/1); SMF 19/22, with shale (N2)	592.45
Dolomitic limestone (5Y6/1); SMF 23	592.64
Dolomitic limestone (5Y6/1); SMF 19, alternating with calcitic dolomite (N4); SMF 19	592.82
Calcitic dolomite (N3/N4); SMF 23	593.15
Calcitic dolomite (N3/N4); SMF 24	593.17
Dolomitic limestone (5Y6/1); SMF 23, grading into calcitic dolomite (N4); SMF 23	593.30
Dolomitic limestone (5Y6/1); SMF 19, moderately bioturbated	593.40
Shale (N2)	593.49
Dolomitic limestone (5Y6/1); SMF 19	593.50
Dolomitic limestone (5Y6/1); SMF 24 and calcitic dolomite (N3); SMF 24, as lithoclasts	593.69
Dolomitic limestone (N4/N5); SMF 23, cut by sparite veinlets, sharp upper boundary	594.40
Dolomitic limestone (5Y6/1); SMF 24, with shale (N2)	594.43
Calcitic dolomite (N4); SMF 23, sparite veinlets	594.69
Dolomitic limestone (5Y6/1,N6); SMF 19/24, mixed with	

Lithofacies	Nomenclature	Depth (m)
	fine to granular quartzose and quartzitic sandstone, sandstone composed 30 (by vol.) of unit	594.91
Dolomitic limestone (5Y6/1); SMF 19/24, alternating	with calcitic dolomite (N4); SMF 19/24, laminae 2 to 3 cm thick often cut by sandstone or carbonate dykes near the base	595.04
Shale (N2) and fine quartzose sandstone (N7), with	dolomitic limestone (5Y6/1): SMF 24	595.08
Dolomitic limestone (5Y6/1); SMF 19/23/24, alternating	with calcitic dolomite (N4); SMF 19/23/24, often broken by zones of medium to coarse quartzose sandstone (N7)	595.39
Dolomitic limestone (5Y6/1), SMF 19/24, with soft	sediment load structures intermixed with shale	595.49
Dolomitic limestone (5Y5/1, 5Y6/1); SMF 19, with soft	sediment load structures and drag folds, sparite vugs	595.51
Dolomitic limestone (5Y6/1); SMF 24 , sparite infilling	of gastropod molds	595.74
Shale (N2)		595.87
Dolomitic limestone (5Y5/1); SMF 23		595.88
Shale (N2/N3) with dolomitic limestone (5Y5/1); SMF 19		596.01
Dolomitic limestone (5Y6/1,N6) SMF 19/23/24, lamination	inclined 15° from assumed horizontal, desiccation cracks and mud chips abundant, fine quartzose sandstone (N7), dykes common, grading into calcitic	

Lithofacies	Nomenclature	Depth(m)
	dolomite (N3); SMF 19/23	596.52
	Calcitic dolomite (N3); SMF 23, sparite filled veinlets and vugs common	597.00
	Calcitic dolomite (N3/N4); SMF 19, with shale (N2)	597.10
	Calcitic dolomite (N3); SMF 19, alternating with dolomitic limestone (N3); SMF 19	597.94
	Dolomitic limestone (5Y6/1); SMF 19 with both regular and irregular laminae	598.52
	Calcitic dolomite (5Y5/1); SMF 19 and dolomitic limestone (5Y6/1); SMF 19, both argillaceous	598.69
	Dolomitic limestone (5Y5/1); SMF 23 grading into limestone (5Y5/1); SMF 23	598.83
	Shale (N2) alternating with dolomitic limestone (5Y6/1); SMF 23	598.90
	Dolomitic limestone (5Y5/1); SMF 23	599.05
	Dolomitic limestone (5Y5/1); SMF 24, alternating with fine and medium quartzose and quartzitic sandstone	599.67
	Dolomitic limestone (5Y5/1); SMF 19, alternating with calcitic dolomite (N3/N4); SMF 19 and shale (N2)	600.04
	Dolomitic limestone (5Y5/1); SMF 23, sharp upper boundary	600.15
	Dolomitic limestone (5Y5/1); SMF 19/24, alternating with calcitic dolomite (N4); SMF 19/24, deformed laminae and sparite vugs common	600.32
	Calcitic dolomite (N3); SMF 23, grading into dolomite (N3); SMF 23	600.44
	Shale (N2)	600.47

Lithofacies Nomenclature	Depth (m)
Calcitic dolomite (N3); SMF 23	600.58
Shale (N2)	600.65
Calcitic dolomite (N3) SMF 19/23	601.04
Shale (N2)	601.10
Shale (N2) grading into argillaceous calcitic dolomite (N4); SMF 19	601.51
Shale (N2)	601.52
Calcitic dolomite (N3); SMF 19/23	601.76
Calcitic dolomite (N3); SMF 19 alternating with shale (N2)	601.78
Dolomitic limestone (5Y5/1); SMF 19/24, sparite vugs, sharp erosional lower boundary	602.07
Dolomite (5Y5/1); SMF 19/24, alternating with calcitic dolomite (N4, 5Y5/1); SMF 19/24, desiccation cracks common	603.44
Dolomite (5Y6/1); SMF 19, alternating with calcitic dolomite (5Y6/1); SMF 19	604.03
Shale (N2), alternating with calcitic dolomite (N4); SMF 24	604.23
Dolomite (N4); SMF 19/24, rip-up clasts and desiccation cracks increasing in abundances toward base	605.07
Shale (N2); interlayered with calcitic dolomite (N4); SMF 19	605.24
Calcitic dolomite (N4); SMF 19/24, alternating with dolomitic limestone (N3); SMF 19/24, desiccation cracks increase toward base	605.52

Lithofacies	Nomenclature	Depth(m)
Shale (N2), with calcitic dolomite (N3); SMF 24 lithoclasts		605.57
Shale N2)		605.60
Dolomitic limestone (5Y5/1); SMF 19, abundant sparite vugs		605.79
Dolomitic limestone (N2,5Y5/1); SMF 19/24		605.95
Dolomitic limestone (5Y6/1); SMF 19/20		606.54
Calcitic dolomite (N6,5Y6/1); SMF 19		606.67
Calcitic dolomite (5Y6/1); SMF 24		606.83
Dolomitic limestone (5Y6/1); SMF 23		607.05
Shale (N2)		607.08
Dolomitic limestone (5Y6/1); SMF 19		607.11
Shale (N2)		607.13
Dolomititic limestone (5Y6/1); SMF 19/20		607.32
Dolomitic limestone (5Y6/1); SMF 23		607.38
Shale (N2)		607.39
Dolomitic limestone (5Y6/1); SMF 19/23		607.50
Shale (N2)		607.56
Dolomitic limestone (5Y6/1); SMF 23 interlayered with fine to medium quartzose sandstone, molds of selenite crystals ?		607.87
Dolomitic limestone (5Y6/1); SMF 19, strongly bioturbated		608.39
Dolomitic limestone (5Y6/1); SMF 23, with irregular shale (N2) laminae		608.75
Dolomitic limestone (5Y6/1); SMF 19/24, strongly		

Lithofacies	Nomenclature	Depth (m)
	bioturbated near base	608.84
Dolomitic limestone (N6); SMF 23		608.91
Dolomitic limestone (5Y5/1,5Y6/1); SMF 19/24, rip - up	clasts and desiccation cracks abundant near base	609.42
Dolomitic limestone (N4, 5Y5/1); SMF 23		609.80
Dolomitic limestone (5Y6/1); SMF 19, strongly	bioturbated	609.94
Dolomitic limestone (N4,5Y6/1); SMF 19/20, bulbous	stromatolites	610.52
Dolomitic limestone (5Y6/1); SMF 19/23, strongly	bioturbated, laminae poorly defined	610.63
Shale (N2)		610.66
Dolomitic limestone (N4); SMF 19, with laminae of very	fine to fine quartzose sandstone	610.68
Dolomitic limestone (5Y6/1); SMF 24		610.73
Dolomititic limestone (5Y6/1); SMF 19/24		610.85
Shale (N2)		610.87
Dolomitic limestone (5Y6/1); SMF 19/20, with fine	quartzose sandstone , alternating with calcitic dolomite (5Y5/1); SMF 19/2	611.21
Calcitic dolomite (5Y6/1); SMF 19, alternating with	dolomitic limestone (5Y6/1); SMF 19	611.26
Calcitic dolomite (5Y6/1); SMF 24		611.29
Calcitic dolomite (5Y6/1); SMF 23		611.34
Shale (N2)		611.37
Calcitic dolomite (5Y6/1); SMF 23		611.44

Lithofacies Nomenclature	Depth (m)
Shale (N2)	611.47
Calcitic dolomite (5Y6/1); SMF 23	611.58
Calcitic Dolomite (5Y6/1); SMF 19, strongly bioturbated	611.80
Shale (N2)	611.84
Calcitic dolomite (5Y6/1); SMF 19	611.87
Shale (N2)	611.90
Calcitic dolomite (5Y6/1); SMF 23, selenite crystals?	611.91
Shale (N2)	612.07
Calcitic dolomite (N5); 19/23, selenite crystals	612.08
Calcitic dolomite (N5); SMF 23, with shale (N2)	612.13
Dolomitic limestone (5Y6/1); SMF 20	612.28
Dolomitic limestone (5Y6/1); SMF 24, desiccation cracks and rip-up clasts	612.64
Dolomitic limestone (5Y6/1); SMF 19, strongly bioturb.	612.70
Shale (N2)	612.76
Calcitic dolomite (5Y6/1); SMF 19/24	612.78
Shale (N2)	612.87
Calcitic dolomite (5Y6/1); SMF 23	612.90
Shale (N2)	612.93
Calcitic dolomite (5Y6/1); SMF 23	612.95
Calcitic dolomite (5Y6/1); SMF 19/24, desiccation cracks and rip-up clasts common	613.00
Shale (N2)	613.15
Calcitic dolomite (5Y6/1), SMF 24, interlayered with fine quartzose sandstone	613.18
Calcitic dolomite (N4, 5Y6/1); SMF 19/23, alternating with dolomitic limestone (N4); SMF 19	613.41

Lithofacies Nomenclature	Depth (m)
Dolomitic limestone (N4); SMF 19, argillaceous	613.46
Dolomitic limestone (N4); SMF 19/23, sparite veinlets	613.52
Dolomitic limestone (5Y5/1); SMF 23, sparite veinlets and shale (N2)	614.02
Dolomitic limestone (N4/N5); SMF 19/20?, soft sediment deformation	614.30
Dolomitic limestone (N5); SMF 23	614.54
Dolomitic limestone (N4/N5); SMF 19/24, rip-up clasts in medium quartzose sandstone at base	614.57
Shale (N2)	614.62
Dolomitic limestone (5Y5/1); SMF 19/23	614.63
Dolomitic limestone (5Y5/1); SMF 19	614.68
Dolomitic limestone (5Y6/1); SMF 19/23, strongly bioturbated	614.89
Calcitic dolomite (5Y5/1); SMF 23, sparite vugs	615.17
Dolomite (5Y5/1); SMF 19, argillaceous	615.75
Calcitic dolomite (N5,5Y6/1); SMF 19/20/23	616.50
Shale (N2)	616.52
Dolomitic limestone (N5,5Y5/1); SMF 11/23, alternating with shale (N2) at 3 to cm intervals, lower 5 cm grade into SMF 19	616.76
Dolomitic limestone (5Y6/1); SMF 20/21?	616.93
Shale (N2)	617.04
Dolomitic limestone (5Y6/1); SMF 23 with irregular shale (N2) laminae	617.09
Dolomitic limestone (5Y6/1); SMF 19	617.49

Lithofacies Nomenclature	Depth (m)
Dolomitic limestone (5Y5/1); SMF 23	617.61
Dolomitic limestone (5Y5/1); SMF 24	618.20
Dolomitic limestone (5Y5/1); SMF 19/23, moderately bioturbated	618.25
Dolomitic limestone (5Y5/1); SMF 23	618.44
Shale (N2)	618.57
Dolomitic limestone (5Y5/1); SMF 23, with shale (N2) laminae	618.59
Dolomitic limestone (5Y5/1); SMF 23, upper boundary sharp	618.64
Dolomitic limestone (5Y5/1); SMF 24, desiccation cracks and rip-up clasts abundant	618.73
Shale (N2)	618.84
Dolomitic limestone (5Y5/1); SMF 23, sparite vugs common	618.86
Shale (N2) with clasts of dolomitic limestone (5Y5/1); SMF 24	620.02
Dolomitic limestone (5Y5/1); SMF 19/23	620.16
Dolomitic limestone (5Y6/1); SMF 24	620.33
Dolomitic limestone (5Y6/1); SMF 23, sparite vugs common	620.40
Dolomitic limestone (5Y6/1, 5Y7/1); SMF 19, laminae thicken toward base	620.88
Calcitic dolomite (N4/N5); SMF 23, sparite vugs common	621.48
Calcitic dolomite (N5); SMF 19/23	623.11
Calcitic dolomite (N5); SMF 19	623.37
Calcitic dolomite (N4/N5); SMF 19/23 alternating with	

Lithofacies Nomenclature Depth (m)

dolomitic limestone (N4/N5); SMF 19/23 ..... 624.54

Dolomitic limestone (N4/N5); SMF 19/23, argillaceous . 625.14

Dolomitic limestone (N4/N5); SMF 24, argillaceous 625.75

Dolomitic limestone (N4/N5); SMF 19/23 ..... 625.89

Dolomitic limestone (N6); SMF 19, strongly bioturbated 626.97

Dolomitic limestone (N4/N); SMF 19/23 ..... 627.19

Calcitic dolomite (N6); SMF 19/23, SMF 19 increasing with shale (N2) and degree of bioturbation toward base 628.19

Dolomitic limestone (N4/N6); SMF 19/23 ..... 630.02

Dolomitic limestone (N4/N5); SMF 19/20?/23/24, shale (N2) increase toward base 631.27

Dolomitic limestone (N4/N6); SMF 19 ..... 632.05

Dolomitic limestone (N4/N6); SMF 23 ..... 632.25

Dolomitic limestone (N4/N6); SMF 24 ..... 632.46

Dolomitic limestone (N4/N6); SMF 23/24 ..... 632.57

Dolomitic limestone (N4/N6); SMF 19/23 ..... 632.70

Dolomitic limestone (N6); SMF 19, with shale (N2) 633.68

Calcitic dolomite (N6); SMF 23 ..... 634.89

Calcitic dolmite (N6); SMF 19 ..... 635.16

Calcitic dolomite (N5); SMF 23 ..... 636.80

Dolomitic limestone (N5); SMF 19, strongly bioturbated 637.26

Dolomitic limestone (N5); SMF 24 ..... 637.67

Dolomitic limestone (N5); SMF 19/23 ..... 637.85

Dolomitic limestone (N5); SMF 19/24 ..... 637.97

Dolomitic limestone (N5); SMF 19/23 ..... 638.32

Lithofacies Nomenclature	Depth (m)
Dolomitic limestone (N5); SMF 19, strongly bioturbated	640.41
Shale (N2)	640.44
Dolomitic limestone (N5); SMF 19/23	640.47
Dolomitic limestone (N5); SMF 23/24	641.00
Dolomitic limestone (N5); SMF 19/24	641.40
Dolomitic limestone (N5); SMF 20/21?	641.51
Calcitic dolomite (N4); SMF 23	641.72
Calcitic dolomite (N4/N5); SMF 19/23/24, strongly bioturbated in zones	642.72
Shale (N2)	643.54
Calcitic dolomite (N4); SMF 19, strongly bioturbated	643.57
Calcitic dolomite (N4/N5); SMF 19/23, laminae poorly defined	643.66
Calcitic dolomite (N4/N5); SMF 23, becoming argillaceous toward base	643.85
Dolomitic limestone (N4/N5); SMF 19, alternating with calcitic dolomite (N4/N5); SMF 19	644.09
Dolomitic limestone (N4); SMF 23, with shale (N2) laminae	644.14
Shale (N2)	644.34
Dolomitic limestone (N4/N5); SMF 19/24, strongly bioturbated, lithoclasts and gastropod bioclasts in medium quartzose sandstone at base	644.36
Limestone (N4, 5Y5/1); SMF 23	644.67
Dolomitic limestone (5Y5/1); SMF 23, shale at 3 to 5 cm intervals	645.26

Lithofacies	Nomenclature	Depth (m)
	Dolomitic limestone (N5,5Y5/1); SMF 19/24, alternating with limestone (N5, 5Y5/1); SMF 19/24, laminae poorly defined	645.38
	Dolomitic limestone (N5,5Y5/1); SMF 13/19/24, alternating with limestone (N5, 5Y5/1);SMF 13/19/24,onkoids	645.57
	Limestone (N5,5Y5/1); SMF 19/23, laminae poorly defined	645.87
	Limestone (N5,5Y5/1); SMF 19	646.81
	Dolomitic limestone (5Y6/1, 5Y7/1), SMF 23	646.94
	Dolomitic limestone (5Y7/1); SMF 19/21/24, alternating with calcitic dolomite (5Y7/1); SMF 19/24	647.06
	Dolomitic limestone (5Y6/1, 5Y7/1); SMF 19/23, alternating with calcitic dolomite (5Y6/1, 5Y7/1); SMF 19/23, SMF 23 increasing toward base	647.22
	Calcitic dolomite (N5,5Y5/1); SMF 19/20	647.42
	Calcitic dolomite (N5); SMF 19/23/24	647.94
	Dolomite (N4); SMF 19, interlayered with fine quartzose sandstone, sparite filled ostrocod? shells	648.56
	Dolomiti (N4/N5); SMF 19/23 alternating with fine quartzose sandstone, sparite vugs common near base	648.88
	Calcitic dolomite (N5); SMF 24, interlayered with medium quartzose sandstone	650.25
	Calcitic dolomite (N5); SMF 23	650.37
	Calcitic dolomite (N5); SMF 24	651.05

Lithofacies Nomenclature	Depth (m)
Calcitic dolomite (N4/N5); SMF 19/23	651.32
Calcitic dolomite (N5); SMF 19, alternating with dolomitic limestone (N5); SMF 19, strongly bioturbated, brachiopod shell fragments and flaser of shale (N2) common, sparite vugs	651.97
Dolomitic limestone (N5); SMF 19	653.21
Dolomitic limestone (N5); SMF 24, soft sediment deformation	653.63
Dolomitic limestone (N5); SMF 19	653.63
Dolomitic limestone (N5); SMF 24	655.07
Shale (N2)	655.12
Dolomitic limestone (N5); SMF 19, strongly bioturbated; brachiopod and ostracode shell fragments	655.13
Shale (N2)	655.81
Dolomitic limestone (N5); SMF 23, with isolated shale (N2) laminae and sparite vugs	655.82
Dolomitic limestone (N5); SMF 19	656.10
Dolomitic limestone (N5); SMF 19, argillaceous	656.39
Shale (N2)	656.91
Dolomitic limestone (N5/N6); SMF 19/24	656.93
Dolomitic limestone (N5/N6); SMF 19/20/22/24	657.37
Dolomitic limestone (N5/N6); SMF 19, alternating with limestone (N5/N6); SMF 19, ostracode bioclasts increasing toward base	657.40
Dolomitic limestone (N5/N6); SMF 19, sharp upper boundary	657.57

Lithofacies	Nomenclature	Depth (m)
Dolomitic limestone (N4/N5); SMF 19, sharp upper boundary, ostracode and brachiopod bioclasts, sparite vugs		657.90
Dolomitic limestone (N5/N6); SMF 19, alternating at 9 to 14 cm with 1 to 2 cm thick shale (N2) laminae		658.01
Dolomitic limestone (N5/N6); SMF 19/24		658.46
Dolomitic limestone (N5); SMF 19/23		658.69
Dolomitic limestone (N5); SMF 19, with shale (N2)		659.02
Dolomitic limestone (N5); SMF 19/23, with gastropod bioclasts common		659.89
Dolomitic limestone (N5); SMF 23, grading downward into calcitic dolomite (N5); SMF 23		660.80
Dolomitic limestone (N5, 5Y5/1); SMF 19/24		660.98
Calcitic dolomite (5Y6/1); SMF 24		661.20
Calcitic dolomite (5Y6/1); SMF 19/24, SMF 24 occurring in 3 narrow zones		661.31
Calcitic dolomite (5Y6/1); SMF 19, small scale current ripples		661.54
Calcitic dolomite (5Y6/1); SMF 19/24, with flaser beds, fine to medium quartzose sandstone in SMF 24		662.33
Calcitic dolomite (N5); SMF 19, sparite veinlets		662.82
Calcitic dolomite (5Y6/1); SMF 19/24 , soft sediment deformation		662.86
Calcitic dolomite (N5); SMF 19/23		662.93
Shale (N2)		663.30
Calcitic dolomite (N6/N7); SMF 19/24, occurring in		

Lithofacies Nomenclature Depth (m)

7 zones 663.57

Calcitic dolomite (N6/N7); SMF 24 ..... 664.12

Buck Bridge Formation

March Member

Calcitic dolomite (N6/N7); SMF 24, sharp upper boundary , intermixed with fine to medium quartzose sandstone 664.38

Fine to medium quartzose sandstone (5YR9/1), even parallel laminae, moderately bioturbated 664.49

Shale (N2) 664.55

Dolomitic limestone (N6/N7); SMF 19/24, sandy, sparite vugs common 664.56

Fine to medium quartzose sandstone (N8), unlaminated grading downward into dolomitic limestone (N6/N7); SMF 24 ..... 665.10

Dolomitic limestone (N6/N7); SMF 19, with zones of fine to medium quartzose sandstone (N7), parallel laminae 665.70

Fine to medium sandstone (N7); even, parallel laminae interlayered with dolomitic limestone (N6), SMF 19, sand 40 to 60% of unit 666.34

Dolomite (N5); SMF 24, mixed with fine quartzose sandstone and dolomitic limestone (N6/N7); SMF 19 clasts 666.60

Lithofacies	Nomenclature	Depth (m)
	Dolomite (N5); SMF 24, intermixed with shale (N2) and fine to medium quartzose sandstone, sparite vugs increasing in abundants toward base	666.78
	Dolomite (N5); SMF 24, desiccation cracks infilled with fine to medium quartzose sandstone	667.00
	Fine quartzose sandstone (N8/N9); even parallel laminae, flaser bedding	667.10
	Fine quartzose sandstone (N8/N9); even parallel laminae, dolomitic limestone (N5/N6); SMF 24, rip-up clasts	667.57
	Dolomitic limestone (N5/N6); SMF 24, with flaser bedding, sharp upper and lower boundaries	668.22
	Dolomitc limestone (N5/N6); SMF 24, with flaser bedding, grading downward into very fine quartzose sandstone	668.34
	Fine quartzose sandstone (N8); small scale ripples	668.56
Heuvelton member		
	Very fine to fine quartzitic sandstone (N7/N8); flaser bedding, laminae 2 to 8 cm thick (ave. 3 cm), small scale ripples (RI 5 to 14)	668.78
	Fine quartzose sandstone (N7); with bifurcated wavy flaser bedding	669.69
	Fine quartzose sandstone (5PB5/2); unlaminated	669.88
	Fine quartzose sandstone (N8); even parallel laminae	

Lithofacies	Nomenclature	Depth (m)
	disrupted in 2 narrow zones	670.16
Silty	to very fine quartzose sandstone (N8); lamination disrupted, quantity of silt and carbonate cement increasing toward base	670.28
Dolomitic	limestone (5PB5/2); SMF 24, grading into silt and fine quartzose sandstone (N8), sparite vugs common	670.38
Dolomitic	limestone (5PB5/2); SMF 23/24, grading down into very fine quartzose sandstone (N8).....	670.70
Shale	(N2)	670.81
Very fine	quartzose sandstone (N8); even parallel laminae, *Chondrite?* burrows	670.82
Very fine to fine	quartzose sandstone (N8, 5PB5/2); even parallel laminae, bedding 5 to 12 cm thick, lower 60 cm has increase in shale(N2) and 5PB5/2 colouration toward the base, erosional boundaries at 4 cm intervals	671.17
Fine to medium	quartzose sandstone (N8); even parallel laminae, erosional boundaries at 7 to 8 cm intervals	672.60
Fine to medium	quartzose sandstone (N8); ripples up to 2.5 cm high (asymmetric),even, parallel laminae .	673.44
Dolomitic	limestone (N4); SMF 19/24, alternating with shale (N2) at 0.3 to 1 cm intervals	673.68
Quartzose	paraconglomerate (5B7/1); clasts up to -4.5ϕ, quartz with pyrite veinlets and fluid vacuoles,	

Lithofacies	Nomenclature	Depth (m)
	dolomitic limestone (N5); SMF 19/24, cement	673.72
	Fine to coarse quartzose sandstone (N9); flaser bedding	673.80
	Quartzose paraconglomerate (5B7/6); clasts up to -3ϕ size, dolomitic limestone (N4); SMF 24, cement	673.95
	Silty to very fine quartzose sandstone (N9); even, parallel laminae	673.99
	Dolomitic limestone (N4, 5PB5/1); SMF 19, with shale(N2) laminations, soft sediment deformation common	674.04
	Fine to medium quartzitic sandstone (N8); even, parallel laminae, flaser bedding common	674.22
	Medium quartzose sandstone (5PB5/1); SMF 19, even, parallel laminae 5 mm thick	675.69
	Fine to medium quartzitic sandstone (N8); without lamination	675.77
	Very fine to fine quartzose sandstone (N8); without lamination	675.88
	Polymictic paraconglomerate (N8,5PB5/1); clasts of metaquartzite (N8), up to -3 ϕ size, intermixed with dolomitic limestone (5PB5/1); SMF 24, rip-up clasts, dolomitic limestone (5PB5/1); SMF 24, cement	675.95
	Fine to medium quartzose sandstone (N8); even, parallel laminae, flaser bedding in zones, erosional boundaries (5 zones)	676.04
	Fine to coarse quartzitic sandstone(N8); even, parallel	

Lithofacies	Nomeclature	Depth (m)
	laminae, flaser bedding at regular intervals	676.27
Very fine to fine quartzose sandstone (N7); even parallel	laminae, small scale ripples and flaser bedding occurring in 7 zones	677.57
Fine to coarse quartzose sandstone (5PB5/1); even,	parallel laminae.....	679.64
Fine to coarse quartzose sandstone (N8); even parallel	laminae and flaser bedding	679.74
Fine to coarse quartzose sandstone (5PB5/1); even,	parallel laminae, shale (N2) at irregular intervals, brachiopod bioclasts common	679.94
Fine quartzose sandstone (5PB5/1); even, parallel laminae	and flaser bedding occurring in 5 zones	680.26
Fine to medium quartzose sandstone (N8/N9); even,	parallel laminae	682.16
Fine to medium quartzose sandstone (5PB5/1); flaser	bedding, shale increasing toward base	682.35
Very fine to fine quartzose sandstone (5PB5/1); even,	parallel laminae and flaser bedding , moderately bioturbated	683.18
Fine to medium quartzose sandstone (5PB5/1); even, parallel	laminae	684.64
Fine to coarse quartzitic sandstone (N8); even, parallel	laminae grading into unlaminated bedding in 4 zones	685.13
Fine quartzitic sandstone (N8); poorly defined laminae	occasionally broken by wavy flaser bedding	685.55

Lithofacies	Nomenclature	Depth (m)
	Fine Quartzitic sandstone (N8); strongly bioturbated ..	685.70
	Shale (N2)	685.80
	Fine to medium quartzose sandstone (5PB5/1); even, parallel laminae with flaser bedding zones	686.04
	Fine to medium quartzose sandstone (N8); even, parallel laminae to flaser bedding, flaser bedding becoming more abundant toward base	687.10
	Fine to medium quartzose sandstone (N8); even, parallel laminae, unlaminated and flaser bedding, laminae 2 to 3 cm thick	687.45
	Very coarse quartzose sandstone (N8); clasts up to -3ϕ size, limestone (N7); SMF 23, cement	688.62
	Very fine quartzose sandstone (N7/N8); flaser bedding .	688.67
	Very fine to fine quartzose sandstone (5PB5/1); even, parallel laminae and wavy flaser bedding	688.98
	Fine to medium quartzose sandstone (N7, 5PB8/1); unlaminated, 3 zones of colour gradation	689.51
	Fine to medium quartzitic sandstone (N8); unlaminated bedding alternating with flaser bedding, strongly bioturbated	690.12
	Fine to medium quartzose sandstone (N8); graded bedding from 5 to 15 cm thick	692.81
	Fine to medium quartzose sandstone (N8); unlaminated ..	693.53
	Fine to medium quartzose sandstone (5PB5/1); laminae disrupted by moderate bioturbation	694.38
	Silty to fine quartzose sandstone (N8); unlaminated with	

Lithofacies	Nomenclature	Depth (m)
	flaser bedding in narrow zones	694.69
	Fine to medium quartzose sandstone (N8, 5 B5/1); even, parallel laminae grading into unlaminated beds (35 zones), each zone marked by thin flaser bedding boundary	695.98
	Fine to medium quartzose sandstone (N7); even, parallel laminae alternating with flaser bedding (5 zones), carbonate and mud increasing toward base	698.91
	Fine to medium quartzose sandstone (N5); unlaminated	699.32
	Fine to medium quartzose sandstone (N7/N8); unlaminated beds grading into polymictic paraconglomerate of limestone (N5); SMF 23, clasts and metaquartzite clasts up to -3ϕ size	699.52
	Fine to medium quartzose sandstone (N8/N9); even, parallel laminae with zones of coarse clasts, flaser bedding of dolomitic limestone (N5)	700.13
	Fine to medium quartzose sandstone (5Y6/1); erosional boundaries with dolomite rip-up clasts	700.59
	Fine to medium quartzose sandstone (5PB5/1); alternating with medium quartzose sandstone (5Y6/1), dolomite (5Y6/1); SMF 19/23/24 and dolomitic limestone (N6/N7); SMF 19/23/24, beds	701.43
	Silty to fine quartzose sandstone (N5); unlaminated and flaser bedding	702.56
	Very fine quartzitic sandstone (N3); unlaminated	702.76
	Dolomitic limestone (N5); SMF 24	702.88

Lithofacies	Nomenclature	Depth (m)
	Very fine quartzose sandstone (N2); unlaminated	702.97
	Fine to medium quartzitic sandstone (N7/N8); colouration at 4 to 11 cm spacing	703.18
	Dolomitic limestone (5PB5/1); SMF 24, wavy flaser bedding	703.46
	Fine to medium quartzitic sandstone (N7/N8); even, parallel laminae to unlaminated bedding occurring at 4 to 11 cm intervals	703.56
	Dolomitic limestone (5PB5/1); SMF 19/24, grading toward fine to medium quartzose sandstone (N7/N8); sharp upper boundary	704.42
	Fine to medium quartzose sandstone (N8); unlaminated and flaser bedding grading toward fine quartzitic sandstone (N8); with flaser bedding	705.61
	Fine to coarse quartzose sandstone (5PB5/1); erosional boundaries with zones of large clasts up to -2ϕ size	706.76
	Fine to medium quartzitic sandstone (N8); even, parallel laminae and flaser bedding	706.88
	Fine to medium quartzose sandstone (N8); even, parallel laminae, unlaminated and flaser bedding, slightly to moderately bioturbated, bioturbation increasing toward base.....	708.05
	Fine to medium quartzitic sandstone (N8); even, parallel laminae, unlaminated and flaser bedding, small scale cross strata (2 to 4 cm high) at 2 to 4 cm	

Lithofacies	Nomenclature	Depth (m)
	intervals, desiccation cracks and bioturbation increasing toward base	712.31
	Fine to medium quartzose sandstone (5B9/1); flaser bedding disrupted by bioturbation and desiccation cracks, brachiopod bioclasts common	712.79
	Fine quartzitic sandstone (N8); unlaminated beds with shale (N2)	712.89
	Fine to medium quartzose sandstone (5B9/1); even, parallel laminae, moderately bioturbated, burrows up to 3 cm deep, brachiopod bioclasts are common	712.99
	Fine to medium quartzitic sandstone (N8); even parallel laminae	713.37
	Fine to medium quartzose sandstone (N8, 5B9/1); even, parallel laminae, strongly bioturbated at irregular zones, brachiopod bioclasts common	713.58
	Fine to medium quartzose sandstone (5PB6/2); even, parallel laminae and cross strata up to 3 cm high, moderately bioturbated	713.90
	Fine to medium quartzose sandstone (N8); even, parallel laminae, unlaminated and flaser bedding mixed with dolomitic limestone (5B9/1)	714.46
	Shale (N2)	714.70
	Fine to medium quartzose sandstone (N8); even, parallel laminae and cross strata up to 3 or 4 cm high, symmetric ripples (RI= 2)	714.71

Lithofacies	Nomenclature	Depth (m)
	Fine to medium quartzose sandstone (N8, 5PB6/1); even, parallel laminae and flaser bedding, desiccation cracks common, colour grades into N8 toward base	715.70
	Fine to medium quartzose sandstone (N8); even, parallel laminae and cross strata up to 2 cm high, ripples (RI= 1 to 15), bedding 6 to 10 cm thick	715.94
	Fine to medium quartzose sandstone (5PB6/1); even, parallel laminae and flaser bedding, beds 6 to 12 cm thick	718.52
	Fine to medium quartzitic sandstone (N8); planar cross strata up to 4 cm high, brachiopod bioclasts common	719.02
	Fine quartzose sandstone (N8); even, parallel laminae and flaser bedding at 10 cm intervals	719.55
	Fine to medium quartzose sandstone (5PB6/1); even, parallel laminae with shale (N2) at irregular intervals	719.79
	Fine to medium quartzitic sandstone (N8); even, parallel laminae and planar cross strata up to 6 cm high, grading into fine quartzose sandstone (N8) and dolomitic limestone (5PB5/1); SMF 19, toward base	719.94
	Fine to medium quartzose sandstone (N8, 5PB5/1); even, parallel laminae grading downward into dolomitic limestone (5PB5/1); SMF 19, moderately bioturbated	722.07

Lithofacies Nomenclature Depth (m)

Fine to medium quartzitic sandstone (N7/N8); even parallel laminae, unlaminated and flaser bedding, *Diplocraterion* burrows up to 6 cm deep, cross strata from 4 to 5 cm high 723.61

Fine to medium quartzose sandstone (N4, 5PB5/1); even parallel laminae cut by *Diplocraterion* burrows 725.12

Fine to medium quartzose sandstone (N7); even parallel laminae 725.36

Potsdam Formation

Keeseville Member

Fine to medium quartzitic sandstone (5PB6/1); even parallel laminae, moderately bioturbated 726.44

Very fine to fine quartzitic sandstone (N7/N8); even parallel laminae, moderately bioturbated 729.39

Shale (N5) 729.53

Fine to medium quartzitic sandstone (N5/N8); unlaminated, colour darkening toward base 729.63

Fine to medium quartzitic sandstone (N8); unlaminated bedding with narrow zones of N5 or N6 colour laminae, in places moderately bioturbated 729.69

Fine to medium quartzitic sandstone (N8); even parallel laminae up to 1 cm thick, coarse to granular sandstone and shale (N2) in narrow

Lithofacies	Nomenclature	Depth (m)
	disrupted zones	730.59
Fine quartzitic sandstone	(N8, 5PB6/1); even laminae, moderately bioturbated, in zones laminae show alternating colours, cross strata 5 cm high	734.26
Medium to coarse quartzitic sandstone	(N8); even parallel laminae interlayered with shale (N2), granular sandstone at 5 to 8 cm intervals, ripples 1 to 2 cm in length (RI = 1 to 4)	736.09
Fine to medium quartzitic sandstone	(N8); even parallel laminae intermixed with orthoquartzitic comglomerates, clasts up to -6ϕ size	737.05
Fine to medium quartzitic sandstone	(N8); even parallel laminae, unlaminated bedding interlayered with shale (N4), burrows abundant, grading into orthoquartzitic conglomerate with -4ϕ size clasts near base	737.92
Fine quartzitic sandstone	(N8), even parallel laminae alternating with orthoquartzitic conglomerates in 4 zones	739.14
Fine to medium quartzitic sandstone	(N8); even parallel laminae, low bioturbation, cross strata 3 to 6 cm high, grading downward into flaser bedding	740.97
Fine quartzitic sandstone	(N3/N6); even parallel laminae, isolated clasts of microcline up to -1ϕ size, quartz grains increasing in size toward	

Lithofacies	Nomenclature	Depth (m)
	the base	741.97
	Fine to medium quartzitic sandstone (N5/N7); even parallel laminae, unlaminated and flaser bedding, shale (N2) clasts up to -1ϕ size	742.18
	Fine to medium quartzitic sandstone (N5/N7); even parallel laminae cut by shale (N3) laminae at 15 cm intervals, current ripples up to 2 cm in length	747.67
	Shale (N2)	748.28
	Fine to medium quartzitic sandstone (N7/N8); even parallel laminae, shale (N2) interlayered in middle of unit at 15 to 19 cm intervals	748.34
	Fine to medium quartzitic sandstone(9N5/N7); even laminae beds8 to 10 cm thick, cross strata 8 cm high, narrow coarse sandstone laminae toward base	749.50
	Fine to medium quartzitic sandstone (N7/N8), even parallel laminae interlayered with shale (N3) laminae, bioturbation low	751.94
	Shale (N2)	753.14
	Medium quartzitic sandstone (N7); even parallel laminae, interlayered with shale (N5)	753.16
	Fine to medium quartzitic sandstone (N6); even laminae interlayered with shale (N4), cross strata 11 cm high	756.00
	Fine to medium quartzitic sandstone (N8); moderately bioturbated, interlayered with shale (N2/N7)	

Lithofacies Nomenclature	Depth (m)
laminae that thicken with depth	756.13
Shale (N5)	763.52
Very fine to medium quartzitic sandstone (N5/N7); even parallel laminae in graded bedding 60 cm thick ..	763.59
Fine to medium quartzitic sandstone (N5/N8); interlayered with shale (N2) at 12 cm intervals, shale up to 2 cm thick	766.57
Fine to medium quartzitic sandstone (N8); poorly sorted, brachiopod bioclasts common, interlayered with shale (N4), flaser bedding, thin zones with large quartz clasts up to -4ϕ size	776.84
Shale (N4)	786.56
Fine to medium quartzitic sandstone (N8); interlayered with shale (N4)	786.59

Ausable Member

Silt to medium quartzitic sandstone (N9); grading into silt to medium subarkose sandstone (5YR8/1) with even parallal laminae that are graded, feldspar appears fresh with mininium visible chemical alteration	788.25
Fine to medium subarkose to arkose (5G9/1, 5R8/2); even lamination with graded beds, colour intensity and feldspar content increasing toward base, 5G9/1 associated with coarser sediment laminae	

Lithofacies	Nomenclature	Depth (m)

and 5R8/2 with finer grain laminae, flaser bedding common, asymmetric ripple up to 5 mm size 790.95

Orthoquartzitic conglomerate (N7) within an arkose (5R8/2) matrix, metaquartzite clasts up to -5ϕ size 798.27

Basal member

Fine to medium subarkose to arkose (5R8/4); even lamination, heavy minerals common with their size increasing toward base, quartz grains become increasingly angular with depth, shale (N3) laminae common often surrounded by 5G9/6 laminae, ripples up to 5 mm high (RI ≈ 10) 798.41

Medium to coarse subarkose to arkose (5R8/4); interlayered with shale (N3), arkosic conglomerate with metaquartzic clasts up to -5ϕ size and microcline clasts up to -2.5ϕ size, grains subangular 826.92

End of core 835.15

Appendix 2

Location of Samples

Sample Code	Lot	Concession	Township	County	Province
1	16	IV	Escott	Leeds	Ontario
3	15	IV	Yonge	Leeds	Ontario
4	14	IV	Yonge	Leeds	Ontario
6	6	III	Yonge	Leeds	Ontario
7	5	IV	Yonge	Leeds	Ontario
8	11	III	Yonge	Leeds	Ontario
9	17	III	Yonge	Leeds	Ontario
10	11	I	Yonge	Leeds	Ontario
11	27	I	Elizabethtown	Leeds	Ontario
12	15	IV	Yonge	Leeds	Ontario
13	16	V	Yonge	Leeds	Ontario
14	16	V	Yonge	Leeds	Ontario
15	24	IX	Elizabethtown	Leeds	Ontario
16	12	VII	Yonge	Leeds	Ontario
17	12	VI	Yonge	Leeds	Ontario
18	12	VI	Yonge	Leeds	Ontario
19	12	VIII	Yonge	Leeds	Ontario
20	6	III	Yonge	Leeds	Ontario
21	16 -.18	VII	Lansdowne	Leeds	Ontario
22	24	I	Yonge	Leeds	Ontario
23	22	I	Leeds	Leeds	Ontario
24	34	V	Leeds	Leeds	Ontario
25	38	V	Pittsburgh	Leeds	Ontario

Sample Code	Lot	Concession	Township	County	Province
26	13	III	Pittsburgh	Leeds	Ontario
27	23	II	Crosby North	Leeds	Ontario
28	24	II	Crosby North	Leeds	Ontario
29	26	II	Crosby North	Leeds	Ontario
30	31	I	Crosby North	Leeds	Ontario
31	26	III	Crosby North	Leeds	Ontario
32	31	VI	Crosby North	Leeds	Ontario
33	39	VII	Crosby North	Leeds	Ontario
34	1	IV	Pittsburgh	Leeds	Ontario
35	19 - 24	X - XI	Storrington	Leeds	Ontario
36	13	IX	Storrington	Leeds	Ontario
37	15 - 18	IX	Storrington	Leeds	Ontario
41	5	IV	Crosby South	Leeds	Ontario
42	25	V	Bastard	Leeds	Ontario
44	24	V	Bastard	Leeds	Ontario
45	6	IV	Crosby South	Leeds	Ontario
46	23	V	Bastard	Leeds	Ontario
47	24	VI	Bastard	Leeds	Ontario
48	23	VII	Bastard	Leeds	Ontario
50	22	VIII	Bastard	Leeds	Ontario
51	22	X	Bastard	Leeds	Ontario
52	12	XIII	Lansdowne	Leeds	Ontario
53	2	VII	Yonge	Leeds	Ontario
54	15	IX	Yonge	Leeds	Ontario
55	21	IX	Yonge	Leeds	Ontario
56	25	X	Lansdowne	Leeds	Ontario

Sample Code	Lot	Concession	Township	County	Province
57	22 - 23	XIII	Lansdowne	Leeds	Ontario
58	4	XI	Lansdowne	Leeds	Ontario
59	5	XI	Lansdowne	Leeds	Ontario
60	4	XI	Lansdowne	Leeds	Ontario
61	21 - 22	VII	Bastard	Leeds	Ontario
62	5 -6	IV	Crosby South	Leeds	Ontario
63	9	I	Burgess South	Leeds	Ontario
401-1A	22	I	Elizabethtown	Leeds	Ontario
401-1B	22	I	Elizabethtown	Leeds	Ontario
401-1C	21	I	Elizabethtown	Leeds	Ontario
401-2	24	I	Elizabethtown	Leeds	Ontario
401-3	27 - 28	I	Elizabethtown	Leeds	Ontario
401-4	28	I	Elizabethtown	Leeds	Ontario
401-5	29	I	Elizabethtown	Leeds	Ontario
401-6	10	I	Yonge	Leeds	Ontario
ST-1	23	II	Nepean	Carleton	Ontario
0-1	30	V	Nepean	Carleton	Ontario
0-2	3	II	Nepean	Carleton	Ontario
0-3	4	II	Nepean	Carleton	Ontario
0-4	6, 7, 8	I	Nepean	Carleton	Ontario
0-5	21	I	March	Carleton	Ontario
0-6	4	II	Torbolton	Carleton	Ontario
0-7	19	IV	March	Carleton	Ontario
0-8	21	IV	March	Carleton	Ontario
C-1	22	VI	Drummond	Lanark	Ontario
C-2	1	V	Ramsay	Lanark	Ontario

Sample Code	Lot	Concession	Township	County	Province
C-3	5	VII	Ramsay	Lanark	Ontario
C-4	11	VII	Ramsay	Lanark	Ontario
DW-1	29	V	Montague	Lanark	Ontario
DW-2	23	I	Elmsley South	Lanark	Ontario
DW-3	25	VII	Elmsley North	Lanark	Ontario
DW-4	24	VII	Elmsley North	Lanark	Ontario
DW-7	1	IV	Burgess South	Lanark	Ontario
DW-8	21	II	Elmsley South	Lanark	Ontario
DW-9	21	VI	Elmsley North	Lanark	Ontario
DW-10	25	VII	Elmsley North	Lanark	Ontario
DW-12	24	X	Elmsley North	Lanark	Ontario
RR2	4	I	Bathurst	Lanark	Ontario
WRR3	21	XII	Bedford	Frontenac	Ontario
HW16	7	IX	Oxford	Grenville	Ontario
CH1	85	II	Havelock	Huntington	Quebec
CH1A	2	III	Franklin	Huntington	Quebec
CH2A	23	VIII	Huntington	Huntington	Quebec
CH2B	187	V	Hemmingford	Huntington	Quebec
CH3				Huntington	Quebec
CH3A				Huntington	Quebec
NY-1	13 km east of Alexandria Bay on Highway 26			Jefferson	New York State

Appendix 3

INCLUSIVE GRAPHIC STATISTICS

Population of sieved samples = 290

Notation		Mean	Standard Deviation
Md	Median		
Me	Graphic mean	2.49ϕ	0.73ϕ
S_I	Inclusive Graphic Standard Deviation	1.08ϕ	0.51ϕ
S_{KI}	Inclusive Graphic Skewness	0.27	0.17
K'_G	Transformed Kurtosis	0.53	0.07
1%	1st percentile clast size	0.73ϕ	0.85ϕ
CTϕ	Coarse truncation point grain size	1.54ϕ	0.83ϕ
CT%	Population C fraction of sample	15.8 %	17.0 %
BWϕ	Backwash point grain size	2.13ϕ	0.42ϕ
FTϕ	Fine truncation point grain size	3.19ϕ	0.34ϕ
FT%	Population B fraction of sample	23.7 %	19.4 %
Mud%	Insoluble (in HCL) fraction of Pan (> 4ϕ)	13.71%	13.96%
Carb%	Total soluble (in HCL) fraction of sample	9.68%	17.37%

Appendix 3 Inclusive Graphic Statistic

Code	Md	Me	S_I	S_{kI}	K'_G	1%	CTØ	%	FT Ø	%	BWØ	Mud%	Carb%
1-a	1.70	2.05	0.95	0.48	0.42	0.55	1.80	60	3.00	25	-	3	nil
b	2.70	3.12	1.71	0.36	0.41	0.65	1.75	30	3.50	37	3.00	37	4
c	2.95	3.02	0.95	0.19	0.48	1.53	1.50	1	3.50	30	2.25	17	under 1
d	2.75	2.78	0.97	0.06	0.45	1.05	2.00	28	3.50	26	-	11	under 1
e	2.00	2.38	1.13	0.61	0.57	1.00	1.73	30	3.50	16	2.50	12	1
3-a	2.75	2.78	0.83	0.06	0.43	1.20	1.00	1	3.45	25	2.05	.7	under 1
4-a	3.50	3.19	0.91	0.42	0.50	1.60	2.65	18	3.70	60	-	17	5
6-a	2.80	3.12	1.60	0.36	0.50	0.90	0.50	11	3.30	38	2.20	26	5
7-a	1.85	2.20	1.05	0.37	0.52	0.75	1.60	28	3.40	14	2.50	9	under 1
8-a	1.85	2.11	0.97	0.56	0.53	1.00	0.58	5	3.50	10	1.85	7	under 1
8-c	3.35	3.45	1.16	0.18	0.51	1.30	1.50	3	3.50	43	2.50	21	.2
8-e	1.80	2.09	1.08	0.53	0.49	0.70	0.50	<1	3.50	14	2.20	6	under 1
8-f	1.60	1.91	1.07	0.55	0.47	0.90	2.00	23	3.00	18	2.00	6	under 1
8-g	2.20	2.49	0.90	0.49	0.45	0.90	1.50	11	3.40	22	2.20	7	under 1
9-a	2.00	2.07	0.87	0.49	0.54	0.50	0.50	1	3.30	13	2.10	3	under 1
9(2)b	2.30	2.47	0.83	0.34	0.48	0.90	2.30	48	3.50	15	3.00	4	1
10-b	1.80	2.09	1.08	0.40	0.49	1.82	1.50	<1	3.50	40	2.20	23	19

Appendix 3 Inclusive Graphic Statistic

Code	Md	Me	S_I	S_{KI}	K_G'	1%	CTØ	%	FTØ	%	BWØ	Mud%	Carb%
10-d	3.40	3.65	1.22	0.33	0.50	1.75	1.50	<1	3.50	45	3.00	35	16
10-e	3.18	3.40	1.21	0.31	0.48	0.60	1.50	<1	3.20	48	2.20	18	29
10-f	3.17	3.11	0.74	-0.05	0.59	0.75	1.50	<1	3.50	22	2.0/3.0	11	25
10-g	3.38	3.56	1.26	0.25	0.51	0.60	1.50	<1	3.50	44	2.00	34	30
10-i	2.20	2.20	1.61	-0.24	0.73	-3.50	0.50	9	2.70	26	1.50	6	2
10-j(a)	1.90	1.80	0.76	0.09	0.67	0.65	0.50	<1	3.50	11	1.5/2.5	7	nil
10-j(b)	1.75	1.77	1.22	-0.18	0.73	-3.20	0.90	11	3.50	3	2.5/3.0	1	nil
10-k	1.90	1.98	0.62	0.30	0.49	0.55	1.oo	2	3.00	8	2.00	2	nil
10-l	1.82	1.81	0.64	0.22	0.50	0.69	0.40	<1	3.40	5	2.00	3	nil
10-m	2.05	2.21	0.86	0.16	0.42	-1.00	1.10	6	3.50	5	2.00	4	nil
10-n	2.05	2.35	0.86	0.39	0.52	1.00	0.90	<1	3.50	6	1.5/2.6	4	under 1
11-a	3.55	3.43	1.42	-0.08	0.88	0.47	1.50	8	3.20	62	2.10	37	17
11-b	3.05	3.02	0.93	-0.16	0.47	1.00	1.50	3	3.20	46	2.30	17	12
11-c	4.00	4.12	1.27	0.15	0.49	1.90	2.00	3	3.50	65	-	14	51
11-g	3.60	3.96	2.55	0.32	0.48	0.30	0.50	2	3.60	19	1.00	44	35
11-h	2.30	2.00	1.22	0.30	0.53	1.00	1.80	8	3.30	54	-	13	1
12-a	2.45	2.68	0.83	0.42	0.53	1.20	2.00	18	2.50	44	-	9	35

Appendix 3 Inclusive Graphic Statistic

Code	Md	Me	S_I	S_{KI}	K_G'	1%	CTØ	%	FTØ	%	BWØ	Mud%	Carb%
13-a	2.75	2.82	0.89	0.12	0.44	1.05	2.30	34	3.60	23	-	9	35
13-b	2.15	2.27	0.75	0.14	0.52	0.90	2.00	24	3.00	35	-	6	under 1
14-a	4.03	3.37	1.14	-0.95	0.43	1.18	1.50	13	3.00	61	-	51	49
15-b	1.18	3.66	1.33	0.00	0.49	1.18	-	nil	1.80	92	-	41	70
16-a	3.00	3.06	1.26	0.14	0.48	1.10	1.80	19	3.50	34	-	24	20
16-b	3.10	3.68	1.88	0.54	0.54	1.20	2.00	10	3.50	34	-	24	13
17-a	2.20	2.36	1.11	0.32	0.50	1.65	1.10	5	3.40	16	1.60	11	1
17-c	2.20	2.45	0.96	0.34	0.47	1.75	1.50	15	3.20	24	2.00	11	under 1
17-d	2.32	2.42	1.00	0.25	0.55	1.60	0.70	<1	3.10	20	1.80	10	under 1
17-e	2.20	2.37	1.02	0.40	0.48	1.65	1.60	30	3.50	16	3.00	9	2
17-f	2.76	3.08	1.67	0.38	0.51	1.95	1.70	22	3.50	30	-	25	17
17-g	1.30	1.44	1.13	0.36	0.51	0.32	0.50	3	3.10	4	1.0/1.5	2	nil
17-h	2.15	2.40	1.09	0.39	0.52	0.70	1.00	4	3.00	28	1.80	11	under 1
18-a	2.08	2.14	0.88	0.13	0.45	0.60	1.60	36	3.50	7	2.50	5	3
18-b	1.88	1.99	0.96	0.24	0.48	0.45	0.50	1	3.40	7	1.30	5	under 1
18-c	2.22	2.44	1.12	0.31	0.47	0.70	0.50	<1	1.70	65	-	11	1
18-d	3.25	3.22	0.78	-0.07	0.54	1.10	3.00	32	3.50	33	-	15	10

Appendix 3 Inclusive Graphic Statistic

Code	Md	Me	S_I	S_{KI}	K'_G	1%	CTØ	%	FTØ	%	BWØ	Mud%	Carb%
18-e	2.40	2.55	1.26	0.20	0.48	0.30	1.80	35	3.50	22	2.5/3.0	14	40
19-a	2.34	2.54	1.20	0.40	0.57	1.00	1.70	30	3.30	19	-	14	under 1
19-b	2.35	2.32	0.97	0.16	0.61	0.80	0.50	<1	3.20	12	1.5/2.1	8	under 1
19-c	1.65	1.86	1.15	0.52	0.64	0.50	0.30	<1	3.30	1	1.2/2.8	7	under 1
19-d	3.78	3.49	0.76	-0.53	0.55	1.45	2.50	15	3.50	71	-	29	12
19-e	-3.45	-2.03	2.15	0.91	0.77	-3.80	1.40	84	1.40	2	-	2	nil
19-f	2.08	2.35	1.24	0.55	0.61	1.05	1.50	16	3.50	16	2.20	13	nil
19-g	1.90	2.08	0.89	0.45	0.57	0.45	1.00	2	2.80	18	1.80	7	nil
19-h	2.35	2.59	1.08	0.42	0.57	1.00	0.70	<1	3.30	21	2.15	13	under 1
20-a	1.60	1.59	0.57	0.07	0.55	0.35	0.90	8	3.50	2	2.30	1	under 1
20-b	2.22	2.43	1.18	0.40	0.50	0.70	1.00	5	3.50	19	2.25	13	3
20-c	1.85	1.94	0.85	0.37	0.65	0.60	0.50	<1	3.50	6	2.25	6	2
21-a	1.07	1.14	0.72	0.27	0.55	0.10	0.50	18	2.30	8	1.40	1	nil
21-c	1.74	1.88	0.93	0.36	0.60	0.05	1.10	16	3.30	10	2.10	6	nil
21-e	1.22	1.27	0.63	0.18	0.54	0.50	0.00	<1	3.50	2	-	2	nil
22-a	1.95	2.12	1.10	0.47	0.60	0.40	0.04	1	3.50	11	2.20	9	under 1
23-b	1.70	1.74	0.74	0.18	0.50	0.25	1.85	58	3.50	3	-	1	nil

Appendix 3 - Inclusive Graphic Statistic

Code	Md	Me	S_I	$S_{K\,I}$	K_G'	1%	CTØ	%	FTØ	%	BWØ	Mud%	Carb%
23-c	2.00	2.19	1.00	0.48	0.55	0.75	1.00	4	3.30	3	1.90	8	nil
24-a	1.70	1.88	1.43	0.76	0.78	0.65	1.00	4	3.30	9	1.5/2.1	9	under 1
24-b	1.70	1.80	0.72	0.33	0.50	0.70	1.30	32	3.50	3	2.50	3	nil
24-c	2.10	2.17	0.66	0.29	0.55	0.95	1.30	4	3.30	6	2.20	4	1
25-a	2.08	2.09	1.09	0.17	0.47	0.65	1.10	19	3.50	10	-	7	nil
25-b	1.90	2.02	1.04	0.29	0.52	0.50	1.00	14	3.50	10	2.00	6	nil
25-c	1.90	2.09	1.18	0.46	0.56	0.55	0.50	1	3.50	10	1.0/2.0	8	nil
26-c	3.00	4.57	3.59	0.72	0.44	0.20	1.80	28	3.30	46	-	41	27
27-a	1.75	1.97	0.93	0.35	0.52	-1.25	0.50	2	3.50	9	-	4	nil
27-b	2.45	2.48	0.60	0.13	0.53	0.33	2.10	30	3.10	14	-	3	nil
28-a	1.90	2.01	0.82	0.24	0.50	0.80	1.00	8	3.50	6	2.00	3	1
28-b	2.50	2.52	0.82	0.06	0.47	0.65	0.50	<1	3.50	11	1.30	5	nil
29-b	2.10	2.24	1.09	0.41	0.59	0.90	0.50	<1	3.30	14	1.70	11	5
30-a	1.74	1.90	0.80	0.38	0.55	0.70	1.80	5	3.30	6	-	5	under 1
31-a	2.20	2.48	1.34	0.47	0.59	0.78	1.00	2	3.40	19	1.70	14	under 1
31-b	2.00	2.30	1.28	0.43	0.56	0.80	1.50	33	3.50	17	2.00	13	under 1
31-c(1)	1.90	2.01	0.82	0.07	0.69	0.80	1.00	1	3.30	8	2.20	7	under 1

Appendix 3 Inclusive Graphic Statistic

Code	Md	Me	S_I	S_{KI}	K'_G	1%	CTØ/	%	FTØ	%	BWØ	Mud%	Carb%
31-c(2)	1.55	1.55	0.63	-0.08	0.63	-3.00	1.00	2	3.20	1	2.00	1	nil
31-d	1.95	2.38	1.51	0.55	0.65	0.25	0.50	5	3.50	17	1.4/2.0	15	under 1
32-a	2.57	2.84	1.34	0.40	0.59	0.50	1.00	2	3.40	23	2.30	18	under 1
32-b	2.25	2.38	0.80	0.40	0.60	1.15	2.20	54	3.40	9	-	7	under 1
32-c	2.45	2.45	0.69	0.19	0.68	1.23	1.50	7	3.00	10	2.00	6	under 1
33-a	3.05	3.03	1.22	0.02	0.49	1.00	1.50	11	2.50	32	-	23	nil
33-b	2.65	3.31	2.61	0.49	0.63	0.10	0.90	10	3.50	28	-	26	9
33-c	2.50	2.59	1.30	0.26	0.55	0.75	1.70	26	3.50	18	3.00	15	50
33-d	1.55	1.78	1.06	0.42	0.56	0.00	1.70	58	3.30	10	-	7	nil
34-a	5.47	5.46	1.23	0.01	0.49	3.20	2.00	<1	3.50	95	3.00	89	48
35-a	1.85	1.85	0.90	0.13	0.51	0.32	1.00	17	3.20	8	-	4	nil
35-a(2)	0.90	0.77	1.62	0.21	0.62	-2.70	0.00	18	3.00	7	1.50	3	nil
35-b(2)	2.00	2.00	0.63	-0.05	0.51	0.20	1.00	10	3.10	4	1.5/2.5	2	nil
36-a	2.10	2.31	0.91	0.46	0.51	0.80	0.50	<1	3.20	18	2.10	7	1
36-b	1.53	1.65	0.63	0.52	0.61	0.65	1.80	28	2.80	8	1.80	2	nil
36-c	1.55	1.73	0.72	0.60	0.58	0.60	0.50	<1	3.00	8	1.70	2	nil
36-d	1.40	1.50	0.68	0.42	0.58	0.45	1.30	45	3.20	5	2.00	4	under 1

Appendix 3 Inclusive Graphic Statistic

Code	Md	Me	S_I	S_{K_I}	K'_G	1%	CTØ	%	FTØ	%	BWØ	Mud%	Carb%
37-a	1.00	1.05	0.71	0.18	0.53	-0.50	0.00	5	2.70	3	2.00	1	nil
37-b	0.98	1.05	0.50	0.31	0.53	-0.10	0.30	4	2.30	3	1.10	1	nil
41-a	1.08	1.13	0.55	0.18	0.50	0.00	1.00	45	3.50	2	2.30	1	nil
41-b	1.15	1.15	0.67	-0.04	0.49	-0.80	0.60	18	3.50	1	2.30	1	nil
42-a	2.00	2.06	0.72	0.26	0.57	0.80	2.00	52	2.80	15	-	5	under 1
44-b	3.90	4.15	2.36	0.15	0.44	0.82	2.10	30	3.00	63	-	41	78
45-b	2.15	3.07	2.61	0.64	0.71	-1.80	1.20	9	3.40	22	2.20	21	12
45-c	1.80	1.82	1.56	-0.22	0.72	-3.50	0.80	12	3.50	6	2.50	3	nil
45-d	2.10	2.32	0.95	0.42	0.56	0.90	1.00	2	3.50	13	2.20	9	under 1
45-e	2.25	2.45	1.00	0.32	0.49	0.75	0.20	<1	3.00	27	2.00	8	under 1
46-a	3.50	3.77	1.88	0.24	0.44	0.90	0.50	<1	3.10	48	1.5/2.5	48	51
47-a	2.10	2.25	0.88	0.21	0.42	0.80	1.00	5	3.10	7	1.70	4	under 1
47-b	2.05	2.16	0.90	0.15	0.39	0.55	1.00	8	3.10	8	2.00	3	under 1
47-c	2.00	2.20	0.85	0.39	0.51	0.93	1.70	40	3.20	11	-	5	under 1
47-d	2.03	2.24	0.69	0.41	0.61	1.00	1.80	32	3.50	5	2.50	3	1
47-e	1.78	1.72	0.68	0.00	0.51	0.42	1.50	45	3.30	7	2.20	2	nil
48-a	2.35	2.50	1.02	0.35	0.50	0.95	1.20	3	3.10	7	2.10	4	nil

Appendix 3 Inclusive Graphic Statistic

Code	Md	Me	S_I	K_I	K'_G	1%	CTØ	%	FTØ	%	BWØ	Mud%	Carb%
48-b	1.88	2.10	0.87	0.56	0.57	0.75	1.00	<1	3.10	10	1.80	4	under 1
48-c	2.50	2.54	1.21	0.19	0.53	0.72	0.50	<1	3.00	28	1.2/2.0	12	2
48-d	2.16	2.27	0.77	0.31	0.45	0.85	1.10	5	3.50	8	2.0/3.0	9	4
48-e	2.30	2.55	1.19	0.46	0.57	1.03	1.00	<1	3.20	24	1.6/2.7	12	1
48-f	2.50	2.69	0.99	0.32	0.53	1.30	1.50	9	3.20	24	2.25	13	1
48-g	2.05	2.28	0.87	0.45	0.51	1.00	2.00	46	2.80	18	-	7	under 1
48-h	2.26	2.38	0.91	0.29	0.51	1.00	2.20	55	3.20	12	-	8	under 1
48-i	2.40	2.64	1.13	0.40	0.52	1.00	2.10	42	3.50	2	-	14	2
48-j	2.40	2.55	1.00	0.32	0.54	0.93	1.00	1	3.50	16	2.20	11	1
48-k	2.40	2.63	1.11	0.38	0.56	0.80	1.00	2	3.20	22	2.20	14	2
48-l	1.65	1.83	0.70	0.49	0.59	0.70	1.80	59	2.60	15	-	5	nil
50-a	2.50	2.57	0.84	0.07	0.56	0.05	1.80	14	3.00	28	2.50	6	under 1
50-b	2.00	2.08	0.93	0.24	0.57	0.40	0.60	3	3.50	9	2.0/3.0	6	under 1
50-c	2.50	2.67	1.07	0.26	0.52	0.78	1.00	2	2.80	40	-	13	under 1
51-a	1.75	1.93	0.84	0.43	0.61	0.45	1.00	6	2.20	25	1.50	5	under 1
51-b	1.90	2.07	0.78	0.37	0.54	0.80	1.50	23	2.20	32	-	3	nil
52-a	1.36	1.71	1.01	0.52	0.49	0.30	0.60	1	3.40	13	1.1/2.3	3	nil

Appendix 3 Inclusive Graphic Statistic

Code	Md	Me	S_I	S_{K_I}	K'_G	1%	CTØ	%	FTØ	%	BWØ	Mud%	Carb%
52-b	3.25	3.17	0.72	0.19	0.50	1.65	1.50	<1	3.00	32	2.0/2.5	11	2
52-c	1.75	1.97	0.98	0.39	0.54	0.55	0.50	1	3.20	15	1.2/2.2	6	1
52-d	2.30	2.48	0.89	0.27	0.48	0.80	1.00	2	3.50	15	2.30	6	1
52-e	2.08	2.26	0.87	0.32	0.54	0.70	2.00	48	3.50	12	2.50	6	under 1
53-a	2.80	2.81	1.40	0.10	0.48	0.65	1.50	24	3.50	30	2.50	24	77
53-b	2.40	2.80	1.79	0.36	0.45	0.31	0.51	2	3.00	40	1.0/1.6	26	18
53-c	3.05	3.22	1.43	0.23	0.44	1.10	1.00	<1	2.00	73	-	31	2
54-a	2.95	2.97	1.39	0.19	0.49	0.90	1.50	8	3.50	35	2.00	27	15
54-b	3.00	3.13	1.05	0.37	0.55	1.40	1.50	2	3.20	33	2.50	20	14
54-c	2.80	2.88	1.09	0.16	0.46	1.25	1.50	2	3.50	24	2.0/3.2	18	8
54-d	2.96	2.90	0.87	0.05	0.50	1.17	1.00	<1	3.20	36	1.5/2.0	11	20
55-a	3.35	3.50	0.96	0.25	0.48	1.82	1.60	14	-	-	-	30	23
55-b	2.70	2.78	1.16	0.17	0.50	0.88	1.60	14	3.00	40	2.0/2.5	17	13
55-c	4.80	4.48	0.42	-0.04	0.50	3.40	2.50	<1	3.50	99	3.00	88	61
56-b	1.72	2.17	1.35	0.61	0.60	0.52	1.80	53	2.80	23	-	14	48
56-d	2.95	2.91	1.25	0.09	0.60	0.70	1.50	12	3.50	25	2.50	16	21
57-a	2.70	2.92	1.12	0.32	0.45	1.30	1.40	3	3.50	31	3.20	20	6

Appendix 3 Inclusive Graphic Statistic

Code	Md	Me	S_I	S_{K_I}	K'_G	1%	CTØ	%	FTØ	%	BWØ	Mud%	Carb%
57-b	2.31	2.36	1.10	0.09	0.46	0.25	1.60	28	3.42	19	3.10	7	5
57-d	2.35	2.62	1.02	0.47	0.54	1.30	1.55	28	3.42	19	2.20	13	10
57-e	2.15	2.30	0.95	0.25	0.51	0.62	1.30	<1	3.20	22	2.20	6	5
57-f	2.70	2.87	1.16	0.40	0.65	1.30	1.80	11	3.20	26	2.50	16	4
57-g	2.10	2.32	1.04	0.32	0.46	0.55	1.60	30	3.10	26	-	9	7
57-h	2.10	2.38	1.03	0.37	0.48	0.60	2.10	50	3.50	18	3.00	8	6
58-a	2.05	2.25	1.08	0.35	0.47	0.75	0.50	<1	3.50	15	2.20	9	6
59-a	2.60	2.73	0.77	0.21	0.56	1.15	1.00	<1	3.00	32	1.5/2.0	8	6
60-a	2.10	2.21	1.17	0.12	0.52	-2.30	0.80	10	3.60	11	2.00	7	5
60-b	1.70	1.02	1.67	0.48	0.58	-2.95	0.50	23	2.70	13	1.15	4	3
60-c	1.65	1.71	0.70	0.20	0.56	0.45	1.50	40	2.50	12	-	2	nil
61-a	3.18	3.13	0.77	-0.03	0.46	1.60	2.20	18	3.50	38	2.60	24	18
61-b	1.92	1.96	0.75	0.15	0.45	0.83	1.20	20	3.50	3	-	2	nil
61-c	1.75	2.15	1.44	0.72	0.72	0.90	1.80	55	2.70	20	-	13	7
61-d	2.30	2.80	1.53	0.72	0.55	0.80	0.00	<1	3.30	2	0.9/1.5	20	4
61-e	2.05	2.32	1.26	0.60	0.68	1.00	0.50	<1	3.30	16	2.20	13	10
61-f	1.70	1.90	0.75	0.51	0.38	0.65	1.00	2	3.00	12	2.00	5	3

Appendix 3 Inclusive Graphic Statistic

Code	Md	Me	S_I	S_{KI}	K'_G	1%	CTØ	%	FTØ	%	BWØ	Mud%	Carb%
61-g	2.00	2.02	0.76	0.20	0.52	0.73	0.50	<1	3.20	8	1.60	5	6
61-h	1.80	1.88	0.70	0.41	0.63	0.75	0.50	<1	3.50	7	2.20	4	3
61-i	2.20	2.73	1.50	0.54	0.61	0.70	2.00	42	2.70	26	-	41	27
61-j	2.90	2.92	0.82	0.05	0.58	0.80	2.10	26	2.10	74	-	17	12
61-k	2.90	2.92	1.06	0.06	0.48	0.80	2.30	15	3.00	55	-	17	13
61-l	2.00	2.22	0.87	0.66	0.56	0.85	2.20	64	3.00	18	-	6	1
61-m	2.40	2.61	1.00	0.41	0.59	0.90	1.30	2	3.20	22	2.50	12	9
61-n	2.20	2.55	1.23	0.53	0.61	0.90	2.20	52	3.10	22	-	12	29
61-0	1.55	1.85	0.89	0.54	0.51	0.55	1.00	9	3.50	9	1.5/3.0	5	under 1
61-p	1.95	2.00	0.71	0.16	0.48	0.70	0.50	<1	3.50	3	1.50	1	nil
61-q	1.75	1.81	0.60	0.63	0.35	0.55	1.30	30	3.20	5	-	3	1
61-r	1.70	1.90	0.70	0.51	0.54	0.68	1.70	45	3.00	8	-	4	under 1
61-s	1.49	1.59	0.62	0.32	0.54	0.80	1.80	73	3.00	5	-	2	under 1
61-t	3.00	3.48	1.75	0.48	0.57	1.60	1.20	<1	3.40	34	2.20	26	2
61-u	2.05	2.19	0.89	0.44	0.57	1.00	1.00	2	3.00	15	2.00	7	under 1
61-v	2.00	2.14	0.97	0.34	0.54	0.78	1.30	16	3.00	17	2.00	7	under 1
61-w	2.25	2.58	1.28	0.50	0.57	0.95	1.00	2	3.50	20	2.00	15	9

Appendix 3 Inclusive Graphic Statistic

Code	Md	Me	S_I	S_{KI}	K_G	1%	CTØ	%	FTØ	%	BWØ	Mud%	Carb%
61-x	2.12	2.13	0.73	0.12	0.47	1.08	1.50	13	3.00	14	-	7	5
61-y	2.10	2.14	0.85	0.19	0.51	0.90	0.50	<1	3.20	12	1.50	5	4
61-z	2.25	2.38	0.99	0.28	0.49	1.00	1.00	2	3.40	15	2.00	9	7
61-aa	1.80	2.03	0.80	0.51	0.54	1.00	1.50	26	3.20	10	2.00	5	under 1
61-bb	1.90	2.04	0.80	0.38	0.52	1.00	1.50	22	3.10	8	2.60	4	under 1
61-cc	1.88	1.95	0.55	0.18	0.69	1.08	2.00	45	3.00	15	-	6	under 1
61-dd	1.80	1.83	0.60	0.24	0.53	0.93	1.60	42	3.50	6	2.60	3	1
61-ee	1.88	1.92	0.64	0.22	0.58	1.00	2.00	63	3.50	6	2.60	4	under 1
61-ff	1.95	2.18	0.89	0.50	0.59	1.05	1.50	19	3.40	10	2.20	7	1
61-gg	1.88	2.20	1.04	0.49	0.53	0.73	1.50	28	2.60	28	2.00	9	4
61-hh	2.36	2.51	0.97	0.35	0.54	1.10	1.60	25	3.00	35	-	10	8
61-ii	2.22	2.27	0.81	0.05	0.55	1.12	2.00	40	3.00	16	-	5	3
61-jj	2.04	2.12	0.82	0.29	0.60	0.82	1.00	30	3.30	7	1.70	5	4
61-kk	2.45	2.52	0.94	0.29	0.55	1.00	1.20	2	3.50	12	2.20	10	7
61-ll	3.20	3.36	1.34	0.23	0.50	1.35	1.50	3	3.50	40	2.00	28	8
61-mm	2.60	2.73	1.09	0.32	0.63	0.85	1.20	2	3.30	20	1.80	14	11
61-nn	3.35	2.74	1.70	0.39	0.47	1.43	1.50	1	3.40	50	2.30	39	5

Appendix 3 Inclusive Graphic Statistic

Code	Md	Me	S_I	S_{K_I}	K'_G	1%	CTØ	%	FTØ	%	BWØ	Mud%	Carb%
61-oo	2.60	3.38	2.05	0.63	0.53	1.05	2.00	26	2.80	42	2.00	31	15
61-pp	4.15	4.38	2.18	0.22	0.47	1.50	2.10	14	3.50	60	-	50	8
61-qq	1.95	1.95	0.48	0.13	0.58	1.11	1.50	12	3.10	5	2.30	4	3
61-rr	1.94	1.97	0.48	0.21	0.59	1.08	2.50	73	3.50	6	-	2	1
61-ss	2.30	2.34	0.59	0.32	0.61	1.55	2.00	23	2.80	15	-	6	4
61-tt	2.20	2.60	1.21	0.60	0.56	1.24	2.20	50	3.50	20	-	15	3
61-uu	2.50	2.47	0.70	-0.01	0.44	1.31	1.80	19	3.50	8	-	3	2
62-b	1.70	1.77	0.61	0.22	0.49	0.53	0.90	3	3.33	2	1.50	1	nil
63-a	2.00	2.38	1.55	0.42	0.50	0.15	0.50	2	3.00	30	1.0/1.8	17	12
63-b	2.15	2.18	0.64	0.16	0.52	0.90	2.00	42	3.10	8	2.50	4	3
401													
1A-a	2.50	2.54	1.08	0.09	0.51	1.80	1.00	7	3.30	23	-	10	8
1A-b	3.45	3.31	0.87	-0.17	0.47	0.83	1.50	6	3.40	56	2.30	22	17
1A-c	1.68	1.69	0.67	0.12	0.46	0.72	1.00	16	3.10	3	1.50	2	1
1A-i	4.20	4.30	1.44	0.13	0.48	1.75	1.50	<1	3.50	67	2.20	55	28
1A-j	3.42	3.37	0.80	-0.06	0.48	1.55	2.10	9	3.50	47	-	25	19
1B-b	2.12	2.28	1.34	0.28	0.53	0.10	1.60	38	3.40	18	-	13	27

Appendix 3 Inclusive Graphic Statistic

Code 401	Md	Me	S_I	S_{KI}	K'_G	1%	CTØ	%	FTØ	%	BWØ	Mud%	Carb%
1B-c	2.45	2.51	0.96	0.10	0.47	0.70	1.70	20	3.50	14	-	6	5
1B-d	2.15	2.73	1.84	0.61	0.64	0.70	1.70	32	3.50	22	2.70	19	32
1B-e	2.60	2.65	0.97	0.05	0.44	0.65	1.80	23	3.50	22	-	9	7
1B-f	2.45	3.12	1.94	0.55	0.48	0.70	1.80	34	3.00	35	-	29	39
1B-g	2.55	2.62	1.00	0.10	0.46	0.63	1.80	22	3.50	22	-	10	8
1C-a	3.60	3.76	1.62	0.15	0.48	1.00	1.50	6	2.80	70	2.00	39	27
1C-b	2.30	2.47	1.33	0.49	0.69	1.08	1.50	10	3.20	16	2.20	14	13
1C-c	2.35	2.51	1.02	0.26	0.50	1.00	0.80	<1	3.00	26	1.60	10	7
2-a	2.15	2.20	1.05	0.18	0.50	0.76	1.00	11	3.20	16	1.50	8	6
3-b	2.55	2.56	0.96	0.05	0.50	0.75	1.40	10	3.50	17	3.00	7	5
3-d	3.00	2.95	1.48	-0.12	0.44	0.30	1.50	15	3.50	40	2.20	19	15
4-c	2.50	2.62	1.00	0.18	0.47	0.70	2.20	42	3.00	38	-	15	6
4-d	3.30	4.43	3.05	0.59	0.47	1.20	2.20	30	3.40	50	-	44	13
4-e	3.02	2.99	0.89	0.00	0.47	1.40	1.50	3	3.50	73	2.2/3.1	12	4
5-c	2.60	2.65	0.97	0.12	0.50	0.90	1.00	2	3.10	31	1.70	10	2
5-d	3.60	3.51	1.64	-0.02	0.48	0.70	1.50	14	3.50	51	2.0/2.8	40	13

Appendix 3 Inclusive Graphic Statistic

Code 401	Md	Me	S_I	S_{KI}	K'_G	1%	CTØ	%	FTØ	%	BWØ	Mud%	Carb%
5-e	1.58	1.59	0.63	0.15	0.52	0.95	0.50	<1	3.00	5	1.0/2.0	1	nil
5-f	2.35	2.45	1.16	0.37	0.66	0.62	1.50	12	3.50	14	2.80	12	4
5-g	2.80	2.93	1.46	0.12	0.47	0.30	1.30	13	3.50	13	2.50	23	13
5-i	3.20	3.07	0.93	-0.13	0.46	1.30	2.10	18	3.30	46	-	17	6
6-b	2.40	2.87	1.69	0.59	0.67	1.00	1.70	21	3.40	34	-	18	7
6-c	1.90	2.03	0.84	0.35	0.58	0.80	0.50	<1	2.60	18	1.50	6	2
6-d	1.70	1.77	0.69	0.29	0.51	0.80	1.20	23	3.20	6	2.50	38	44
6-e	3.60	3.68	1.54	0.11	0.45	0.75	2.00	24	2.30	76	-	40	25
6-f	2.60	2.72	1.03	0.19	0.52	1.00	1.80	19	3.00	32	-	16	5
6-g	2.40	2.45	1.03	0.10	0.51	0.30	1.40	18	3.00	30	-	6	1
6-h	2.15	2.45	1.23	0.49	0.59	0.80	1.50	15	3.20	20	2.10	14	23
6-i	2.70	3.70	2.46	0.69	0.58	1.12	2.20	10	3.15	35	-	30	64
6-j	2.30	2.42	0.78	0.23	0.56	1.00	1.80	20	3.50	13	2.70	4	1
6-k	3.05	3.39	1.56	0.36	0.51	1.00	2.20	20	3.40	40	-	30	47
6-l	2.65	2.94	1.49	0.34	0.49	0.85	1.50	14	3.20	36	2.30	23	9
6-m	3.60	3.57	1.32	0.04	0.44	1.67	0.50	<1	3.60	51	2.0/2.5	39	17

Appendix 3 Inclusive Graphic Statistic

Code	Md	Me	S_I	S_{KI}	K'_G	1%	CTØ	%	FTØ	%	BWØ	Mud%	Carb%
401													
6-n	3.20	3.50	1.44	0.38	0.58	1.26	2.00	10	3.50	33	3.00	21	4
ST-1	2.70	2.70	2.00	0.02	0.51	0.78	1.60	15	2.40	60	-	9	nil
O													
1-a	1.05	1.17	0.65	0.45	0.61	0.30	1.20	66	3.40	3	2.20	2	nil
1-b	2.20	2.38	0.93	0.28	0.53	0.86	1.10	5	2.80	26	2.10	6	nil
1-c	2.80	2.57	1.94	0.14	0.66	0.55	1.20	17	2.80	49	-	10	2
1-d	2.40	2.41	0.75	0.06	0.47	1.00	1.78	25	3.50	6	-	57	14
1-e	1.90	2.12	1.10	0.30	0.42	0.56	1.20	28	3.25	20	2.00	7	nil
2-b	3.42	3.07	1.23	-0.33	0.42	0.60	1.50	15	3.40	52	2.15	24	18
2-c	2.60	2.58	1.02	0.01	0.47	0.50	1.00	8	2.90	32	-	66	67
C													
1-a	3.55	3.35	0.95	-0.31	0.56	1.05	1.75	11	3.17	28	-	49	54
1-b	2.08	2.14	1.01	0.16	0.44	0.80	1.00	9	3.00	20	2.01	5	nil
1-c	2.00	2.14	0.87	0.24	0.61	0.81	1.00	10	3.50	10	2.10	33	6
2-a	1.70	2.10	1.14	0.31	0.43	0.60	1.00	14	3.20	27	1.65	8	2
3-a	2.25	2.25	0.93	0.04	0.42	0.60	1.50	30	3.50	8	2.90	4	24

Appendix 3

Code	Md	Me	S_I	S_{KI}	K'_G	1%	CTØ	Inclusive %	Graphic FTØ	Graphic %	Graphic BWØ	Statistic Mud%	Statistic Carb%
C													
3-b	2.80	2.53	0.92	-0.32	0.42	1.00	1.00	4	3.50	10	2.00	4	nil
3-c	2.45	2.39	0.77	-0.12	0.41	1.86	1.80	30	3.50	4	3.00	4	under 1
3-d	2.80	2.77	0.59	-0.02	0.61	1.13	2.40	20	3.25	14	-	5	under 1
4-a	2.75	2.73	0.67	0.05	0.65	0.90	1.00	1	3.20	18	2.40	7	nil
4-b	2.40	2.39	0.79	0.51	0.49	0.95	1.50	12	3.50	7	1.50	4	under 1
DW													
1-a	2.50	2.70	0.75	-0.14	0.52	0.90	1.20	8	3.50	5	2.50	3	under 1
2-a	1.32	1.54	0.77	0.47	0.57	0.44	2.00	80	2.90	9	-	4	nil
3-a	1.50	1.62	0.72	0.41	0.63	0.50	1.40	40	-	-	-	4	nil
4-a	2.75	3.55	2.25	0.58	0.50	1.08	1.50	10	2.80	30	2.10	31	65
4-b	3.48	3.51	1.59	0.02	0.50	1.78	2.00	2	3.50	50	3.00	3	82
4-c	3.60	3.61	1.18	0.02	0.50	1.73	1.50	<1	2.50	87	2.00	32	47
4-d	3.40	3.41	0.43	0.01	0.46	2.10	1.50	<1	2.50	98	2.00	41	51
7-a	2.00	2.19	0.80	0.39	0.59	0.60	1.35	7	3.10	10	2.25	3	nil
8-b	3.97	3.96	0.55	0.06	0.47	2.80	2.00	<1	3.50	79	2.25	47	82
8-e	3.78	3.64	1.76	0.06	0.44	0.75	1.50	14	3.30	62	2.05	45	40

Appendix 3

Inclusive Graphic Statistic

Code	Md	Me	S_I	S_{KI}	K_G'	1%	CTØ	%	FTØ	%	BWØ	Mud%	Carb%
DW													
8-h	2.07	2.43	1.22	0.65	0.68	1.80	1.50	25	2.60	48	-	15	33
9-a	1.60	1.85	1.09	0.34	0.57	-2.70	0.20	3	1.80	36	1.00	3	nil
9-b	2.30	2.30	0.73	0.06	0.53	0.68	0.10	<1	3.00	15	2.50	3	nil
9-c	1.95	2.08	0.66	0.38	0.63	0.80	0.50	<1	2.60	14	-	3	nil
9-d	2.03	2.19	0.80	0.33	0.57	0.60	1.50	16	2.30	11	2.30	5	under 1
10-a	2.60	2.53	0.99	-0.08	0.55	0.55	1.00	8	2.90	30	1.90	7	2
12-a	2.00	2.27	0.94	0.37	0.48	0.73	1.00	5	3.50	15	2.10	4	1
NY-1	2.70	3.87	1.92	0.46	0.44	1.01	1.50	7	3.50	40	2.0/2.5	35	24
Thinsections Estimates													
CH1	-	1.89	1.48	-0.22	0.46	-	0.50	20	3.70	1	2.40	45	nil
CH1A	-	1.77	0.78	-0.04	0.47	-	0.80	7	3.00	13	-	13	nil
CH2A	-	1.77	0.65	-0.06	0.44	-	0.80	13	-	-	-	-	18
CH2B	-	3.40	0.68	0.03	0.53	-	0.90	4	3.50	2	-	3	nil
CH3	-	2.72	0.57	0.24	0.50	2.30	2.20	6	2.85	50	-	89	96
CH3A	-	1.37	0.68	0.35	0.62	0.80	0.63	5	3.20	11	-	2	66

Appendix 4

MOMENT STATISTISTICS

Sample Code	$\bar{X}_1$	m_2	m_3	m_4	G_1	G_2
Thinsection Estimates						
CH2A	1.77ϕ	0.60ϕ			0.20ϕ	
CH2B	3.40ϕ	0.62ϕ			0.24ϕ	
CH3	2.72ϕ	0.54ϕ			0.3 ϕ	
CH3A	1.37ϕ	0.63ϕ			0.35ϕ	

Total number of samples = 295

Notation

$\bar{X}_1$ = First moment (mean) = 2.75 ± 0.04ϕ

m_2 = Second moment (sorting) = 1.05 ± 0.03ϕ

m_3 = Third moment

m_4 = Fourth moment

G_1 = Moment coefficient of skewness ($\frac{m_3}{m_2 3/2}$) = 0.47

G_2 = Moment coefficient of kurtosis ($\frac{m_4}{m_2^2}$)

Friedman's Equations (1962)

(sieve) $\bar{X}_1$ = 1.0550 ($\bar{X}_1$ from thinsection) - 0.3602

(sieve) m_2 = 0.7177 (m_2 from thinsection) + 0.1356

(sieve) G_1 = 0.3647 (G_1 from thinsection) + 0.2241

Appendix 4 Moment Statistics

Code	$\bar{X}_1$	m_2	m_3	m_4	G_1	G_2
1-a	2.33	1.02	0.79	2.84	0.77	2.73
1-b	3.27	2.09	0.27	6.24	0.09	1.42
1-c	3.37	0.74	0.24	1.49	0.37	2.70
1-d	3.07	1.06	0.36	2.54	0.33	2.27
1-e	2.74	1.12	1.14	3.78	0.96	3.03
3-a	2.99	0.86	-0.38	2.34	-0.49	3.20
4-a	3.58	0.91	-0.35	2.30	-0.41	2.77
6-a	3.25	1.52	0.43	4.06	0.23	1.76
7-a	2.70	1.07	0.76	3.41	0.68	2.95
8-a	2.44	1.01	1.04	3.75	1.03	3.68
8-c	3.67	1.06	-0.12	2.29	-0.11	2.04
8-e	2.28	1.07	0.81	2.88	0.73	2.50
8-f	2.12	1.11	0.94	3.22	0.80	2.60
8-g	2.76	0.78	0.26	1.33	0.38	2.18
9-a	2.31	0.77	0.41	1.77	0.70	3.01
9-(2)b	2.73	0.67	0.18	1.12	0.34	2.48
10-b	3.67	1.02	0.09	1.18	0.08	1.74
10-d	3.84	0.94	-0.003	1.47	-0.003	1.66
10-e	3.64	1.06	0.10	1.97	0.09	1.75
10-f	3.37	0.42	-0.05	0.48	-0.19	2.79
10-g	3.75	1.06	-0.10	2.03	-0.09	1.80
10-i	2.12	3.34	-11.31	69.97	-1.85	6.27
10-j(a)	2.27	0.94	1.23	4.89	1.40	5.51
10-j(b)	1.77	2.08	-4.28	25.22	-1.42	5.82
10-k	2.29	0.47	0.29	0.91	0.92	4.18

Appendix 4 Moment Statistics

Code	$\bar{X}_1$	m_2	m_3	m_4	G_1	G_2
10-l	2.35	0.80	0.57	2.83	0.79	4.38
10-m	2.42	0.86	0.10	5.15	0.12	0.96
10-n	2.28	0.42	0.12	0.60	0.45	3.35
11-a	3.68	1.57	-0.87	4.81	-0.45	1.96
11-b	3.32	1.03	0.26	2.17	0.25	2.04
11-c	4.19	0.86	-0.50	1.52	-0.63	2.07
11-g	3.83	1.37	-0.62	3.42	-0.39	1.82
11-h	2.95	1.30	0.52	3.64	0.35	2.16
12-a	2.91	0.63	0.26	1.00	0.52	2.56
13-a	3.07	0.73	0.08	1.05	0.13	1.97
13-b	2.93	0.63	0.02	1.00	0.04	2.49
14-a	4.18	1.69	-2.66	8.32	-1.20	2.90
15-b	3.79	1.28	-0.44	3.09	-0.31	1.90
16-a	3.32	1.33	0.27	3.25	0.18	1.84
16-b	3.53	1.17	0.18	2.56	0.14	1.87
17-a	2.68	1.24	1.03	4.14	0.74	2.68
17-c	2.73	1.15	0.94	3.63	0.76	2.74
17-d	2.75	1.03	0.76	3.32	0.73	3.14
17-e	2.59	0.94	0.43	2.07	0.47	2.33
17-f	3.18	1.55	0.50	4.31	0.26	1.79
17-g	1.75	0.69	0.94	3.14	1.62	6.49
17-h	2.67	1.28	1.04	4.34	0.72	2.66
18-a	2.83	1.33	0.30	3.08	0.20	1.74
18-b	2.28	0.92	0.50	2.21	0.57	2.62
18-c	2.77	1.09	0.14	2.18	0.12	1.82

Appendix 4 Moment Statistics

Code	$\bar{X}_1$	m_2	m_3	m_4	G_1	G_2
18-d	3.42	0.56	-0.26	1.03	-0.62	3.26
18-e	2.78	1.23	0.15	2.67	0.11	1.78
19-a	2.82	1.17	1.03	3.74	0.81	2.72
19-b	2.56	0.95	0.99	3.61	1.06	3.97
19-c	2.21	1.10	1.26	5.73	1.10	4.76
19-d	3.80	0.56	-0.51	1.14	-1.23	3.64
19-e	-2.17	5.39	22.54	137.52	1.80	4.73
19-f	2.70	1.19	1.30	4.24	1.00	2.98
19-g	2.43	0.96	1.09	3.96	1.16	4.31
19-h	2.89	1.10	0.88	3.36	0.76	2.76
20-a	1.91	0.45	0.37	1.46	1.24	7.21
20-b	2.73	1.34	1.03	4.48	0.66	2.50
20-c	2.28	0.80	1.03	3.49	1.43	5.42
21-a	1.43	0.64	0.71	2.29	1.38	5.58
21-a	1.43	0.64	0.71	2.29	1.38	5.58
21-c	2.20	1.00	1.30	4.42	1.31	4.44
21-e	1.60	0.56	0.63	2.47	1.48	7.81
22-a	2.88	5.34	30.28	225.98	2.46	7.93
23-b	2.15	0.85	1.28	5.33	1.63	7.39
23-c	2.37	0.99	1.19	4.52	1.20	4.59
24-a	2.68	1.02	0.67	3.39	0.65	3.25
24-b	2.53	0.76	0.06	1.37	0.09	2.36
24-c	2.52	0.70	0.23	1.53	0.39	3.08
25-a	2.44	1.16	0.88	4.02	0.70	2.97
25-b	2.35	1.13	0.92	4.07	0.76	3.19

Appendix 4 Moment Statistics

Code	$\bar{X}_1$	m_2	m_3	m_4	G_1	G_2
25-c	2.42	1.20	1.09	4.52	0.84	3.17
26-c	3.37	2.29	-0.47	7.44	-0.14	1.42
27-a	2.20	1.01	0.01	4.92	0.01	4.85
27-b	2.93	0.47	0.15	0.87	0.60	3.97
28-a	2.31	0.69	0.35	1.41	0.62	2.99
28-b	2.82	0.75	0.16	2.07	0.24	3.66
29-b	2.60	1.06	1.18	3.98	1.07	3.52
30-a	2.23	0.79	0.96	3.15	1.37	5.07
31-a	2.95	1.25	0.64	3.78	0.46	2.42
31-b	2.66	1.39	1.18	5.01	0.73	2.61
31-c(1)	2.40	0.74	1.12	3.20	1.74	5.93
31-c(2)	1.76	0.76	-1.48	6.55	-2.25	11.47
31-d	2.63	1.51	1.30	6.28	0.70	2.76
32-a	3.05	1.28	0.63	3.90	0.43	2.37
32-b	2.67	0.73	0.78	2.32	1.26	4.41
32-c	2.73	0.60	0.62	1.83	1.34	5.17
33-a	3.35	1.37	-0.06	3.66	-0.04	1.96
33-b	3.00	1.99	0.36	7.60	0.13	1.93
33-c	2.87	1.31	0.80	4.07	0.53	2.38
33-d	2.11	1.22	1.46	5.83	1.08	3.89
34-a	4.85	0.19	-0.24	0.45	-2.98	12.73
35-a	2.15	0.80	0.39	2.10	0.55	3.28
35-a(2)	1.10	2.53	-0.89	21.99	-0.22	3.43
35-b(2)	2.20	0.50	0.08	1.04	0.24	4.21
36-a	2.64	0.95	0.78	2.90	0.85	3.24

Appendix 4 Moment Statistics

Code	$\bar{X}_1$	m_2	m_3	m_4	G_1	G_2
36-b	1.97	0.51	0.53	1.46	1.44	5.55
36-c	2.02	0.68	0.88	2.67	1.56	5.76
36-d	1.85	0.75	1.23	4.19	1.90	7.42
37-a	1.35	0.73	0.69	3.56	1.10	6.64
37-b	1.34	0.38	0.38	1.37	1.63	9.42
41-a	1.31	0.66	0.20	3.13	0.38	7.20
41-b	1.42	0.66	0.41	3.10	0.77	7.09
42-a	2.40	0.72	0.83	2.63	1.35	5.08
44-b	3.74	1.88	1.15	5.56	-0.44	1.57
45-b	2.69	2.36	-0.90	19.17	-0.25	3.44
45-c	1.72	3.34	-8.95	59.47	-1.47	5.34
45-d	2.64	0.98	0.97	3.33	0.99	3.44
45-e	2.69	0.89	0.31	1.77	0.37	2.26
46-a	3.71	1.83	-0.71	5.04	-0.32	1.50
47-a	2.39	0.74	0.64	2.39	1.00	4.37
47-b	2.40	0.87	0.52	2.81	0.64	3.15
47-c	2.48	0.80	0.74	2.47	1.03	3.85
47-d	2.41	0.46	0.32	0.91	1.05	4.36
47-e	1.98	0.62	0.69	2.42	1.43	6.32
48-a	2.39	0.61	0.74	2.26	1.57	6.12
48-b	2.29	0.79	0.88	2.91	1.25	4.67
48-c	2.87	1.34	0.48	4.14	0.31	2.32
48-d	2.66	1.04	0.80	3.22	0.75	2.98
48 e	2.90	1.04	0.71	2.96	0.67	2.72
48-f	2.97	1.00	0.71	2.78	0.71	2.78

Appendix 4 Moment Statistics

Code	$\bar{X}_1$	m_2	m_3	m_4	G_1	G_2
48-g	2.61	0.90	0.89	2.82	1.04	3.48
48-h	2.78	0.93	0.59	2.45	0.65	2.81
48-i	2.90	1.18	0.89	3.50	0.70	2.52
48-j	2.87	1.01	0.78	2.97	0.78	2.93
48-k	2.93	1.13	0.80	3.41	0.67	2.68
48-l	2.23	0.86	1.19	3.71	1.49	5.02
50-a	2.79	0.76	-0.16	1.96	-0.24	3.44
50-b	2.51	1.08	0.69	3.50	0.61	3.00
50-c	2.96	1.09	0.60	3.11	0.52	2.62
51-a	2.24	0.87	1.14	3.59	1.42	4.77
51-b	2.33	0.65	0.47	1.42	0.91	3.40
52-a	1.94	1.08	1.09	3.31	0.97	2.85
52-b	3.44	0.49	-0.16	0.60	-0.47	2.49
52-c	2.23	0.93	0.78	2.58	0.88	3.01
52-d	2.71	0.74	0.20	1.37	0.32	2.48
52-e	2.50	0.75	0.49	1.63	0.74	2.87
53-a	3.08	1.76	0.48	5.50	0.20	1.78
53-b	3.03	2.31	0.27	8.14	0.08	1.52
53-c	3.44	1.51	-0.02	3.66	-0.01	1.62
54-a	3.44	1.44	0.36	3.60	0.17	1.73
54-b	3.40	0.93	0.36	1.95	0.40	2.26
54-c	3.13	0.91	0.31	2.16	0.39	2.62
54-d	3.15	0.65	-0.02	0.94	-0.04	3.6
55-a	3.77	0.86	0.11	1.30	0.14	1.74
55-b	3.10	1.23	0.46	3.38	0.34	2.28

Appendix 4 Moment Statistics

Code	$\bar{X}_1$	m_2	m_3	m_4	G_1	G_2
55-c	4.87	0.13	-0.14	0.19	-2.76	10.79
56-b	2.47	1.51	1.86	6.52	1.01	2.86
56-d	3.25	1.20	-0.11	3.45	-0.08	2.41
57-a	3.11	1.28	0.94	3.51	0.65	2.13
57-c	2.60	1.09	0.22	2.32	0.19	1.94
57-d	2.96	1.00	0.85	2.77	0.85	2.76
57-e	2.57	0.96	0.79	3.01	0.84	3.25
57-e	3.08	1.03	0.80	2.71	0.77	2.58
57-g	2.65	1.00	0.29	2.04	0.29	2.02
57-h	2.62	0.95	0.41	1.96	0.44	2.18
58-a	2.65	1.21	0.86	3.74	0.65	2.57
59-a	2.92	0.61	0.11	0.98	0.23	2.64
60-a	2.33	1.76	-1.51	17.69	-0.65	5.72
60-b	1.69	3.37	-4.24	31.83	-0.69	2.81
60-c	2.02	0.58	0.60	2.14	1.33	6.42
61-a	3.51	1.00	0.24	1.90	0.23	1.89
61-b	2.30	0.67	0.46	1.78	0.84	4.03
61-c	2.48	1.31	1.99	6.06	1.33	3.45
61-d	2.85	1.38	1.24	4.60	0.76	2.41
61-e	2.68	1.12	1.38	4.27	1.16	3.38
61-	2.27	0.76	1.03	3.08	1.54	5.36
61-g	2.37	0.76	0.77	2.76	1.16	4.77
61-h	2.22	0.69	0.89	2.80	1.54	5.85
61-i	2.84	1.60	1.60	5.77	0.79	2.25
61-j	3.17	1.11	0.34	2.86	0.29	2.32

Appendix 4 Moment Statistics

Code	$\bar{X}_1$	m_2	m_3	m_4	G_1	G_2
61-k	3.20	1.17	0.28	3.11	0.22	2.26
61-l	2.[illegible]	0.85	0.95	3.03	1.21	4.16
61-m	2.89	0.98	0.85	3.10	0.88	3.24
61-n	2.81	1.18	1.13	3.96	0.88	2.83
61-o	2.19	0.95	1.11	3.73	1.19	4.10
61-p	2.24	0.52	0.15	0.82	0.32	3.05
61-q	2.12	0.71	0.72	2.54	1.18	4.97
61-r	2.24	0.70	0.80	2.64	1.36	5.36
61-s	1.99	0.46	0.64	1.97	1.85	8.09
61-t	3.44	1.14	0.39	2.51	0.32	1.93
61-u	2.54	0.86	0.98	3.12	1.22	4.19
61-v	2.49	0.99	0.98	3.55	0.99	3.60
61-w	2.88	1.26	0.93	3.91	0.66	2.46
61-x	2.65	0.85	0.78	2.71	1.00	3.78
61-y	2.46	0.84	0.75	2.77	0.97	3.91
61-z	2.69	1.01	0.84	3.15	0.83	3.08
61-aa	2.38	0.79	0.92	2.86	1.32	4.59
61-bb	2.41	0.71	0.70	2.46	1.15	4.82
61-cc	2.53	0.77	0.81	2.60	1.19	4.41
61-dd	2.17	0.56	0.66	2.05	1.55	6.47
61-ee	2.25	0.57	0.79	2.40	1.80	7.27
61-ff	2.57	0.95	0.96	3.15	1.04	3.49
61-gg	2.50	1.13	1.23	4.17	1.03	2.28
61-hh	2.80	0.95	0.87	2.88	0.94	3.17
61-ii	2.64	0.82	0.82	2.66	1.10	3.94

Appendix 4 Moment Statistics

Code	$\bar{X}_1$	m_2	m_3	m_4	G_1	G_2
61-jj	2.46	0.72	0.69	2.34	1.12	4.46
61-kk	2.88	0.89	0.71	2.71	0.85	3.90
61-ll	3.51	1.21	0.15	2.60	0.11	1.78
61-mm	2.97	1.03	0.73	3.14	0.69	2.96
61-nn	3.77	1.24	-0.21	2.44	-0.15	1.58
61-oo	3.26	1.57	0.70	5.99	0.35	1.62
61-pp	4.00	1.35	-0.96	3.36	-0.62	1.86
61-qq	2.58	0.71	0.50	1.96	0.83	3.87
61-rr	2.29	0.42	0.52	1.54	1.94	8.90
61-ss	2.70	0.58	0.54	2.01	1.22	6.04
61-tt	2.91	1.14	1.06	3.42	0.87	2.63
61-uu	2.74	0.57	0.32	1.23	0.74	3.80
62-b	2.12	0.48	0.30	1.24	0.90	5.34
63-a	2.62	1.30	1.38	7.60	0.53	2.11
63-b	2.52	0.61	0.49	1.77	1.03	4.75
401						
1A-a	2.77	0.98	0.07	2.14	0.07	2.21
1A-b	3.66	0.86	0.002	1.49	0.002	2.04
1A-c	2.01	0.6	0.62	2.31	1.24	5.85
1A-e	4.23	0.88	-0.64	1.80	-0.77	2.31
1A-j	3.70	0.88	-0.05	1.65	-0.06	2.11
1B-b	2.57	1.52	1.21	5.63	0.65	2.44
1B-c	2.75	0.81	0.11	1.46	0.15	2.24
1B-d	2.82	1.57	1.31	5.44	0.67	2.22
1B-e	2.89	0.91	0.002	1.62	0.003	2.06

Appendix 4 Moment Statistics

Code 401	$\bar{X}_1$	m_2	m_3	m_4	G_1	G_2
1B-f	3.12	1.88	0.79	5.51	0.31	1.57
1B-g	2.87	0.92	0.07	1.74	0.08	2.07
1C-a	3.68	1.53	-0.55	3.96	-0.29	1.68
1C-b	2.84	1.07	1.06	3.54	0.95	3.08
1C-c	2.79	1.08	0.80	3.28	0.72	2.83
2-a	2.49	1.00	0.39	2.34	0.39	2.34
3-b	2.83	0.82	0.03	1.55	0.04	2.30
3-d	3.19	1.57	-0.05	4.54	-0.02	1.84
4-c	2.88	0.91	0.10	1.70	0.12	2.04
4-d	3.65	1.75	-0.48	4.37	-0.21	1.43
4-e	3.20	0.68	-0.10	1.05	-0.18	2.27
5-c	2.90	0.82	0.11	1.52	0.14	2.26
5-d	3.44	1.83	-0.33	5.19	-0.13	1.55
5-e	1.89	0.55	0.16	2.27	0.39	7.49
5-f	2.80	1.01	0.89	3.31	0.88	3.25
5-g	3.13	1.68	0.14	5.70	0.06	2.02
5-i	3.31	0.74	-0.17	1.08	-0.26	1.95
6-b	2.93	1.29	1.10	4.03	0.75	2.43
6-c	2.32	0.72	0.63	1.93	1.01	3.69
6-d	2.35	0.71	0.51	2.16	0.85	4.30
6-e	3.77	1.39	-0.61	3.55	-0.37	1.83
6-f	3.09	1.11	0.50	3.06	0.43	2.50
6-g	2.69	0.93	0.15	1.97	0.16	2.26
6-h	2.76	1.23	1.16	4.19	0.85	2.78

Appendix 4 Moment Statistics

Code	$\bar{X}_1$	m_2	m_3	m_4	G_1	G_2
401						
6-i	3.32	1.46	0.60	3.57	0.34	1.68
6-j	2.66	0.63	0.24	1.12	0.47	2.79
6-k	3.49	1.33	0.07	3.20	0.04	1.80
6-l	3.12	1.57	0.62	4.46	0.32	1.82
6-m	3. 8	1.28	-0.36	2.60	-0.25	1.59
6-n	3.49	0.99	0.13	2.24	0.13	2.26
ST-1	2.96	0.97	0.25	2.65	0.26	2.82
O						
1-a	1.54	0.70	1.14	3.65	1.95	7.46
1-b	2.62	0.73	0.31	1.45	0.51	2.72
1-c	2.90	1.38	0.07	4.08	0.04	2.15
1-d	3.96	1.60	-1.24	4.48	-0.61	1.75
1-e	2.40	1.29	0.97	4.25	0.66	2.54
2-b	3.35	1.66	-0.41	4.83	-0.19	1.75
2-c	3.22	1.56	0.17	4.51	0.09	1.85
C						
1-a	3.69	1.07	-0.57	2.95	-0.52	2.59
1-b	2.56	0.97	0.51	2.57	0.53	2.70
1-c	3.03	1.80	0.78	5.70	0.32	1.76
2-a	2.43	1.45	1.25	5.12	0.72	2.45
3-a	2.51	0.98	0.41	2.36	0.42	2.45
3-b	2.80	0.91	0.004	2.15	0.004	2.61
3-c	2.68	0.68	0.004	1.10	0.01	2.38
3-d	3.07	0.52	0.19	1.20	0.51	4.51

Appendix 4 Moment Statistics

Code	$\bar{X}_1$	m_2	m_3	m_4	G_1	G_2
C						
4-a	3.05	0.61	0.25	1.56	0.53	4.20
4-b	2.70	0.68	0.35	1.66	0.62	3.58
DW						
1-a	2.70	0.65	0.17	1.45	0.32	3.47
2-a	1.83	0.82	1.27	4.25	1.72	6.35
3-a	1.95	0.68	1.09	3.59	1.95	7.83
4-a	3.31	1.74	0.36	4.54	0.16	1.50
4-b	3.31	0.70	-2.11	8.47	-3.57	17.08
4-c	3.85	0.98	-0.25	1.80	-0.28	2.08
4-d	4.60	0.46	-0.43	0.75	-1.36	3.52
7-a	2.41	0.61	0.34	1.35	0.72	3.69
8-b	4.87	0.16	-0.19	0.31	-3.63	12.71
8-e	4.40	1.32	-2.63	7.94	-1.73	4.53
8-h	2.67	1.54	1.35	5.70	0.71	2.39
9-a	1.85	1.94	-2.21	16.41	-0.81	4.29
9-b	2.60	0.57	0.04	1.11	0.10	3.41
9-c	2.34	0.56	0.42	1.27	1.01	4.11
9-d	2.46	0.77	0.74	2.65	1.09	4.45
10-a	2.70	0.89	-0.02	2.07	-0.02	2.58
12-a	2.50	0.86	0.46	1.75	0.58	2.38
NY-1	3.54	1.50	0.09	3.80	0.05	1.68
Thinsection Estimate						
CH1	1.89	1.20			1.40	
CH1A	1.77	0.47			0.21	

Appendix 5

Insoluble Mud Size Distribution

Code	Formation	Member	Me	S_I	S_K	K'_G
8-c	Potsdam	Keeseville	5.87	0.78	0.06	0.36
10-e	Theresa		4.80	0.71	0.38	0.52
11-c	Theresa		5.19	0.92	0.45	0.56
11-e	Buck Bridge	Heuvelton	5.04	0.97	0.41	0.48
56-d	Buck Bridge	March	4.88	0.90	0.48	0.61
57-c	Buck Bridge	March	5.24	0.83	0.04	0.40
61-nn 401	Buck Bridge	Heuvelton	5.45	1.14	0.26	0.45
4-g 401	Theresa		5.70	1.07	0.04	0.40
6-g C	Theresa		5.34	0.88	0.25	0.60
1-a	Buck Bridge	March	5.03	0.82	0.12	0.54

Overall Value

$Me = 5.25 \pm 0.11$ Ø

$S_I = 0.90 \pm 0.04$ Ø

$S_K = 0.25 \pm 0.06$

$K'_G = 0.50 \pm 0.03$

Appendix 6

ESTIMATED PALEOWAVE AND CURRENT CONDITIONS UNDER WHICH RIPPLES FORMED

λ = ripple length (cm)

RI = ripple index

RSI = ripple symmetry index

u_t = shear velocity required to initiate formation of ripple (cm/sec).

Wave parameters

T = estimated wave period.(sec)

H = estimated wave height (cm)

L = estimated wave length (cm)

$\bar{h}$ = estimated water depth (cm)

Current parameters

u_* = estimated bed shear stress on ripple(cm/sec).

$\bar{U}$ = estimated mean current velocity (cm/sec).

Refer to text, chapter 5 for explanation of methods used to obtain parameters.

Number of samples = 200

mean λ = 3.10 ± 0.12 cm

mean u_t = 9.07 ± 0.11 cm/sec

mean T = 1.36 ± 0.07 sec

mean H = 6.93 ± 0.29 cm

mean L = 250.39 ± 13.49 cm

mean h = 48.89± 1.97 cm

mean u_* = 1.31 ± 0.10 cm/sec

mean $\bar{U}$ = 27.40± 2.22 cm/sec

Appendix 6

ESTIMATED PALEOWAVE AND CURRENT CONDITIONS

Sample Code	Wave						Current			
	λ	u_t	T	H	L	h	RSI	RI	u_*	$\bar{U}$
8-a	3.0	9.76	1.21	5.4	200	42	1.0	10	0.1	1.3
8-b	4.0	9.31	1.60	12.0	362	63	2.3	13	1.3	28.6
8-c	1.0	5.83	0.67	4.5	69	21	2.3	10	1.3	28.8
	2.4	7.25	1.30	4.4	237	54	1.8	3	1.8	33.7
	4.5	8.49	2.05	8.9	561	102	1.0	11	0.1	1.4
8-d	2.0	8.84	0.88	5.6	113	27	3.0	10	2.1	43.1
8-d(2)	3.5	10.18	1.90	7.1	246	49	4.0	10	2.9	61.4
8-e	1.0	7.44	0.53	4.5	42	13	1.0	10	<0.1	0.1
	1.5	8.32	0.72	5.0	75	20	1.0	8	<0.1	0.3
	3.1	9.87	1.23	6.7	208	43	1.0	10	<0.1	0.3
8-f	1.0	7.68	0.51	4.5	39	12	4.0	10	2.4	48.7
	1.5	8.50	0.69	5.0	71	19	4.0	15	2.3	49.6
	4.0	10.86	1.45	7.5	276	52	1.0	8	<-0.1	-0.4
8-g	2.0	8.26	0.95	5.6	130	31	1.0	10	<0.1	0.8
	3.2	9.29	1.35	6.8	249	51	1.0	16	<0.1	0.7
9(2)b	2.0	8.29	0.95	5.6	129	31	4.0	10	2.7	57.7
	3.0	9.17	1.28	6.6	227	48	1.4	10	0.6	13.3
10-a	2.4	9.26	1.02	6.0	146	33	1.0	8	<0.1	0.4
	7.0	9.96	2.27	10.2	618	97	2.5	4	3.4	62.4
10-b	1.3	7.95	0.64	4.8	61	17	6.5	4	5.0	107.4
	4.2	10.65	1.56	7.8	313	58	1.0	14	0.1	3.1
10-d	2.6	7.21	1.42	6.3	279	61	12.0	13	5.3	120.6
	4.0	8.03	1.96	7.5	505	96	1.0	13	0.1	1.8

Sample Code	λ	u_t	Wave T	Wave H	L	h	RSI	RI	Current u_*	Current $\bar{U}$
10-j(1)	4.5	11.46	1.54	8.0	308	56	1.0	15	<-0.1	-0.8
10-j(2)	1.4	9.67	0.64	4.9	61	17	1.8	7	1.1	20.7
10-l	1.8	8.53	0.83	5.4	99	25	1.7	9	0.9	19.1
	3.2	8.54	1.28	7.4	216	42	1.1	11	0.1	2.1
10-m	3.5	9.73	1.41	7.1	269	54	2.5	12	1.8	38.3
11-d	1.0	5.23	0.75	4.5	85	27	1.0	5	0.1	2.0
	4.2	7.49	2.20	7.8	638	118	1.0	9	0.1	2.2
3-a	1.7	7.54	0.89	5.3	114	29	2.4	6	1.8	36.9
	2.8	8.54	1.29	6.4	230	50	4.8	9	3.5	74.5
	4.8	9.77	1.93	8.3	477	85	1.0	10	<0.1	0.9
12-a	3.2	8.99	1.40	6.8	266	54	3.5	8	2.9	59.9
14-a	4.2	8.53	1.93	7.8	489	91	1.0	7	0.1	1.7
16-c	3.0	7.85	1.50	6.6	310	65	3.0	8	2.4	51.8
	6.0	9.33	2.53	9.3	788	131	1.6	8	1.2	26.3
17-a	2.2	8.65	1.00	5.8	142	33	2.8	11	1.9	40.5
17-h	6.0	11.09	2.12	9.3	557	92	2.0	8	1.7	34.5
	6.5	11.26	2.27	9.8	624	100	1.0	8	<-0.1	-0.1
18-c	0.9	6.26	0.57	4.4	48	16	1.0	9	0.1	1.1
	3.6	9.65	1.46	8.2	277	50	1.6	36	0.5	12.8
	4.5	10.20	1.73	8.0	389	71	1.5	10	0.8	17.1
19-g	2.0	8.86	0.89	6.3	109	24	1.0	10	-0.1	-1.8
	2.4	9.28	1.02	5.6	113	27	1.0	12	<0.1	0.6
	3.5	10.19	1.35	7.1	245	49	6.0	9	4.4	90.2
19-h	2.5	8.58	1.14	6.1	183	41	1.4	13	0.6	12.2
	5.0	10.20	1.92	8.5	470	82	1.5	17	0.7	15.4

Sample Code	λ	u_t	T	Wave H	L	h	RSI	RI	Current u_*	$\bar{U}$
20-a	3.0	10.68	1.10	6.8	166	34	2.0	10	0.7	14.2
20-b	5.0	10.49	1.87	8.4	445	78	4.0	12.5	3.1	66.3
20-c	2.4	9.51	0.99	6.0	138	31	1.4	12	0.5	11.3
21-e	4.0	12.13	1.29	7.5	221	42	1.0	4	-0.1	-2.2
22-a	3.0	9.74	1.21	5.6	201	42	9.0	15	4.6	100.5
23-a	5.0	11.30	1.74	8.5	383	67	2.4	16	1.6	35.3
23-c	1.2	7.65	0.62	4.7	57	16	3.0	12	1.8	42.9
	6.5	11.68	2.19	9.8	580	93	1.0	13	<-0.1	-0.5
24-a	3.8	10.77	1.39	7.4	255	49	1.0	13	<-0.1	-0.4
	1.4	8.39	0.66	4.9	64	18	6.0	14	3.2	68.0
24-b	2.0	9.30	0.84	5.6	102	25	1.9	10	1.1	23.1
24-c	3.0	9.66	1.22	6.6	204	43	2.0	10	1.3	27.9
25-a	4.0	10.52	1.49	7.5	294	56	1.0	10	<0.1	0.1
27-a	3.3	10.24	1.27	7.6	217	44	2.3	17	1.4	30.7
	5.0	11.36	1.78	8.5	380	66	1.0	10	<-0.1	-0.1
27-b	3.0	9.15	1.29	6.6	228	48	6.0	15	3.5	78.7
28-b	2.2	8.41	1.03	5.8	150	35	2.1	11	1.3	28.1
	5.0	10.33	1.90	8.5	459	80	1.0	13	<0.1	0.3
30-a	8.0	12.93	2.43	11.1	688	103	1.1	11	0.1	-2.4
31-a	1.3	7.43	0.69	4.8	70	20	3.3	13	1.9	48.4
31-a	2.0	8.27	0.95	5.6	129	31	1.0	10	<0.1	0.8
	2.4	8.66	1.09	6.0	167	38	1.4	12	0.6	12.2
31-b	1.0	7.18	0.55	4.5	45	14	2.3	10	1.3	27.3
	2.4	8.93	1.06	6.5	154	33	1.0	12	<-0.1	-0.5
31-c(1)	8.2	12.77	2.52	11.2	739	110	1.7	16	1.2	26.1

Sample	Wave								Current	
Code	λ	u_t	T	H	L	h	RSI	RI	u_*	$\bar{U}$
32-b	1.2	7.41	0.64	4.7	60	18	1.0	6	<0.1	0.9
	1.5	7.83	0.75	5.0	83	23	2.0	10	1.2	24.7
	3.6	9.75	1.45	7.2	282	56	1.0	12	<0.1	0.6
32-c	2.5	9.79	1.12	6.1	175	39	2.1	8	1.5	30.9
33-b	2.7	7.72	1.37	6.1	175	39	2.9	14	1.9	41.0
33-c	3.6	9.40	1.50	7.2	303	60	1.4	13	0.6	13.0
	4.0	9.65	1.62	7.5	350	67	3.0	8	2.6	54.3
	4.2	9.71	1.66	7.8	373	69	1.8	21	0.9	21.4
33-d	14.0	15.19	3.62	15.3	1363	171	3.3	11	3.4	70.7
34-a	1.2	4.34	1.09	6.5	162	35	2.0	12	0.9	21.9
	1.8	4.81	1.47	6.5	299	64	2.6	18	1.4	34.2
	3.0	5.46	2.16	6.6	639	134	1.0	30	0.1	2.2
35-a	4.4	11.23	1.54	7.9	308	57	1.2	22	0.2	5.5
	4.5	11.30	1.56	8.0	317	58	1.3	23	0.5	11.4
36-a	4.0	11.20	1.40	7.5	260	49	7.5	13	4.6	96.9
36-c	9.0	13.72	2.58	11.7	759	110	1.2	18	0.2	5.3
42-a	2.4	9.31	1.01	6.0	144	33	1.0	10	<0.1	0.5
	2.5	9.40	1.04	6.1	153	34	1.5	5	0.9	17.6
	3.0	9.84	1.20	6.6	197	41	1.0	10	<0.1	0.2
	3.1	9.93	1.23	6.7	206	43	2.0	8	1.5	29.5
43-b	1.0	6.24	0.63	4.5	60	19	4.0	10	2.4	51.4
	4.0	8.83	1.78	7.5	418	79	1.0	13	0.1	1.3
45-c	2.0	8.27	0.85	5.6	103	25	1.2	13	0.3	5.7
45-e	2.0	8.31	0.94	5.6	128	31	3.0	10	2.1	43.9
	3.5	9.56	1.44	7.1	278	55	1.3	12	0.5	10.0

Sample Code	Wave λ	u_t	T	H	L	h	RSI	RI	Current u_*	$\bar{U}$
47-a	3.0	9.53	1.24	6.6	210	44	3.2	10	2.4	50.7
	3.0	9.53	1.24	6.6	210	44	1.1	15	0.2	3.5
47-b	3.4	9.98	1.34	7.1	241	48	1.9	5	1.6	31.3
	3.5	9.98	1.37	7.1	252	50	1.7	6	1.2	24.4
47-c	3.5	9.99	1.38	7.1	255	51	1.5	18	0.6	14.1
	3.9	10.26	1.49	7.5	294	56	2.9	8	2.5	50.9
47-d	3.1	10.15	1.27	6.7	219	45	2.1	8	1.6	31.9
47-e	2.2	9.66	0.89	5.8	114	26	2.2	11	1.4	28 5
	5.0	11.86	1.66	8.5	348	61	4.0	17	2.7	59.9
48-b	1.1	7.61	0.57	4.6	48	14	2.6	11	1.5	31.4
	3.7	10.30	1.41	7.3	265	52	1.9	13	1.2	24.9
48-c	4.5	10.02	1.76	8.0	402	73	2.0	6	1.9	35.5
48-d	2.0	8.58	0.92	4.7	52	15	1.0	10	<0.1	1.0
48-f	1.2	7.02	0.67	4.7	67	19	5.0	6	3.5	68.8
	6.5	10.71	2.38	9.8	689	111	2.3	13	1.7	38.5
48-h	3.0	9.31	1.27	6.6	220	46	2.0	10	1.3	28.1
51-a	1.2	8.01	0.59	4.7	52	15	1.0	12	<-0.1	-0.1
52-c	2.3	9.36	0.97	5.9	132	30	9.0	12	4.7	98.4
52-d	4.0	9.84	1.60	7.5	337	64	1.0	10	<0.1	0.7
53-a	1.1	8.59	0.50	4.6	38	11	1.2	11	0.2	3.7
	1.5	9.27	0.63	5.0	59	16	4.0	8	2.8	54.8
54-a	3.5	8.74	1.57	7.1	333	66	2.1	7	1.7	35.3
57-d	2.5	8.53	1.15	6.1	185	41	1.1	8	0.2	4.4
	3.8	9.48	1.57	7.4	329	63	1.6	10	0.9	19.5
58-a	1.5	8.00	0.73	5.0	80	22	2.7	9	1.8	37.6
	2.0	8.61	0.91	5.6	119	29	5.6	10	3.6	74.7

Sample Code	Wave λ	u_t	T	H	L	h	RSI	RI	Current u_*	$\bar{U}$
59-a	2.0	7.92	0.99	5.6	141	34	1.5	10	0.7	15.0
	3.0	8.77	1.34	6.6	248	52	1.7	15	0.9	19.7
60-c	2.0	9.45	0.83	5.6	99	24	1.5	7	0.7	12.9
	5.0	11.88	1.65	8.5	347	61	5.3	7	4.8	95.0
61-a	5.0	8.29	2.11	8.5	567	99	1.5	12	0.8	17.5
61-g	3.5	10.30	1.33	7.1	240	48	4.7	18	2.9	64.5
	2.3	9.28	0.97	5.9	134	31	2.3	8	1.7	34.0
61-h	3.5	10.56	1.30	7.1	228	46	1.0	11	0.0	0.0
	3.3	10.41	1.25	7.0	210	42	1.2	12	0.3	6.0
61-i	1.8	7.71	0.92	5.4	122	30	1.0	6	0.1	1.1
	1.0	6.66	0.59	4.6	52	15	2.3	5	1.6	30.8
61-j	3.4	8.75	1.53	7.1	314	53	2.4	9	1.7	36.3
	1.2	6.74	0.70	4.7	73	21	11.0	6	5.6	112.7
61-l	5.0	10.88	1.80	8.5	414	72	1.0	7	<-0.1	-0.3
	2.0	8.65	0.91	5.6	118	29	5.6	6	4.3	84.0
61-m	3.0	8.95	1.32	6.6	238	50	5.0	6	4.3	86.0
	1.7	7.76	0.86	5.3	108	27	3.2	8	2.3	47.4
61-n	3.0	9.04	1.30	6.6	233	49	5.0	7	4.1	82.5
61-q	2.0	9.29	0.85	5.6	103	25	5.6	10	3.6	73.6
	2.1	9.29	0.85	5.7	110	26	5.0	11	3.2	67.0
	6.0	12.23	1.93	9.3	459	76	1.0	10	-0.1	-1.1
61-bb	5.3	11.39	1.83	8.8	420	72	12.0	11	6.7	139.9
401-1a-a	1.4	7.48	0.73	4.9	80	22	1.0	7	<0.1	0.9
	3.3	9.28	1.40	7.0	264	53	1.0	17	<0.1	0.6
401-b-c	1.2	7.24	0.65	4.7	63	18	1.0	18	<0.1	0.6
	2.5	8.70	1.13	6.1	178	40	1.0	8	<0.1	1.0

Sample Code	Wave λ	u_t	T	H	L	h	RSI	RI	Current u_*	$\bar{U}$
401-b-d	1.1	6.82	0.63	4.6	50	18	4.0	6	2.9	57.7
	1.3	7.11	0.72	4.8	77	22	3.3	4	2.9	54.8
401-b-f	1.2	6.51	0.72	4.7	78	23	1.0	4	0.1	1.6
	2.5	7.82	1.25	6.1	220	49	1.0	8	0.1	1.6
401-b-h	2.5	8.54	1.15	6.1	185	41	1.0	8	0.1	1.0
401-c-a	2.5	7.01	1.40	6.1	275	61	1.0	13	0.2	3.6
401-2-a	3.0	9.61	1.23	6.6	206	43	1.0	10	<0.1	0.4
401-3-a	7.0	11.15	2.46	10.2	727	114	1.1	9	0.2	4.3
401-3-c	5.0	9.91	1.98	8.5	499	87	1.5	7	1.0	19.6
401-3-d	2.7	8.22	1.29	6.4	231	50	1.0	7	0.1	1.4
	4.5	9.33	1.89	8.0	464	85	1.0	9	0.1	1.2
401-4-f	4.3	9.15	1.85	7.9	443	82	1.0	14	<0.1	1.1
401-5-a	1.5	7.47	0.79	5.0	92	25	1.0	3	0.1	1.4
	1.7	7.71	0.87	5.3	109	28	1.0	10	<0.1	1.0
401-6-b	2.0	7.73	1.02	5.7	147	35	1.5	10	0.7	14.9
401-6-d	2.5	9.89	0.99	6.1	138	31	1.1	8	0.2	3.3
401-6-e	5.0	8.44	2.32	8.5	686	120	1.5	7	1.0	20.9
401-6-g	8.0	11.76	2.67	11.1	833	125	4.7	8	4.7	95.9
401-6-f	3.0	8.78	1.34	6.6	247	52	1.0	15	<0.1	1.0
	4.3	9.61	1.76	7.9	402	74	1.0	43	<0.1	0.6
401-6-i	1.8	6.52	1.08	5.4	170	43	1.5	9	0.7	15.9
	2.2	6.86	1.26	5.8	226	53	13.0	22	4.5	109.9
401-6-n	2.0	6.93	1.13	5.6	185	44	1.0	10	0.1	1.7
401-6-o	2.2	7.10	1.22	6.7	202	42	6.3	7	4.3	88.5
	2.3	7.17	1.30	5.9	224	51	3.6	12	2.4	53.3
	4.8	8.63	2.19	8.3	612	109	1.4	12	0.7	14.9

Sample Code	Wave λ	u_t	T	H	L	h	RSI	RI	Current u_*	$\bar{U}$
C-3 -a	1.6	8.20	0.96	5.6	132	32	1.0	8	<0.1	0.9
	2.0	8.20	0.96	5.6	132	32	1.0	10	<0.1	0.9
	3.0	8.86	1.36	6.6	252	53	1.0	11	0.1	1.2
	3.2	9.07	1.29	6.8	275	56	1.8	6	0.2	4.1
C-4-a	2.0	7.89	1.00	5.6	143	34	1.5	10	0.7	14.9
	2.9	8.65	1.32	6.5	239	51	2.0	15	1.2	26.2
C-4-b	1.8	8.18	0.86	5.4	108	27	3.0	9	2.1	43.7
	2.0	8.39	0.93	5.6	125	30	3.0	10	2.1	43.7
DW-3-a	3.5	9.89	1.39	7.1	260	52	1.0	7	<0.1	0.5
DW-2-a	3.5	11.20	1.23	7.1	203	40	1.9	12	1.1	23.7
DW-9-d	7.0	11.67	2.36	10.2	664	104	1.3	14	0.5	10.2
O-2-a	1.2	6.57	0.71	4.7	77	22	1.0	6	0.1	1.2
	2.4	7.81	1.20	6.1	204	45	1.0	5	0.1	1.4
	2.5	7.90	1.24	6.7	211	44	1.0	8	<0.1	0.4
O-2-c	2.7	8.67	1.21	6.4	203	44	1.0	9	<0.1	0.9
O-4-a	2.9	9.04	1.26	6.5	219	47	16.4	15	6.1	134.6
	2.0	8.24	0.95	5.6	130	31	2.3	10	1.5	31.8
62-b	1.5	11.23	0.52	5.0	41	11	2.0	15	0.9	18.5
	2.8	13.13	0.84	6.4	97	21	1.8	14	0.8	17.1
62-c	1.4	6.91	0.80	4.9	94	26	1.8	14	0.9	19.6
	2.2	7.74	1.12	5.8	177	41	1.2	11	0.3	7.2
62-d	1.5	8.70	0.68	5.0	68	18	6.5	15	3.3	71.0
	2.5	9.89	0.99	6.1	138	31	1.1	13	0.1	3.0

Appendix 7

ESTIMATED PALEOFLOW CONDITIONS UNDER WHICH CROSS STRATA FORMED

H = height of planar cross strata (mean value along bed; cm)

θ = non-dimensional Shield-Bagnold bed shear stress.

Fr = Froude number; 1: single number is convergent value.

2: double numbers, 1st number is highest Fr value obtain by changing θ.

2nd number is estimate Fr value from equation 5-47.

u_* = estimate shear velocity (cm/sec)

h = estimate mean depth under which cross strata formed (cm)

$\bar{U}$ = estimate mean flow velocity under which the cross strata formed (cm/sec)

$H = 15.83 \pm 1.44$ cm

$\theta = 0.86 \pm 0.03$

$u_* = 5.17 \pm 0.24$ cm/sec

$h = 49.12 \pm 3.72$ cm

$\bar{U} = 57.92 \pm 1.37$ cm/sec

Appendix 7

ESTIMATED PALEOFLOW CONDITIONS UNDER WHICH CROSS STRATA FORMED

Sample Code	H	θ	Fr	u_*	h	$\bar{U}$
1-a	4.7	0.42	0.28	4.0	23.7	49.7
	7.5	0.67	0.30	8.0	30.5	60.2
	16.0	1.25	0.30/0.32	6.8	48.2	77.1
1-d	5.0	0.65	0.28	3.8	20.8	46.2
3-a	1.5	0.10	0.24	2.2	11.1	29.6
5-g	9.8	1.25	0.28/0.31	5.0	29.5	56.8
6-a	2.5	0.23	0.26	2.8	14.4	36.0
	3.0	0.29	0.27	3.1	16.4	40.0
6-f	9.8	1.22	0.31	5.3	28.4	59.9
	14.7	1.25	0.22/0.33	4.7	44.2	53.2
7-a	3.7	0.35	0.27	3.4	19.4	43.5
8-b	3.0	0.41	0.27	3.0	15.2	38.2
8-e	10.4	0.89	0.31	5.7	32.9	64.9
8-f	14.7	1.13	0.32	6.7	40.6	73.9
8-g	3.0	0.35	0.27	3.1	15.7	39.3
	11.5	1.25	0.25/0.31	4.7	34.6	53.2
9-a	10.4	1.25	0.26/0.31	4.7	31.3	53.2
10-h	49	1.25	0.09/0.37	4.0	147.4	45.5
	58	1.25	0.10/0.37	4.0	147.0	46.4
10-j(a)	7.4	0.60	0.30	5.1	32.4	62.8
10-j(b)	8.0	0.60	0.30	5.1	33.4	62.8
10-n	7.0	0.74	0.30	4.7	26.3	56.0
	7.4	0.74	0.30	4.7	26.3	56.0

Sample Code	H	θ	Fr	u_*	h	$\overline{U}$
11-a	20.0	1.25	0.17/0.33	4.2	60.2	47.8
11-c	8.0	1.25	0.25/0.30	4.2	24.1	47.8
c	14.5	1.25	0.15/0.32	3.3	43.6	37.6
11-e	3.0	0.76	0.27	2.7	11.0	32.4
11-f	3.0	0.76	0.27	2.7	11.0	32.4
	4.0	0.97	0.28	3.1	11.8	34.9
	7.4	1.25	0.23/0.30	3.5	22.3	39.4
11-h	7.4	0.81	0.30	4.7	25.6	55.1
	12.3	1.25	0.30/0.31	5.9	37.0	66.4
13-a	15	1.25	0.24/0.32	5.2	45.1	59.0
14-a	2.5	0.47	0.26	2.6	12.2	33.1
16-a	0.8	0.11	0.22	1.4	5.7	19.2
	7.4	0.40	0.22	5.4	37.7	67.6
	12	1.25	0.25/0.31	4.8	36.1	54.3
16-b	12.3	0.63	0.31	6.7	36.1	54.3
	7.4	1.10	0.30	4.5	20.4	50.0
16-c	5.0	0.99	0.28	3.5	14.5	38.7
17-a	22.7	1.25	0.21/0.34	6.1	77.3	69.0
	23	1.25	0.23/0.34	6.1	69.2	69.2
	45	1.25	0.16/0.36	6.1	135.4	69.2
17-b	14.7	1.25	0.27/0.32	5.8	44.2	66.0
17-e	25.7	1.25	0.21/0.34	6.1	77.3	69.0
18-a	30	1.25	0.21/0.35	6.6	90.3	74.7
19-a	10.5	0.91	0.31	5.6	32.6	64.2
19-c	25	1.25	0.23/0.34	6.6	75.2	74.7
23-a	20	1.25	0.30/0.33	7.6	60.2	85.8

Sample Code	H	θ	Fr	u_*	h	$\overline{U}$
24-a	15	1.00	0.32	6.8	41.5	74.9
	40	1.25	0.20/0.35	7.2	120.4	81.8
27-a	20	1.25	0.28/0.33	7.0	60.2	79.2
27-b	20.3	1.25	0.28/0.38	7.0	61.1	79.3
	60.5	1.25	0.13/0.37	5.9	183.0	66.4
28-a	61	1.25	0.16/0.37	6.9	183.0	78.0
	59	1.25	0.17/0.37	6.9	180.5	78.2
30-a	31	1.25	0.24/0.35	7.2	91.5	82.0
	30	1.25	0.23/0.35	7.2	90.3	81.2
31-a	1.8	0.20	0.28	4.1	10.7	30.6
	7.0	0.80	0.30	4.6	25.5	54.5
	30	1.25	0.19/0.35	5.9	90.3	66.4
	30.4	1.25	0.19/0.35	5.7	91.5	66.6
31-b	4.0	0.42	0.28	3.6	20.1	45.6
31-c(1)	29	1.25	0.20/0.34	6.9	86.7	78.2
32-a	2.5	1.25	0.29	4.4	24.5	53.1
33-c	10.5	1.17	0.31	5.5	29.3	60.6
35-a	60.8	1.25	0.17/0.37	7.3	183.0	82.6
38-a	7.4	0.37	0.30	5.3	38.4	67.6
	7.6	0.41	0.30	5.5	37.7	68.8
41-a	7	0.40	0.30	5.3	35.7	66.9
	10	0.53	0.31	6.2	45.8	76.8
	16	0.80	0.32	7.5	56.0	87.6
42-a	4.0	0.37	0.28	3.7	20.7	46.8
47-c	12	1.03	0.31	5.9	33.9	65.5
47-d	30	1.25	0.21/0.35	6.4	90.3	72.2

Sample Code	H	θ	Fr	u_*	h	$\overline{U}$
48-a	5.0	0.57	0.28	3.9	22.5	48.5
	10	1.05	0.31	5.3	28.0	59.5
	15	1.25	0.15/0.36	5.3	128.0	59.5
	46	1.25	0.14/0.36	5.8	138.4	66.0
48-e	30	1.25	0.19/0.35	5.7	90.3	64.8
48-f	15	1.25	0.25/0.32	5.5	45.1	61.7
	48	1.25	0.14/0.36	5.5	144.4	61.7
48-h	12.5	1.25	0.30/0.32	6.1	37.6	68.8
52-a	61	1.25	0.17/0.37	7.7	128.7	86.7
52-c	10	0.41	0.27	3.4	19.2	42.8
	48	1.25	0.18/0.36	7.0	144.4	79.2
52-d	5.5	0.63	0.29	4.2	23.4	50.7
57-a	15.2	1.25	0.23/0.32	5.0	45.7	57.0
57-c	15.2	1.25	0.28/0.32	6.1	45.7	69.2
	5.0	0.53	0.28	4.0	23.3	49.4
	14.0	1.25	0.29/0.32	6.1	42.1	69.2
57-e	3.0	0.31	0.27	4.1	16.1	39.7
57-g	4.3	0.45	0.28	3.7	21.2	46.7
	20.2	1.25	0.24/0.33	6.2	60.8	70.2
	25	1.25	0.24/0.33	6.1	60.2	69.2
57-f	5.0	0.70	0.28	3.8	19.7	46.0
61-a	3.0	0.50	0.27	3.0	14.3	36.9
61-b	4.4	0.37	0.28	3.8	22.8	48.4
	48	1.25	0.18/0.36	7.0	144.4	79.5
61-c	3.6	0.27	0.27	3.4	19.4	43.5

Sample Code	H	θ	Fr	u_*	h	$\overline{U}$
61-c	48	1.25	0.17/0.36	6.5	144.4	73.7
61-g	3.2	0.28	0.27	3.3	17.6	41.7
61.h	7.0	0.60	0.30	5.0	30.6	61.3
	15	1.09	0.32	6.8	41.5	74.9
	30	1.25	0.23/0.35	7.2	90.3	81.8
61-i	2.0	0.24	0.25	2.4	11.4	30.4
61-j	2.4	0.34	0.26	2.6	12.7	33.4
61-l	24	1.25	0.23/0.34	6.4	72.2	72.6
61-m	3.0	0.37	0.27	3.1	15.6	38.7
61-n	3.2	0.36	0.27	3.1	15.7	39.0
61-q	24	1.25	0.27/0.34	7.4	72.2	83.8
61-s	7.0	0.50	0.30	5.1	33.4	63.0
61-t	15.5	1.25	0.19/0.32	4.2	46.6	47.0
61-u	4.0	0.40	0.28	3.7	20.4	46.3
61-w	30	1.25	0.18/0.33	5.7	90.3	64.1
61-x	4.6	0.42	0.28	3.8	22.7	48.4
	48	1.25	0.17/0.36	6.6	144.4	75.0
61-y	9.6	0.86	0.31	5.5	31.4	63.1
61-aa	4.0	0.36	0.28	3.7	20.9	46.7
61-dd	5.0	0.40	0.28	4.2	25.5	52.5
61-ff	5.1	0.48	0.28	4.0	24.7	50.4
61-hh	15	1.25	0.27/0.32	5.8	45.1	65.7
61-jj	2.2	0.20	0.28	2.7	13.1	34.6
	1.4	0.12	0.24	2.1	9.7	27.6
	2.5	0.22	0.26	2.8	14.5	36.1
	16	1.25	0.29/0.32	6.7	48.2	75.2

Sample Code	H	θ	Fr	u_*	h	$\overline{U}$
61-mm	40	1.25	0.15/0.35	5.4	120.4	60.9
	24	1.25	0.19/0.34	5.4	72.2	60.9
61-rr	11	0.89	0.31/0.33	5.9	34.5	67.8
401-1-f	20	1.25	0.15/0.33	5.0	60.2	42.8
401-1c-c	10.2	0.73	0.31	3.7	38.7	70.1
401-1c-e	2.5	0.60	0.26	2.5	10.9	31.1
	7.4	1.25	0.24/0.31	3.7	27.9	41.5
	9.8	1.25	0.21/0.31	3.7	29.5	41.5
401-3-c	2.0	0.25	0.25	2.4	11.3	30.8
401-5-g	9.8	1.25	0.28/0.33	5.0	29.5	56.8
401-6-f	9.8	1.22	0.31	5.3	28.4	59.9
	14.7	1.25	0.25/0.32	5.4	44.2	61.1
401-6-j	5.0	0.54	0.28	3.9	23.1	48.8
	3.0	0.56	0.27	3.0	13.6	36.4
	8.0	0.57	0.30	5.3	36.0	65.8
DW-1-a	4.0	0.65	0.26	2.5	10.2	30.3
DW-1-b	4.0	0.27	0.28	3.7	22.1	47.7
	10	0.33	0.28	4.1	26.6	52.3
DW-2-a	5.0	0.32	0.28	4.1	26.7	52.4
DW-7-a	1.7	0.44	0.25	2.1	8.5	26.3
DW-8-c	24	1.25	0.20/0.34	5.6	72.2	63.7
DW-9-a	5.7	0.46	0.29	4.4	30.0	55.6
DW-9-c	4.0	0.37	0.28	3.7	20.7	46.5
Dw-12-a	2.5	0.24	0.26	2.8	14.2	35.7
C-2-a	3.0	0.27	0.27	3.1	16.6	39.9
C-2-b	2.5	0.23	0.26	2.8	14.4	36.5